PHYSICAL-CHEMICAL INTERACTIONS AND COMPOSITION-STRUCTURE-PROPERTY MODIFICATIONS DURING PROCESSING: FOOD QUALITY, NUTRITION, AND HEALTH, 2nd Edition

EDITED BY: Qiang Xia, Brian D. Green and Zhonghua Liu

PUBLISHED IN: Frontiers in Nutrition

frontiers Research Topics

ISSN 1664-8714
ISBN 978-2-8325-5091-5
DOI 10.3389/978-2-8325-5091-5

About Frontiers

Frontiers is more than just an open-access publisher of scholarly articles: it is a pioneering approach to the world of academia, radically improving the way scholarly research is managed. The grand vision of Frontiers is a world where all people have an equal opportunity to seek, share and generate knowledge. Frontiers provides immediate and permanent online open access to all its publications, but this alone is not enough to realize our grand goals.

Frontiers Journal Series

The Frontiers Journal Series is a multi-tier and interdisciplinary set of open-access, online journals, promising a paradigm shift from the current review, selection and dissemination processes in academic publishing. All Frontiers journals are driven by researchers for researchers; therefore, they constitute a service to the scholarly community. At the same time, the Frontiers Journal Series operates on a revolutionary invention, the tiered publishing system, initially addressing specific communities of scholars, and gradually climbing up to broader public understanding, thus serving the interests of the lay society, too.

Dedication to Quality

Each Frontiers article is a landmark of the highest quality, thanks to genuinely collaborative interactions between authors and review editors, who include some of the world's best academicians. Research must be certified by peers before entering a stream of knowledge that may eventually reach the public - and shape society; therefore, Frontiers only applies the most rigorous and unbiased reviews.
Frontiers revolutionizes research publishing by freely delivering the most outstanding research, evaluated with no bias from both the academic and social point of view. By applying the most advanced information technologies, Frontiers is catapulting scholarly publishing into a new generation.

What are Frontiers Research Topics?

Frontiers Research Topics are very popular trademarks of the Frontiers Journals Series: they are collections of at least ten articles, all centered on a particular subject. With their unique mix of varied contributions from Original Research to Review Articles, Frontiers Research Topics unify the most influential researchers, the latest key findings and historical advances in a hot research area! Find out more on how to host your own Frontiers Research Topic or contribute to one as an author by contacting the Frontiers Editorial Office: frontiersin.org/about/contact

PHYSICAL-CHEMICAL INTERACTIONS AND COMPOSITION-STRUCTURE-PROPERTY MODIFICATIONS DURING PROCESSING: FOOD QUALITY, NUTRITION, AND HEALTH, 2nd Edition

Topic Editors:
Qiang Xia, Ningbo University, China
Brian D. Green, Queen's University Belfast, United Kingdom
Zhonghua Liu, Hunan Agricultural University, China

Publisher's note: This is a 2nd edition due to an article retraction.

Citation: Xia, Q., Green, B. D., Liu, Z., eds. (2024). Physical-Chemical Interactions and Composition-Structure-Property Modifications During Processing: Food Quality, Nutrition, and Health, 2nd Edition. Lausanne: Frontiers Media SA.
doi: 10.3389/978-2-8325-5091-5

Table of Contents

05 ***Editorial: Physical-Chemical Interactions and Composition-Structure-Property Modifications During Processing: Food Quality, Nutrition, and Health***
Qiang Xia, Brain D. Green and Zhonghua Liu

08 ***Understanding the Structure, Thermal, Pasting, and Rheological Properties of Potato and Pea Starches Affected by Annealing Using Plasma-Activated Water***
Yizhe Yan, Baixiang Peng, Bin Niu, Xiaolong Ji, Yuan He and Miaomiao Shi

21 ***From Fish Scale Gelatin to Tyrosinase Inhibitor: A Novel Peptides Screening Approach Application***
Zi-Zi Hu, Xiao-Mei Sha, Lu Zhang, Min-Jun Zha and Zong-Cai Tu

34 ***Molecular Authentication of Twelve Meat Species Through a Promising Two-Tube Hexaplex Polymerase Chain Reaction Technique***
Zhendong Cai, Guowei Zhong, Qianqian Liu, Xingqiao Yang, Xiaoxia Zhang, Song Zhou, Xiaoqun Zeng, Zhen Wu and Daodong Pan

43 ***Effects of Quinoa Flour on Wheat Dough Quality, Baking Quality, and* in vitro *Starch Digestibility of the Crispy Biscuits***
Yanrong Ma, Daying Wu, Lei Guo, Youhua Yao, Xiaohua Yao, Zhonghua Wang, Kunlun Wu, Xinyou Cao and Xin Gao

56 ***Chemical Comparison of Monk Fruit Products Processed by Different Drying Methods Using High-Performance Thin-Layer Chromatography Combined With Chemometric Analysis***
Hui-Jie Hong, Qi Yang, Qiao Liu, Fong Leong and Xiao-Jia Chen

63 ***Application of Machine Vision System in Food Detection***
Zhifei Xiao, Jilai Wang, Lu Han, Shubiao Guo and Qinghao Cui

70 ***Research Status and Prospect for Vibration, Noise and Temperature Rise-Based Effect of Food Transport Pumps on the Characteristics of Liquid Foods***
XiaoQi Jia, Songyu Li, Bo Li, Li Zhang, Qiangmin Ding, Panlong Gao and ZuChao Zhu

76 ***Photolysis for the Removal and Transformation of Pesticide Residues During Food Processing: A State-of-the-Art Minireview***
Qian Xiao, Xiaoxu Xuan, Grzegorz Boczkaj, Joon Yong Yoon and Xun Sun

82 ***Advanced Lipidomics in the Modern Meat Industry: Quality Traceability, Processing Requirement, and Health Concerns***
Chengliang Li, Burcu Ozturk-Kerimoglu, Lichao He, Min Zhang, Jiajing Pan, Yuanyi Liu, Yan Zhang, Shanfeng Huang, Yue Wu and Guofeng Jin

94 ***Influence of Fluid Food Viscosity on Internal Flow Characteristics of Conveying Pump***
XiaoQi Jia, Qingyang Chu, ZuChao Zhu, Qiangmin Ding and Panlong Gao

107 ***Effects of Ozone Water Combined With Ultra-High Pressure on Quality and Microorganism of Catfish Fillets (*Lctalurus punctatus*) During Refrigeration***
Yuzhao Ling, Mingzhu Zhou, Yu Qiao, Guangquan Xiong, Lingyun Wei, Lan Wang, Wenjin Wu, Liu Shi, Anzi Ding and Xin Li

118 ***Effect of Microbial Interaction on Flavor Quality in Chinese Baijiu Fsermentation***
Lei Gao, Jian Zhou and Guiqiang He

frontiers | Frontiers in Nutrition

TYPE Editorial
PUBLISHED 18 October 2022
DOI 10.3389/fnut.2022.1044382

OPEN ACCESS

EDITED AND REVIEWED BY
Michael Rychlik,
Technical University of Munich, Germany

*CORRESPONDENCE
Qiang Xia
xqiang0713@hotmail.com;
xiaqiang@nbu.edu.cn
Zhonghua Liu
zhonghua-liu@hotmail.com

SPECIALTY SECTION
This article was submitted to Food Chemistry, a section of the journal Frontiers in Nutrition

RECEIVED 14 September 2022
ACCEPTED 04 October 2022
PUBLISHED 18 October 2022

CITATION
Xia Q, Green BD and Liu Z (2022) Editorial: Physical-chemical interactions and composition-structure-property modifications during processing: Food quality, nutrition, and health. *Front. Nutr.* 9:1044382. doi: 10.3389/fnut.2022.1044382

Editorial: Physical-chemical interactions and composition-structure-property modifications during processing: Food quality, nutrition, and health

Qiang Xia[1]*, Brain D. Green[2] and Zhonghua Liu[3]*

[1]Key Laboratory of Animal Protein Food Processing Technology of Zhejiang Province, College of Food and Pharmaceutical Science, Ningbo University, Ningbo, China, [2]Institute for Global Food Security, Queen's University Belfast, Belfast, United Kingdom, [3]Key Laboratory of Tea Science of Ministry of Education, Hunan Agricultural University, Changsha, China

KEYWORDS

composition-structure-property, thermal treatments, nonthermal processing, process development and optimization, physicochemical interactions

Editorial on the Research Topic
Physical-chemical interactions and composition-structure-property modifications during processing: Food quality, nutrition, and health

Recent years have witnessed the role of industrial food processing in driving the creation and transformation of a modernized and facilitated lifestyle by providing efficient food supply chains and sustainable diets (1–3), particularly for those effective, eco-friendly and energy-saving pretreatment or manufacturing technologies. Different food unit operations aim at assuring physicochemical stability and microbiological and nutrition safety, and simultaneously obtaining desired modifications in the composition and structure of food matrices, accompanied by positive health implications (4). Therefore, the correlation between extrinsic processing factors and composition-structure-properties response has been one of major focuses of food science research, largely relying on food matrices and the applied technique types (5, 6). In this regard, thermal conditions receive the most attention considering their generalization and high applicability. For current food industries, multiple processing techniques, process optimization strategies, and the exploitation of new food sources have been largely developed. Resultantly, the presence of new-type physicochemical interaction behavior and phenomenon among minor/major components and composition-structure-property relation modifications exerted by emerging processing methods or patterns or in new combination patterns require more elaborate characterization, analysis, and summarization over the response of quality, nutritional and health properties

of final products, in order to achieve the tailored production of nutritional and health foods (7, 8). Particularly, healthier food can be obtained *via* suitable food re-formulation and microstructure designing (9), relying on the accumulation of knowledge about the correlation between food structure, the gastrointestinal fate of nutrients and satiety response.

The current Research Topic aims at highlighting the progress and roles of processes-induced physicochemical modifications and interaction behavior of different intrinsic food components, particularly at molecular levels, in regulating the changes of quality, storability, nutrition and health characteristics of food products. In this collection, a total of 13 papers have been published, related to the development of analysis, evaluation and characterization techniques for the complicated network of chemical and compositional differences, machine imaging, introduction and summarization of the newly developed processing techniques and the effects, as well as the processing and nutrition attributes of food materials with new origins (Jia, Chu et al., Hong et al., Ma et al.).

Novel characterization techniques and methodologies applied to monitor compositional variations or differences during processing are expected in this Research Topic. Li et al. summarized advanced lipidomics applied to muscle origin differentiation and meat processing, with the aspects of quality traceability, processing requirement, and health concerns involved. Cai et al. reported a two-tube hexaplex polymerase chain reaction technique used for molecular authentication which may occur in commercial meat processing. Another mini-review performed by Xiao, Wang et al. reported the application of a machine vision system for food quality monitoring during processing. Effects of novel processing techniques and varied combination patterns on the chemical modifications during processing are also reported in this collection, as observed in the cases of plasma-activated water (Yan et al.), hydrodynamic cavitation (Sun et al.), and photolysis (Xiao, Xuan et al.). These cases suggested that the major food physicochemical attributes during processing and transportation can be modified significantly, depending on many process parameters, as exemplified by the correlation between food safety properties and rotary motion conditions (e.g., vibration, noise, and temperature rise) of food transport pumps (Jia, Li, et al.).

In conclusion, it can be inferred from these papers of this collection that scientific and technical challenges during food processing have been overcome to a large degree, with both novel processing techniques and detection/characterization strategies developed. However, there are some research aspects that should be highlighted in future related work, as exemplified by the following items: (i) metabolic and omic characterization of bio-processing foods; (ii) interaction patterns between food components as affected by processing parameters, as well as its effects on nutritional properties (e.g., digestibility, bioaccessibility, bioavailability, etc.); (iii) comparison of chemical modifications of food components (e.g., protein, lipid, carbohydrates, phytochemicals, etc.) between traditional thermal processing and emerging nonthermal processing processes or the combined patterns.

Author contributions

QX: drafted the manuscript. BG and ZL: conceptualized, reviewed, and edited the manuscript. All authors contributed to the article and approved the submitted version.

Funding

This work is financially supported by the National Natural Science Foundation of China (32101862) and Natural Science Foundation of Zhejiang Province (LQ20C200007).

Conflict of interest

The authors declare that the research was conducted in the absence of any commercial or financial relationships that could be construed as a potential conflict of interest.

Publisher's note

References

1. Augustin MA, Riley M, Stockmann R, Bennett L, Kahl A, Lockett T, et al. Role of food processing in food and nutrition security. *Trends Food Sci Technol.* (2016) 56:115–25. doi: 10.1016/j.tifs.2016.08.005

2. Xu L, Zheng Y, Zhou C, Pan D, Geng F, Cao J, et al. A structural explanation for enhanced binding behaviors between β-lactoglobulin and alkene-aldehydes upon heat-and ultrasonication-induced protein unfolding. *Food Hydrocoll.* (2022) 130:107682. doi: 10.1016/j.foodhyd.2022.107682

3. Zhang X, Zheng Y, Kumar Awasthi M, Zhou C, Barba FJ, Cai Z, et al. Strategic thermosonication-mediated modulation of lactic acid bacteria acidification kinetics for enhanced (post)-fermentation performance. *Bioresour Technol.* (2022) 361:127739. doi: 10.1016/j.biortech.2022.127739

4. Dima C, Assadpour E, Dima S, Jafari SM. Bioactive-loaded nanocarriers for functional foods: from designing to bioavailability. *Curr Opin Food.* (2020) 33:21–9. doi: 10.1016/j.cofs.2019.11.006

5. Xia Q, Tao H, Huang P, Wang L, Mei J, Li Y. Minerals *in vitro* bioaccessibility and changes in textural and structural characteristics of uncooked pre-germinated brown rice influenced by ultra-high pressure. *Food Control.* (2017) 71:336–45. doi: 10.1016/j.foodcont.2016.07.018

6. Xia Q, Zheng Y, Liu Z, Cao J, Chen X, Liu L, et al. Nonthermally driven volatilome evolution of food matrices: the case of high pressure processing. *Trends Food Sci Technol.* (2020) 106:365–81. doi: 10.1016/j.tifs.2020.10.026

7. Calligaris S, Moretton M, Melchior S, Mosca AC, Pellegrini N, Anese MJF, et al. Designing food for the elderly: the critical impact of food structure. *Food Funct.* (2022) 13:6467–83. doi: 10.1039/D2FO00099G

8. Kaufmann SF, Palzer S. Food structure engineering for nutrition, health and wellness. In: *Advances in Food Process Engineering Research and Applications*. Boston, MA: Springer (2013). p. 429–43. doi: 10.1007/978-1-4614-7906-2_20

9. Bhat ZF, Morton JD, Bekhit AEDA, Kumar S, Bhat HF. Effect of processing technologies on the digestibility of egg proteins. *Compr Rev Food Sci Food Saf 20.* (2021) 4703–38. doi: 10.1111/1541-4337.12805

frontiers in Nutrition

ORIGINAL RESEARCH
published: 07 February 2022
doi: 10.3389/fnut.2022.842662

Understanding the Structure, Thermal, Pasting, and Rheological Properties of Potato and Pea Starches Affected by Annealing Using Plasma-Activated Water

Yizhe Yan[1]*, *Baixiang Peng*[1], *Bin Niu*[2], *Xiaolong Ji*[1], *Yuan He*[1] and *Miaomiao Shi*[1]*

[1] Henan Key Laboratory of Cold Chain Food Quality and Safety Control, College of Food and Bioengineering, Zhengzhou University of Light Industry, Zhengzhou, China, [2] College of Food Science and Technology, Henan Agricultural University, Zhengzhou, China

In this research, annealing (ANN) using plasma-activated water (PAW) was first employed to modify potato and pea starches. Compared with the conventional ANN using distilled water (DW), the granular morphology of two starches was not significantly affected by PAW-ANN. The results of X-ray diffraction (XRD) and Fourier transform infrared (FTIR) spectroscopy showed that PAW-ANN could reduce the long and short-range ordered structure of potato starch while improving the long and short-range ordered structure of pea starch. Differential scanning calorimetry (DSC) analysis indicated that PAW-ANN lowered the gelatinization enthalpy of potato starch and increased the gelatinization enthalpy of pea starch. The analysis of viscosity and dynamic rheological characteristics illustrated that PAW-ANN reduced the peak viscosity and improved the gel strength of starch pastes. PAW-ANN represents a novel modification method for modifying the structure, reducing the viscosity, improving the gel strength of starch, and is very promising for applying in starch-based hydrogels and food additives.

Keywords: plasma-activated water, annealing, structure, physicochemical properties, potato starch, pea starch

OPEN ACCESS

Edited by:
Qiang Xia,
Ningbo University, China

Reviewed by:
Lijun Sun,
Northwest A&F University, China
Qunyu Gao,
South China University of Technology, China

***Correspondence:**
Yizhe Yan
yanyizhe@zzuli.edu.cn
Miaomiao Shi
chengzi3090@126.com

Specialty section:
This article was submitted to Food Chemistry, a section of the journal Frontiers in Nutrition

Received: *24 December 2021*
Accepted: *04 January 2022*
Published: *07 February 2022*

Citation:
Yan Y, Peng B, Niu B, Ji X, He Y and Shi M (2022) Understanding the Structure, Thermal, Pasting, and Rheological Properties of Potato and Pea Starches Affected by Annealing Using Plasma-Activated Water. Front. Nutr. 9:842662. doi: 10.3389/fnut.2022.842662

INTRODUCTION

Starch is a significant carbohydrate source for most organisms, which has been widely applied in the food industry, such as papermaking, adhesives and biodegradable plastics, sweeteners, pasta products, and some fermented products (1). Native starch has the limitations of poor hydration performance, low thermal stability, low shear resistance, and high retrogradation rate, while modified starch performs well in terms of compatibility and has a low retrogradation rate, pasty gelation tendency, and gel shrinkage (2). Therefore, modified starch is preferred in the food industry instead of native starch. The modification of starch usually has the following three methods, namely, physical, chemical, and enzyme modification (3). Among them, physical modification is relatively safe and low-cost, and can greatly reduce waste generation (4).

Annealing (ANN) is usually to treat starch for a period of time at a high moisture content (more than 40%, w/w) and a low temperature (below 60°C). As a green modification method, ANN has received extensive attention because it only involves water and heat (5). It can usually change the internal structure and physicochemical properties of starch while not damaging the integrity of

granules, which makes starch easier to be processed and employed in certain specific circumstances. For example, it has been studied that annealed starch was more suitable for application in yogurt, sauce, and low-digestible foods than native starch (6).

Plasma-activated water (PAW) from plasma treatment of distilled water (DW) has the advantages of uniform function, green and environmental protection. PAW will generate an acidic environment and generate active substances, such as hydrogen peroxide, nitric acid, and peroxynitrite, which will cause changes in the pH, redox potential, and conductivity. Recently, PAW has been widely used in food and agriculture yields, such as promoting plant growth, preservation of seafood, and broad-spectrum sterilization (7). However, PAW was rarely applied in the starch modification. According to our preliminary studies, PAW alone had no significant influence on the structure and properties of the starch. Therefore, a combination of PAW and other modified technologies could be an effective strategy. Based on this assumption, we have recently explored the combination of PAW and heat-moisture treatment (HMT) on the structure and properties of maize starches (8). PAW-HMT provided an innovative strategy to regulate the structure and digestibility of starch. However, PAW-HMT effect remained limited compared with the conventional HMT (DW-HMT). Therefore, the development of new PAW combined modifications (such as PAW-ANN and PAW-ultrasound) is desired.

In this research, PAW was first employed during ANN to modify potato and pea starches. After being modified with PAW-ANN, the changes of structure and properties of potato and pea starches were investigated. It is worth mentioning that this green modification method is only involved in plasma, water, and heat. This research will not only propose a new way of starch ANN treatment, but also further expand the application of PAW in starch modification.

MATERIALS AND METHODS

Materials

Native potato starch (13.2% moisture and 21.6% amylose) was obtained from Qinghai Weston Potato Industry Group Co., Ltd. (Xining, China). Native pea starch (11.3% moisture and 30.8% amylose) was obtained from Henan Enmiao Food Co., Ltd. (Zhengzhou, China). A hydrogen peroxide quantitative kit was obtained from Shanghai Sangon Biotech Co., Ltd. (Shanghai, China). Nitrite and nitrate determination kits were obtained from Beyotime Biotechnology Institute (Nantong, China). Other reagents used in this experiment were of analytical grade.

Preparation and Characterization of PAW

The PAW was obtained by treating 100 ml of distilled water through plasma processing equipment (Easton Geake Automation Equipment Co., Ltd., Shenzhen, China) for 120 s. The power was 750 W and the working gas was compressed air (0.18 MPa) (8). The pH/oxidation-reduction potential (ORP) meter and conductivity meter (INESA Scientific Instrument Co., Ltd., Shanghai, China) were, respectively, employed for measuring the pH, ORP, and conductivity of the PAW. Additionally, the content of H_2O_2, NO^{2-}, and NO^{3-} were determined by corresponding assay kits. Notably, PAW was suggested to be further used within 12 h.

ANN of Potato and Pea Starches With PAW or DW

After drying at 45°C, the moisture content of potato and pea starches (30 g, dry basis) is about 5%. Then, the moisture content of them was adjusted to 60% using DW or PAW, respectively. The starch samples were put into the reactor with sufficient stirring and then heated in an air oven at 50°C for 12 h. Finally, modified starches were obtained through washing, drying, and sieving and marked as DW-Potato, DW-Pea, PAW-Potato, and PAW-Pea, respectively.

Scanning Electron Microscopy

Morphology of native and modified starch granules was observed using a scanning electron microscope (JSM-6490LV, JEOL, Japan). A small amount of dry-based samples were adhered to the double-sided conductive adhesive and coated with gold in the ion sputtering device (Polaron Sputter Coat System, Model 5001, UK) for 120 s (8). The imaging acceleration voltage of Scanning electron microscopy (SEM) was 20 kV. A micrograph of representative particles was chosen and taken at a magnification of ×1,000.

Polarization Light Microscopy

A suspension of starch samples (1%, w/w) was obtained by using a solvent of glycerol and water (1:1, v/v) and observed under polarized light microscopy (PLM) (BX53M, Olympus Co., Ltd., Japan). The images were observed and taken at ×200 for all starch samples.

X-Ray Diffraction

Before analysis of X-ray diffraction (XRD), starch samples needed balancing water over a saturated NaCl solution at room temperature for 1 week (9). Starch samples were analyzed by using an X-ray diffractometer (D8 Advance, Bruker, Karlsruhe, Germany). The detailed test conditions and relative crystallinity (RC) calculation of the starch samples were based on our previous study (8).

Fourier Transform Infrared Spectroscopy

Fourier transform infrared (FTIR) spectra of starch samples were determined by using an FTIR spectrometer (Vertex 70, Bruker, Karlsruhe, Germany). Before the test, potassium bromide should be dried at 105°C for 6 h. A certain amount of samples and potassium bromide (mass ratio: 1:100) were taken in an agate mortar, mixed, and grinded for about 2 min. The ground mixed samples were placed in a tableing mold and compressed with a tableting machine, where the pressure was maintained within the range of 10 MPa for about 1 min and then taken out for testing. Test conditions: scanning wave number 4,000–400 cm^{-1}, resolution 4 cm^{-1}, scanning time 64 s. The spectra were analyzed by OMNIC8.2 (Version 8.2, Thermo Nicolet Inc., Madison, WI, USA). The absorbance ratio at 1,047/1,022 cm^{-1} ($R_{1047/1022}$) can be obtained by deconvolution with a peak width of 38 cm^{-1}

TABLE 1 | Physicochemical properties and content of active substances of distilled water (DW) and plasma-activated water (PAW).

Water	pH	Conductivity (μS/cm)	ORP (mV)	H_2O_2 (μmol/L)	NO_2^- (μmol/L)	NO_3^- (μmol/L)
DW	6.40 ± 0.05^a	4.55 ± 0.48^b	247.00 ± 2.65^b	ND	ND	ND
PAW	2.72 ± 0.01^b	764.67 ± 1.53^a	569.67 ± 1.53^a	131.32 ± 0.91	$1{,}905.22 \pm 0.75$	$2{,}075.17 \pm 2.69$

Values are means ± SD; means with the same letters in a column for the same starch do not differ significantly ($p > 0.05$). ND, Not detected.

and enhancement factor of 19 and employed to characterize the short-range ordered structure of starch molecules (8).

Differential Scanning Calorimetry

Thermal properties of native and modified starches were obtained by using a differential scanning calorimeter (Q20, TA Instruments Inc., Newcastle, DE, USA). The starch (3 mg, dry basis) and distilled water were added with a microliter syringe to a total weight of 12 mg into an aluminum pan. The samples were equilibrated at room temperature for 12 h. Subsequently, the sample pans were gradually scanned from 30 to 120°C at a heating rate of 10°C/min (8).

Rapid Viscosity Analyzer

Pasting characteristics of the starch samples were obtained by using a rapid viscosity analyzer (RVA4500, Perten Instruments, Hägersten, Sweden). Starch samples were suspended in distilled water to make a total weight of 28.0 g (8% dry starch, w/w) and then analyzed using RVA Standard Procedure 1 profile. The samples were equilibrated at 50°C for 1 min, heated to 95°C within 222 s, held at 95°C for 150 s, cooled back to 50°C for 228 s, and then equilibrated at 50°C for 2 min. During this process, the paddle speed was kept at 960 rpm for the first 10 s, and then kept at 160 rpm. The pasting curves and parameters were obtained by RVA system software.

Dynamic Rheological Properties

The dynamic rheological properties of starch pastes from the RVA experiment were analyzed by using a rheometer (Discovery HR-1, TA Instruments Inc., Newcastle, DE, USA). Sample pastes were transferred to the rheometer plate (40 mm diameter and 1,000 μm gap) and equilibrated for 5 min at 25°C. The strain was set at 1% and the frequency was taken at 0.1–20 Hz. G', G'', and tan δ (G''/G') of samples were recorded.

Statistical Analysis

All experimental data were recorded as the means ± SDs. ANOVA followed by *post-hoc* Duncan's multiple range tests ($p < 0.05$) was conducted to determine the significant differences between mean values using the SPSS 26.0 Statistical Software Program (SPSS Inc., Chicago, IL, USA).

RESULTS AND DISCUSSION

Characterization of PAW

After 2 min of plasma treatment, the pH of PAW dropped rapidly from 6.4 to 2.72, the conductivity value increased from 4.55 to 764.67 μS/cm, and the ORP value increased from 247 to 569.67 mV (**Table 1**). The measured conductivity value can be used to detect whether there were active ions in the water, and the ORP can be used to reflect the macroscopic oxidation–reduction performance of all substances in the aqueous solution, depending on the concentration and strength of the oxidant in the solution. During the plasma discharge process, a large number of active chemical substances, such as reactive hydroxyl radicals, singlet oxygen, superoxide, ozone, and active molecule nitrogen species, were generated. These substances interacted with water molecules to further generate H^+, H_2O_2, NO, NO^{2-}, NO^{3-}, $ONOO^-$, and so on, which led to the changes in the pH value, conductivity value, and ORP value of the aqueous solution (10). In addition, after plasma treatment, the content of H_2O_2, NO^{2-}, and NO^{3-} was increased from zero to 131.32, 1,905.22, and 2,075.17 μmol/L, respectively (**Table 1**), which further verified the above fact.

Granular Morphology

Scanning Electron Microscopy

The SEM micrographs of native and modified starch samples are displayed in **Figure 1**. Native potato starch granules were oval or spherical, with various sizes and smooth surfaces. The potato starch granules treated with DW-ANN and PAW-ANN had obvious dents and cracks. Native pea starch granules were slender, kidney-shaped, of different sizes, and had many folds (11). After DW-ANN and PAW-ANN, the shape of most pea starch granules did not change significantly, but the surface folds of the granules were deepened, and a few granules appeared with dents and cracks. However, PAW-ANN did not give significantly different results from DW-ANN for two starches.

Polarized Light Microscopy

The PLM micrographs of native and modified starch samples are displayed in **Figure 2**. Native starch granules showed a characteristic birefringence pattern (Maltese cross). The strength of birefringence was related to the overall size, relative crystallinity, and crystallite orientation of the crystal grains (12). The polarized cross of native potato starch was complete and obvious. In contrast, the polarized cross of modified potato starch became fuzzy and the shape of the particles became irregular with cracks, which were similar to the observation by SEM. The difference in the polarized cross between native and modified pea starches was not obviously observed. Notably, there was no significant difference between PAW-ANN and DW-ANN for the two starches.

Crystalline Structure

X-ray diffractograms of starch samples are displayed in **Figure 3**. Potato starch showed the characteristic diffraction peaks at $2\theta =$

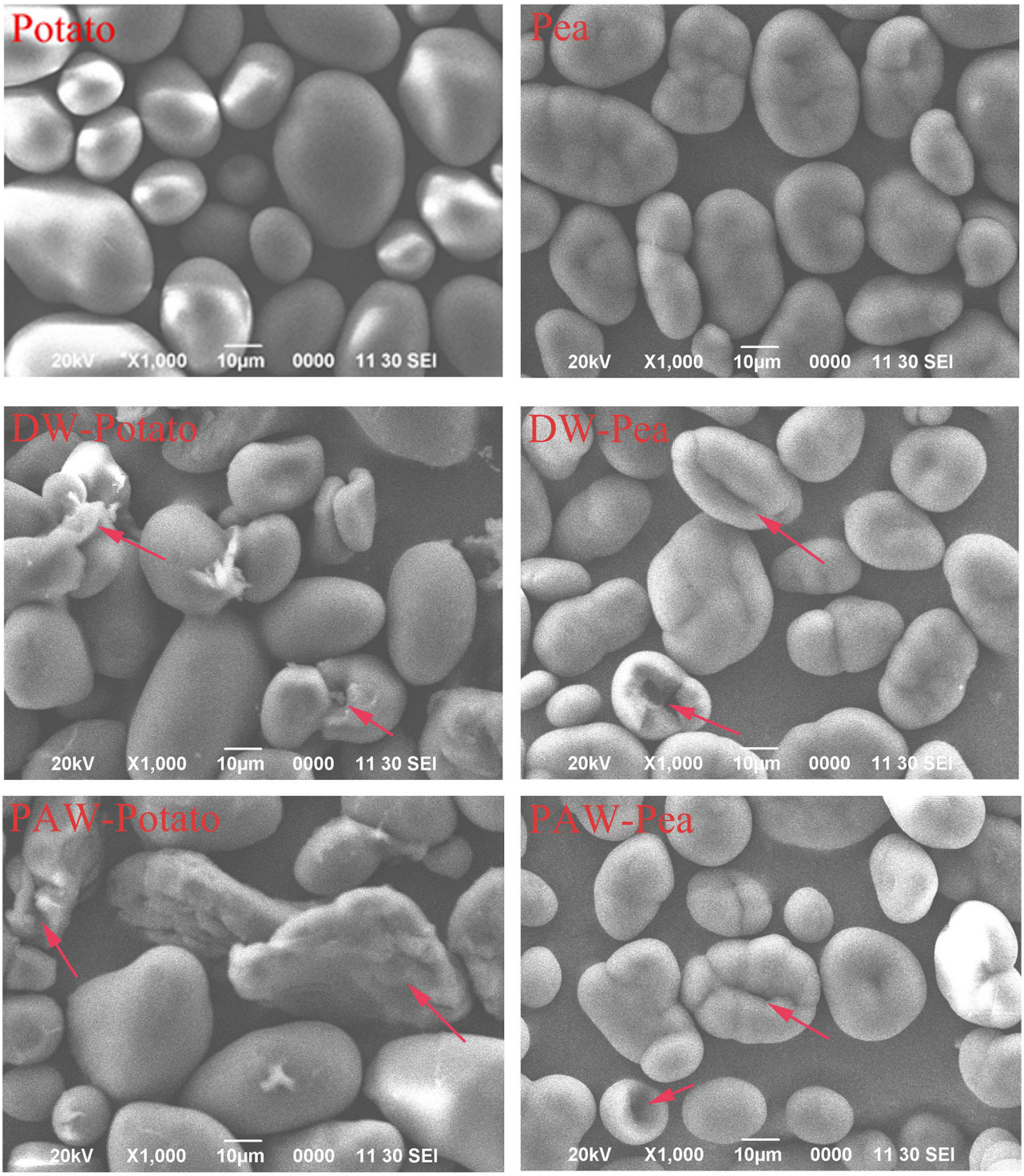

FIGURE 1 | Scanning electron microscopy (SEM) images of native and modified starches.

5.6, 17.1, 22.2, and 24.1 degrees, which was classified to the B-type structure (13). According to **Table 2**, the relative crystallinity (RC) of ANN-modified potato starch (DW-Potato and PAW-Potato) was lower compared with native potato starch. This might be because the double helix molecules of the B-type crystal structure were more sparsely arranged in space, forming a spiral cavity center (14), so ANN was more likely to destroy its crystal structure. This can be confirmed from the observations of the

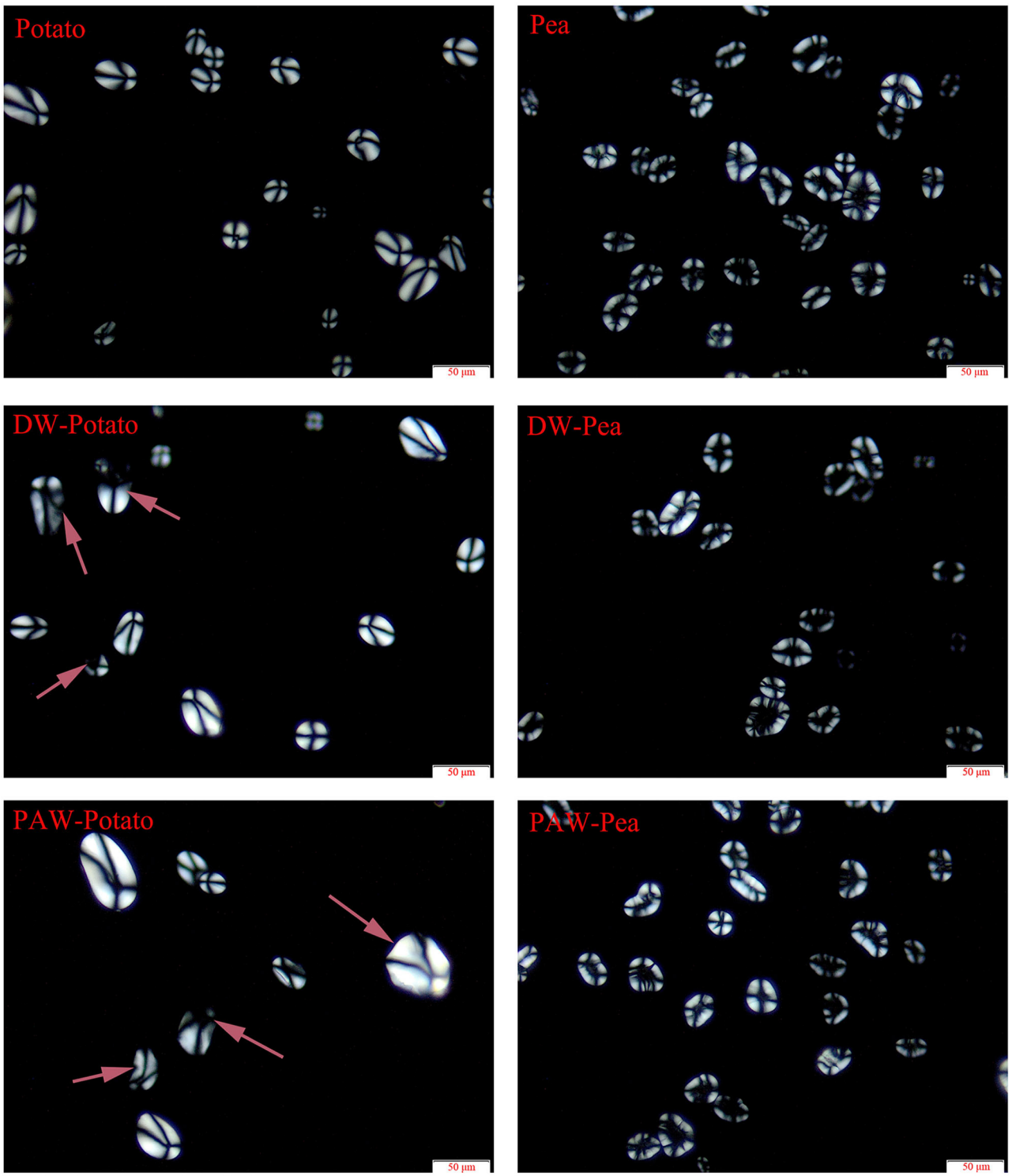

FIGURE 2 | Polarized light microscopy (PLM) images of native and modified starches.

SEM and PLM of DW-Potato and PAW-Potato. In addition, the RC of PAW-Potato was lower than that of DW-Potato, which may be attributed to the acidic content of PAW. ANN could increase the sensitivity of potato starch to acid hydrolysis, resulting in its crystal structure being more easily hydrolyzed (15). The characteristic diffraction peaks of pea starch were

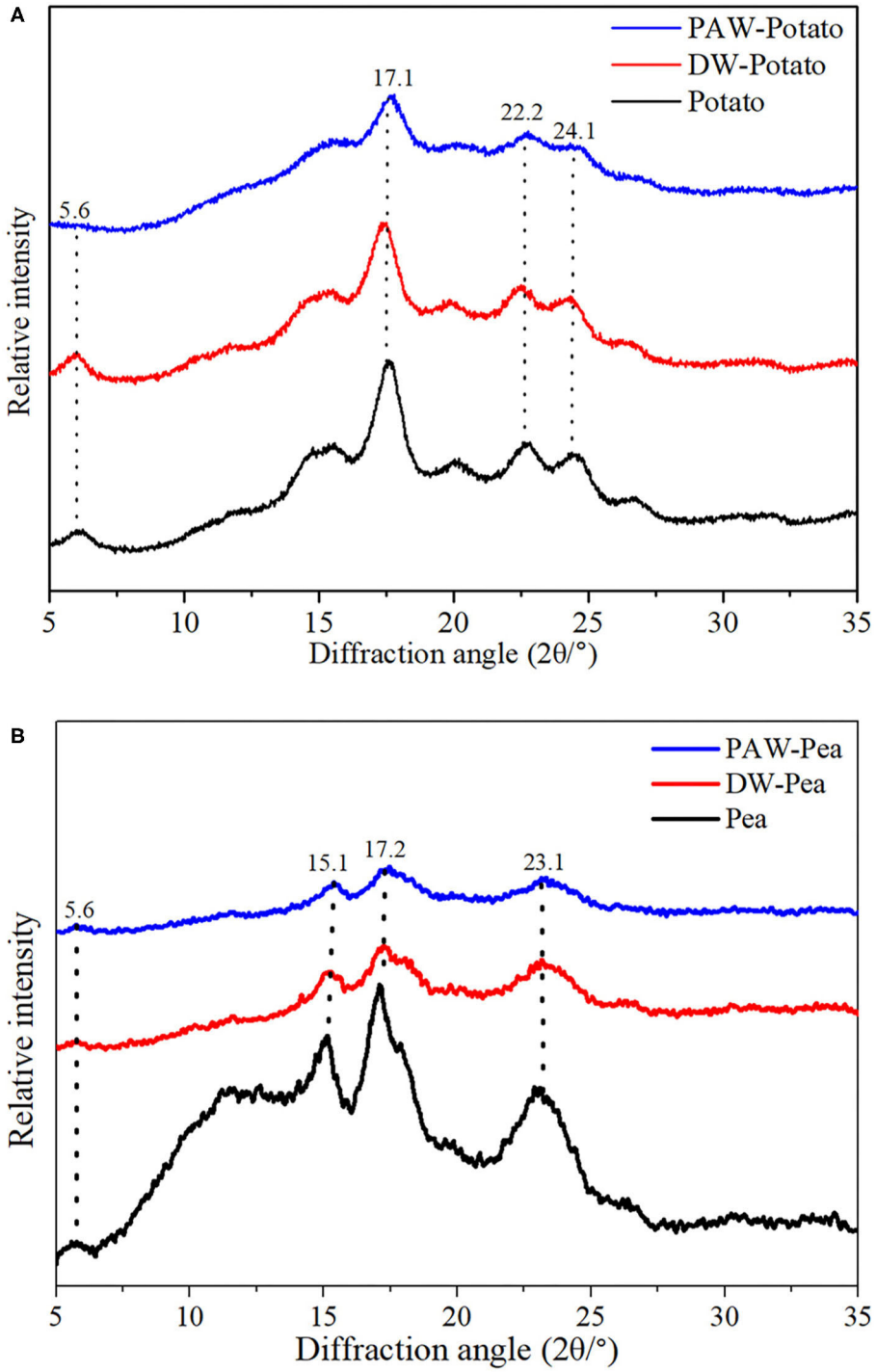

FIGURE 3 | X-ray diffraction (XRD) patterns of native and modified starches. **(A)** Native, distilled water-annealing (DW-ANN) treated, and plasma-activated water-annealing (PAW-ANN) treated potato starch. **(B)** Native, DW-ANN treated, and PAW-ANN treated pea starch.

mainly shown at $2\theta = 5.6$, 15.1, 17.2, and 23.1°, which belonged to the diffraction of C-type starch (16). It can be concluded from **Table 2** that the crystallinity of ANN-modified pea starch (DW-Pea and PAW-Pea) was higher than that of native pea starch. This might be because ANN made the initially weak or imperfect crystallites of pea starch gradually disappeared, while the remaining crystallites became more perfect due to melting and recrystallization (17). In addition, the RC of PAW-Pea was

TABLE 2 | Long-range, short-range ordered structure, and thermal properties of native and modified starches.

Samples	RC (%)	$R_{1047/1022}$	T_o (°C)	T_p (°C)	T_c (°C)	ΔH (J/g)
Potato	25.16 ± 0.35[a]	0.905 ± 0.003[a]	57.34 ± 0.24[c]	61.59 ± 0.23[b]	72.10 ± 0.67[b]	12.27 ± 0.43[a]
DW-Potato	22.13 ± 0.21[b]	0.862 ± 0.025[a]	62.32 ± 0.18[a]	66.32 ± 0.17[a]	74.33 ± 0.72[a]	9.39 ± 0.18[b]
PAW-Potato	15.20 ± 0.41[c]	0.783 ± 0.057[b]	61.86 ± 0.16[b]	66.04 ± 0.11[a]	73.32 ± 0.38[a]	7.31 ± 0.20[c]
Pea	25.40 ± 0.26[c]	0.877 ± 0.018[b]	57.92 ± 0.04[b]	65.07 ± 0.06[b]	75.58 ± 0.06[b]	6.69 ± 0.20[c]
DW-Pea	30.53 ± 0.31[b]	0.905 ± 0.011[ab]	66.97 ± 0.01[a]	69.74 ± 0.02[a]	76.25 ± 0.12[b]	8.50 ± 0.23[b]
PAW-Pea	34.93 ± 0.25[a]	0.934 ± 0.001[a]	66.92 ± 0.05[a]	69.76 ± 0.03[a]	78.42 ± 0.44[a]	9.66 ± 0.11[a]

Values are means ± SD; means with the same letters in a column for the same starch do not differ significantly ($p > 0.05$).

higher than that of DW-Pea, indicating that PAW can improve the RC of pea starch during ANN. This may be due to more hydrolysis of the amorphous area by the acidic components of PAW, resulting in a better orientation of the hydrolyzed starch crystallites (18).

Short-Range Ordered Structure

The spectra of all starches showed similar trends, indicating that no new functional groups were formed (**Figure 4**). Studies have shown that the IR bands at 1,047 and 1,022 cm^{-1} were related to the ordered structure and amorphous structure of starch, respectively (19). The absorbance ratio of them ($R_{1047/1022}$) can indicate the relative content of the short-range ordered structure of starch. $R_{1047/1022}$ of native and modified starches followed the order: Potato > DW-Potato > PAW-Potato; Pea < DW-Pea < PAW-Pea (**Table 2**). For potato starch, $R_{1047/1022}$ decreased successively because ANN caused starch granules to form granular pores, ruptures, and cracks, resulting in damage to the internal ordered structure. The presence of PAW further aggravated the destruction process. For pea starch, $R_{1047/1022}$ increased sequentially, which might be due to the high moisture content and moderate heat energy existing in the ANN process that could produce more effective double helix stacking (6). Moreover, the acidic components of PAW could affect amorphous regions of starch and generate more short-chain amylose to form a new double helices structure. The result of $R_{1047/1022}$ was in agreement with the result of XRD.

Thermal Properties

The differential scanning calorimetry (DSC) curves of native and modified starches are shown in **Figure 5**. **Table 2** presented the gelatinization transition temperatures (To, Tp, and Tc) and gelatinization enthalpy (ΔH). ANN resulted in a significant increase in the gelatinization temperatures of starch because ANN enhanced the interaction between amylose and amylose or amylopectin (20), inhibiting granule swelling and delaying gelatinization. However, the gelatinization temperatures of starches treated by DW-ANN and PAW-ANN were not significantly different. For potato starch, DW-ANN reduced the ΔH, and PAW-ANN can reduce the ΔH more, from 12.27 to 7.31 J/g. The decrease of the ΔH after ANN indicated the dissociation of unstable double helices in some starch granules (21), and the addition of PAW made this change more dramatic. For pea starch, DW-ANN increased the ΔH, and PAW-ANN can increase the ΔH more, from 6.69 to 9.66 J/g. The increase of the ΔH after ANN indicated more increase of effective double helix stacking in pea starch granules (22). After PAW-ANN, the increase of ΔH was due to the formation of new double helices, which was caused by the hydrolysis of amorphous regions (23). The ΔH result was in line with XRD and FTIR results.

Pasting Properties

The pasting characteristics curves of native and modified starches are presented in **Figure 6**. The viscosity change of starch granules under heating and shearing was attributed to the tightly deformed granule arrangement, the friction between the expanded granules, and the content of leached amylose and amylopectin (24). After ANN, the peak viscosity of both potato and pea starches decreased, and the peak viscosity of modified potato starch decreased more. This might be associated with a significant increase in the interaction between amylose and amylose or amylopectin, inhibiting granule swelling, which was concluded from the increase of the gelatinization temperatures of starch (25). Moreover, compared with DW-ANN, PAW-ANN resulted in a lower peak viscosity. The decrease of viscosity could be because the starch chains were largely affected by acid hydrolysis, which generated fragmentation of starch chains (26).

Dynamic Rheological Properties

The dynamic rheological properties of native and modified starch pastes are displayed in **Figure 7**. G′ and G″ are used to represent the elasticity and viscosity of starch gels, respectively (27). Tan δ was the ratio of G″ and G′, which represents the viscoelastic properties of the starch gels (28). It can be illustrated from the **Figures 7A–D** that the G′ and G″ of all starch pastes increased with increasing sweeping frequency and G′ was larger than G″ (tan δ < 1), revealing that starch pastes were a typical weak gel structure and more elastic (29). After ANN, all modified starches showed higher G′ and G″, which explained that the gel strength of starch was enhanced. This may be because, during ANN, the rearrangement of amylose units formed on the surface of starch granules through larger pores and cracks increased the gel strength of starch (30). This can be demonstrated from the tan δ (**Figures 7E,F**). The starch pastes after ANN had a smaller tan δ, indicating that the solid properties of the modified starch pastes were enhanced with

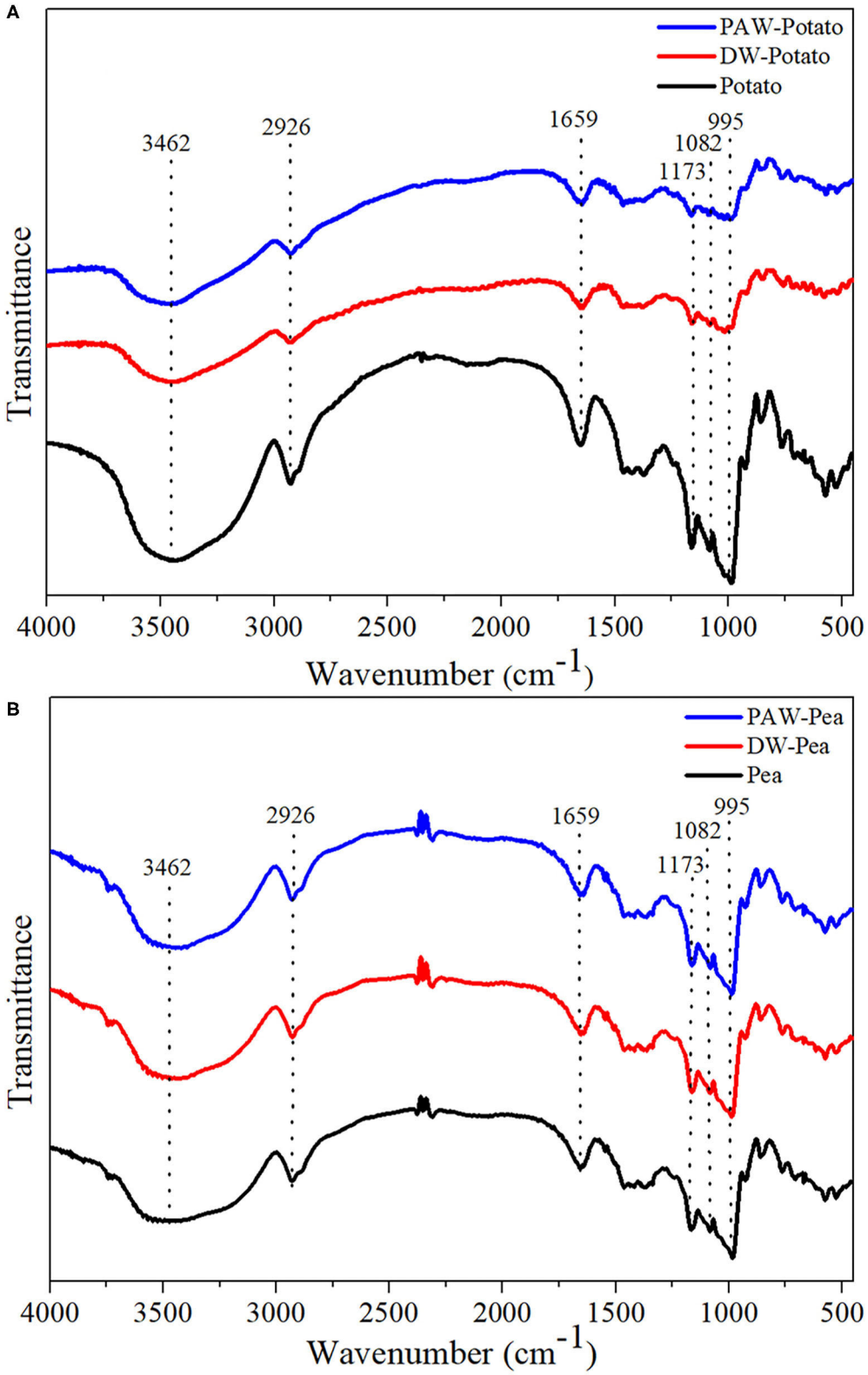

FIGURE 4 | Fourier transform infrared (FTIR) spectra of native and modified starches. **(A)** Native, DW-ANN treated, and PAW-ANN treated potato starch. **(B)** Native, DW-ANN treated, and PAW-ANN treated pea starch.

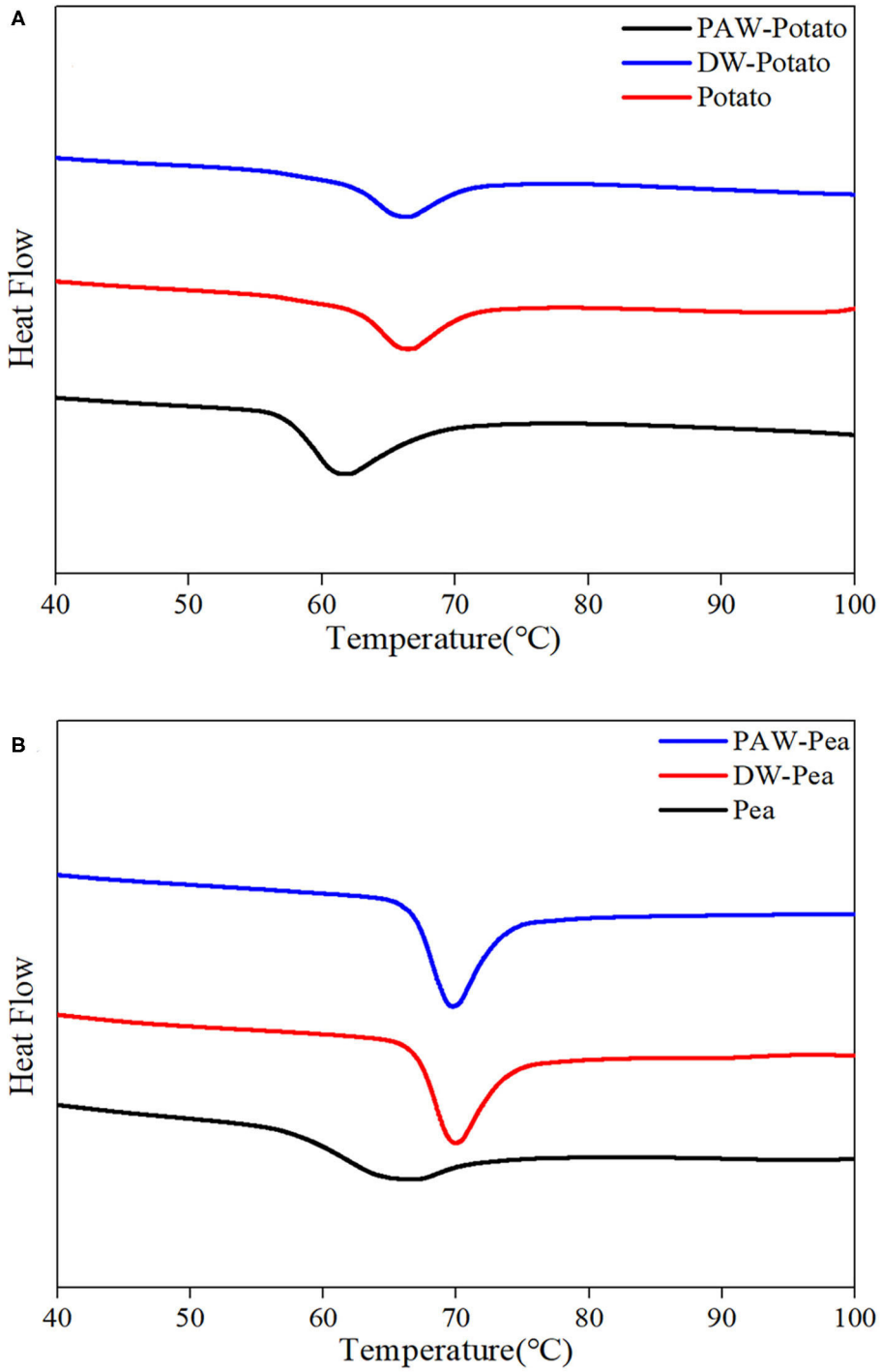

FIGURE 5 | Thermal properties of native and modified starches. **(A)** Native, DW-ANN treated, and PAW-ANN treated potato starch. **(B)** Native, DW-ANN treated, and PAW-ANN treated pea starch.

the higher gel strength. In addition, pea starch had lower tan δ than potato starch. Notably, compared with DW-ANN, PAW-ANN resulted in larger G′ and G″, and smaller tan δ, which indicated that the starch treated by PAW-ANN had higher gel strength than that treated by DW-ANN. Therefore, PAW-ANN modified starches had the highest gel strength and will be a potential gelling agent for soft candies, ice cream, and meat foods production.

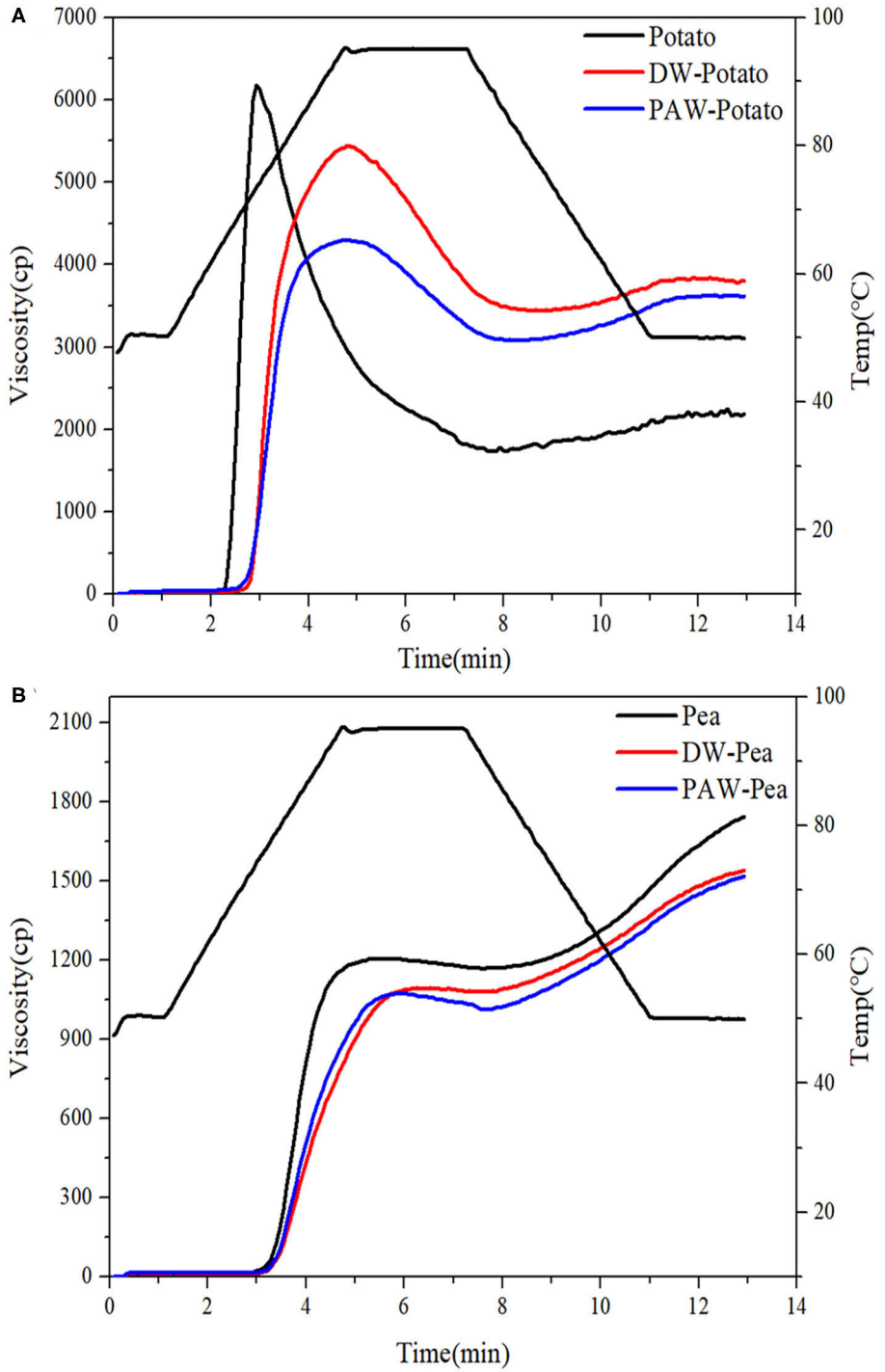

FIGURE 6 | Pasting curves of native and modified starches. **(A)** Native, DW-ANN treated, and PAW-ANN treated potato starch. **(B)** Native, DW-ANN treated, and PAW-ANN treated pea starch.

CONCLUSION

In summary, PAW-ANN as a completely novel starch modification method, had an obvious effect on the structure, thermal, pasting, and rheological properties of potato and pea starches. The impact of PAW-ANN on the granular morphology of two starches was not significantly different from the conventional DW-ANN. Compared with DW-ANN, PAW-ANN increased long and short-range ordered structure, and gelatinization enthalpy of pea starch while decreasing these

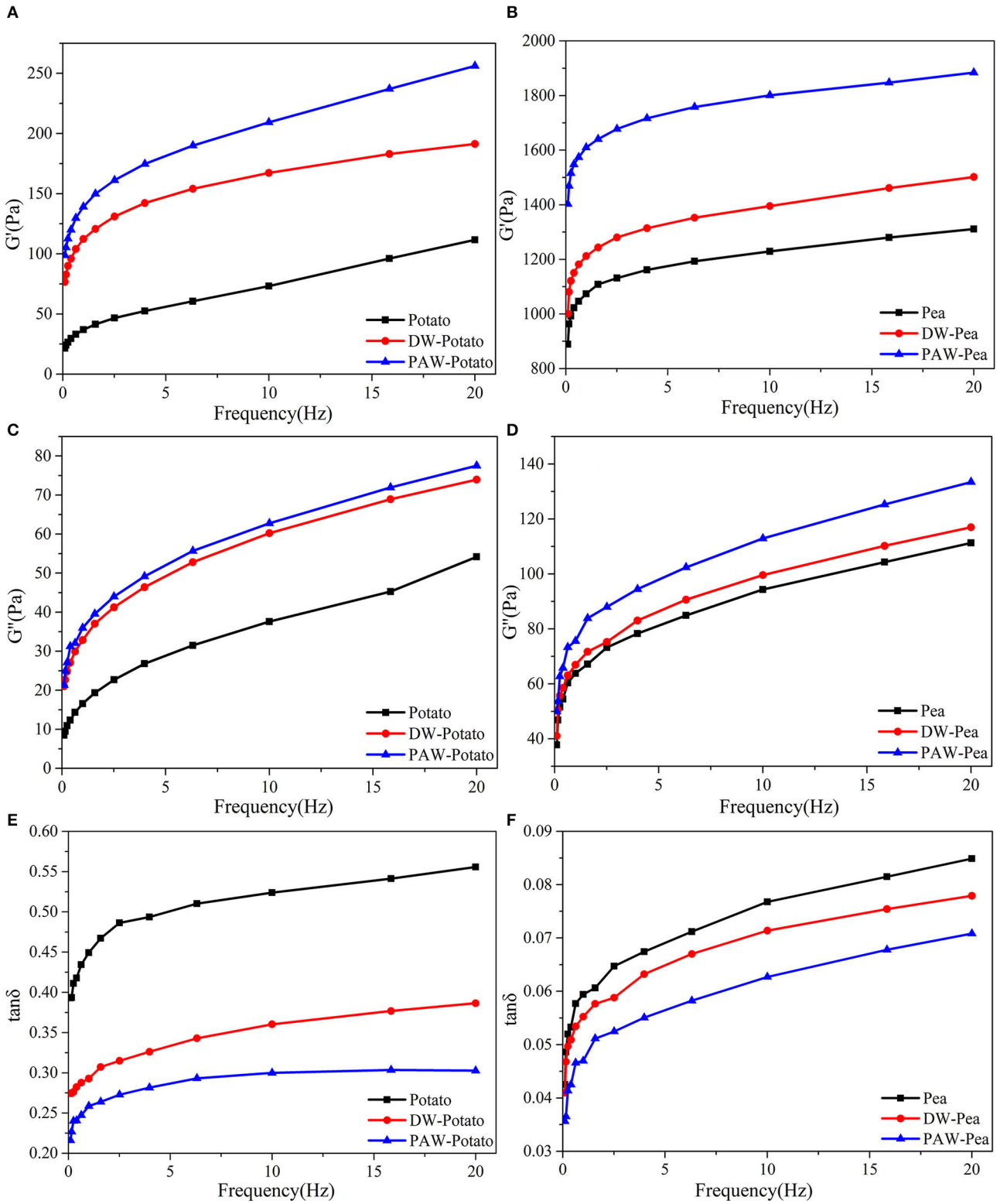

FIGURE 7 | Dynamic rheological curves of native and modified starches. **(A)** Storage modulus (G′) of native, DW-ANN treated, and PAW-ANN treated potato starch. **(B)** Storage modulus (G′) of native, DW-ANN treated, and PAW-ANN treated pea starch. **(C)** Loss modulus (G″) of native, DW-ANN treated, and PAW-ANN treated potato starch. **(D)** Loss modulus (G″) of native, DW-ANN treated, and PAW-ANN treated pea starch. **(E)** loss tangent (tan δ) of native, DW-ANN treated, and PAW-ANN treated potato starch. **(F)** Loss tangent (tan δ) of native, DW-ANN treated, and PAW-ANN treated pea starch.

indicators of potato starch. In addition, PAW-ANN resulted in the lowest peak viscosity and the highest gel strength of the paste for two starches. Although, the exact mechanism was not clear, an acidic component in PAW might be an important factor for starch modification according to previous studies and above experimental results. This research showed that PAW-ANN provided innovative insights and novel technologies for the production of new modified starches applied to starch-based hydrogels and food additives.

DATA AVAILABILITY STATEMENT

The original contributions presented in the study are included in the article/supplementary material, further inquiries can be directed to the corresponding author/s.

AUTHOR CONTRIBUTIONS

YY contributed to the conception, design, and funding of the study. BP, XJ, and YH organized the database. BP wrote the first draft of the manuscript. BN and MS contributed to writing-review and editing. All authors contributed to the article and approved the submitted version.

FUNDING

We are grateful to the National Natural Science Foundation of China (32101945), the Program for Science and Technology Innovation Talents in Universities of Henan Province (20HASTIT037), and the Henan Youth Talent Support Project (2020HYTP046).

REFERENCES

1. Fujita A. Starch. In: *Encyclopedia of Applied Plant Sciences, 2nd Edn.* Amsterdam: Academic Press; Elsevier (2017). p. 106–11.
2. Kaur M, Singh S. Influence of heat-moisture treatment (HMT) on physicochemical and functional properties of starches from different Indian oat (*Avena sativa* L.) cultivars. *Int J Biol Macromol.* (2019) 122:312–9. doi: 10.1016/j.ijbiomac.2018.10.197
3. Yadav BS, Guleria P, Yadav RB. Hydrothermal modification of indian water chestnut starch: influence of heat-moisture treatment and annealing on the physicochemical, gelatinization and pasting characteristics. *LWT Food Sci Technol.* (2013) 53:211–7. doi: 10.1016/j.lwt.2013.02.007
4. Zhang F, Zhang Y, Thakur K, Zhang J, Wei Z. Structural and physicochemical characteristics of lycoris starch treated with different physical methods. *Food Chem.* (2018) 275:8–14. doi: 10.1016/j.foodchem.2018.09.079
5. Guo B, Wang Y, Pang M, Wu J, Hu X, Huang Z, et al. Annealing treatment of amylose and amylopectin extracted from rice starch. *Int J Biol Macromol.* (2020) 164:3496–500. doi: 10.1016/j.ijbiomac.2020.08.245
6. Chung H, Liu Q, Hoover R. Impact of annealing and heat-moisture treatment on rapidly digestible, slowly digestible and resistant starch levels in native and gelatinized corn, pea and lentil starches. *Carbohydr Polym.* (2009) 75:436–47. doi: 10.1016/j.carbpol.2008.08.006
7. Thirumdas R, Kothakota A, Annapure U, Siliveru, K, Blundell R, et al. Plasma activated water (PAW): chemistry, physico-chemical properties, applications in food and agriculture. *Trends Food Sci Technol.* (2018) 77:21–31. doi: 10.1016/j.tifs.2018.05.007
8. Yan Y, Feng L, Shi M, Cui C, Liu Y. Effect of plasma-activated water on the structure and in vitro digestibility of waxy and normal maize starches during heat-moisture treatment. *Food Chem.* (2020) 306:125589. doi: 10.1016/j.foodchem.2019.125589
9. Wang S, Wang J, Wang S, Wang S. Annealing improves paste viscosity and stability of starch. *Food Hydrocoll.* (2017) 62:203–11. doi: 10.1016/j.foodhyd.2016.08.006
10. Adhikari B, Adhikari M, Ghimire B, Park G, Choi EH. Cold atmospheric plasma-activated water irrigation induces defense hormone and gene expression in tomato seedlings. *Sci Rep.* (2019) 9:16080. doi: 10.1038/s41598-019-52646-z
11. Piecyk M, Druzynska B, Oltarzewska A, Wolosiak R, Worobiej E, Ostrowska-Ligeza E. Effect of hydrothermal modifications on properties and digestibility of grass pea starch. *Int J Biol Macromol.* (2018) 118:2113–20. doi: 10.1016/j.ijbiomac.2018.07.063
12. Zhang B, Li X, Liu J, Xie F, Chen L. Supramolecular structure of A- and B-type granules of wheat starch. *Food Hydrocoll.* (2013) 31:68–73. doi: 10.1016/j.foodhyd.2012.10.006
13. Varatharajan V, Hoover R, Li J, Vasanthan T, Nantanga KKM, Seetharaman K, et al. Impact of structural changes due to heat-moisture treatment at different temperatures on the susceptibility of normal and waxy potato starches towards hydrolysis by porcine pancreatic alpha amylase. *Food Res Int.* (2011) 44:2594–606. doi: 10.1016/j.foodres.2011.04.050
14. Witt T, Doutch J, Gilbert EP, Gilbert RG. Relations between molecular, crystalline, and lamellar structures of amylopectin. *Biomacromolecules.* (2012) 13:4273–82. doi: 10.1021/bm301586x
15. Nakazawa Y, Wang Y. Acid hydrolysis of native and annealed starches and branch-structure of their naegeli dextrins. *Carbohydr Res.* (2003) 338:2871–82. doi: 10.1016/j.carres.2003.09.005
16. Shi M, Zhang Z, Yu S, Wang K, Gilbert RG, Gao Q. Pea starch (*Pisum sativum* L.) with slow digestion property produced using beta-amylase and transglucosidase. *Food Chem.* (2014) 164:317–23. doi: 10.1016/j.foodchem.2014.05.045
17. Lorenz K, Collins F, Kulp K. Steeping of starch at various temperatures-effects on functional properties. *Starch.* (1980) 32:181–6. doi: 10.1002/star.19800320602
18. Zhang H, Hou H, Liu P, Wang W, Dong H. Effects of acid hydrolysis on the physicochemical properties of pea starch and its film forming capacity. *Food Hydrocoll.* (2019) 87:173–9. doi: 10.1016/j.foodhyd.2018.08.009
19. Capron I, Robert P, Colonna P, Brogly M, Planchot V. Starch in rubbery and glassy states by FTIR spectroscopy. *Carbohydr Polym.* (2007) 68:249–59. doi: 10.1016/j.carbpol.2006.12.015
20. Zhang B, Wu C, Li H, Hu X, Jin Z, Tian Y, et al. Long-term annealing of C-type kudzu starch: effect on crystalline type and other physicochemical properties. *Starch Stärke.* (2015) 67:577–84. doi: 10.1002/star.201500003
21. Bahrani SA, Loisel C, Rezzoug SA, Cohendoz S, Buleon A, Maache-Rezzoug Z. Physicochemical and crystalline properties of standard maize starch hydrothermally treated by direct steaming. *Carbohydr Polym.* (2017) 157:380–90. doi: 10.1016/j.carbpol.2016.10.009
22. Chung KM, Moon TW, Chun JK. Influence of annealing on gel properties of mung bean starch. *Cereal Chem.* (2000) 77:567–71. doi: 10.1094/CCHEM.2000.77.5.567
23. Wang L, Wang Y. Structures and physicochemical properties of acid-thinned corn, potato and rice starches. *Starch Stärke.* (2001) 53:570–6. doi: 10.1002/1521-379X(200111)53:11<570::AID-STAR570>3.0.CO;2-S
24. Sasaki T, Yasui I, Matsuki J, Satake T. Comparison of physical properties of wheat starch gels with different amylose content. *Cereal Chem.* (2002) 79:861–6. doi: 10.1094/CCHEM.2002.79.6.861
25. Lan H, Hoover R, Jayakody L, Liu Q, Donner E, Baga M, et al. Impact of annealing on the molecular structure and physicochemical properties of normal, waxy and high amylose bread wheat starches. *Food Chem.* (2008) 111:663–75. doi: 10.1016/j.foodchem.2008.04.055
26. Zambelli RA, Galvao A, de Mendonca LG, Leao MVD, Carneiro SV, Lima ACS, et al. Effect of different levels of acetic, citric and lactic acid in the cassava

starch modification on physical, rheological, thermal and microstructural properties. *Food Sci Technol Res.* (2018) 24:747–54. doi: 10.3136/fstr.24.747
27. Sudheesh C, Sunooj KV, Sinha SK, George J, Kumar S, Murugesan P, et al. Impact of energetic neutral nitrogen atoms created by glow discharge air plasma on the physico-chemical and rheological properties of kithul starch. *Food Chem.* (2019) 294:194–202. doi: 10.1016/j.foodchem.2019.05.067
28. Chen L, Tian Y, Bai Y, Wang J, Jiao A, Jin Z. Effect of frying on the pasting and rheological properties of normal maize starch. *Food Hydrocoll.* (2018) 77:85–95. doi: 10.1016/j.foodhyd.2017.09.024
29. Meriem-Benziane M, Abdul-Wahab SA, Benaicha M, Belhadri M. Investigating the rheological properties of light crude oil and the characteristics of its emulsions in order to improve pipeline flow. *Fuel.* (2012) 95:97–107. doi: 10.1016/j.fuel.2011.10.007
30. Sudheesh C, Sunooj KV, Anjali KU, Aaliya B, Navaf M, Kumar S, et al. Effect of lysine incorporation, annealing and heat moisture treatment alone and in combination on the physico-chemical, retrogradation, rheological properties and in vitro digestibility of kithul (*Caryota urens* L.) starch. *Int J Food Sci Technol.* (2020) 55:2391–8. doi: 10.1111/ijfs.14488

Conflict of Interest: The authors declare that the research was conducted in the absence of any commercial or financial relationships that could be construed as a potential conflict of interest.

frontiers in Nutrition

ORIGINAL RESEARCH
published: 18 March 2022
doi: 10.3389/fnut.2022.853442

From Fish Scale Gelatin to Tyrosinase Inhibitor: A Novel Peptides Screening Approach Application

Zi-Zi Hu[1], *Xiao-Mei Sha*[1]*, *Lu Zhang*[1], *Min-Jun Zha*[1] and *Zong-Cai Tu*[1,2]*

[1] National R&D Center for Freshwater Fish Processing, College of Chemistry and Chemical Engineering & College of Life Science, Jiangxi Normal University, Nanchang, China, [2] State Key Laboratory of Food Science and Technology, Nanchang University, Nanchang, China

Bioaffinity ultrafiltration combined with LC-Orbitrap-MS/MS was applied for the first time to achieve rapid screening and identification of tyrosinase inhibitory peptides (TYIPs) from grass carp scale gelatin hydrolysates. The binding mode of TYIPs with tyrosinase was investigated by molecular docking technology. The whitening effect of TYIPs was further studied by evaluating the tyrosinase activity and melanin content in mouse B16F10 cells. Four new TYIPs were screened from hydrolysates, among which DLGFLARGF showed the strongest tyrosinase inhibition with an IC_{50} value of 3.09 mM. Molecular docking showed that hydrogen bonds were the main driving force in the interaction between the peptide DLGFLARGF and tyrosinase. The addition of DLGFLARGF significantly inhibited the tyrosinase activity and melanin production of B16F10 melanoma cells. These results suggest that DLGFLARGF is a promising skin whitening agent for the treatment of potential pigment-related diseases.

Keywords: grass carp scale gelatin, tyrosinase inhibitory peptides, bioaffinity ultrafiltration, LC-Orbitrap-MS/MS, whitening

OPEN ACCESS

Edited by:
Qiang Xia,
Ningbo University, China

Reviewed by:
Hongshun Yang,
National University of Singapore, Singapore
Liqiang Zou,
Nanchang University, China

***Correspondence:**
Xiao-Mei Sha
shaxiaomei1987@sina.com
Zong-Cai Tu
004756@jxnu.edu.cn

Specialty section:
This article was submitted to Food Chemistry, a section of the journal Frontiers in Nutrition

Received: *12 January 2022*
Accepted: *07 February 2022*
Published: *18 March 2022*

Citation:
Hu Z-Z, Sha X-M, Zhang L, Zha M-J and Tu Z-C (2022) From Fish Scale Gelatin to Tyrosinase Inhibitor: A Novel Peptides Screening Approach Application. Front. Nutr. 9:853442. doi: 10.3389/fnut.2022.853442

INTRODUCTION

Gelatin has a rich sources and is widely used in the food and medicine industries (1–5). The hydrolysis product of gelatin is collagen peptide, which is a mixture of peptides. After separation and purification, specific bioactive peptides could be obtained that have a wide range of significant functional activities. At present, the functional activities of collagen peptides such as antioxidant activity (6), angiotensin-converting enzyme inhibition activity (7), anti-tumor activity (8), and antibacterial activity (9) have been studied. Recent studies have shown that many active peptides contain some hydrophobic amino acids, uncharged polar amino acids, aromatic amino acids, etc., which have the ability to inhibit the production of melanin (10, 11).

The production of melanin is regulated by enzymes such as tyrosinase, tyrosinase-binding protein-1 (dopa pigment isomerase), and tyrosinase-binding protein-2 (melanin precursor oxidase) (12). Tyrosinase (EC1.14.18.1) is a multifunctional enzyme with three histidine (His) residues and two Cu ions in the active center, which is widely found in fungi, plants and animals. Tyrosinase oxidizes tyrosine to produce dopamine and then continues to oxidize dopamine to produce dopamine quinone. Dopamine quinone is a very active molecule that can generate a polymer complex or brownish pigment when it reacts with amino acids or proteins, finally producing melanin (13). Substances with tyrosinase inhibition activity are commonly found in whitening foods. At present, tyrosinase inhibitors widely used in foods have been reported, including arbutin,

kojic acid, oxidative resveratrol, etc. (14). However, studies have shown that these substances show limiting effects and certain side effects, including the lack of good permeability, high toxicity and poor stability (15). Scientists have recently become interested in the tyrosinase inhibitory activity of extracts from natural sources, due to the benefits of mild functional activity, simple absorption, and excellent skin compatibility (16–18). Active polypeptide is composed of 2–20 amino acids, which has the above advantages that could provide the possibility for its application in foods (19).

The conventional procedures for screening active peptides from complex protein hydrolysates include the preparation of hydrolysates, bioassay-guided separation, purification and peptide sequence identification. In general, traditional methods require multi-step extraction and separation with organic solvents, resulting in low efficiency, serious environmental pollution, time-consuming and laborious (20, 21). The combination of bioaffinity ultrafiltration and liquid chromatography-mass spectrometry based on the interaction between small molecule ligands and enzyme active sites is an effective approach for a powerful approach for identifying biologically active compounds from complex mixtures (22). It has been widely used to screen and identify a variety of biologically active compounds from natural extracts and traditional Chinese medicine (23). Qin et al. (24) established a bioaffinity ultrafiltration-high performance liquid chromatography-electrospray ionization-time of flight-mass spectrometry (BAUF-HPLC-ESI-TOF/MS) method to identify potential new bioactive substances. This method has been demonstrated to be a quick way to obtain high-purity, high-activity bioactive substances. However, there is no report about screening tyrosinase inhibitor peptides by this method.

In this paper, a rapid screening and identification method for the tyrosinase inhibitory peptides (TYIPs) in the hydrolysis of fish scale (by-products during freshwater fish production) gelatin was established for the first time based on ultrafiltration and Nano-LC-Orbitrap-MS/MS. Then, molecular docking was used to determine the interaction of the identified peptide with tyrosinase in order to investigate the biological activity and mechanism. Finally, the effect of peptides on B16F10's ability to produce melanin was further studied.

MATERIALS AND METHODS

Materials

Grass carp scale gelatin was obtained from the laboratory. Alcalase (≥200,000 units/g) was purchased from Solarbio Chemical Co. (Shanghai, China). Mushroom tyrosinase (6,680 U/mg) and 3,4-dihydroxyphenylalanine (L-DOPA) were purchased from Sigma-Aldrich (St. Louis, MO, USA). The murine melanoma B16F10 cells (CL0039) were acquired from Fenghui Biological Technology Co., Ltd. (Hunan, China). All the other reagents were analytical grade.

Preparation of TYIPs From Fish Scale Gelatin

The grass carp scale gelatin was prepared according to the method of Sha et al. (25). According to previous experiments, the optimal enzymatic hydrolysis conditions for preparing TYIPs were: substrate concentration of 125 mg/ml, alcalase dosage of 1%, pH 9.0, enzymatic hydrolysis temperature of 60°C, and enzymatic hydrolysis time of 2 h.

Analysis of the Tyrosinase Inhibitory Activity

The determination of the tyrosinase inhibitory activity was made according to Uysal et al. (26). Sample solutions (50 μl) with the appropriate concentration were reacted with 50 μl of 200 mM pH 6.8 phosphate buffer saline (PBS) solution and 50 μl of tyrosinase at room temperature for 15 mins. Then, 50 μl of 2.5 mM L-DOPA was added, and allowed to react at 30°C for 10 min. The absorbance (As) at 475 nm was finally measured with a microplate reader (Synergy H1, BioTek Co., Ltd., USA). Taking the reaction system without enzyme and sample as a blank. Kojic acid (2 mg/ml) used as the positive control, and the rate of tyrosinase inhibition could be calculated using the following equation:

$$Tyrosinase\ inhibition\ rate/\% = \frac{(A_c - A_b) - (A_s - A_b)}{(A_c - A_b)} \times 100\% \quad (1)$$

where, As is the absorbance of the sample after reaction; Ac is the absorbance of the reaction system with distilled water instead of the sample; Ab is the absorbance of the reaction system with distilled water instead of tyrosinase.

Analysis of the Amino Acid Composition

The amino acid composition was determined based on the report of Chen et al. (27) with appropriate modifications. The samples were hydrolyzed with 6 M HCl at 110°C for 24 h prior to composition analysis with a High-Speed Amino Acid Analyzer Model L-8900 (Hitachi Co., Japan).

Analysis of Molecular Weight Distribution

The molecular weight (MW) distribution was determined using an Agilent 1260 Infinity HPLC system (Agilent Technologies, Inc., Santa Clara, CA, USA) equipped with a waters XBridge Protein BEH 125Å SEC (3.5 μm, 7.8 × 300 mm) (28). Hydrolysates were eluted with water (0.1% FA) and acetonitrile (60:40, V/V) at a flow rate of 0.4 ml/min. The injection volume was 10 μl. The detection wavelength was 220 nm (28). The MW of peptides was calculated based on the calibration curve constructed with cytochrome C (12,384 Da), aprotinin (6,511.51 Da), bacitracin (1,422.69 Da), L-oxidized glutathione (612.63 Da) and hydroxyproline (131.13 Da).

Rapid Screening of TYIPs

Bioaffinity Ultrafiltration

The screening method was slightly modified based on the previous report (22). The inhibitory activity of tyrosinase was evaluated at 1–6 mg/ml to obtain the best binding concentration.

4 ml of hydrolysis product (5 mg/ml) and 2 ml of mushroom tyrosinase (10 U/ml) were incubated for 1 h at 37°C. Inactivated mushroom tyrosinase (heated in a

boiling water bath for 10 mins) was also prepared as a blank group. The detailed method is shown in **Figure 2A**. Filtrates, including peptides binding active tyrosinase (PAT) and peptides binding inactive tyrosinase (PIT), were collected and freeze-dried for tyrosinase inhibition evaluation and peptide identification.

Peptide Identification

The amino acid sequence of the components obtained in 2.6.1 was determined by Nano-LC-ESI-Q-Orbitrap-MS/MS. Peptides were separated on an AcclaimR PepMap RSLC (50 μm ×150 mm, C18, 2 μm, 100 Å) column at a flow rate of 220 nl/min. Mobile phase A and B was consisted of 0.1% formic acid aqueous solution and 0.1% acetonitrile solution, respectively. Gradient elution conditions were as follows: 0–2 min, 4–12% B; 2–25 min, 12–22% B; 25–32 min, 22–32% B; 32–37 min, 32–75% B; 37–40 min, 75% B (isoelution). The positive ion scanning mode was adopted, and the mass spectrometry data were collected using Xcalibur 2.2 SP1 software, with a mass range of 250–1,250 m/z and a resolution of 70,000. The top 20 peptides were selected for fragmentation according to the signal strength of the first mass spectrometry, and the fragmentation mode was HCD with an energy of 27%. The parent ion map was analyzed by Xcalibur software and De Novo was sequenced using PEAKS Studio 7.0 software to obtain the amino acid sequence of peptides. The peptides identified in this paper met the requirements of false discovery rate (FDR) $\leq$ 5% and average local confidence score (ALC) $\geq$ 95%.

Molecular Docking and Peptides Synthesis

The X-ray crystal structure of Agaricus bisporus tyrosinase (2Y9W) was downloaded from the Protein Data Bank (https://www.rcsb.org/structure/2Y9W) (29), and three-dimensional (3D) structure of TYIPs segment were obtained by ChemBio 3D Ultra 14.0. Based on the 3D crystal structure of tyrosinase, the computer-aided technology was used to analyze the action mode and site of peptide segment with tyrosinase, and to clarify the action mechanism. The specific docking process was as follows: first, the AutoDock tool is used to remove water molecules from tyrosinase and add Gasteiger charges and hydrogen atoms to tyrosinase molecules. Then, the AutoDock tool was used again to dock ligand small molecules (peptides) with tyrosinase. The docking process and calculation were carried out according to default parameters. The coordinates of the docking center of the peptide with tyrosinase were (64, 70, 116). Results were obtained based on the lowest free energy.

Cell Culture

B16F10 cells were kept in Dulbecco's modified eagle medium supplemented with 10% heat-inactivated fetal bovine serum, and cells were cultured at 37°C in an atmosphere with 5% CO_2. These cells were then used for cell viability, tyrosinase inhibition and melanin content determination.

Determination of the Cell Viabilities of B16F10 Melanoma Cells

The previously described cell counting kit-8 (CCK-8) assay was used to assess cell viability (30). The cells were incubated in a 96-well plate with 5×10^4 cells per well in a 5% humid CO_2 atmosphere at 37°C for 24 h. DLGFLARGF was added to the cells at concentrations of 0, 0.1, 0.2, 0.4, 0.8 and 1.6 mg/ml, while 0.75 mg/ml of kojic acid was used as a positive control. The cells were re-incubated for 24 h under the same conditions. The cells were then treated with the CCK-8 reagent and incubated at 37°C for 1 h. Cell viability is calculated by reading the absorbance value at 450 nm. The calculation formula is shown below.

$$Cell\ viability/\% = \frac{(A_s - A_b)}{(A_c - A_b)} \times 100\% \quad (2)$$

where, As is the absorbance of experimental wells (medium containing cells, CCK-8, sample to be tested); Ac is the absorbance of control well (medium containing cells, CCK-8, no sample to be tested); Ab is the absorbance of blank wells (medium without cells and samples to be tested, CCK-8).

Determination of Tyrosinase Activity in B16F10

The tyrosinase inhibition was determined according to the method of Ullah et al. (31). B16F10 cells were seeded into 96-well plates at a rate of 5×10^4 cells per well and incubated at 37°C in a humid atmosphere of 5% CO_2 for 24 h. The cells were then treated with kojic acid (0.75 mg/ml) and DLGFLARGF (0, 0.1, 0.2, 0.4, 0.8 and 1.6 mg/ml), and re-incubated for 24 h under the same conditions. The cells were then washed with PBS buffer, lysed with lysate buffer [100 μl containing 50 mM PBS, 0.1 mM phenylmethanesulfonyl fluoride (5 μl) and Triton X-100 (5 μl)], and frozen at −80°C for 30 min. The cell lysate was then centrifuged at 12,000 rpm at 4°C for 30 min and transferred to a 96-well plate with a total volume of 100 μl (80 μl lysate supernatant and 20 μl 10 mM L-DOPA) and incubated for 30 min at 37°C. The absorbance was measured at 450 nm using an enzyme-linked immunosorbent assay (ELISA) reader.

Determination of Melanin Content in B16F10

After cultivated according to the instructions above, the cells were digested with 0.25% trypsin when reached to 80–90% confluence to make a single cell suspension. Fresh culture medium was used to adjust the cell concentration to 1×10^6 cells/ml, 2 ml of which was inoculated in a 6-well culture plate for incubation overnight. When the cells adhered, the supernatant was discarded and the cells were rinsed with PBS once. 2 ml fresh culture medium was added again for incubation under CO_2 for 48 h. The supernatant was discarded after the incubation, and the adhered cells were rinsed with PBS and then dispersed with trypsin. The dispersed cells were collected and centrifuged at 1,500 r/min for 10 min. The precipitation was added with

1 ml NaOH (1 mol/L) containing 10% dimethyl sulfoxide for 1 h water bath at 80°C before being transferred to a 96-well culture plate. Measured the optical density value of each well at 405 nm with a microplate reader, and calculated the melanin content (32).

$$Melanin\ content/\% = \frac{(A_s - A_b)}{(A_c - A_b)} \times 100\% \quad (3)$$

TABLE 1 | Amino acid composition of fish scale gelatin hydrolysate.

Amino acid	Content (g per 100 g)	Amino acid	Content (g per 100 g)
Asp	4.58 ± 0.16	Ile*	1.03 ± 0.02
Thr	2.00 ± 0.05	Leu*	2.60 ± 0.08
Ser	2.49 ± 0.05	Tyr	0.41 ± 0.05
Glu	7.82 ± 0.16	Phe*	1.53 ± 0.03
Gly	16.71 ± 0.03	Lys	2.83 ± 0.03
Ala*	5.58 ± 0.04	His	0.26 ± 0.01
Cys	0.05 ± 0.01	Arg	6.74 ± 0.01
Val*	1.83 ± 0.04	Pro*	9.43 ± 0.07
Met*	1.24 ± 0.07		

Hydrophobic amino acid.

TABLE 2 | Molecular weight distribution of fish scale gelatin hydrolysate.

Component	Molecular weight range (Da)	Retention time (min)	Relative content (%)	Peak molecular weight (Da)
I	9,217–4,642	14.05–15.64	9.75	4,974
II	4,642–3,358	15.64–16.39	8.80	4,044
III	3,358–1,992	16.39–17.60	17.05	2,560
IV	1,992–904	17.60–19.43	29.65	1,441
V	904–503	19.43–20.67	10.51	568
VI	503–180	20.67–23.17	16.12	452

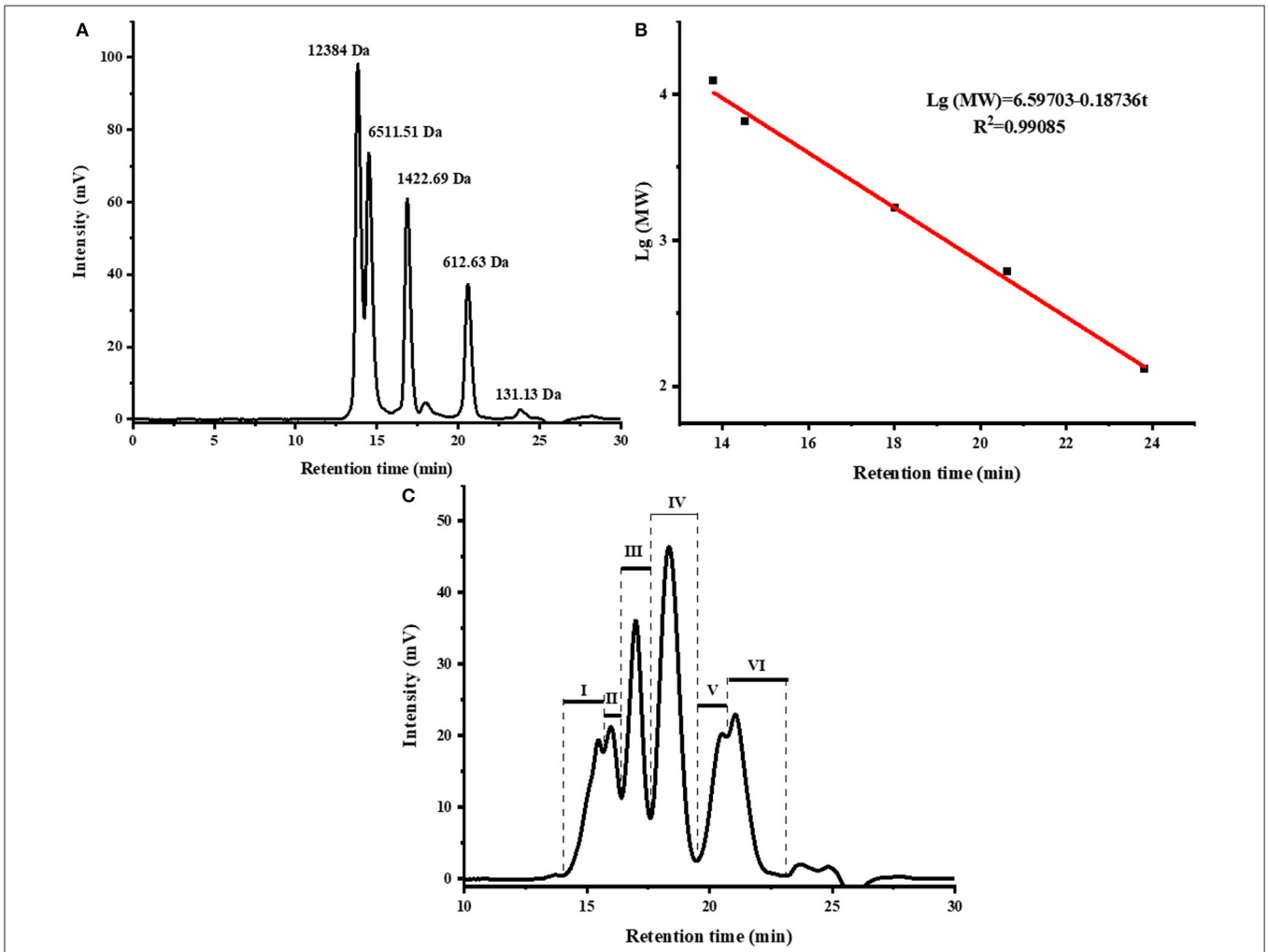

FIGURE 1 | The size exclusion chromatogram of standards **(A)**, molecular weight distribution curve of standards **(B)**, and the size exclusion chromatogram of fish scale gelatin hydrolysates, I, II, III, IV, V, VI represent the different components obtained **(C)**.

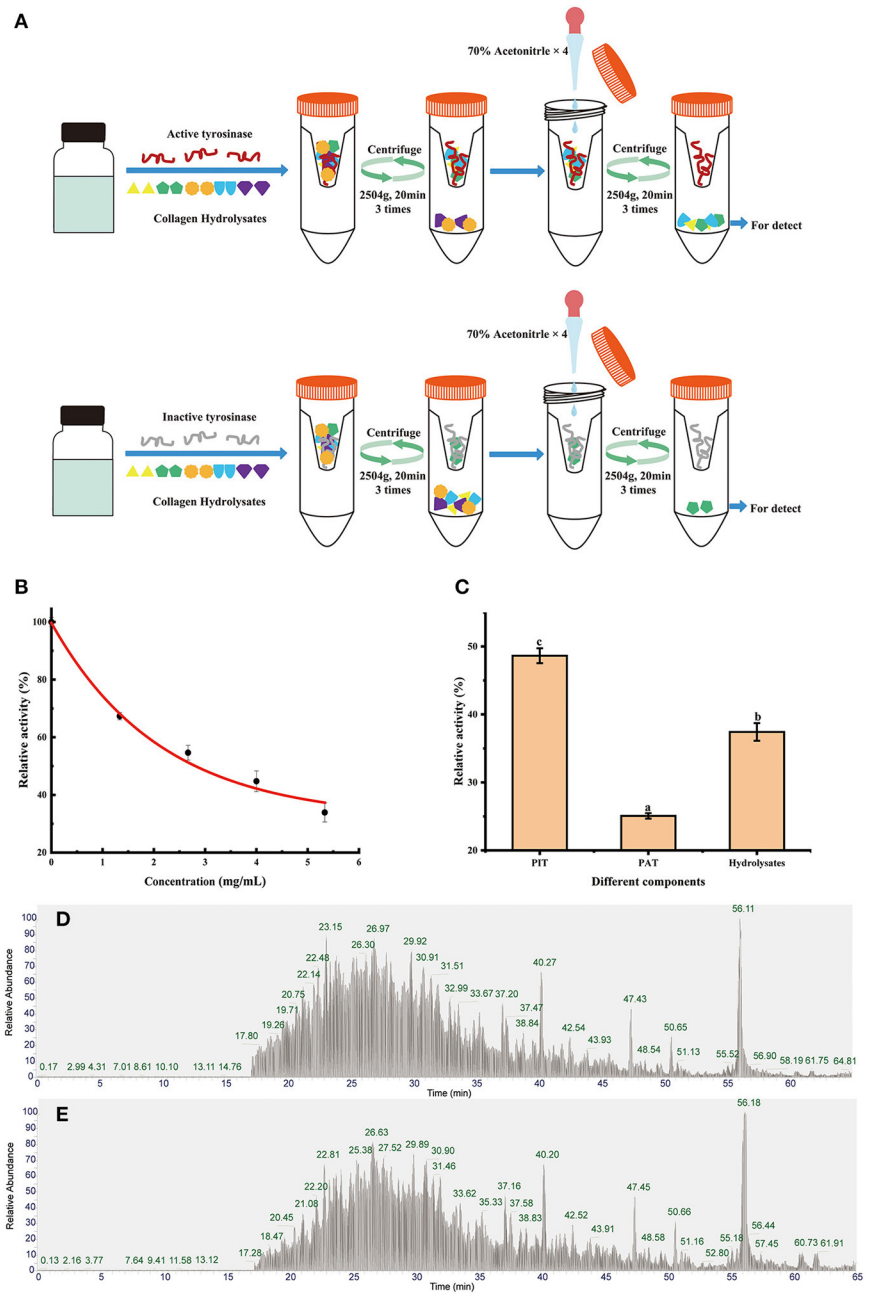

FIGURE 2 | Diagrams of biological affinity ultrafiltration—liquid mass spectrometry screening methods **(A)**, the tyrosinase activity of hydrolysates **(B)**, ultrafiltration fractions **(C)**, the total ion chromatography (TIC) of PAT **(D)**, and PIT **(E)**. Different lowercase letters represent significant differences between different groups ($p < 0.05$).

where, As is the absorbance of experimental wells; Ac is the absorbance of control well; Ab is the absorbance of blank wells.

Statistical Analysis

In each analysis, three parallel tests were performed. The results were presented in the form of mean ± standard deviation (SD). SPSS Statistics 20 software (IBM, Armonk, NY, USA) was used to perform one-way analysis of variance (ANOVA, $P < 0.05$) and Duncan's multiple range test to analyze the differences between samples.

RESULTS AND DISCUSSION

Amino Acid Composition and Molecular Weight Distribution of Hydrolysates

The amino acid composition of hydrolysates was shown in **Table 1** and the total amount of amino acids was 67.12 g in 100 g hydrolysates. Many amino acid residues in collagen peptides are associated to tyrosinase inhibitory activity, according to the structure-activity relationship investigation between the peptide chain and melanin production inhibition (10, 33, 34).

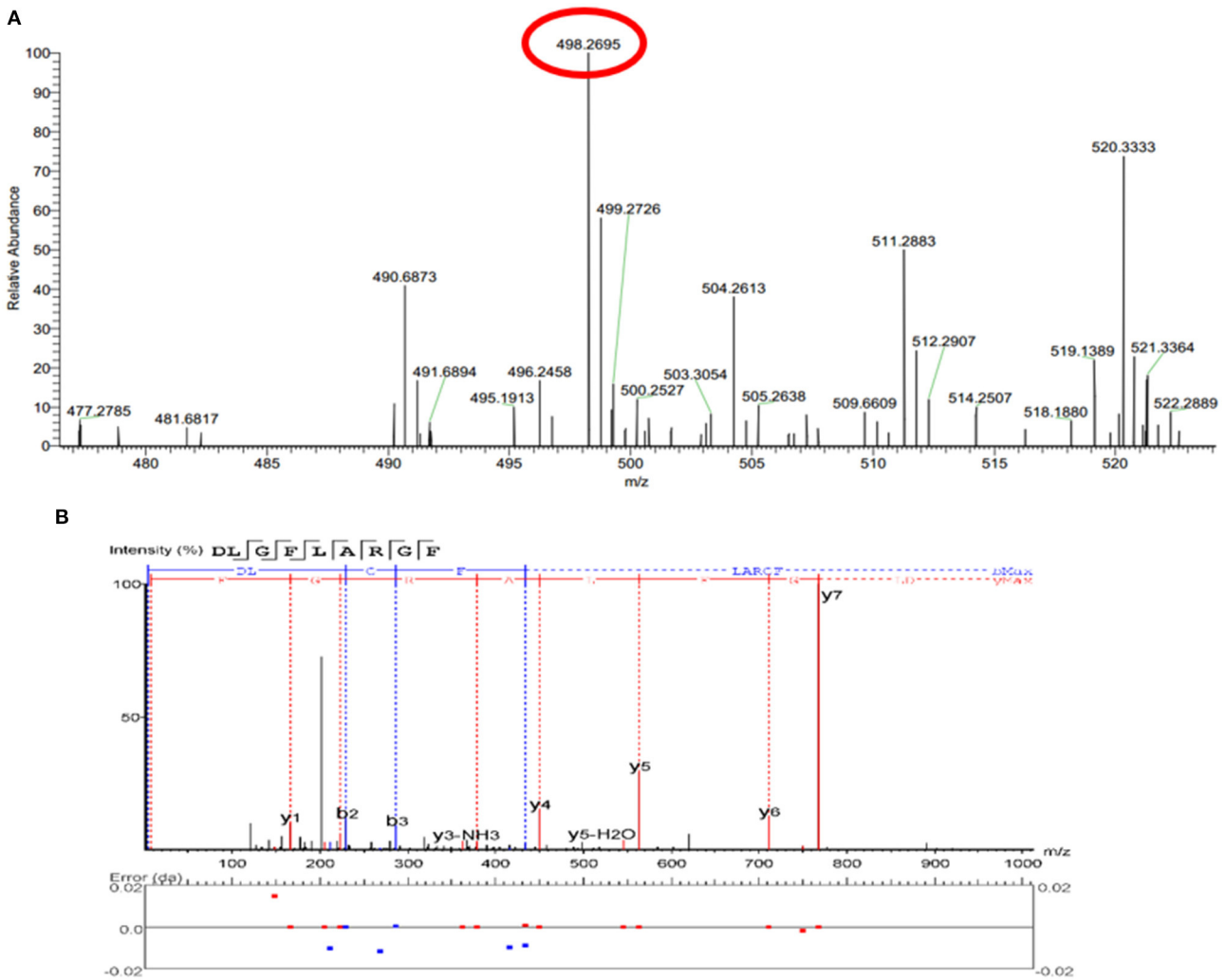

FIGURE 3 | The full MS scan spectrum **(A)** and the full MS/MS spectrum **(B)** of DLGFLARGF.

Val (V), Ala (A), Leu (L) and Ile (I) are four aliphatic hydrophobic amino acids that can directly interact with enzymes to inhibit the formation of dopaquinone, hence inhibiting melanin production, and have an additive effect. As shown in **Table 1**, the total amount of these four amino acids was 11.04 g/100 g hydrolysates, accounting for 16.45% of the total amino acid content. Arg (R) residues enhance cell penetration and facilitate the interaction between peptides and tyrosinase; Phe (F) is similar in structure to Tyr (Y) (the natural substrate of tyrosinase), which facilitates the binding of peptides and enzymes (10). The contents of these two amino acids were 6.74 g/100 g and 1.53 g/100 g in hydrolysates, respectively. Cys (C), Ser (S) and Thr (T) can form a complex with the enzymatic reaction product (dopaquinone) to prevent the conversion of dopaquinone into melanin, instead of inhibiting enzyme activity. The total amount of these three amino acids was 4.54 g/100 g in hydrolysates. Asp (D) and Glu (E) are negatively charged amino acid residues, which are not conducive to binding to tyrosinase. The total amount of these two amino acids was 12.40 g/100 g hydrolysates, accounting for 18.47% of the total amino acid. From what has been discussed above, the content of amino acids beneficial to inhibiting melanin was up to 35.44%. These results suggested that hydrolysates may have strong tyrosinase inhibitory activity.

The MW distribution reflects the hydrolysis degree of fish scale gelatin (35). Peptides with different MW have different tyrosinase inhibition abilities (36). As shown in **Figure 1** and **Table 2**, there were mainly six peaks (I-VI), indicating that the hydrolysate contained six components, and the MW distribution of components I, II, III, IV, V and VI were 9,217–4,642 Da, 4,642–3,358 Da, 3,358–1,992 Da, 1,992–904 Da, 904–503 Da and 503–180 Da, respectively. The MW of the hydrolysates were mainly concentrated in components III, IV, V and VI, whose relative contents were 17.05, 29.65, 10.51, and 16.12%, accounting for more than 73% of the total contents. In addition, the MW of hydrolysates was mainly concentrated below 1,992 Da, accounting for 56.28% of proteolytic products. Alcalase is a non-specific protease that can cleave many sites in a protein at

TABLE 3 | Identification of peptides unique to PAT by LC–ESI–Q–Orbitrap–MS/MS.

No.	Peptide	RT (min)	Length	ALC (%)	m/z	Mass	Local confidence (%)
1	PGPVGVKL	27.98	8	99	383.7446	765.4749	99 100 100 100 100 100 100 100
2	LDALNENK	20.2	8	99	458.7404	915.4661	100 100 100 99 98 99 98 100
3	VPGPM	25.62	5	98	500.2538	499.2465	99 99 100 99 98
4	GPVGSF	29.02	6	98	563.2829	562.2751	97 98 99 99 100 100
5	TGPLGL	34.4	6	98	557.3301	556.322	97 98 99 99 99 100
6	FDLGFLAR*	42.62	8	98	469.7591	937.5021	99 99 99 98 98 97 97 99
7	FSGM	24.61	4	97	441.1804	440.1729	96 96 100 99
8	WSVEF*	45.45	5	97	667.3090	666.3013	93 95 100 100 100
9	GEPGLLGM	42.87	8	97	773.3893	772.3789	89 95 97 98 99 100 99 100
10	GPPGLGQR	20.59	8	96	391.2201	780.4242	99 99 100 98 97 94 90 95
11	WQLTL*	47.88	5	96	660.3729	659.3643	97 94 99 96 95
12	EAPDPF	50.31	6	95	675.3026	674.2911	96 94 97 98 92 96
13	LVGPAGPTQR	21.96	10	95	498.2855	994.5560	100 100 100 100 99 99 91 86 85 93
14	DAPGLLRGF	35.7	9	95	473.2618	944.5079	79 88 100 100 100 99 97 95 99
15	DLGFLARGF*	45.92	9	95	498.2695	994.5236	81 82 99 100 100 99 98 99 99
16	GFTGM	28.03	5	95	512.2175	511.2101	90 92 98 99 97

*The above refers to the molecular mass less than or equal to 1,000 Da. The proportion of amino acids that are marked with * means that the contribution of tyrosinase inhibition is greater than or equal to 0.6.*

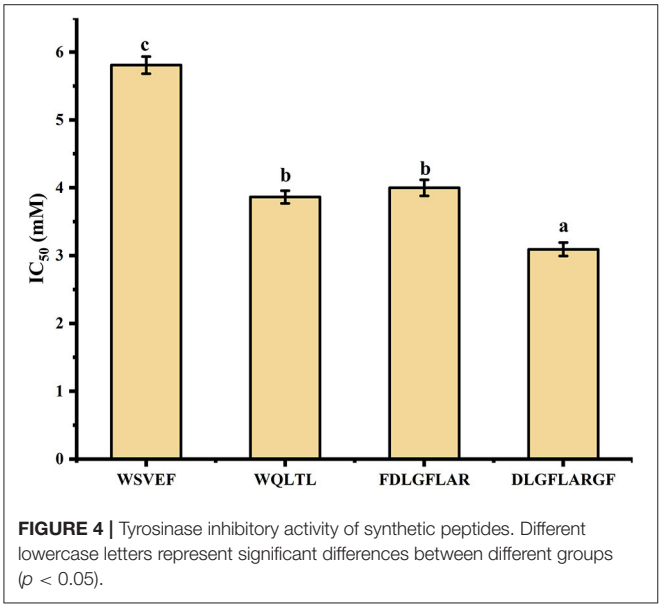

FIGURE 4 | Tyrosinase inhibitory activity of synthetic peptides. Different lowercase letters represent significant differences between different groups ($p < 0.05$).

random and generate a higher number of low MW peptides (37), which are attractive for higher biofunctional activity (38).

Enrichment and Identification of Potential TYIPs

Appropriate concentration and ratio are required in order to achieve a saturated state of binding. **Figure 2B** shows the tyrosinase activity residual rate of hydrolysates with different concentrations. Significant dose-dependence was observed in the concentration range of 0–5.33 mg/ml, which indicated that most of the active sites of tyrosinase can be bound by peptides. However, the inhibitory effect per milligram of inhibitor decreased as the hydrolysates concentration increased. In order to retain an ideal tyrosinase inhibitory activity, the concentration of hydrolysates was set at 5 mg/ml with tyrosinase inhibitory activity rate at 61.7% for screening.

After bioaffinity ultrafiltration, tyrosinase inhibitions of PAT and PIT were evaluated. The results are shown in **Figure 2C**. The inhibition rate of tyrosinase on PAT was 74.92%, while the corresponding inhibition rates of PIT and hydrolysates were 51.37 and 62.58%, respectively. This suggests that certain peptides in the hydrolysates can specifically bind to the active site of tyrosinase and can be enriched effectively by bioaffinity ultrafiltration, resulting in a higher inhibition of PAT than PIT and hydrolysates.

The peptide composition in PAT and PIT was identified by Nano-LC-Q-Orbitrap-MS/MS to screen potential TYIPs. The total ion chromatograms were shown in **Figures 2D,E**. By matching the b and y series ions detected in the MS/MS spectrum with that recorded in database (uniprot-taxonomy Anabantaria 201912), the exact amino acid sequence of each peptide can be drawn. For example, peptide 9 (**Figure 3A**) has MS ion 498.2695^{2+}, b series of b2 (229.1183^{2+}), b3 (286.1397^{2+}) and b4 (433.2082^{2+}), y1 (166.0863^{2+}), y2 (223.1077^{2+}), y3 (379.2088^{2+}), y4 (450.2459^{2+}), y5 (563.3300^{2+}), y6 (710.3984^{2+}) and y7 (767.4199^{2+}), and the sequence was identified as DLGFLARGF (**Figure 3B**). By this method, 52 of the peptides identified in PAT were not found in PIT. Inhibitors can bind specifically to the active site of tyrosinase and be released by acetonitrile (39), which confirmed the high selectivity of bioaffinity ultrafiltration. Therefore, these specific peptides in PAT are considered as potential TYIPs.

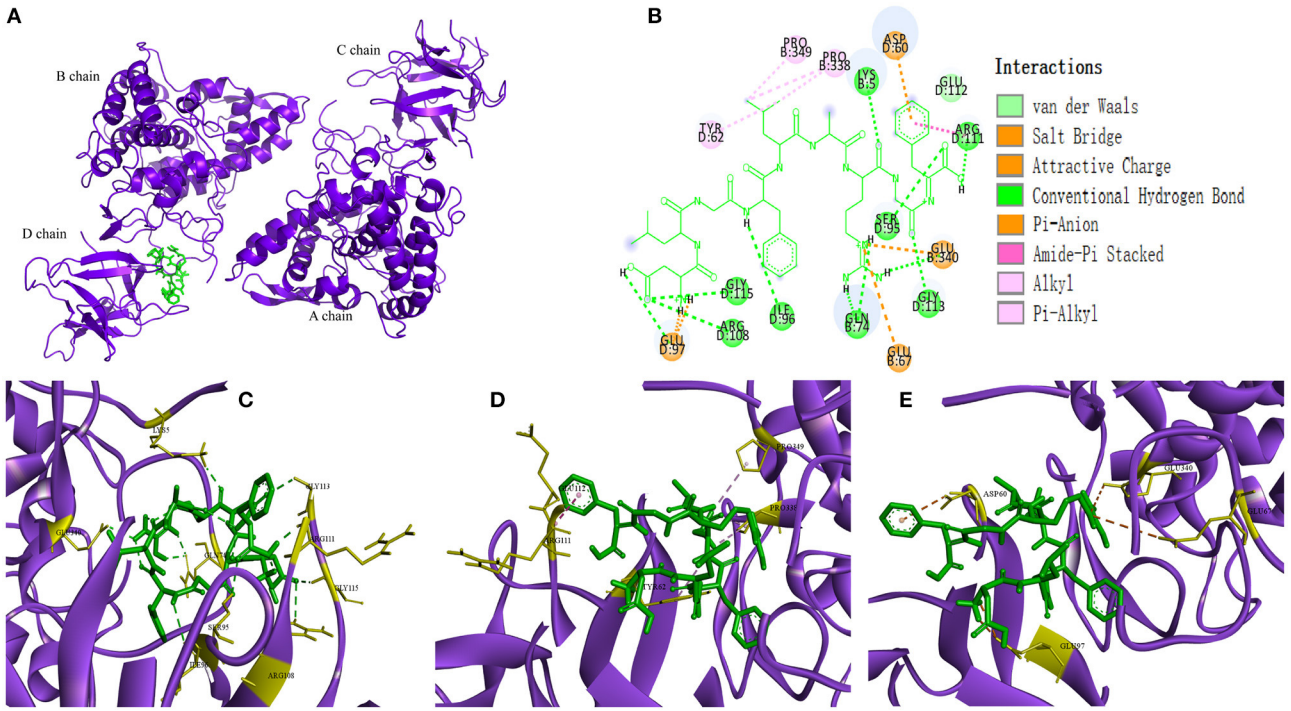

FIGURE 5 | Predicted binding mode of DLGFLARGF and tyrosinase **(A,B)**. Hydrogen bond formed by DLGFLARGF and amino acid residues of tyrosinase **(C)**. Hydrophobic interaction between DLGFLARGF and amino acid residues of tyrosinase **(D)**. Electrostatic interaction between DLGFLARGF and amino acid residues of tyrosinase **(E)**.

Rapid Screening and Tyrosinase Inhibitory Activity Verification

Studies have shown that peptides with lower MW tend to have higher functional activity (38). Therefore, peptides with MW $\leq$ 1,000 Da were selected from the 52 peptides obtained, and 16 peptides (shown in **Table 3**) were obtained for subsequent analysis. Section Amino Acid Composition and Molecular Weight Distribution of Hydrolysates introduced some amino acids that contribute to tyrosinase inhibition, such as Val, Ala, Leu, Ile, Arg, Phe, Cys, Ser, and Thr. According to the screening method from previous study (10), 16 peptides in **Table 3** were counted for their tyrosinase inhibitory contribution ratio of amino acids, and 4 peptides (marked * in **Table 3**) with a contribution ratio of amino acids greater than or equal to 0.6 were obtained, they were discovered to be novel peptides by searching the data on the website http://www.uwm.edu.pl/biochemia/index.php/en/biopep. Therefore, the four peptides were used for subsequent synthesis to verify the tyrosinase inhibitory activity *in vitro*, the purity of the synthetic peptides was more than 95%. The tyrosinase inhibition ability of the synthetic peptide was shown in **Figure 4**. The peptide DLGFLARGF showed the strongest tyrosinase inhibition ability, with an IC_{50} value of 3.09 mM. The IC_{50} of peptides WQLTL, WSEVF and FDLGFLAR were 3.86, 5.81, and 4.00 mM, respectively, and they all showed good tyrosinase inhibitory activity. Similar peptides from natural sources have also been found in other studies, such as Phe-Pro-Tyr (FPY) from defatted walnut (*Juglans regia* L.) meal hydrolysate with an IC_{50} value of 3.22 $\pm$ 0.22 mM (40), and RHAKF from Chinese quince seed protein hydrolysate with IC_{50} value of 1.15 mg/ml (41). In order to further explore the reasons for the difference in tyrosinase inhibition of these four peptides, molecular docking analysis was performed.

Molecular Docking

In recent years, as a computer simulation technology, molecular docking has been widely used to study the possible interaction mechanism between inhibitors and enzymes (42–44). In order to show the binding mode of TYIPs with tyrosinase more intuitively, the AutoDock tool was used, and the results are shown in **Figures 5**, **6**. Peptide DLGFLARGF bonded to the D chain of tyrosinase and interacted with its surrounding amino acid residues, nine hydrogen bonds were formed with Glu 340, Arg 111, Gly 115, Arg 108, Ile 96, Ser 95, Gly 113, Lys 5 and Glu 97 on the enzyme D chain (**Figure 5C**). In addition, amino acid residues Try 62, Pro 338, Pro 349, Glu 112, and Arg 111 can form a hydrophobic pocket on the enzyme D chain, which tightly surround and hold the peptide DLGFLARGF through hydrophobic action (**Figure 5D**). At the same time, electrostatic interaction also occurred between Glu 97, Glu 340, Glu 67, Asp 60 and the peptide DLGFLARGF on the D-chain (as shown in **Figure 5E**). These results intuitively indicated that hydrogen bonding was the main driving force (as shown in **Table 4**) involved in the interaction between

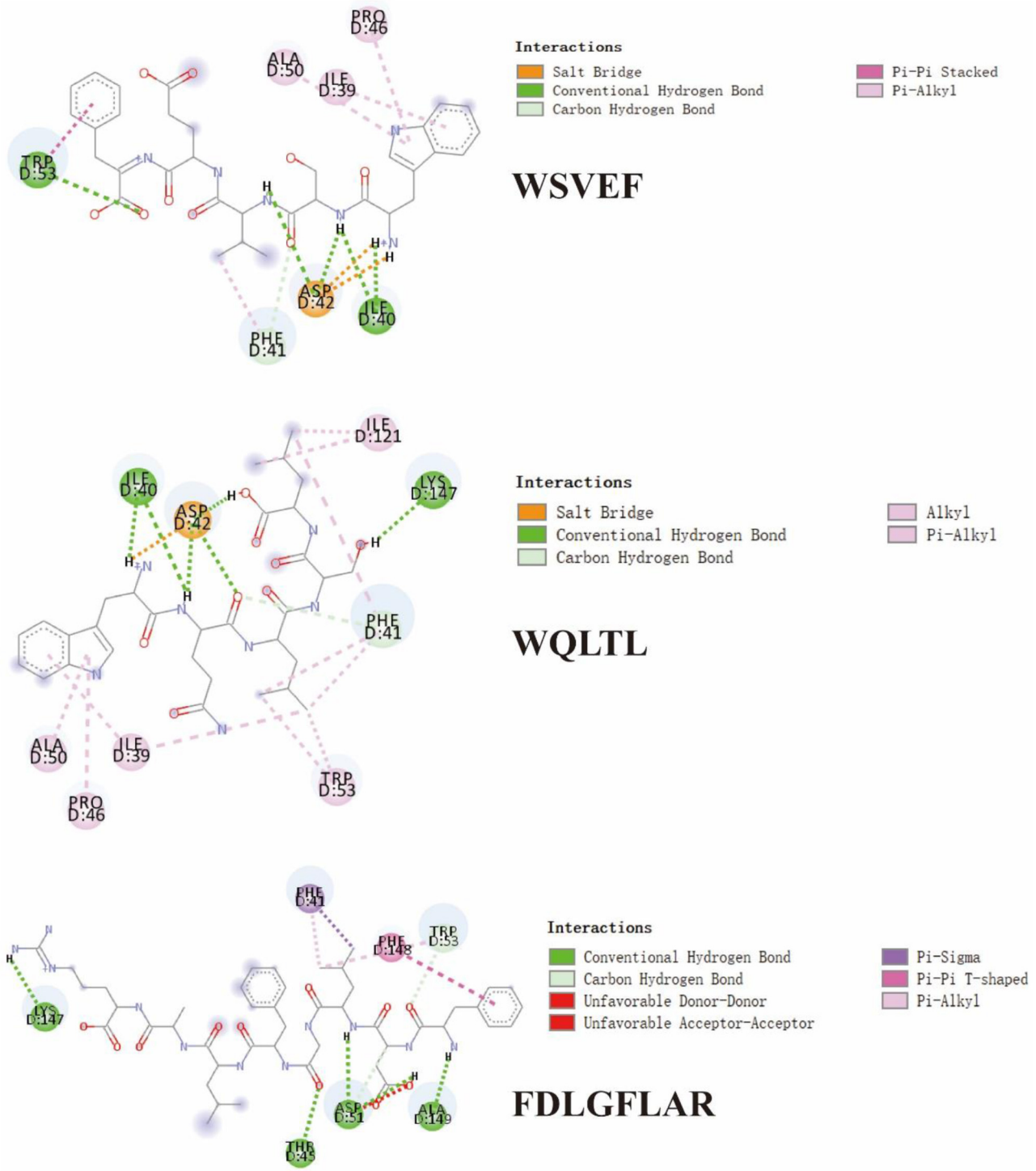

FIGURE 6 | 2D diagram showing interactions between TYIPs and tyrosinase amino acid residue.

peptide DLGFLARGF and tyrosinase. It can be inferred that the peptide DLGFLARGF binds to the inactive center of tyrosinase through hydrogen bonding, and indirectly inhibits the binding of substrate to tyrosinase by changing the conformation of the enzyme, thereby inhibiting the catalytic activity of the enzyme.

TABLE 4 | Docking results according to hydrophobic interaction, electrostatic interaction and hydrogen bond for complex.

	DLGFLARGF	WQLTL	WSEVF	FDLGFLAR
Hydrogen bonds	Glu 340, Arg 111, Gly 115, Arg 108, Ile 96, Ser 95, Gly 113, Lys 5, Glu 97	Asp 42, Lys 147, Ile 40	Asp 42, Ile 40, Trp 53	Ala 149, Asp 51, Thr 45, Lys 147
Electrostatic interaction	Glu 97, Glu 340, Glu 67, Asp 60	Asp 42	Asp 42	No
Hydrophobic interaction	Tyr 62, Pro 338, Pro 349	Ile 121, Ile 39, Pro 46, Ala 50, Trp 53, Phe 41	Trp 53, Phe 41, Pro 46, Ala 50, Ile 39	Phe 148, Trp 53, Phe 41

In **Figure 6** and **Table 4**, it could be seen that driving forces in the peptides WQLTL, WSEVF, and FDLGFLAR were less than DLGFLARGF, which also led to lower tyrosinase inhibitory activity of these peptides. Moreover, molecular docking can also be used to screen enzyme inhibitors based on binding energy changes (45, 46). The three peptides have different binding energies with WQLTL = −8.3 kcal/mol, WSEVF = −9.2 kcal/mol, FDLGFLAR = −6.4 kcal/mol, which was not completely consistent with the trend of tyrosinase inhibition ability in **Figure 4**. This may be because the most stable conformation was selected based on the lowest binding energy, but the peptide conformation in the reaction system may not be the most stable (47). On the other hand, it may also be due to the longer-chain of FDLGFLAR closer to the center of the hydrophobic cavity and the more hydrophobic interactions of WQLTL than WSEVF.

The Effect of DLGFLARGF on B16F10 Melanoma Cells

The CCK-8 method was used to determine the potential cytotoxicity of different concentrations of DLGFLARGF compared with kojic acid (0.75 mg/ml). **Figure 7A** shows the effect of DLGFLARGF and kojic acid on the viability of B16F10 cells. With the increase of DLGFLARGF concentration, the cell survival rate gradually decreased. But within the tested concentration range (0–1.6 mg/ml), no obvious cytotoxicity was obtained (viability > 50%). Therefore, the concentrations of 0, 0.1, 0.2, 0.4, 0.8, and 1.6 mg/ml were selected to study the inhibitory effect of DLGFLARGF on melanin synthesis.

To further evaluate the tyrosinase inhibition of DLGFLARGF, B16F10 melanoma cells were treated with different concentrations of DLGFLARGF and kojic acid (0.75 mg/ml). The result is shown in **Figure 7B**. With the increase of DLGFLARGF concentration, tyrosinase activity gradually decreased, indicating gradually increased tyrosinase inhibitory ability. The inhibition rate was 23.19% for 1.6 mg/ml of DLGFLARGF, which was very close to that of kojic acid with 28.34% inhibition rate under 0.75 mg/ml. According to the previous results, the peptide DLGFLARGF was found to reduce tyrosinase activity by binding to the amino acid residue sites on the D chain of tyrosinase upon entry into the cells, but kojic acid in published study was proved to be docked to the catalytic site of mushroom tyrosinase and thus had a stronger tyrosinase inhibitory activity (48).

The content of melanin can directly determines the degree of skin whiteness. At present, the recognized process of melanin formation is roughly that tyrosine is oxidized to dopa under the action of tyrosinase, and then dopa is oxidized to dopa-quinone, which finally forms eumelanin through a series of reactions. Tyrosinase is the key enzyme for melanin formation (49). As shown in **Figure 7C**, the melanin content gradually decreased as the concentration of DLGFLARGF increased and showed a concentration-dependent relationship, indicating that DLGFLARGF can effectively inhibit the production of melanin. In terms of the inhibitory effects on melanin production, the melanin content was reduced by 55.4% in the cells treated with kojic acid (0.75 mg/ml), while DLGFLARGF reduced by 38.3% at 1.6 mg/ml. Kojic acid had been proved to be better than DLGFLARGF in inhibiting tyrosinase activity. On the other hand, the synthesis of melanin involves various factors besides tyrosinase, and kojic acid could also regulate transcription of tyrosinase pathway genes and bleach produced melanin (50). Moreover, collagen peptide has mild functional activity, easy absorption and high skin compatibility, while kojic acid lacks good permeability in application, and show high toxicity and low activity stability (51).

CONCLUSIONS

In this work, the alcalase hydrolysate of grass carp fish scale gelatin was discovered to have promising tyrosinase inhibitory activity. The tyrosinase inhibition rate of fish scale gelatin treated with alcalase was 61.7% (at 5 mg/ml). The MW distribution of the hydrolysate was mainly below 3,358 Da (73.33%), and the content of amino acids that inhibit melanin was up to 35.44%. A rapid screening method of TYIPs based on bioaffinity ultrafiltration combined with LC-Orbitrap-MS/MS was established. 52 peptides were identified from PAT, among which 4 new peptides were screened. The peptide DLGFLARGF showed excellent tyrosinase inhibitory activity with an IC_{50} value of 3.09 mM. Hydrogen bonds were the predominant driving force in the interaction between peptide DLGFLARGF and tyrosinase according to molecular docking. In addition, when the concentration of DLGFLARGF reached 1.6 mg/ml, the melanin content and tyrosinase activity decreased to 61.7% and 76.81% of the control group, respectively. The above results indicate that bioaffinity ultrafiltration combined with LC-Orbitrap-MS/MS is an effective method for high-throughput screening of TYIPs. Moreover, DLGFLARGF can be widely used as a tyrosinase inhibitor in the whitening foods and pharmaceuticals.

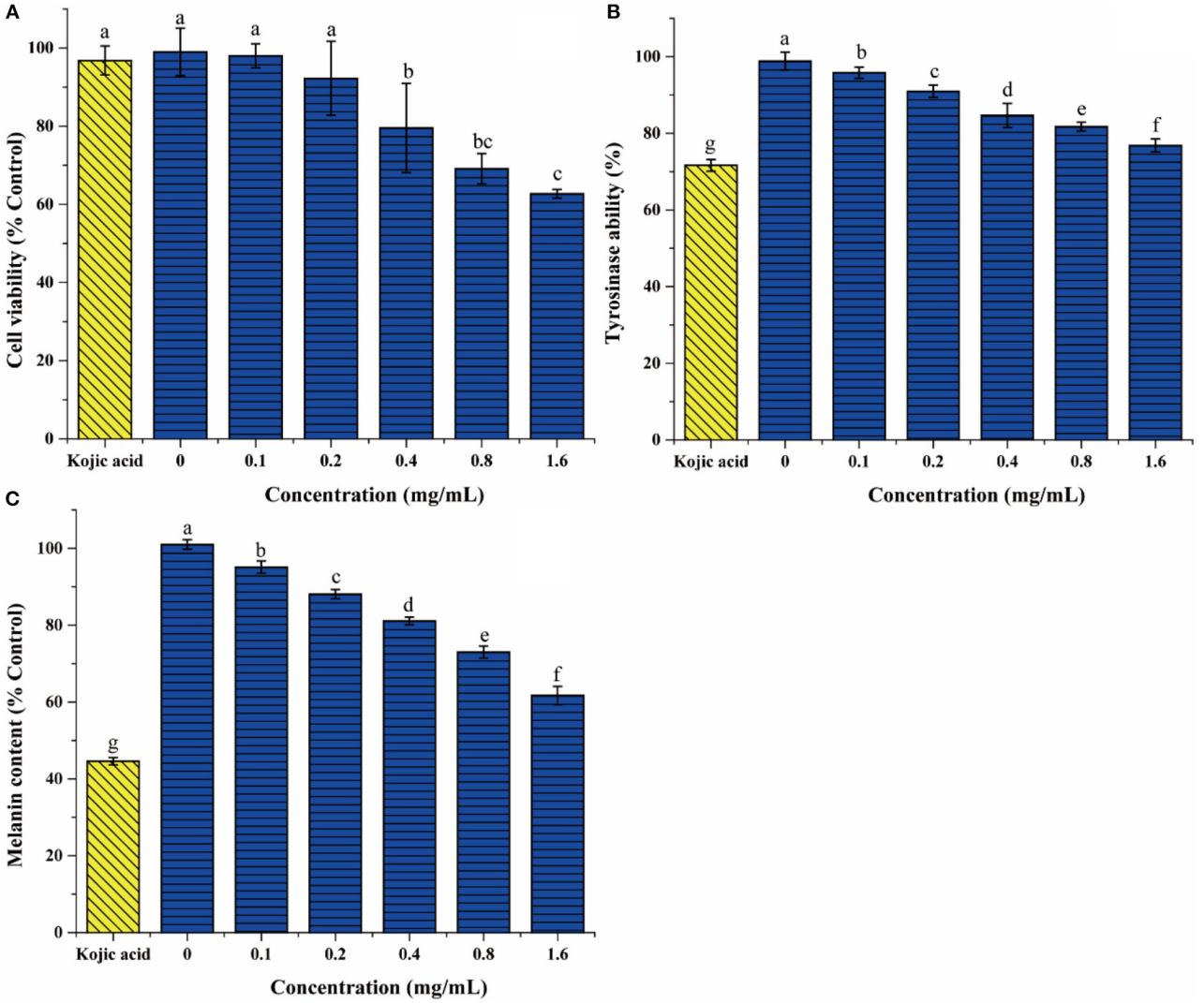

FIGURE 7 | The effect of DLGFLARGF on B16F10 melanoma cells cytotoxicity **(A)**, tyrosinase activity **(B)**, and melanin content **(C)**. Kojic acid (0.75 mg/ml) was used as a positive control. The results are expressed as a percentage of the control, and the value is the mean ± SD of three independent experiments. According to Duncan's test, different letters indicate that the statistical difference between the two groups is $p < 0.05$.

DATA AVAILABILITY STATEMENT

The original contributions presented in the study are included in the article/supplementary material, further inquiries can be directed to the corresponding authors.

AUTHOR CONTRIBUTIONS

Z-ZH: experiments, data curation, and writing-original draft. X-MS: supervision, review, and editing. LZ: investigation, methodology, review, and editing. M-JZ: experiments. Z-CT: project administration, supervision, and funding acquisition. All authors contributed to the article and approved the submitted version.

FUNDING

This study was supported by the National Key R&D Program of China (No. 2018YFD0901101).

REFERENCES

1. Sha XM, Hu ZZ, Tu ZC, Zhang LZ, Duan DL, Huang T, et al. Influence of dynamic high pressure microfluidization on functional properties and structure of gelatin from bighead carp (*Hypophthalmichthys nobilis*) scale. *J Food Process Preserv.* (2018) 42:e13607. doi: 10.1111/jfpp.13607
2. Sow LC, Nicholas ZYT, Wong CW, Yang H. Combination of sodium alginate with tilapia fish gelatin for improved texture

properties and nanostructure modification. *Food Hydrocoll.* (2019) 94:459–67. doi: 10.1016/j.foodhyd.2019.03.041
3. Sow LC, Tana SJ, Yang H. Rheological properties and structure modification in liquid and gel of tilapia skin gelatin by the addition of low acyl gellan. *Food Hydrocoll.* (2019) 90:9–18. doi: 10.1016/j.foodhyd.2018.12.006
4. Zhao X, Zhou Y, Zhao L, Chen L, He Y, Yang H. Vacuum impregnation of fish gelatin combined with grape seed extract inhibits protein oxidation and degradation of chilled tilapia fillets. *Food Chem.* (2019) 294:316–25. doi: 10.1016/j.foodchem.2019.05.054
5. Xin Y, Chai M, Chen F, Hou Y, Lai S, Yang H. Comparative study on the gel properties and nanostructures of gelatins from chicken, porcine, and tilapia skin. *J Food Sci.* (2021) 86:1936–45. doi: 10.1111/1750-3841.15700
6. Zhang YF, Duan X, Zhuang YL. Purification and characterization of novel antioxidant peptides from enzymatic hydrolysates of tilapia (*Oreochromis niloticus*) skin gelatin. *Peptides.* (2012) 38:13–21. doi: 10.1016/j.peptides.2012.08.014
7. Lin L, Lv S, Li BF. Angiotensin-I-converting enzyme (ACE)-inhibitory and antihypertensive properties of squid skin gelatin hydrolysates. *Food Chem.* (2012) 131:225–30. doi: 10.1016/j.foodchem.2011.08.064
8. Wang FH, Dong XF, Xiu P, Zhong JT, Wei HL, Xu ZZ, et al. T7 peptide inhibits angiogenesis via downregulation of angiopoietin-2 and autophagy. *Oncol Rep.* (2015) 33:675–84. doi: 10.3892/or.2014.3653
9. Ennaas N, Hammami R, Beaulieu L, Fliss I. Purification and characterization of four antibacterial peptides from protamex hydrolysate of Atlantic mackerel (Scomber scombrus) by-products. *Biochem Biophys Res Commun.* (2015) 462:195–200. doi: 10.1016/j.bbrc.2015.04.091
10. Schurink M, van Berkel WJH, Wichers HJ, Boeriu CG. Novel peptides with tyrosinase inhibitory activity. *Peptides.* (2007) 28:485–95. doi: 10.1016/j.peptides.2006.11.023
11. Wu JJ, Lin JC, Wang CH, Jong TT, Yang HL, Hsu SL, et al. Extraction of antioxidative compounds from wine lees using supercritical fluids and associated anti-tyrosinase activity. *J Supercrit Fluids.* (2009) 50:33–41. doi: 10.1016/j.supflu.2009.04.010
12. Kameyama K, Sakai C, Kuge S, Nishiyama S, Tomita Y, Ito S, et al. The expression of tyrosinase, tyrosinase-related proteins 1 and 2 (TRP1 and TRP2), the silver protein, and a melanogenic inhibitor in human melanoma cells of differing melanogenic activities. *Pigm Cell Res.* (1995) 8:97–104. doi: 10.1111/j.1600-0749.1995.tb00648.x
13. Patil S, Sistla S, Jadhav J. Screening of inhibitors for mushroom tyrosinase using surface plasmon resonance. *J Agric Food Chem.* (2014) 62:11594–601. doi: 10.1021/jf5039585
14. Lee SY, Baek N. and Nam T-g, Natural, semisynthetic and synthetic tyrosinase inhibitors. *J Enzyme Inhib Med Chem.* (2016) 31:1–13. doi: 10.3109/14756366.2015.1004058
15. Song X, Hu X, Zhang Y, Pan J, Gong D, Zhang G. Inhibitory mechanism of epicatechin gallate on tyrosinase: inhibitory interaction, conformational change and computational simulation. *Food Funct.* (2020) 11:4892–902. doi: 10.1039/D0FO00003E
16. Hemachandran H, Jain F, Mohan S, Kumar DT, Priya Doss CG, Ramamoorthy S. Glandular hair constituents of *Mallotus philippinensis* Muell. fruit act as tyrosinase inhibitors: Insights from enzyme kinetics and simulation study. *Int J Biol Macromol.* (2018) 107:1675–82. doi: 10.1016/j.ijbiomac.2017.10.036
17. Anantharaman A, Hemachandran H, Mohan S, Ayyathan DM, Kumar DT, Doss CGP, et al. Induction of apoptosis by apocarotenoids in B16 melanoma cells through ROS-mediated mitochondrial-dependent pathway. *J Funct Foods.* (2016) 20:346–57. doi: 10.1016/j.jff.2015.11.019
18. Hridya H, Amrita A, Mohan S, Gopalakrishnan M, Dakshinamurthy TK, Doss GP, et al. Functionality study of santalin as tyrosinase inhibitor: a potential depigmentation agent. *Int J Biol Macromol.* (2016) 86:383–9. doi: 10.1016/j.ijbiomac.2016.01.098
19. Thaha A, Wang BS, Chang YW, Hsia SM, Huang TC, Shiau CY, et al. Food-derived bioactive peptides with antioxidative capacity, xanthine oxidase and tyrosinase inhibitory activity. *Processes.* (2021) 9:747. doi: 10.3390/pr9050747
20. Wu QY, Jia JQ, Yan H, Du JJ, Gui ZZ. A novel angiotensin-I converting enzyme (ACE) inhibitory peptide from gastrointestinal protease hydrolysate of silkworm pupa (*Bombyx mori*) protein: biochemical characterization and molecular docking study. *Peptides.* (2015) 68:17–24. doi: 10.1016/j.peptides.2014.07.026
21. Zhong C, Sun LC, Yan LJ, Lin YC, Liu GM, Cao MJ. Production, optimisation and characterisation of angiotensin converting enzyme inhibitory peptides from sea cucumber (*Stichopus japonicus*) gonad. *Food Funct.* (2018) 9:594–603. doi: 10.1039/c7fo01388d
22. Wang L, Liu YF, Luo Y, Huang KY, Wu ZQ. Quickly screening for potential alpha-glucosidase inhibitors from guava leaves tea by bioaffinity ultrafiltration coupled with HPLC-ESI-TOF/MS method. *J Agric Food Chem.* (2018) 66:1576–82. doi: 10.1021/acs.jafc.7b05280
23. Zhang L, Xu L, Ye YH, Zhu MF, Li J, Tu ZC, et al. Phytochemical profiles and screening of alpha-glucosidase inhibitors of four Acer species leaves with ultra-filtration combined with UPLC-QTOF-MS/MS. *Ind Crop Prod.* (2019) 129:156–68. doi: 10.1016/j.indcrop.2018.11.051
24. Qin SS, Ren YR, Fu X, Shen J, Chen X, Wang Q, et al. Multiple ligand detection and affinity measurement by ultrafiltration and mass spectrometry analysis applied to fragment mixture screening. *Anal Chim Acta.* (2015) 886:98–106. doi: 10.1016/j.aca.2015.06.017
25. Sha XM, Tu ZC, Liu W, Wang H, Shi Y, Huang T, et al. Effect of ammonium sulfate fractional precipitation on gel strength and characteristics of gelatin from bighead carp (*Hypophthalmichthys nobilis*) scale. *Food Hydrocoll.* (2014) 36:173–80. doi: 10.1016/j.foodhyd.2013.09.024
26. Uysal S, Zengin G, Locatelli M, Bahadori MB, Mocan A, Bellagamba G, et al. Cytotoxic and enzyme inhibitory potential of two potentilla species (P-speciosa L. and P-reptans Willd) and their chemical composition. *Front Pharmacol.* (2017) 8:290. doi: 10.3389/Fphar.2017.00290
27. Chen X, Wu JH, Li L, Wang SY. Cryoprotective activity and action mechanism of antifreeze peptides obtained from tilapia scales on *Streptococcus thermophilus* during cold stress. *J Agric Food Chem.* (2019) 67:1918–26. doi: 10.1021/acs.jafc.8b06514
28. Jiang X, Cui ZQ, Wang LH, Xu HJ, Zhang YG. Production of bioactive peptides from corn gluten meal by solid-state fermentation with *Bacillus subtilis* MTCC5480 and evaluation of its antioxidant capacity *in vivo*. *LWT-Food Sci Technol.* (2020) 131:109767. doi: 10.1016/j.lwt.2020.109767
29. Ismaya WT, Rozeboom HJ, Weijn A, Mes JJ, Fusetti F, Wichers HJ, et al. Crystal Structure of Agaricus bisporus Mushroom Tyrosinase: Identity of the Tetramer Subunits and Interaction with Tropolone. *Biochemistry.* (2011) 50:5477–86. doi: 10.1021/bi200395t
30. Munetaka I, Hideyuki T, Masanobu S, Kazumi S, Yosuke O, Keiyu U. A combined assay of cell vability and *in vitro* cytotoxicity with a highly water-soluble tetrazolium salt, neutral red and crystal violet. *Biol Pharm Bull.* (1996) 19:1518–20. doi: 10.1248/bpb.19.1518
31. Ullah S, Park Y, Park C, Lee S, Kang D, Yang J, et al. Antioxidant, anti-tyrosinase and anti-melanogenic effects of (E)-2,3-diphenylacrylic acid derivatives. *Bioorg Med Chem.* (2019) 27:2192–200. doi: 10.1016/j.bmc.2019.04.020
32. Zhang X, Li J, Li Y, Liu Z, Lin Y, Huang J. Anti-melanogenic effects of epigallocatechin-3-gallate (EGCG), epicatechin-3-gallate (ECG) and gallocatechin-3-gallate (GCG) via down-regulation of cAMP/CREB /MITF signaling pathway in B16F10 melanoma cells. *Fitoterapia.* (2020) 145:104634. doi: 10.1016/j.fitote.2020.104634
33. Futaki S. Membrane-permeable arginine-rich peptides and the translocation mechanisms. *Adv Drug Delivery Rev.* (2005) 57:547–58. doi: 10.1016/j.addr.2004.10.009
34. Ishikawa M, Kawase I, Ishii F. Combination of amino acids reduces pigmentation in B16F0 melanoma cells. *Biol Pharm Bull.* (2007) 30:677–81. doi: 10.1248/Bpb.30.677
35. Chen SY, Yang Q, Chen X, Tian YQ, Liu ZY, Wang SY. Bioactive peptides derived from crimson snapper and *in vivo* anti-aging effects on fat diet-induced high fat *Drosophila melanogaster*. *Food Funct.* (2020) 11:524–33. doi: 10.1039/c9fo01414d
36. Zhuang YL, Sun LP, Zhao X, Wang JF, Hou H, Li BF. Antioxidant and melanogenesis-inhibitory activities of collagen peptide from jellyfish (*Rhopilema esculentum*). *J Sci Food Agric.* (2009) 89:1722–7. doi: 10.1002/jsfa.3645
37. Maqsoudlou A, Mahoonak AS, Mora L, Mohebodini H, Toldrá F, Ghorbani M. Peptide identification in alcalase hydrolysated pollen and comparison of its bioactivity with royal jelly. *Food Res Int.* (2019) 116:905–15. doi: 10.1016/j.foodres.2018.09.027

38. Chen N, Yang HM, Sun Y, Niu J, Liu S. Purification and identification of antioxidant peptides from walnut (*Juglans regia* L) protein hydrolysates. *Peptides.* (2012) 38:344–9. doi: 10.1016/j.peptides.2012.09.017
39. Mulabagal V, Calderon AI. Development of an ultrafiltration-liquid chromatography/mass spectrometry (UF-LC/MS) based ligand-binding assay and an LC/MS based functional assay for mycobacterium tuberculosis shikimate kinase. *Anal Chem.* (2010) 82:3616–21. doi: 10.1021/ac902849g
40. Feng YX, Wang ZC, Chen JX, Li HR, Wang YB, Ren DF, et al. Separation, identification, and molecular docking of tyrosinase inhibitory peptides from the hydrolysates of defatted walnut (*Juglans regia* L). meal. *Food Chem.* (2021) 353:129471. doi: 10.1016/j.foodchem.2021.129471
41. Deng YJ, Huang LX, Zhang CH, Xie PJ, Cheng J, Wang X, et al. Skin-care functions of peptides prepared from Chinese quince seed protein: sequences analysis, tyrosinase inhibition and molecular docking study. *Ind Crop Prod.* (2020) 148:112331. doi: 10.1016/j.indcrop.2020.112331
42. Chai WM, Lin MZ, Song FJ, Wang YX, Xu KL, Huang JX, et al. Rifampicin as a novel tyrosinase inhibitor: Inhibitory activity and mechanism. *Int J Biol Macromol.* (2017) 102:425–30. doi: 10.1016/j.ijbiomac.2017.04.058
43. Hridya H, Amrita A, Sankari M, Doss CGP, Gopalakrishnan M, Gopalakrishnan C, et al. Inhibitory effect of brazilein on tyrosinase and melanin synthesis: kinetics and in silico approach. *Int J Biol Macromol.* (2015) 81:228–34. doi: 10.1016/j.ijbiomac.2015.07.064
44. Wang YJ, Zhang GW, Yan JK, Gong DM. Inhibitory effect of morin on tyrosinase: Insights from spectroscopic and molecular docking studies. *Food Chem.* (2014) 163:226–33. doi: 10.1016/j.foodchem.2014.04.106
45. Kharazmi Khorassani J, Asoodeh A, Tanzadehpanah H. Antioxidant and angiotensin-converting enzyme-ACE-inhibitory activity of thymosin alpha-1-Thα1-peptide. *Bioorg Chem.* (2019) 87:743–52. doi: 10.1016/j.bioorg.2019.04.003
46. Wu HX, Liu YL, Guo MR, Xie JL, Jiang XM. A virtual screening method for inhibitory peptides of angiotensin I-converting enzyme. *J Food Sci.* (2014) 79:C1635–42. doi: 10.1111/1750-3841.12559
47. Ma TX, Fu QQ, Mei QG, Tu ZC, Zhang L. Extraction optimization and screening of angiotensin-converting enzyme inhibitory peptides from *Channa striatus* through bioaffinity ultrafiltration coupled with LC-Orbitrap-MS/MS and molecular docking. *Food Chem.* (2021) 354:129589. doi: 10.1016/j.foodchem.2021.129589
48. Söhretoglu D, Sari S, Barut B, Özel A. Tyrosinase inhibition by some flavonoids: Inhibitory activity, mechanism by *in vitro* and *in silico* studies. *Bioorg Chem.* (2018) 81:168–74. doi: 10.1016/j.bioorg.2018.08.020
49. Halaban. R, Patton RS, Cheng E, Svedine S, Trombetta ES, Wahl ML, et al. Abnormal acidification of melanoma cells induces tyrosinase retention in the early secretory pathway. *J. Biol. Chem.* (2002) 277:14821–8. doi: 10.1074/jbc.M111497200
50. Meng W, Zhang C, Xiao D. The effect of different activated carbon and bleaching temperature on kojic acid bleaching. Berlin: Springer (2015). p. 325–33.
51. Nerya O, Musa R, Khatib S, Tamir S, Vaya J. Chalcones as potent tyrosinase inhibitors: the effect of hydroxyl positions and numbers. *Phytochemistry.* (2004) 65:1389–95. doi: 10.1016/j.phytochem.2004.04.016

Conflict of Interest: The authors declare that the research was conducted in the absence of any commercial or financial relationships that could be construed as a potential conflict of interest.

The reviewer LZ declared a shared affiliation with the author Z-CT to the handling editor at the time of review.

Publisher's Note: All claims expressed in this article are solely those of the authors and do not necessarily represent those of their affiliated organizations, or those of the publisher, the editors and the reviewers. Any product that may be evaluated in this article, or claim that may be made by its manufacturer, is not guaranteed or endorsed by the publisher.

frontiers in Nutrition

BRIEF RESEARCH REPORT
published: 24 March 2022
doi: 10.3389/fnut.2022.813962

Molecular Authentication of Twelve Meat Species Through a Promising Two-Tube Hexaplex Polymerase Chain Reaction Technique

Zhendong Cai[1†], Guowei Zhong[2†], Qianqian Liu[3], Xingqiao Yang[1], Xiaoxia Zhang[4], Song Zhou[1], Xiaoqun Zeng[1], Zhen Wu[1] and Daodong Pan[1*]*

[1] Key Laboratory of Animal Protein Deep Processing Technology of Zhejiang Province, College of Food and Pharmaceutical Sciences, Ningbo University, Ningbo, China, [2] Center for Global Health, School of Public Health, Nanjing Medical University, Nanjing, China, [3] Institute of Environmental Research at Greater Bay Area, Guangzhou University, Guangzhou, China, [4] Ordos Agriculture and Animal Husbandry Technology Extension Centre, Ordos, China

OPEN ACCESS

Edited by:
A. M. Abd El-Aty,
Cairo University, Egypt

Reviewed by:
Aly Farag El Sheikha,
Jiangxi Agricultural University, China
Emel Oz,
Atatürk University, Turkey
Lixia Lu,
Nanjing Tech University, China
M. A. Motalib Hossain,
University of Malaya, Malaysia

***Correspondence:**
Qianqian Liu
csuliuqian@foxmail.com
Daodong Pan
daodongpan@163.com

[†] These authors have contributed equally to this work

Specialty section:
This article was submitted to Food Chemistry, a section of the journal Frontiers in Nutrition

Received: 12 November 2021
Accepted: 18 February 2022
Published: 24 March 2022

Citation:
Cai Z, Zhong G, Liu Q, Yang X, Zhang X, Zhou S, Zeng X, Wu Z and Pan D (2022) Molecular Authentication of Twelve Meat Species Through a Promising Two-Tube Hexaplex Polymerase Chain Reaction Technique. Front. Nutr. 9:813962. doi: 10.3389/fnut.2022.813962

Frequent meat frauds have aroused significant social attention. The aim of this study is to construct a two-tube hexaplex polymerase chain reaction (PCR) method offering accurate molecular authentication of twelve meat species in actual adulteration event. Deoxyribonucleic acid (DNA) sequencing demonstrates that designed primers can specifically amplify target species from genomic DNA mixture of six species in each tube reaction, which showed 100% accuracy of horse (148 bp), pigeon (218 bp), camel (283 bp), rabbit (370 bp), ostrich (536 bp), and beef (610 bp) as well as turkey (124 bp), dog (149 bp), chicken (196 bp), duck (277 bp), cat (380 bp), and goose (468 bp). A species-specific primer pair produced the target band in the presence of target genomic DNA but not non-target species. Through multiplex PCR assays with serial concentration of the DNA mixture of six species in each PCR reaction, the detection limit (LOD) of the two-tube hexaplex PCR assay reached up to 0.05–0.1 ng. Using genomic DNA isolated from both boiled and microwave-cooked meat as templates, PCR amplification generated expected PCR products. These findings demonstrate that the proposed method is specific, sensitive and reproducible, and is adequate for food inspection. Most importantly, this method was successfully applied to detect meat frauds in commercial meat products. Therefore, this method is of great importance with a good application foreground.

Keywords: molecular authentication, hexaplex PCR, meat adulteration, species-specific primer, commercial foodstuffs

INTRODUCTION

Meat products contribute essential nutrients to human such as proteins, fatty acids, trace elements, and vitamins, especially for the richest protein source (1). Based on the growing demand for animal protein-based foods, meat frauds such as counterfeiting and mislabeling have become a severe global issue (2–4). Over the last two decades, events of meat adulteration have occurred globally because of pursuit of extra economic benefits (2).The notorious horsemeat scandal in the European

Union in 2013 is a high-profile food fraud incident, which has shaken consumer trust in food industries throughout the globe (5). Besides, meat adulteration not only breaks market rules but also violates ethical norms and religious laws. As known, pork has strictly restricted consumption in Islam and Judaism, and beef is prohibited in Hindus (6, 7). In addition, meat fraud risks food safety and even threatens public health because of metabolic disorders, allergies, or infectious diseases. As reported, forbidden ingredients such as fox and mouse are occasionally mixed into edible meat products (3, 8). Nevertheless, allergic reactions can be triggered by some meat species especially for sensitized patients (9). Hence, authentication of meat products is necessary to protect consumers from meat fraud and ensure public health in dietary practices.

A reliable, sensitive, and low-cost analytical technique is of great importance to ensure food quality and protect consumers from being deceived. Techniques have been greatly improved recently due because of progress in molecular biology. Deoxyribonucleic acid (DNA) molecules are present in cells and possess excellent stability under high temperature and pressure and chemical processing, suggesting that DNA-based analytical methods are reliable for detection of meat frauds. Polymerase chain reaction (PCR) techniques such as species-specific PCR, multiplex PCR, PCR-RFLP, real-time PCR, random amplified polymorphic DNA (RAPD), and DNA barcoding have evolved as preferred methods for meat fraud detection (2, 10, 11). Recently, both multiplex and real-time PCR techniques have been widely applied for meat fraud detection (12). Real-time PCR provides more detailed information regarding the identification and quantification of meat species (13). However, the matrix may interfere with the amplification process, such that accurate quantification could only be achieved in the presence of a proper reference material (13), indicating that it is difficult to quantify meat fractions in real-world foodstuffs. In addition, real-time PCR assays depend on suitable equipment and trained professionals. In contrast, multiplex PCR is a particularly desirable method, which can efficiently authenticate more species and visually observed through simple agarose gel analysis, suggesting that multiplex PCR assays can be easily implemented with minimum effort but much gain to verify the identification of meat species.

Mitochondrial DNA (mtDNA) harboring multiple copies in all cells possess intraspecies conservation and interspecies polymorphism, so mitochondrial genes are preferred targets for meat fraud detection. Here, using mtDNA genes including NADH dehydrogenase subunits 5 and 6, 12S and 16S rRNAs, cytochrome c oxidase subunits I and II, D-loop, and cytochrome *b* as targets, species-specific primers for twelve animal species (horse, pigeon, camel, rabbit, ostrich, beef, turkey, dog, chicken, duck, cat, and goose) are designed and screened based on tests of cross-reactivity, specificity, sensitivity, and robustness. A two-tube hexaplex PCR assay, which efficiently detects twelve animal origins, is ultimately developed with twelve pairs of species-specific primers. Moreover, this method is adequate for assessment of fraud incidences in commercial meat products.

MATERIALS AND METHODS

Sample Collection and Deoxyribonucleic Acid Extraction

According to a previous approach (14), fresh meat samples of the twelve animal species were purchased from local retailers and markets in Ningbo City, People's Republic of China. Commercial samples in triplicates were purchased on different dates from local supermarkets and online supermarket platforms. All the samples were transported under ice-chilled state and were stored at −80°C to inhibit DNA degradation until further use for DNA extraction. Genomic DNA was isolated by using the EasyPure® Genomic DNA Kit (TransGen Biotech Co., Ltd., Beijing, China) according to the manufacturer's instructions. DNA concentration was measured with a NanoDrop 2000 UV-Vis spectrophotometer (Thermo Scientific, Wilmington, NC, United States).

Design of Species-Specific Primers

Because of high divergence and conservation of mitochondrial sequences within the animal species, mitochondrial genes were selected as targets for designing primers (15). The mitochondrial genes shown in **Table 1** are retrieved from the National Center of Biotechnology Information (NCBI) database. Combining the Oligo 7.0 and BLAST programs, species-specific primers were designed based on physical parameters of cross-reactivity, melting temperature, self-complementarity, and secondary structures. To check *in silico* specificity, the primers were aligned against target and non-target animal species, including 14 land animals of horse (*Equus caballus*), pigeon (*Columba livia*), camel (*Camelus bactrianus*), rabbit (*Oryctolagus cuniculus*), ostrich (*Struthio camelus*), cattle (*Bos taurus*), turkey (*Meleagris gallopavo*), dog (*Canis lupus*), chicken (*Gallus gallus*), duck (*Anas platyrhynchos*), cat (*Felis catus*), goose (*Anser cygnoides*), and pig (*Sus scrofa*), sheep (*Ovis aries*), and 3 aquatic species of small yellow croaker (*Larimichthys polyactis*), tuna (*Thunnus orientalis*), and black carp (*Mylopharyngodon piceus*) using a ClustalW sequence alignment program and the MEGA6 software. Finally, a cross-amplifcation reaction was individually examined to validate the species-specificity of primer pairs by simplex PCR assays. Optimized sequences of primer sets in detail are shown in **Table 1**.

Simplex and Multiplex Polymerase Chain Reaction Assays

Polymerase chain reaction assays were performed as previously described (14). Simplex PCR for each species with its own primers was carried out using an EasyTaq® DNA Polymerase kit (TransGen Biotech Co., Ltd., Beijing, China). The PCR reaction system included 2.5 μl EasyTaq® Buffer (10 x), 2 μl dNTPs (2.5 mM), 0.5 μl EasyTaq DNA Polymerase (5 units μl^{-1}),0.5 μl each primer (10 μM), 1 μl genomic DNA (1 ng μl^{-1}), and refilled ddH_2O to 25 μl. PCR reaction was initiated by 5-min denaturation at 94°C, followed by 34 cycles of 94°C for 30 s, 63°C for 30 s, 72°C for 45 s, and final elongation at 72°C for 5 min. For multiplex PCR, the PCR reaction system included 2.5 μl EasyTaq® Buffer (10 x), 2 μl dNTPs (2.5 mM),0.5–1 μl

TABLE 1 | Oligonucleotide primers for the meat species used in this study.

Primers	Genes	Sequence (5′-3′ direction)	Amplicons (bp)	Reference or source
Horse	NADH dehydrogenase subunit 5	CCCCGCTTCCTCCCTCTGA TAGGTATGGTTATTTCCGGGACG	148	This study
Pigeon	NADH dehydrogenase subunit 5	GGCCCAGAAAGCATCACCTC ATTGGTATAGCGATTAGGGACAG	218	This study
Camel	16S rRNA	CTAGCCCAGAAAATACCACAT CATAGACGAGTTCGCTCCGTA	283	This study
Rabbit	NADH dehydrogenase subunit 5	AATCCGCTTCTACCCCTTG TATACCTGTGAGGGCCAGACT	370	This study
Ostrich	16S rRNA	AGCGCCCTCTAGCTCATCC GCTGCTTTAGGGCCAACGTG	536	This study
Beef	Cytochrome c oxidase subunit I	ATGAGCCCACCATATATTCACT TGTCGTGGTTAAGTCTACAGTCA	610	This study
Turkey	Cytochrome c oxidase subunit II	AGTTGACCACCGTATAGTAGTCC TCGTCCTGGGATTGCATCTGTCT	124	This study
Dog	D-loop	CCCTTGCTCGTAATGTCCCT CGAGATGTCCCATTTGCGAGA	149	This study
Chicken	12S rRNA	CAGGTATCAGGCACACTCAGC CACTCTTTACGCCGGGTAGC	196	This study
Duck	NADH dehydrogenase subunit 6	CCACGCGAATAAAGCATAGCC TTTCGTTTGTAGCCCTGGTG	277	This study
Cat	Cytochrome c oxidase subunit I	TCTTAGCAGCGGGAATCACT AAGAGTAGCCAGTCAACTAAACA	380	This study
Goose	Cytochrome b	TCGCCTTCTCCTCAGTAGCTC TGTCGCAGTCTGATACGATT	468	This study
Eukaryotes	12S rRNA	CAACTGGGATTAGATACCCCACTAT GAGGGTGACGGGCGGTGTGT	456	(24)
Eukaryotes	16S rRNA	AAGACGAGAAGACCCTATGGA GATTGCGCTGTTATCCCTAGGGTA	240	(25)
Eukaryotes	18S rRNA	AGGATCCATTGGAGGGCAAGT TCCAACTACGAGCTTTTTAACTGCA	99	(26)

EasyTaq DNA Polymerase (5 units μl^{-1}),0.5 μl each primer of all six species (10 μM),1 μl genomic DNA of each species at indicated concentrations from 10 to 0.1 ng μl^{-1}, and refilled ddH_2O to 25 μl. Using the same PCR amplification condition as that of simplex PCR, a two-tube hexaplex PCR assay was developed using two sets of six species-specific primer pairs and corresponding DNA mixture of six species in two tubes. All PCR fragments were amplified using T100 Thermal Cycler (Bio-Rad, Germany). PCR products were loaded into 4% agarose gel using 4S GelRed Nucleic Acid Stain and were visualized by Gel Doc XR + System with Image Lab Software (BIO-RAD) (16).

Sequencing of Polymerase Chain Reaction Products

Deoxyribonucleic acid (DNA) sequencing was performed as previously described with some modifications (17). The PCR product was isolated, purified, and then cloned into a *pEASY*®-T5 zero cloning vector (TransGen Biotech Co., Ltd., Beijing, China). PCR amplification with vector primers M13F and M13R was carried out using the template of plasmid DNA and then sequenced. Sequencing was accomplished with an automated DNA sequencer (Applied Biosystems, Foster City, CA, United States). The DNA base composition of the sequence was determined by a BLAST search against the NCBI nucleotide database.

Specificity, Sensitivity, and Reproducibility of the Primers

The specificity of each primer pair was assessed using template DNA extracted from the twelve species by simplex and multiplex PCR assays. The results were run on 4% agarose gel and then visualized for proper amplification. The sensitivity of multiplex PCR was determined by g serial dilutions of the premixed genomic DNA templates of six target species in each tube reaction. Ten concentrations ranging from 10 to 0.01 ng and species-specific primers of six species were used for PCR amplification. The limit of detection and dynamic range were analyzed through 4% agarose gel and electropherograms. For the reproducibility test, meat samples of all the species were boiled at 97–99°C for 30 min. Other meat samples of all the species were, respectively microwave-cooked at 750 W for 10 min. After both heat processing treatments, genomic DNA of each species was extracted and used for PCR amplification to examine reproducibility (17).

TABLE 2 | Results of multiplex PCR assay performed on commercial meat products.

Products (number)	Detected species											
	Horse	**Pigeon**	**Camel**	**Rabbit**	**Ostrich**	**Beef**	**Turkey**	**Dog**	**Chicken**	**Duck**	**Cat**	**Goose**
Beef (15)												
Meat balls (5)						5/5			1/5[a], 1/5[b]	1/5[b]		
Meat slices (5)						5/5			1/5[a]	1/5[b]		
Kebab (5)	1/5[a]				1/5[b]	5/5						
Horse (10)												
Meat slices (2)	2/2		1/2[a]									
Sausages (5)	5/5								1/5[a]	1/5[a], 1/5[b]		
Jerky (3)	3/3											
Camel (10)												
Drysaltery (3)			3/3		1/3[a]							
Dry meat stripe (2)			2/2									
Jerky (5)	1/5[a]		5/5									
Ostrich (10)												
Drysaltery (3)					3/3		1/3[a]					
Jerky (4)		1/4[b]			4/4				1/4[a]			
Sauce braised meat (3)					3/3							
Turkey (10)												
Cutlets (5)							5/5		1/5[a]			1/5[b]
Meat slices (3)							3/3		1/3[a]			
Jerky (2)							2/2					

In each row, the meat samples labeled with same letter (a or b) represent the identical meat samples, while different letters indicate a difference in meat samples.

Commercial Samples

A total of 55 samples including raw and heat processing of meat balls (5), meat slices (10), kebab (5), sausages (5), jerky (14), drysalter (6), dry meat stripe (2), cutlets (5), and sauce braised meat (3) were purchased from markets as well as online supermarket platforms. Genomic DNA of each sample was isolated and used as the template for meat authentication using the proposed hexaplex PCR method. Detailed information of the samples is listed in **Table 2**.

RESULTS

Specificity of Polymerase Chain Reaction Assay

To obtain species-specific primers for horse, pigeon, camel, rabbit, ostrich, beef, turkey, dog, chicken, duck, cat, and goose, candidate primers for each of the animal species were designed using the Oligo 7.0 and BLAST programs. First, the specificity of each species-specific primer pair was individually checked by simplex PCR assays through cross-amplification reaction with 16 non-target species including all the twelve species indicated, and all of which showed no cross-reactivity (data not shown). PCR amplification showed distinct bands with a predicted size of 148 bp, 218 bp, 283 bp, 370 bp, 536 bp, and 610 bp for the horse, pigeon, camel, rabbit, ostrich, and beef species, respectively (**Supplementary Figure 1A**). As positive controls, three universal eukaryotic primer pairs, which target 18S rRNA, 16S rRNA, and 12S rRNA genes, were employed in one tube PCR reaction. As seen in **Supplementary Figure 1B**, all the meat samples generated a predicted size of 99 bp, 240 bp, and 456 bp with similar intensities, suggesting good quality of template DNAs of each meat resource. In addition, using genomic DNA of single species as the template, the target band could be produced in the presence of a complete mixture of six primer pairs but not five non-target primer pairs (**Supplementary Figure 1C**). Likewise, a species-specific primer pair produced the target band in the presence of DNA mixture of six meat species but not five non-target species (**Supplementary Figure 1D**).

The primer specificity for turkey, dog, chicken, duck, cat, and goose was also investigated. As shown in **Supplementary Figure 2A**, the PCR amplification shows the predicted bands for turkey (124 bp), dog (149 bp), chicken (196 bp), duck (277 bp), cat (380 bp), and goose (468 bp). Using three universal eukaryotic primer pairs, the PCR assay demonstrated that good quality of genomic DNA was present in all six meat samples, ensuring the accuracy of the experiment (**Supplementary Figure 2B**). Using the genomic DNA of single species as the template, PCR amplification generated the target band in the presence of a complete mixture of six primer pairs but not five non-target ones (**Supplementary Figure 2C**). PCR amplification with each species-specific primer pair generated the target band in the presence of the template DNA mixture of six meat species but not five non-target species (**Supplementary Figure 2D**).

To further confirm the accuracy of PCR amplification, amplicons for all the species in **Supplementary Figures 1D, 2D** are individually cloned and sequenced. Target species with 100% accuracy was verified by a BLAST search against the NCBI nucleotide database. Partial data of DNA sequencing for

each target species are shown in **Supplementary Figures 3A,B**. Collectively, all the experiments conclude that the designed primers are highly specific and are adequate for food inspection.

Sensitivity of Multiplex Polymerase Chain Reaction Assay

After optimization of simplex PCR for individual species, multiplex PCRs starting from duplex, triplex, tetraplex, and pentaplex were attempted to be constructed, and a two-tube hexaplex PCR assay was ultimately developed using six pairs of species-specific primers in each tube. To reveal the limit of detection (LOD) and dynamic range of the two hexaplex PCR assays, PCR assays were performed with the serial concentration of each DNA template ranging from 10 to 0.01 ng per PCR reaction. Visible bands were matched with intact peak patterns, while weak bands were equipped with defective peak patterns. As template DNA amounts of each species were less than 0.1 ng, PCR fragments were almost invisible for the horse, pigeon, camel, rabbit, ostrich, and beef species in one tube

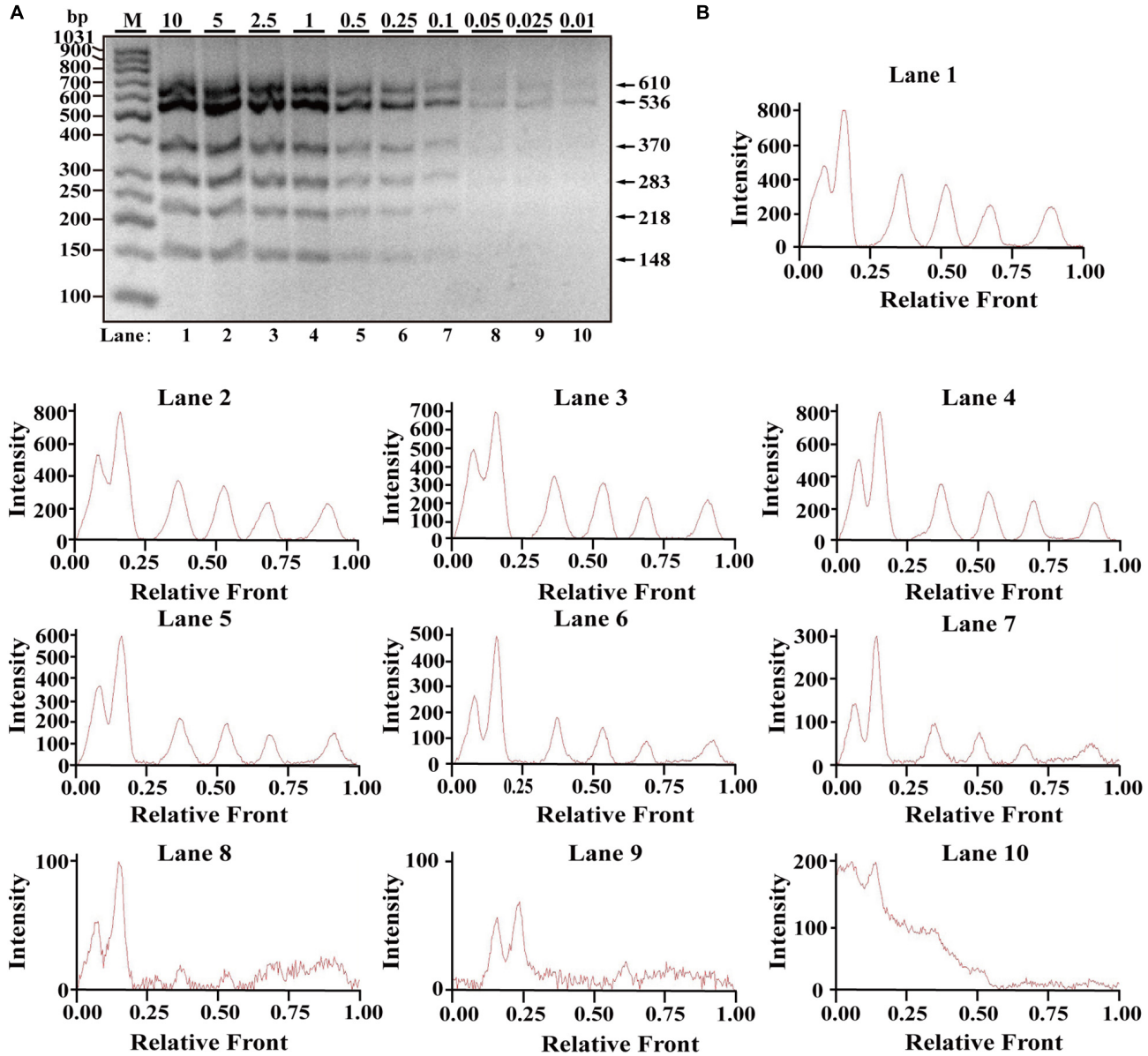

FIGURE 1 | Validation of the sensitivity of the one-tube hexaplex PCR assay. **(A)** Gel image of multiplex PCR fragments amplified with six primer pairs and DNA mixture of six species: horse, pigeon, camel, rabbit, ostrich, and beef under the indicated concentration in a single PCR reaction. **(B)** Using Image Lab Software, electropherograms were drawn based on bands. Lanes 1–10 are represented labels of 10, 5, 2.5, 1, 0.5, 0.25, 0.1, 0.05, 0.025, and 0.01 in **(A)**. The value of number in the horizontal line means the relative position of peaks distant from the top of agarose gel. The value of number at the vertical line means the fluorescent intensity of PCR fragments using 4S GelRed Nucleic Acid Stain. Lane M is ladder DNA.

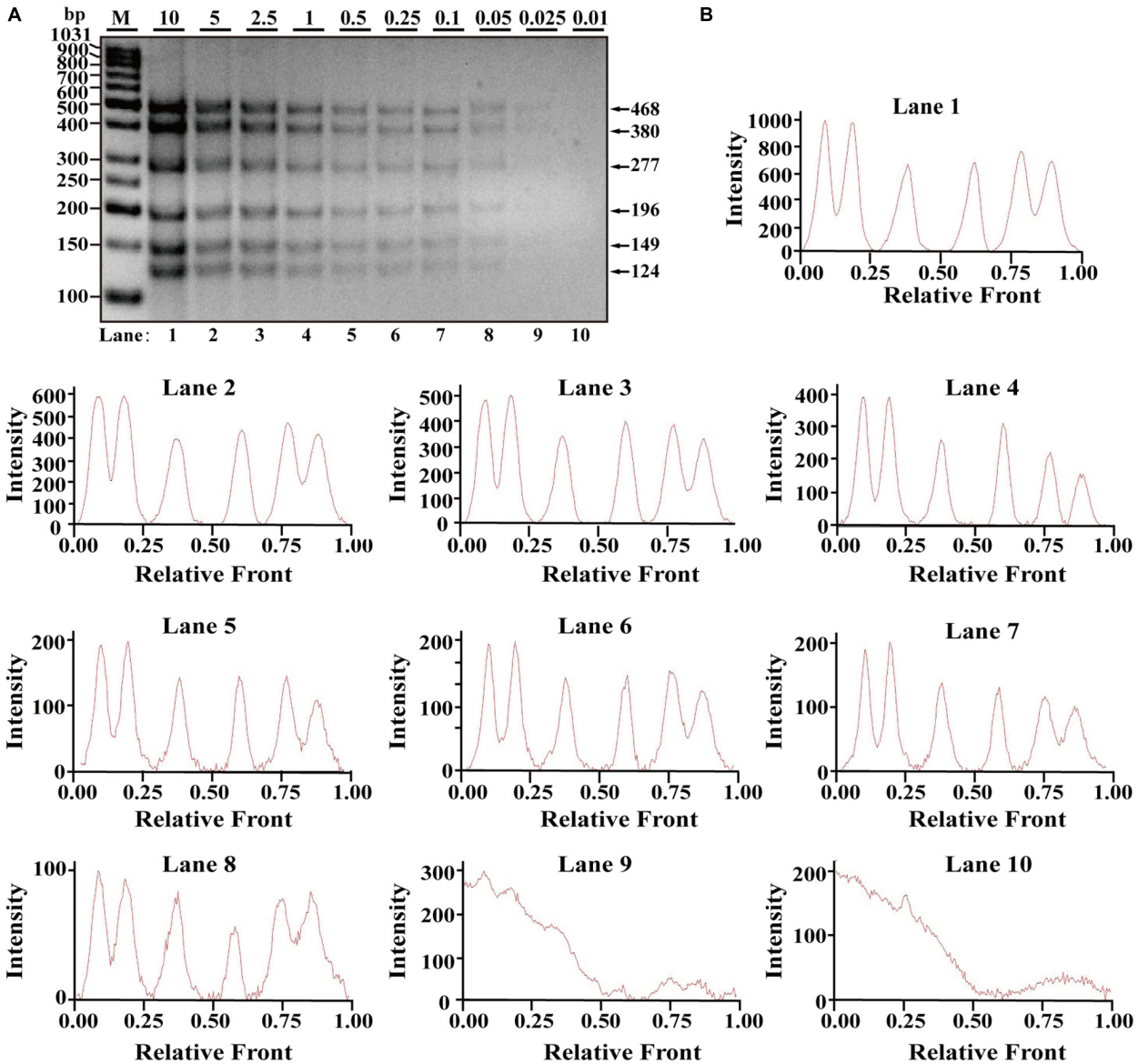

FIGURE 2 | Validation of the sensitivity of the one-tube hexaplex PCR assay. **(A)** Gel image of multiplex PCR fragments amplified with six primer pairs and DNA mixture of six species: turkey, dog, chicken, duck, cat, and goose under the indicated concentration in a single PCR reaction. **(B)** Using Image Lab Software, electropherograms were drawn based on bands. Lanes 1–10 are represented labels of 10, 5, 2.5, 1, 0.5, 0.25, 0.1, 0.05, 0.025, and 0.01 in **(A)**. The value of number in the horizontal line means the relative position of peaks distant from the top of agarose gel. The value of number at the vertical line means the fluorescent intensity of PCR fragments using 4S GelRed Nucleic Acid Stain. Lane M is ladder DNA.

reaction (**Figure 1A**). On the whole, fluorescence intensities were gradually decreased by reducing the content of genomic DNA template, reflecting their reduced PCR products. With decreasing fluorescence intensity, there were six visible peak patterns in lines 1–7 but not lines 8–10 (**Figure 1B**), suggesting that the threshold value of genomic DNA was about 0.1 ng. Therefore, the LOD of hexaplex PCR method for the horse, pigeon, camel, rabbit, ostrich, and beef species was approximately 0.1 ng in one tube reaction. Likewise, it was concluded that the detection threshold of the hexaplex PCR method for turkey, dog, chicken, duck, cat, and goose in the other tube reaction was about 0.05 ng template DNA, which has six bands as shown in **Figure 2A** and six peaks as shown in **Figure 2B**.

Reproducibility of Polymerase Chain Reaction Assay in Heat-Processed Meat

To determine the availability of primers for detecting animal origin in thermally processed meat, both boiled and microwave-cooked treatments were selected to process raw meat tissues. The genomic DNA of each species was isolated from heat processed

meat tissues. PCR amplification generated the expected PCR products with 100% accuracy as that of raw meat samples in heat processing animal species of horse, pigeon, camel, rabbit, ostrich and beef, respectively (**Supplementary Figures 4A,B**). Similar results are obtained from PCR amplification of the turkey, dog, chicken, duck, cat, and goose species, as shown in **Supplementary Figures 4C,D**. Taken together, the results suggest that the designed primers are qualified for detecting meat ingredients in real-world meat products.

Application of Multiplex Polymerase Chain Reaction Assay in Commercial Meat Products

Since some food items such as meatballs, meat slices, kebab, drysalter, and jerky are highly popular and have high consumption rate, 55 commercial samples were randomly selected for multiplex PCR analysis. As summarized in **Table 2**, most of the meat samples declared to be having 100% pure meat content contained the identical ingredients as labeled. However, some shocking findings that samples were adulterated with extra ingredients were unmasked. As illustrated, 6 of 15 (40%) beef samples, 3 of 10 (30%) horse samples, 2 of 10 (20%) camel samples, 3 of 10 (30%) ostrich samples, and 3 of 10 (30%) turkey samples contained meat ingredients that were unlisted. From this survey, the incidence of meat frauds is still rampant until now, especially for some kinds of poultry meat that are fraudulently mixed or counterfeited with red meat. The survey further corroborates the availability of this two-tube hexaplex PCR assay in authenticating commonly consumed meat ingredients.

DISCUSSION

The multiplex PCR technique is a highly effective method for detecting multiple targets in a single platform, which dramatically cuts the cost and time of analysis through a simple agarose gel analysis (18–20). Notably, with the increase of primers and multiplicity of PCR reaction, mutual interference of PCR components causes lower efficiency and even the failure of amplification (7). Through analyses of some bodies of literature recently published, multiplex PCRs are summarized and shown in **Table 3**. Multiplex PCRs such as duplex, triplex, tetraplex, pentaplex (quintuple), and hexaplex (sextuple) have been broadly reported for meat authentication, while most multiplex PCR assays have authenticated less than eight meat species. To our knowledge, relatively little is known about multiplex PCRs that discriminate more than ten animal species. Although two studies have authenticated ten and fourteen animal species, they are achieved by two-tube multiplex PCR assays (7, 17). Notably, fourteen animal species were detected by two-tube independent pentaplex PCR assays with ten pairs of primers, three of them used degenerate primers (7). However, the degenerate primers inaccurately distinguish sheep and goat in ovis, dog, fox, and raccoon-dog in Canidae, and chicken and duck in

TABLE 3 | Comparative analysis of multiplex PCR assays for the identification of meat species.

Multiplex PCR type	Species number	Detection items	Detection limit	Detection method	References or source
Multiplex (two-tube)	12	Horse, pigeon, camel, rabbit, ostrich, beef; turkey, dog, chicken, duck, cat, and goose	0.05–0.1 ng DNA	Gel	This study
Multiplex (two-tube)	14	Cattle, donkey, canidae (dog, fox, raccoon-dog), deer, horse; pig, ovis (sheep, goat), poultry (chicken, duck), cat, and mouse	0.02–0.2 ng DNA	Chip	(7)
Multiplex (two-tube)	10	Beef, sheep, pork, chicken, turkey; cat, dog, mouse, rat, and human	30 pg DNA	Gel	(17)
Octuplex	8	Dog, chicken, cattle, pig, horse, donkey, fox, and rabbit	0.05 ng/μL DNA	Gel	(25)
Heptaplex (RFLP)	7	Beef, buffalo, chicken, duck, goat, sheep, and pork	0.5% for each species	Chip	(4)
Septuple PCR	7	Turkey, goose, pig, sheep, beef, chicken, and duck	0.01–0.05 ng DNA	Gel	(14)
Multiplex	6	Mutton, pork, duck, chicken, horse, cat	9.1% of each species	Gel	(27)
Multiplex	6	Goat, chicken, cattle, sheep, pig, horse	0.25 ng	Gel	(28)
Multiplex	5	Sheep/goat, bovine, chicken, duck, and pig	0.5 ng	Gel	(19)
Pentaplex	5	Dog, duck, buffalo, goat, sheep	0.1–0.32 ng DNA	Gel	(13)
Quadruplex	4	Chicken, mutton, beef, pork	16 pg DNA, 0.01% of each species	Gel	(29)
Quadruple	4	Fox, mink, or raccoon in beef, and mutton	1% for each species	Gel	(30)
Multiplex	4	Buffalo, cattle, pork, and duck	1 pg DNA, 0.1% for each species	Gel	(31)
Quadruple	4	Beef, pork, mutton, and duck	0.1 ng DNA	Gel	(32)
Tetraplex	3	Pig, cattle, and fish	0.001–0.1 ng DNA	Gel	(33)
Multiplex	3	Chicken, duck, and goose	0.05 ng DNA or 1% for each species	Gel	(34)
Multiplex	2	Cattle, horse	0.05 ng DNA	Gel	(3)
Multiplex	2	Cattle, buffalo	2.23–2.31 ng/μL DNA	Gel	(35)

Chip, microchip electrophoresis; Gel, agarose gel electrophoresis.

poultry (7). Our previous study has developed a septuple PCR assay for identifying seven species of turkey, goose, pig, sheep, beef, chicken, and duck in one tube reaction, but it fails to simultaneously authenticate more than seven species (14). In this research, multiplex PCRs have also been found to confront technological challenge, because multiplex PCR with increasing species-specific primers in one reaction sometimes generates loss or unexpected bands. Through screening new species-specific primers and optimizing species combination, a two-tube hexaplex PCR method was ultimately established for accurate authentication of twelve meat species.

Nevertheless, multiplex PCR occasionally causes artifacts because of contamination by alien DNA even at a very low level and generates non-specific target amplification (21). To eliminate the possibility, each species-specific primer pair was individually used for amplifying target species using the DNA mixture of all six species as a template in one PCR reaction. PCR products were subsequently connected into a cloning vector for DNA sequencing, which is highly promising and reliable for determination of nucleotide base sequences. BLAST analysis confirmed species-specific PCR amplification for all the species with 100% accuracy, suggesting that the developed system can accurately amplify each target. Application of the two-tube hexaplex PCR assay in commercial meat products further validated the availability of the developed system. In accordance with other reports, meat fraud with cheap or poor-quality meat has become common worldwide (4, 7). Based on this, accurate verification of meat ingredients is crucial to safeguard consumers from meat fraud and thereby contributes to establish discipline in food business.

According to the data shown in **Table 2**, the proposed method reveals the phenomenon that commercial meat products are frequently adulterated. However, they showed morphological and physical features similar to that of pure meat, indicating that the practice of meat adulteration has been ingeniously performed. Therefore, a reliable analytical technique with high sensitivity is required for meat authentication. In this study, the LOD of the two-tube hexaplex PCR assay reached up to0.05–0.1 ng. Compared with the LOD of multiplex PCR assays shown in **Table 3**, the developed technique is qualified for discriminating meat source. Molecular authentication or molecular traceability of meat species, which is based on the developed multiplex PCR amplification of genomic DNA, has provided an accurate analysis of meat ingredients (22, 23). In this regard, the proposed PCR method targeting mtDNA to authenticate twelve animal species in food products would be especially useful.

CONCLUSION

This study provides a two-tube independent hexaplex PCR assay for molecular authentication of meat fraud, which is a reliable, low-cost, and rapid approach, and offers unambiguous detection and discrimination of twelve animal species. Furthermore, the technique has been corroborated for its accuracy, specificity, sensitivity, and applicability in commercial meat products. The proposed method is of great importance and will have a good application foreground.

DATA AVAILABILITY STATEMENT

The original contributions presented in the study are included in the article/**Supplementary Material**, further inquiries can be directed to the corresponding authors.

AUTHOR CONTRIBUTIONS

ZC, QL, and DP: conception and design of the investigation and study. QL, GZ, XY, XxZ, SZ, XqZ, ZW, and ZC: completion of the experiments. QL, GZ, and ZC: evaluation and analysis of the results. QL, GZ, ZC, and DP: manuscript writing. QL, GZ, XY, XxZ, SZ, XqZ, ZW, ZC, and DP: final approval of the manuscript. All authors contributed to the article and approved the submitted version.

FUNDING

This study was financially supported by the National Natural Science Foundation of China (NSFC) (31901668), National Key R&D Program of China (2021YFD2100104), Natural Science Foundation of Zhejiang Province (LY22C200002), Science and Technology Programs of Zhejiang (2019C02085), Modern Agricultural Technical Foundation of China (CARS-42-25), Scientific Research Fund of Zhejiang Provincial Education Department (Y201940932), Natural Science Foundation of Ningbo (2019A610436 and 2021J108), and School Research Project in Ningbo University (XYL19011).

SUPPLEMENTARY MATERIAL

The Supplementary Material for this article can be found online at: https://www.frontiersin.org/articles/10.3389/fnut.2022.813962/full#supplementary-material

REFERENCES

1. Uddin SMK, Hossain MAM, Chowdhury ZZ, Johan MRB. Short targeting multiplex PCR assay to detect and discriminate beef, buffalo, chicken, duck, goat, sheep and pork DNA in food products. *Food Addit Contam A.* (2021) 38:1273–88. doi: 10.1080/19440049.2021.1925748
2. Li YC, Liu SY, Meng FB, Liu DY, Zhang Y, Wang W, et al. Comparative review and the recent progress in detection technologies of meat product adulteration. *Compr Rev Food Sci Food Saf.* (2020) 19:2256–96. doi: 10.1111/1541-4337.12579
3. Wang WJ, Liu JJ, Zhang QD, Zhou X, Liu B. Multiplex PCR assay for identification and quantification of bovine and equine in minced meats using

novel specific nuclear DNA sequences. *Food Control.* (2019) 105:29–37. doi: 10.1016/j.foodcont.2019.05.016
4. Uddin SMK, Hossain MAM, Chowdhury ZZ, Johan MR. Detection and discrimination of seven highly consumed meat species simultaneously in food products using heptaplex PCR-RFLP assay. *J Food Compos Anal.* (2021) 100:103938. doi: 10.1016/j.jfca.2021.103938
5. Premanandh J. Horse meat scandal – a wake-up call for regulatory authorities. *Food Control.* (2013) 34:568–9. doi: 10.1016/j.foodcont.2013.05.033
6. Li TT, Jalbani YM, Zhang GL, Zhao ZY, Wang ZY, Zhao XY, et al. Detection of goat meat adulteration by real-time PCR based on a reference primer. *Food Chem.* (2019) 277:554–7. doi: 10.1016/j.foodchem.2018.11.009
7. Li JC, Li JP, Xu SG, Xiong SY, Yang JN, Chen X, et al. A rapid and reliable multiplex PCR assay for simultaneous detection of fourteen animal species in two tubes. *Food Chem.* (2019) 295:395–402. doi: 10.1016/j.foodchem.2019.05.112
8. Li JC, Li JP, Liu RX, Wei YX, Wang SW. Identification of eleven meat species in foodstuff by a hexaplex real-time PCR with melting curve analysis. *Food Control.* (2021) 121:107599. doi: 10.1016/j.foodcont.2020.107599
9. Tanabe S, Miyauchi E, Muneshige A, Mio K, Sato C, Sato M. PCR method of detecting pork in foods for verifying allergen labeling and for identifying hidden pork ingredients in processed foods. *Biosci Biotech Biochem.* (2007) 71:1663–7. doi: 10.1271/bbb.70075
10. El Sheikha AF, Mokhtar NFK, Amie C, Lamasudin DU, Isa NM, Mustafa S. Authentication technologies using DNA-based approaches for meats and halal meats determination. *Food Biotechnol.* (2017) 31:281–315. doi: 10.1080/08905436.2017.1369886
11. Mohamad NA, El Sheikha AF, Mustafa S, Mokhtar NFK. Comparison of gene nature used in real-time PCR for porcine identification and quantification: a review. *Food Res Int.* (2013) 50:330–8. doi: 10.1016/j.foodres.2012.10.047
12. Liu GQ, Luo JX, Xu WL, Li CD, Guo YS, Guo L. Improved triplex real-time PCR with endogenous control for synchronous identification of DNA from chicken, duck, and goose meat. *Food Sci Nutr.* (2021) 9:3130–41. doi: 10.1002/fsn3.2272
13. Thanakiatkrai P, Dechnakarin J, Ngasaman R, Kitpipit T. Direct pentaplex PCR assay: an adjunct panel for meat species identification in Asian food products. *Food Chem.* (2019) 271:767–72. doi: 10.1016/j.foodchem.2018.07.143
14. Cai ZD, Zhou S, Liu QQ, Ma H, Yuan XY, Gao JQ, et al. A simple and reliable single tube septuple PCR assay for simultaneous identification of seven meat species. *Foods.* (2021) 10:1083. doi: 10.3390/foods10051083
15. Ali ME, Razzak MA, Abd Hamid SB, Rahman MM, Al Amin M, Abd Rashid NR, et al. Multiplex PCR assay for the detection of five meat species forbidden in Islamic foods. *Food Chem.* (2015) 177:214–24. doi: 10.1016/j.foodchem.2014.12.098
16. Yaman BN, Celik PA, Mutlu MB, Cabuk AA. Combinational analysis of acidophilic bacterial diversity of an iron-rich environment. *Geomicrobiol J.* (2020) 37:877–89. doi: 10.1080/01490451.2020.1795320
17. Prusakova OV, Glukhova XA, Afanas'eva GV, Trizna YA, Nazarova LF, Beletsky IP. A simple and sensitive two-tube multiplex PCR assay for simultaneous detection of ten meat species. *Meat Sci.* (2018) 137:34–40. doi: 10.1016/j.meatsci.2017.10.017
18. Iqbal M, Saleem MS, Imran M, Khan WA, Ashraf K, Zahoor MY, et al. Single tube multiplex PCR assay for the identification of banned meat species. *Food Addit Contam B.* (2020) 13:284–91. doi: 10.1080/19393210.2020.1778098
19. Wang WJ, Wang XK, Zhang QD, Liu ZH, Zhou X, Liu B. A multiplex PCR method for detection of five animal species in processed meat products using novel species-specific nuclear DNA sequences. *Eur Food Res Technol.* (2020) 246:1351–60. doi: 10.1007/s00217-020-03494-z
20. Mafra I, Ferreira IMPLVO, Oliveira MBPP. Food authentication by PCR-based methods. *Eur Food Res Technol.* (2008) 227:649–65. doi: 10.1007/s00217-007-0782-x
21. Doosti A, Dehkordi PG, Rahimi E. Molecular assay to fraud identification of meat products. *J Food Sci Technol.* (2014) 51:148–52. doi: 10.1007/s13197-011-0456-3
22. Mansouri M, Khalilzadeh B, Barzegari A, Shoeibi S, Isildak S, Bargahi N, et al. Design a highly specific sequence for electrochemical evaluation of meat adulteration in cooked sausages. *Biosens Bioelectron.* (2020) 150:111916. doi: 10.1016/j.bios.2019.111916
23. Mokhtar NFK, El Sheikha AF, Azmi NI, Mustafa S. Potential authentication of various meat-based products using simple and efficient DNA extraction method. *J Sci Food Agr.* (2020) 100:1687–93. doi: 10.1002/jsfa.10183
24. Vaithiyanathan S, Vishnuraj MR, Reddy GN, Kulkarni VV. Application of DNA technology to check misrepresentation of animal species in illegally sold meat. *Biocatal Agric Biotechnol.* (2018) 16:564–8. doi: 10.1016/j.bcab.2018.10.012
25. Liu WW, Tao J, Xue M, Ji JG, Zhang YH, Zhang LJ, et al. A multiplex PCR method mediated by universal primers for the identification of eight meat ingredients in food products. *Eur Food Res Technol.* (2019) 245:2385–92. doi: 10.1007/s00217-019-03350-9
26. Martin I, Garcia T, Fajardo V, Rojas M, Pegels N, Hernandez PE, et al. SYBR-Green real-time PCR approach for the detection and quantification of pig DNA in feedstuffs. *Meat Sci.* (2009) 82:252–9. doi: 10.1016/j.meatsci.2009.01.023
27. Xu J, Zhao W, Zhu MR, Wen YJ, Xie T, He XQ, et al. Molecular identification of adulteration in mutton based on mitochondrial 16S rRNA gene. *Mitochondrial DNA A DNA Mapp Seq Anal.* (2016) 27:628–32. doi: 10.3109/19401736.2014.908377
28. Matsunaga T, Chikuni K, Tanabe R, Muroya S, Shibata K, Yamada J, et al. A quick and simple method for the identification of meat species and meat products by PCR assay. *Meat Sci.* (1999) 51:143–8. doi: 10.1016/S0309-1740(98)00112-0
29. Balakrishna K, Sreerohini S, Parida M. Ready-to-use single tube quadruplex PCR for differential identification of mutton, chicken, pork and beef in processed meat samples. *Food Addit Contam A.* (2019) 36:1435–44. doi: 10.1080/19440049.2019.1633477
30. Li XN, Guan YF. Specific identification of the adulterated components in beef or mutton meats using multiplex PCR. *J AOAC Int.* (2019) 102:1181–5. doi: 10.5740/jaoacint.18-0338
31. Wang LP, Hang XR, Geng RQ. Molecular detection of adulteration in commercial buffalo meat products by multiplex PCR assay. *Food Sci Tech Brazil.* (2019) 39:344–8. doi: 10.1590/fst.28717
32. He H, Hong X, Feng Y, Wang Y, Ying J, Liu Q, et al. Application of quadruple multiplex PCR detection for beef, duck, mutton and pork in mixed meat. *J Food Nutr Res.* (2015) 3:392–8. doi: 10.12691/jfnr-3-6-6
33. Sultana S, Hossain MAM, Zaidul ISM, Ali ME. Multiplex PCR to discriminate bovine, porcine, and fish DNA in gelatin and confectionery products. *LWT.* (2018) 92:169–76. doi: 10.1016/j.lwt.2018.02.019
34. Hou B, Meng XR, Zhang LY, Guo JY, Li SW, Jin H. Development of a sensitive and specific multiplex PCR method for the simultaneous detection of chicken, duck and goose DNA in meat products. *Meat Sci.* (2015) 101:90–4. doi: 10.1016/j.meatsci.2014.11.007
35. Dantas VV, Cardoso GVF, Araujo WSC, de Oliveira ACD, da Silva AS, da Silva JB, et al. Application of a multiplex polymerase chain reaction (mPCR) assay to detect fraud by substitution of bovine meat cuts with water buffalo meat in Northern Brazil. *Cyta J Food.* (2019) 17:790–5. doi: 10.1080/19476337.2019.1650832

Conflict of Interest: The authors declare that the research was conducted in the absence of any commercial or financial relationships that could be construed as a potential conflict of interest.

frontiers | Frontiers in Nutrition

ORIGINAL RESEARCH
published: 13 April 2022
doi: 10.3389/fnut.2022.846808

Effects of Quinoa Flour on Wheat Dough Quality, Baking Quality, and *in vitro* Starch Digestibility of the Crispy Biscuits

Yanrong Ma[1], Daying Wu[1], Lei Guo[1], Youhua Yao[2], Xiaohua Yao[2], Zhonghua Wang[1], Kunlun Wu[2], Xinyou Cao[3]* and Xin Gao[1]**

[1] State Key Laboratory of Crop Stress Biology in Arid Areas and College of Agronomy, Northwest A&F University, Yangling, China, [2] State Key Laboratory of Plateau Ecology and Agronomy, Qinghai Key Laboratory of Hulless Barley Genetics and Breeding, Qinghai Subcenter of National Hulless Barley Improvement, Qinghai University, Xining, China, [3] National Engineering Laboratory for Wheat and Maize, Key Laboratory of Wheat Biology and Genetic Improvement in North Yellow and Huai River Valley, Ministry of Agriculture, Crop Research Institute, Shandong Academy of Agricultural Sciences, Jinan, China

OPEN ACCESS

Edited by:
Qiang Xia,
Ningbo University, China

Reviewed by:
Marco Montemurro,
University of Bari Aldo Moro, Italy
Honghai Hu,
Institute of Food Science and Technology (CAAS), China

***Correspondence:**
Kunlun Wu
wklqaaf@163.com
Xinyou Cao
caoxinyou@126.com
Xin Gao
bestgaoxin@nwsuaf.edu.cn

Specialty section:
This article was submitted to Food Chemistry, a section of the journal Frontiers in Nutrition

Received: 31 December 2021
Accepted: 18 March 2022
Published: 13 April 2022

Citation:
Ma Y, Wu D, Guo L, Yao Y, Yao X, Wang Z, Wu K, Cao X and Gao X (2022) Effects of Quinoa Flour on Wheat Dough Quality, Baking Quality, and in vitro Starch Digestibility of the Crispy Biscuits. Front. Nutr. 9:846808. doi: 10.3389/fnut.2022.846808

Quinoa is a pseudo-cereal which has excellent nutritional and functional properties due to its high content of nutrients, such as polyphenols and flavonoids, and therefore quinoa serves as an excellent supplement to make healthy and functional foods. The present study was aimed to evaluate the quality characteristics of wheat doughs and crispy biscuits supplemented with different amount of quinoa flour. The results showed that when more wheat flour was substituted by quinoa flour, proportion of unextractable polymeric protein to the total polymeric protein (UPP%) of the reconstituted doughs decreased and the gluten network structure was destroyed at a certain substitution level. The content of B-type starch and the gelatinization temperature of the reconstituted flours increased. The storage modulus, loss modulus, development time, and stability time of the dough increased as well. Moreover, hardness and toughness of the formulated crispy biscuits significantly decreased. Analyses suggested that starch digestibility was reduced and resistant starch content increased significantly. Taken together, quinoa flour improved dough rheological properties, enhanced the textural properties, and increased resistant starch content in crispy biscuits, thus adding to high nutritional value.

Keywords: quinoa-wheat reconstituted system, crispy biscuits, starch physicochemical properties, dough rheological properties, *in vitro* starch digestibility

INTRODUCTION

Biscuits have become an indispensable bakery product for people worldwide due to their sensory attributes, convenience and countless varieties (1). However, biscuits are made from refined wheat flour, and thus they have unbalanced nutrients and a high glycemic index, disadvantages to patients with chronic diseases such as diabetes, obesity and hypertension (2). It is necessary to substitute part of wheat flour with other nutrition-fortifying flours to produce biscuits with optimal nutritional quality and low starch digestibility.

Quinoa (*Chenopodium quinoa* Willd.), known as a pseudo-cereal, is not only an excellent source of protein, starch, vitamins, and other basic nutrients, but also rich in functional nutrients such as polyphenols, flavonoids, and saponins compared to most cereal grains (3, 4). Despite its nutritional benefits, quinoa has a nutty taste, a different flavor from that of wheat products and its baking quality is poor (4). Therefore, quinoa alone is not a popular staple food. One of its potential usages is to incorporate into biscuit formulations as a supplement, and to improve their nutritional characteristics.

Utilization of quinoa in baked products is not popular owing to its lack of gluten protein to form viscoelastic dough. Dough properties are the dominant factors determining the baking attributes of wheat flour products (5). Rheological property of dough is usually an index of dough viscoelasticity measurement. When wheat flour is mixed with water, gluten proteins absorb water and expand to form gluten network, which confers unique viscoelastic properties on dough. However, crispy biscuits made from the reconstituted flours are expected to have the combined baking properties of wheat dough and the high nutritional properties of quinoa.

The composition and structure of gluten protein have a great role in the dough processing (6). Wheat gluten protein consists of glutenins and gliadins, and determines the viscoelastic behavior of dough. The glutenin polymers are classified into unextractable and extractable polymeric proteins (UPP and EPP) based on solubility in SDS solution (7). UPP%, as one of the commonly used indices to evaluate wheat protein quality, has a positive correlation with dough rheological properties (7, 8). Therefore, it is very promising to introduce this parameter into other non-wheat crops to analyze protein characteristics. UPP% has been used to analyze the protein quality characteristics of hulless barley-wheat reconstituted flour and UPP% of wheat-hulless barley system decreased with the increase of hulless barley proportion (9). The performance of gluten microstructure affects dough behaviors during the dough formation process (10), which can be characterized by the parameters i.e., protein area, protein junctions, and lacunarity used in protein network analysis (11, 12). However, the previous studies have rarely quantitatively analyzed the effect of quinoa supplementation on the microstructure of wheat doughs.

Starch is also a primary ingredient of dough, which is mainly responsible for pasting and thermal properties, water absorption and stability of dough structure, and consequently biscuit quality (13–15). Physicochemical properties of starch are also crucial factors affecting the quality of quinoa products (16). Starch granules with different sizes contribute differently to the dough rheological behavior, and the smaller-sized (B-type) granules improve wheat dough rheological properties (17, 18). Quinoa has a rather low apparent amylose content (4–25%) (19) but high content of super-long-chain amylopectin (20). Apparent amylose affects starch physicochemical properties, including structures, thermal and pasting properties and digestibility of starch (21). Starch is divided as rapidly digestible starch (RDS) (digested within 20 min), slowly digestible starch (SDS) (digested between 20 and 120 min) and resistant starch (RS) (digested beyond 120 min) (22) based on their digestion rate. White bread contains a high content of RDS which leads to an increase in postprandial glucose level during digestion (23). As RS can resist the decomposition of enzymes and slow release of glucose, it plays an important role in regulating blood sugar (24). Therefore, the increase in RS content in diet can contribute to nourishment and human health. Although the nutritional composition and sensory properties of quinoa-fortified bakery products have been extensively investigated (25–28), few studies have reported the relationship between the physiochemical and rheological properties of a quinoa-wheat dough system for the purpose of biscuit bakery.

In this study, quinoa and a wheat variety P13 with weak gluten were used to investigate processing quality and food functional properties of quinoa-wheat doughs and biscuits. The physicochemical properties of starch and gluten, and rheological properties of the reconstituted doughs were determined; and the physicality, texture, sensory evaluation, and starch digestibility of the biscuits were characterized. The results of this study give a new insight into analyzing the processing quality of quinoa-wheat biscuits as functional products.

MATERIALS AND METHODS

Materials

A wheat variety, P13 with weak gluten, was selected as the source of base flour provided by Shandong Academy of Agriculture Sciences. The fine flour was acquired by milling in a Brabender Quadrumat Senior (Hackensack, United States) and then sieved (100 mesh). Quinoa flour was provided by Qinghai University with saponins removed. The samples were stored at 4°C for subsequent experiments.

Determination of Basic Nutritional Components of Quinoa and Wheat Flours

A Diode Array 7,250 NIR spectrometer analyzer (Perten Instrument AB, Sweden) was used to determine moisture and ash content for the quinoa and wheat flours. Protein content was measured according to the AACC methods 46-11A. Component analyses of each flour sample were conducted in triplicate.

Analysis of Functional Components

Extraction Procedure

Quinoa and wheat flour samples (0.5 g for each) were individually dissolved in 50% (v/v) ethanol (10 mL), and the mixture was extracted through reflux in 60°C water bath for 2 h. The total extract was obtained by repeating refluxing and stored at –20°C for further analyses. The sample extract was mainly used for the determination of total flavone and total polyphenol contents.

Total Polyphenol Content Assayed by Folin-Ciocalteau Reagent

Total polyphenol content in the two flour samples was measured using the Folin-Ciocalteau assay according to the method of Alvarez-Jubete et al. (29), applying minor changes. Sample extract (1 mL), Folin-Ciocalteau reagent (1 mL), 1 mM Na_2CO_3 (3 mL)

and distilled water (5 mL) were added into a 10 mL tube. The mixture was placed in the dark for 15 min at 25°C. The absorbance of the mixture was measured at 725 nm using a UV-2100 spectrophotometer (Shanghai, China). Each sample was measured three times. A standard solution was prepared using gallic acid and a calibration curve was obtained using a range of concentrations from 0.01 to 0.06 mg/mL. The results were expressed as gallic acid equivalent (GAE) in mg/g of dry-weight basis. Gallic acid was purchased from Sangon Biotech (Shanghai) Co., Ltd. (Shanghai, China).

Total Flavone Content Assay by Aluminum Nitrate Colorimetric Method

Total flavone content in the two samples was measured using the aluminum nitrate colorimetric method (30) with minor modifications. Sample extract (1.0 mL), 0.72 M $NaNO_2$ (0.15 mL), 0.27 M Al_2 $(NO_3)_3$ (0.15 mL), 1 M NaOH (2.0 mL) and 60% (v/v) ethanol (1.7 mL) were sequentially added into a 5 mL tube. The mixture was incubated for 15 min at 25°C. Absorbance of the mixture was measured at 517 nm using a UV-2100 spectrophotometer (Shanghai, China). Each sample was measured three times. A standard solution was prepared using rutin and a calibration curve was obtained with a range of concentrations from 0.75 to 75 μg/mL. Total flavone content was expressed as mg rutin equivalent (RE)/g of sample. Rutin was purchased from Sangon Biotech (Shanghai) Co., Ltd. (Shanghai, China).

Preparation of Flour Samples

The quinoa flour was added to substitute for wheat flour at five ratios: 10, 15, 20, 25, and 30% (w/w), and the reconstituted flours were designated as Q10, Q15, Q20, Q25, and Q30, with wheat base flour (Q0) as control. The reconstituted flours were kept at 4°C for subsequent experiments.

Analysis of Starch Physicochemical Properties

Isolation of Starch

Wheat starch was isolated from flour following the method reported by Zi et al. (18) with modifications. Wheat starch was extracted with 75% (v/v) ethanol and dried in an oven at 55°C overnight, ground into powder using a blender and sieved through a 200-mesh sieve. Starch in reconstituted flours was also isolated according to the above method.

Starch was isolated from quinoa flour as described by Contreras-Jiménez et al. (31), with minor modifications. The mixture of quinoa flour and distilled water (1:3, w/v) was maintained at 25°C for 1 d. The mixture was sieved (80 mesh), rewashed with 75% (v/v) ethanol and centrifuged at 1,503 × *g* for 20 min to remove the supernatant. The gray layer on the precipitated surface was scraped off and the remaining pellet (quinoa starch) at the bottom were rewashed with 75% (v/v) ethanol and centrifuged. The quinoa starch was obtained by washing the samples for 3–5 times and dried at 60°C for 1 day. The starch sample was ground into fine powder, sifted (200-mesh) and stored at 4°C for subsequent operations.

Measurement of Apparent Amylose Content

Apparent amylose content of individual quinoa and wheat starch sample was measured with an Amylose/Amylopectin Assay Kit (Megazyme International, Ireland Ltd., Bray, Ireland) in triplicate.

Analysis of Size Distribution of Starch Granules

The number of different sized starch granules was determined using a laser diffraction instrument (Microtrac S3500, United States) in triplicate according to the method of Yu et al. (32). The raw data was exported to calculate starch granule number distribution using Microsoft Excel 2019 software.

Thermal Properties

Thermal properties of starch samples were analyzed using a simultaneous thermogravimetric analyzer (STA 7200 RV, HITACHI, Japan) according to an established method (13). Starch sample (3.0 mg) was placed in an aluminum crucible (Ø 5.2 × 2.5 mm) on a sample holder. A blank pan was placed on the reference side sample holder. The experiment was carried out in a dynamic nitrogen environment in the range of 30–300°C, with temperature increasing at a rate of 10°C/min. Four parameters were determined by TA 7000 standard analysis software: onset temperature (T_0), peak of gelatinization temperature (T_p), conclusion temperature (T_c) and gelatinization enthalpy (ΔH_{gel}). The measurement was repeated thrice for each sample.

Determination of UPP% by Size-Exclusion High Performance Liquid Chromatography

UPP and EPP in the reconstituted flours were extracted referring to an established method (33). UPP% in the glutenin fraction was determined as the ratio between peak area of UPP and total peak area of UPP and EPP on an size-exclusion high performance liquid chromatography (SE-HPLC) system (Infinity 1260, Agilent, United States). Each sample was measured with two replicates and the average values were calculated.

Observation of Dough Microstructure

Microstructure of the reconstituted dough samples was visualized by confocal laser scanning microscopy (Olympus, Tokyo, Japan) as described by Bernklau et al. (11). Rhodamine B (0.01 mg/mL) was used for dying the protein. The dough samples were prepared in duplicate. Five independent images (512 × 512 pixel, 423.108 × 423.108 μm) were obtained for each dough sample. The AngioTool 64 version 0.6a (National Cancer Institute, Maryland, United States) was used to qualitatively analyze each image with the three parameters: protein area, protein junctions and lacunarity.

Determination of Dough Rheological Properties

A rheometer (RotoViscol, HAAKE, Germany) was used to determine the small amplitude oscillatory shear measurements of the reconstituted doughs, as described by Wang et al. (34). Storage modulus (G′), loss modulus (G″) and Tan δ (G″/G′) were determined in duplicate.

Mixing properties of the reconstituted doughs were determined using a Mixolab instrument (Mixolab2, Chopin, France) following the method reported by Niu et al. (35). Mixolab analysis was carried out in the process of heating and mixing, which determined the characteristics of gluten strength and starch viscosity of the dough. The dough mixing behaviors were recorded with the standard "Chopin+" protocol. Eleven dough mixing parameters were determined and calculated on the dough processing curve: water absorption (WA), dough development time (DDT), dough stability time (DS), dough development (C1), protein weakening (C2), starch peak viscosity (C3), trough viscosity (C4), final viscosity (C5), protein weakening (%), starch breakdown (C3-C4) and starch retrogradation (C5-C4). Two replications were conducted for each sample.

Preparation of the Formulated Crispy Biscuits and Analysis of Functional Components

Formulated crispy biscuits were made according to AACC method 10–50D with minor modifications. The dough samples were prepared by mixing 100 g reconstituted flour, 15 g shortening, 28.5 g erythritol, 2 g cream, 0.3 g salt, 0.07 g sodium bicarbonate, 0.3 g ammonium bicarbonate, 16 g egg and a proper amount of water (acquired from the Mixolab data: Q0: 10.22 mL; Q20: 10.54 mL; Q25: 10.61 mL; Q30: 10.60 mL) at 22°C, followed by resting for 10 min. Dough was pressed to a thickness of 5.0 mm with a rolling pin, cut with a 50 mm diameter die and baked in an oven at 200°C for 9 min. Two batches of biscuit replicas were prepared and cooled to 25°C for further analyses. Shortening, erythritol, cream, salt and egg were purchased from local supermarket. Additionally, "Observation of dough microstructure" and "Determination of dough rheological properties" were made using dough prepared as described in "Preparation of the formulated crispy biscuits."

The contents of total polyphenol and total flavone in biscuit samples were determined according to the method of quinoa and wheat flours in triplicate.

Evaluation of the Crispy Biscuit Baking Performance

Physical Properties Measurement

Biscuit samples were weighted using a laboratory balance (BSA223S, Sartorius, Germany) and their diameter and thickness were measured using a ruler. Two batches of biscuit replicas were measured and the mean was calculated.

Texture Measurement

Hardness and toughness of the formulated biscuits were measured using TVT Texture Analyzer (TVT 6700, Perten, Sweden) (28). The biscuit sample was placed stably on the center of the base on the testing table. The probe (P-BP70A) and the base (R-TPBR) were selected, the compression height was set to 15.00 mm; the pretest speed was 2.5 mm/s; the test speed was 2.0 mm/s and the posttest speed was 10.0 mm/s. The values are presented as the average of two measurements.

Sensory Evaluation

Sensory characteristics of crispy biscuit samples with different percentages were evaluated using untrained consumers (22–55 years old). The panelists were asked to evaluate the color, shape, structure, flavor and taste of samples and overall acceptability. All parameters were compared with control sample without quinoa addition (Q0). The ratings were on the 9-point hedonic scale ranging from 9 (like extremely) to 1 (dislike extremely) for each characteristic.

In vitro Starch Digestion Assay

Referring to Toutounji et al. (36), *in vitro* digestion of the formulated biscuits was analyzed by sequentially mixing biscuit sample (5 g), sodium acetate solution (40 mL, 0.2 M, pH 6.0) and working enzyme solution (5 mL, 0.66 mL 200 U/mL porcine pancreatin + 1 mL 100 U/mL amyloglucosidase, added up to 50 mL with buffer) in a test tube. The mixture (after being vortexed) was kept in a shaker at 37°C while rotating at 230 rpm for 2 h. The aliquot samples (0.2 mL at each time) of the mixture were collected at 0, 20 and 120 min. The test tubes were immediately heated in 100°C bath for 8 min to denature enzymes and centrifuged at 15,871 × *g* for 10 min. The glucose present in the supernatant was measured at each time point using a D-Glucose Assay kit (GOPOD method, K-GLUC 09/14, Megazyme International, Ireland Ltd., Bray, Ireland) and a UV-2100 spectrophotometer (Shanghai, China). Amyloglucosidase (Aspergillus niger, 100,000 U/mL) was purchased from Macklin Biochemical Co., Ltd. (Shanghai, China), and porcine pancreatin (4 USP) was purchased from Sigma-Aldrich Ltd. (St. Louis, MO, United States).

The relative proportions of RDS, SDS, and RS were calculated (4). The formulas are as follows:

$$RDS(\%) = (G_{20} - G_0) \times 0.9 \times 100$$

$$SDS(\%) = (G_{120} - G_{20}) \times 0.9 \times 100$$

$$RS(\%) = [(TS - RDS - SDS) \div TS] \times 100$$

where G_0, G_{20}, and G_{120} represent the content of glucose (%) released after 0, 20, and 120 min, respectively. TS is total starch content of the sample, and 0.9 is the conversion factor for glucose converted to anhydroglucose (the starch monomer unit).

Statistical Analysis

The resultant data were processed by SPSS software (SPSS Inc., version 22.0 United States). Differences between components of quinoa and wheat flour were assessed by Student's *t*-test ($P \leq 0.05$). The reconstituted flours were analyzed by one-way analysis of variance (ANOVA) and the differences among flour samples were evaluated by least significant difference (LSD) ($P \leq 0.05$).

RESULTS AND DISCUSSION

Compositional Characteristics of Quinoa and Wheat Flours

Ingredients of quinoa and wheat flours are shown in **Table 1**. The results shows that moisture and apparent amylose content of quinoa flour were lower than those of wheat flour. There was significant difference in protein content between quinoa and wheat flours. Quinoa has been used as a supplement to improve nutritional quality and to fortify food products (5). Previous studies have shown that the protein content of quinoa is generally higher than that of common grains (i.e., wheat, corn and barley) (3, 4). Ash content of quinoa flour is higher than that of wheat flour, which may be attributed to crop mineral content (31). The results of this study on compositional characteristics of quinoa and wheat flours are comparable to the previous results (31, 37). As for functional components, quinoa flour contains significantly more total polyphenol and total flavone than wheat flour does. It is generally accepted that polyphenols have beneficial effects on health and polyphenols are the most abundant antioxidants that can scavenge free radicals such as 2,2-diphenyl-1-picrylhydrazyl (DPPH) (38). Therefore, the above result indicates that quinoa has stronger antioxidant capacity than wheat does. Referred to in the earlier studies, total polyphenol content in quinoa ranged from 1.48 to 5.18 mgGAE/g (25, 39). Total flavone content in two quinoa varieties (Salcedo and Altiplano) was 8.69 and 9.14 mg RE/g, respectively (40). The results of the current study were different from the previous results: total polyphenol content in quinoa was relatively high, while total flavone content relatively low, which can be attributed to many factors, such as variations among crop varieties, environmental conditions and cultivation methods. In addition, different polyphenol and flavone extraction methods had significant effects on the results (29). Given that the current results demonstrate quinoa has higher nutritional values than wheat does, the study of the quinoa-wheat flour for biscuit baking is essential.

Analyses of Particle Size Distribution and Thermal Properties of Starch

Different methods can be applied to extract starch from quinoa and wheat, since wheat dough can be separated into starch suspension and gluten by hand washing while quinoa dough can't. The results of particle size distribution of starch showed that the content of B-type granules increased obviously when quinoa flour was added (**Table 2**), which is consistent with the previous findings that most of the quinoa starch granules are composed of small granules (diameter from 1 to 3 μm) (19, 20). Generally, A-type starch granules have higher amylose content (41, 42). As shown in **Table 1**, apparent amylose content of quinoa flour is lower than that of wheat flour, which can be explained that quinoa flour is composed of small granules. Given that more B-type granules can improve the dough rheological properties (9, 17), the reconstituted flours are expected to show better rheological behavior.

The gelatinization properties for wheat starch and quinoa-wheat starches were determined by STA, and the results are shown in **Table 2**. With the increasing proportion of quinoa flour, T_0, T_p, and T_c increase significantly, whereas ΔH_{gel} decreases (**Table 2**). A similar phenomenon has been observed when different proportions of quinoa flour were added to wheat flour and potato starch (27). Thermal properties of starch were closely related to the molecular architecture of crystalline regions of amylopectin (43). Since the long unit chains in amylopectin can allow more flexibility of double helices, which makes the crystalline region of amylopectin more orderly (13, 44), the high content of super-long-chain amylopectin in quinoa may be responsible for increasing gelatinization temperature of starch in the reconstituted flour system. Starch with higher

TABLE 1 | Compositional characteristics of quinoa and wheat flours.

Sample	Moisture (%)	Protein content (%)	Ash content (%)	Apparent amylose content (%)	Total polyphenol content (mgGAE/g)	Total flavone content (mgRE/g)
Quinoa flour	9.64 ± 0.43b	16.81 ± 1.75a	2.17 ± 0.04a	18.74 ± 1.63b	8.76 ± 0.71a	3.00 ± 0.52a
Wheat flour	11.28 ± 0.07a	10.68 ± 0.17b	0.93 ± 0.01b	28.36 ± 1.56a	3.88 ± 0.01b	0.27 ± 0.01b

Values followed by different letters in the same column are significantly different ($P < 0.05$).

TABLE 2 | B-type starch granule content and thermal properties of starch from the reconstituted flours.

Sample	B-type starch granule content (%)	Thermal property			
		T_0 (°C)	T_p (°C)	T_c (°C)	ΔH_{gel} (J/g)
Q0	68.85 ± 2.45b	31.75 ± 0.21e	64.15 ± 0.07c	74.70 ± 0.00c	86.05 ± 0.78a
Q10	68.92 ± 2.22b	31.80 ± 0.14e	63.55 ± 0.92d	73.05 ± 0.21d	82.90 ± 0.00b
Q15	69.95 ± 0.14b	32.05 ± 0.07d	63.95 ± 0.07c	75.15 ± 0.78c	81.05 ± 0.21c
Q20	71.82 ± 1.33b	32.40 ± 0.14c	64.15 ± 0.07c	77.50 ± 0.71b	78.10 ± 2.55d
Q25	72.91 ± 2.15b	32.90 ± 0.00b	65.40 ± 0.00b	77.65 ± 0.21b	74.55 ± 0.78e
Q30	79.07 ± 1.54a	33.50 ± 0.28a	68.45 ± 0.35a	78.85 ± 0.21a	77.75 ± 0.64d

Values followed by different letters in the same column are significantly different ($P < 0.05$).
T_0, onset temperature; T_p, peak of gelatinization temperature; T_c, conclusion temperature; ΔH_{gel}, gelatinization enthalpy.

gelatinization temperature possesses improved molecular order and crystallinity, which requires more energy for gelatinization, and consequently exhibits delayed gelatinization. Different particle size distribution may also cause differences in starch thermal properties. Compared with A granules, B granules showed higher T_0, T_p, and T_c, but lower ΔH_{gel}. With the increase of B/A ratio, gelatinization temperature of mixed starches increased while the ΔH_{gel} decreased (45, 46). Taken together, it can be inferred that the increase of gelatinization temperature and the decrease of ΔH_{gel} may be ascribable to the increase of B-type content in the reconstituted systems.

Analyses of UPP% and Gluten Network Structure of Reconstituted Flours

UPP% is often used as an index to evaluate the wheat quality (6, 9), and in this study it is introduced to evaluate the quinoa quality. Consequently, the UPP% of quinoa-wheat flours was explored and its effect on the dough strength investigated. SE-HPLC measurements showed that the UPP% of the reconstituted flours decreases by 6.27–16.14% compared with Q0, and the graph shows an S-shaped downward trend (**Supplementary Figure 1A**). The results showed addition of quinoa flour significantly lower UPP%, indicating quinoa weakened wheat dough strength. Accordingly, the microstructure of dough was quantitatively analyzed by AngioTool to explore its internal mechanism (**Supplementary Figure 1**). Referred to by Bernklau et al. (11), denser protein cross-linkage contributes to greater stability of gluten and dough, which can be characterized by protein area and protein junctions. Larger protein area and more protein junctions indicates that the gluten protein network structure is more closely connected. The reconstituted doughs except Q10 showed less protein area and fewer protein junctions than Q0 did (**Supplementary Figures 1B,C**), indicating that when quinoa flour was added into wheat flour, the gluten network structure in the dough system deteriorated. The protein area and protein junctions of Q10 increased slightly, without significant difference, compared to those of Q0. Lacunarity reflects the regularity of voids in the network structure and a higher value indicates weaker dough strength (9, 47). With the addition of quinoa flour, lacunarity became larger, indicating the reconstituted doughs became weaker (**Supplementary Figure 1D**).

Combined with the result of UPP%, it can be concluded that the gluten protein quality of the reconstituted doughs became worse with the addition of quinoa flour. The results can be explained by the fact that quinoa does not contain gluten, so that the protein of quinoa cannot connect with wheat gluten to form stable and complete gluten network structure (4). Since the microstructure of the reconstituted doughs was disrupted, the "weakened" doughs are expected to make different crispy biscuits.

Rheology

It is generally recognized that the rheological properties of dough are related to the quality of the final product in some way (48). A rheometer was used to investigate the rheological behavior of

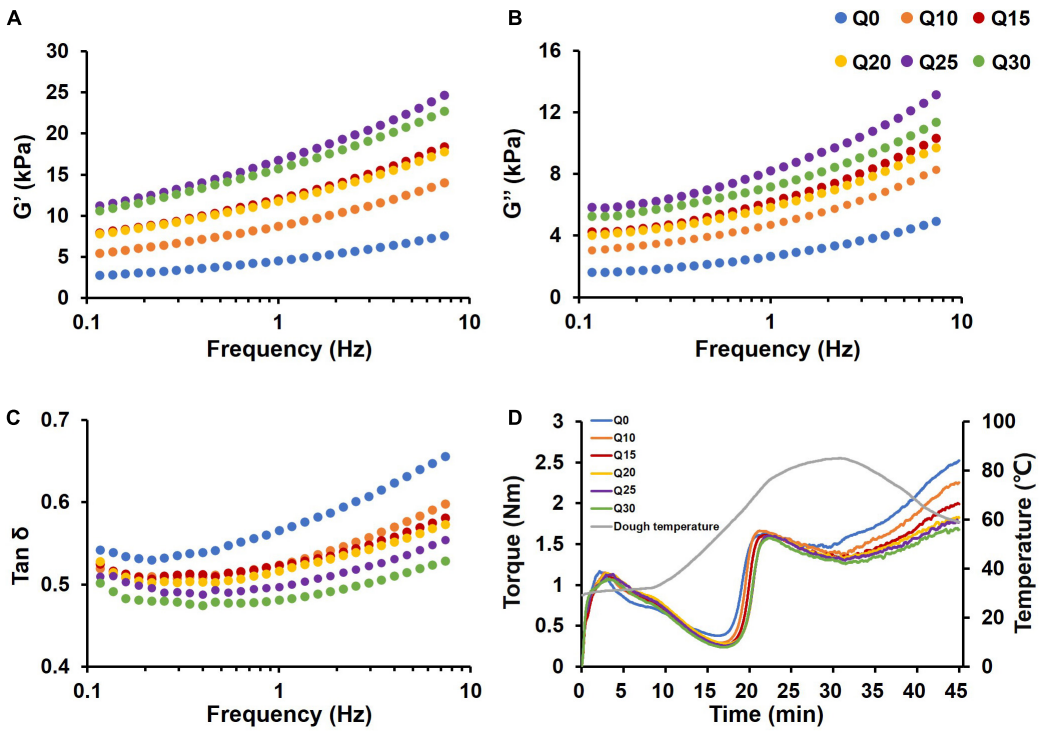

FIGURE 1 | Rheological properties of wheat and quinoa reconstituted doughs. **(A)** Storage modulus (G′). **(B)** Loss modulus (G″). **(C)** Tan δ. **(D)** The mixing profiles of doughs. The data were obtained from two replicates of each sample.

dough. The effect of quinoa flour on the rheological properties of wheat dough was analyzed (**Figure 1**). G′ and G″ represent solid-like and liquid-like characters of the test dough samples, respectively (49). When frequency was in the range of 0.1–10 Hz, G′ and G″ increased in a frequency-dependent manner. G′ was always higher than G″, which led to tan δ < 1 (**Figures 1A–C**), indicating predominance of a solid-like character for the reconstituted dough samples. The reconstituted doughs exhibited higher G′ and G″, compared with Q0. Tan δ decreased with an increased proportion of quinoa flour in dough samples, indicating quinoa flour improved dough viscoelasticity.

It has been generally accepted that UPP% is positively correlated with the dough rheological properties (6, 50). Protein polymers should have disintegrated as inclusion of quinoa flour diluted the gluten network. However, in this study, the rheological properties of the dough were improved. This may be attributed to that the starch of quinoa contains more small-sized granules, which combine more closely with gluten network (9, 51). The improved effect of quinoa starch may offset the decreased effect of the diluted gluten. In the current study, the increased content of smaller-sized starch in the dough system affected physicochemical and structural properties of the wheat dough because the quinoa starch granules embedded in the gluten network structure improve the stability and the rheological properties of the dough.

The dough rheological properties were further analyzed using a Mixolab instrument. Mixolab mixing curves suggested that there was a significant difference in torque among the tested samples at the dough formation stage (0–8 min), and the time from the initial to C1 was significantly lengthened with more quinoa flour added (**Figure 1D**). The Mixolab parameters can reflect the effect of the quinoa on gluten strength and starch pasting properties (**Table 3**). WA of flour is affected by multiple factors including protein and starch (43). The presence of quinoa significantly increased WA of the flours in a linear manner. Given that B-type starch granules with larger surface area can combine more water molecules, and thus increase water absorption of dough (18, 52), we attribute increased WA to inclusion of B-type starch granules in the reconstituted flours. It is noteworthy in this study that DDT and DS of the reconstituted doughs showed a stepwise increase. Inconsistent with the previous studies (30, 53), the absence of gluten in quinoa destroyed the gluten network structure, but prolonged DDT and DS, which can be explained by the assumption that under mechanical force, the protein-protein and protein-starch interactions between quinoa and wheat occurred. Also, high water absorption resulted in more available water in the reconstituted doughs thereby improving the homogeneity and stability of the gluten-starch matrix in the dough system (54). Since the reconstituted doughs showed better performance in the dough development than the control Q0 did, it is clear that quinoa flour at certain substitution levels improved the mixing properties of wheat dough.

When the temperature began to rise, the dough entered the protein weakening stage (C2) (**Figure 1D**). Torque began to drop because of protein denaturation, and continued until starch gelatinization began (30). Protein weakening (%) is described as difference between torque at 8 min and at C2. The protein

TABLE 3 | Effect of quinoa content on the mixing properties of wheat dough.

Sample	WA (%)	DDT (min)	DS (min)	C1 (Nm)	C2 (Nm)	C3 (Nm)	C4 (Nm)	C5 (Nm)	Protein weakening (%)	Breakdown (C3-C4) (Nm)	Setback (C5-C4) (Nm)
Q0	65.85 ± 0.07e	2.19 ± 0.05e	1.95 ± 0.21d	1.17 ± 0.06a	0.38 ± 0.04a	1.63 ± 0.00b	1.45 ± 0.05a	2.52 ± 0.00a	35.10 ± 0.01d	0.17 ± 0.05c	1.07 ± 0.05a
Q10	66.30 ± 0.14d	2.81 ± 0.11d	2.85 ± 0.18c	1.15 ± 0.04ab	0.29 ± 0.01b	1.66 ± 0.02a	1.36 ± 0.02b	2.25 ± 0.01b	50.80 ± 0.01c	0.30 ± 0.00ab	0.89 ± 0.01b
Q15	67.15 ± 0.21c	3.08 ± 0.08c	3.01 ± 0.01c	1.14 ± 0.03b	0.27 ± 0.00c	1.61 ± 0.00b	1.32 ± 0.01c	1.99 ± 0.01c	54.00 ± 0.00b	0.29 ± 0.01ab	0.67 ± 0.00c
Q20	67.90 ± 0.00b	3.12 ± 0.12c	3.62 ± 0.05b	1.15 ± 0.03b	0.28 ± 0.01bc	1.61 ± 0.00b	1.32 ± 0.01c	1.83 ± 0.00d	58.90 ± 0.01a	0.29 ± 0.01b	0.50 ± 0.01d
Q25	68.35 ± 0.21a	3.26 ± 0.08b	3.79 ± 0.12b	1.07 ± 0.00c	0.25 ± 0.04d	1.58 ± 0.01c	1.28 ± 0.02d	1.74 ± 0.02e	55.80 ± 0.01b	0.31 ± 0.01a	0.46 ± 0.00e
Q30	68.30 ± 0.28a	3.57 ± 0.19a	4.54 ± 0.16a	1.08 ± 0.02c	0.25 ± 0.08d	1.58 ± 0.10c	1.28 ± 0.02d	1.69 ± 0.01e	54.50 ± 0.00b	0.30 ± 0.08ab	0.41 ± 0.01f

Values followed by different letters in the same column are significantly different ($P < 0.05$).
WA, water absorption; DDT, dough development time; DS, dough stability time; C1, dough development; C2, protein weakening; C3, starch peak viscosity; C4, trough viscosity; C5, final viscosity.

weakening degree of the reconstituted doughs increased more significantly than that of wheat dough, indicating that quinoa increased protein weakening (**Table 3**), which was consistent with the finding about UPP% (**Supplementary Figure 1**). Similar results were reported by Gujral et al. (53), when hulless barley bran was supplemented to refined wheat flour for chapatti making. This is because the reconstituted doughs contained lower levels of gluten and weakened microstructure, which caused higher protein weakening degree and decreased dough consistence at C2.

As the temperature continued to rise, the dough entered the starch-dominating stage in the mixing process. At C3, starch peak viscosity was determined, which is a pivotal index to evaluate the end-use properties of food products (14). During the stage, torque for Q0 increased greatest (**Figure 1D**). C3 torque of the reconstituted doughs decreased slightly, indicating lower peak viscosity for quinoa than for wheat flour (**Table 3**). This might be attributed to mild variations in water absorption and swelling of small-sized starch granules. Because of the smaller volumes, the B-type starch granules have relatively smaller swelling expansion, which is responsible for lower peak viscosity (41). Besides, other factors, such as the contents of dietary fiber and polyphenols rather than of starch, have been reported to affect pasting properties, which cannot be negligible (20, 30). These components competed with starch granules for water, resulting in a decrease in the available water combined with starch and thus affected the pasting properties of starch.

When the dough temperature continued to rise to the maximum, torque continuously decreased until trough viscosity occurred (during C4). Breakdown is one of parameters that indicates paste stability (55). The breakdown of reconstituted doughs ranged from 0.29 to 0.31 Nm, which is higher than that of Q0 (0.17 Nm), indicating the reconstituted doughs had lower hot-paste stability (**Table 3**). Hot-paste stability is closely related to the exudation of amylose after the starch granule ruptured (56). The difference in structure between quinoa and wheat starch may be more likely to accelerate the leaching of amylose after starch granules fall off, resulting in poor stability.

During the dough cooling stage, torque increased owing to the recrystallization of gelatinized starch granules (53). With the higher ratio of quinoa flour, final viscosity of the reconstituted doughs decreased significantly (**Table 3**). Setback, the difference of torque between C5 and C4, is defined as the process of recrystallization of starch during cooling, which is related to retrogradation tendency of starch (27). With the addition of quinoa flour, setback values showed a downward trend. Shelf life is particularly important for biscuits. Considering the contribution of starch retrogradation to biscuits staling, a decrease in setback value for the reconstituted doughs indicated that the retrogradability of the reconstituted doughs decreased and thereby the shelf-life of biscuits can be extended (21, 57). The possible reason might be that higher polyphenol content in quinoa with higher anti-oxidation ability can inhibit the retrogradation of starch (30). In addition, amylose content is also one of the important factors affecting starch retrogradation (20). Amylopectin has many branches and complex structure, which has a large space barrier and will slow retrogradation in solution; while amylose in solution has little space barrier and is ready to facilitate retrogradation. Therefore, although quinoa flour increased the torque value at protein weakening in the mixing process, it strongly improved starch retrogradability, showing that quinoa starch impacts mixing properties of wheat dough greatly.

The radar graphs were constructed to visualize the comparison among quality characteristics of doughs made from different flours with their components at different levels. Three wheat doughs supplemented with quinoa flours at three ratios (Q20, Q25, and Q30) had better overall scores than Q0 (**Figure 2**), which indicates the three formulations can fulfill the purpose of functional biscuit baking.

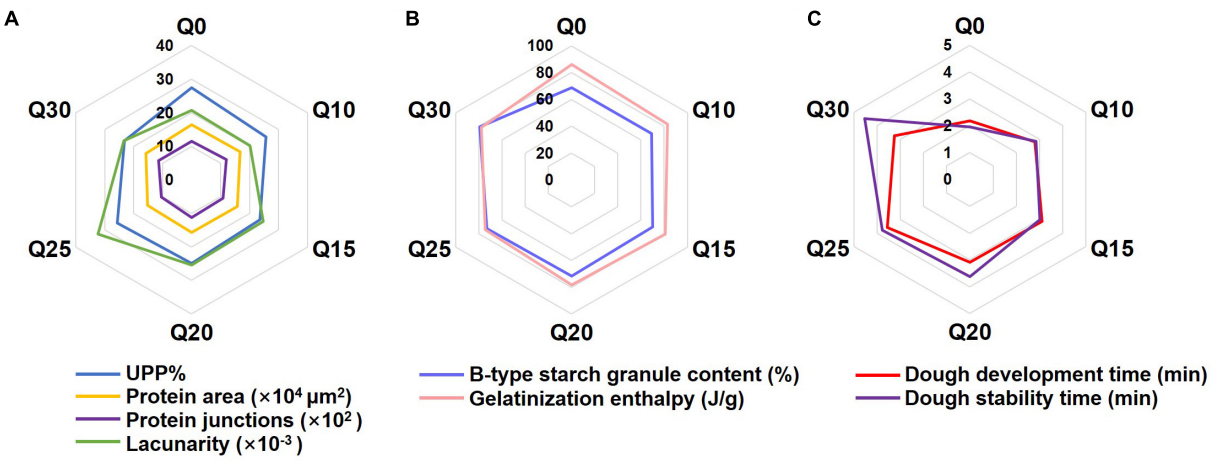

FIGURE 2 | The radar graphs of quality characteristics of wheat and quinoa reconstituted doughs. **(A)** Comparison of UPP%, protein area, protein junctions and lacunarity in wheat and quinoa reconstituted doughs. **(B)** Comparison of B-type starch granule content and gelatinization enthalpy in wheat and quinoa reconstituted doughs. **(C)** Comparison of dough development time and dough stability time in wheat and quinoa reconstituted doughs.

TABLE 4 | Effect of quinoa content on the physical property measurements, textural properties, sensory evaluation, and *in vitro* starch digestibility of crispy biscuits.

	Parameter	Q0	Q20	Q25	Q30
Physical property	Diameter (cm)	5.68 ± 0.02a	5.65 ± 0.06a	5.65 ± 0.11a	5.63 ± 0.04a
	Thickness (mm)	9.96 ± 0.76b	10.52 ± 0.33b	10.85 ± 0.32ab	11.49 ± 0.43a
	Weight (g)	15.93 ± 0.56b	18.47 ± 0.66a	19.15 ± 1.05a	19.29 ± 0.93a
Textural property	Hardness	72.83 ± 1.64a	73.99 ± 9.49a	50.16 ± 8.33b	57.34 ± 4.52b
	Toughness	10.01 ± 0.01a	5.48 ± 0.49bc	6.66 ± 1.56b	5.34 ± 0.76c
Sensory evaluation	Color	8.10 ± 0.26a	7.74 ± 0.10b	7.38 ± 0.20c	6.66 ± 0.12d
	Shape	8.10 ± 0.26a	7.74 ± 0.17b	7.56 ± 0.19b	7.02 ± 0.30c
	Structure	7.20 ± 0.00c	7.56 ± 0.00a	7.38 ± 0.20b	7.20 ± 0.00c
	Flavor	8.10 ± 0.23a	7.38 ± 0.25b	7.02 ± 0.25b	6.12 ± 0.41c
	Overall acceptability	8.00 ± 0.23a	8.12 ± 0.11a	7.77 ± 0.20a	7.10 ± 0.16a
In vitro starch digestibility	RDS (%)	60.80 ± 0.30a	59.21 ± 1.09b	56.70 ± 0.13c	51.47 ± 0.07d
	SDS (%)	1.86 ± 0.53c	1.15 ± 0.03d	3.26 ± 0.63b	4.95 ± 0.13a
	RS (%)	37.34 ± 0.82c	39.64 ± 0.03b	40.04 ± 0.46b	43.58 ± 0.00a

Values followed by different letters in the same row are significantly different ($P < 0.05$).
RDS, rapidly digested starch; SDS, slowly digested starch; RS, resistant starch.

Physical Properties, Texture Profile, and Sensory Evaluation of Crispy Biscuits

Physical property analyses showed that quinoa flours at different substitution ratios had different effects on thickness and weight of biscuits, and the effect was more evident when the quinoa content increased (**Table 4**). Textural properties are important for biscuit quality (15). The analyses of texture properties of the four crispy biscuits showed that hardness and toughness of Q0 was greater than those of Q20, Q25, and Q30 (**Table 4**), which is consistent with the previous report (2). Hardness and toughness are considered as important parameters to evaluate biscuit quality (15). Differences in moisture content of the dough also contribute to differences in biscuits crispiness (58). When quinoa flour was added to wheat flour, WA increased, resulting in an increase in the moisture content of dough (**Table 3**) and a decrease in hardness of the formulated crispy biscuits. Lower hardness and greater toughness are favorable attributes of the crispy biscuits. The above results showed that among the four biscuit samples, Q25 had superior textural attributes.

The results of hedonic sensory scores for crispy biscuits were given in **Table 4**. In terms of color and shape, the scores of Q0, Q20, Q25, and Q30 decreased sequentially. It can also be seen from **Supplementary Figure 2** that the appearance and color of Q20 were better than that of Q25 and Q30. The biscuits displayed varied colors from light to dark brown (**Supplementary Figure 2**), which may be attributed to browning because of Maillard or caramelization reactions. This agrees with the report that temperature and quinoa flour instead of wheat flour affect the browning of biscuits (59). Additionally, the deeper browning of quinoa samples reported in previous studies is due to high levels of polyphenols and ash (2), which is consistent with the results of this study. The inclusion of quinoa in crispy biscuits resulted in increased scores for structure compared to Q0. However, supplement of quinoa in crispy biscuits reduced scores for flavor. In spite of undesirable results in terms of color, shape, and flavor, Q20 ensured satisfactory overall consumer acceptability of formulated crispy biscuit. Although the use of quinoa flour resulted in a slight decrease in the overall acceptability values, all formulated crispy biscuits including Q30, which was substituted with most quinoa, remained within the range that consumers appreciate with the overall rating acceptable.

In vitro Starch Digestibility

Analysis of *in vitro* starch digestibility of the crispy biscuits shows that RDS, SDS, and RS content of Q0 are 60.80, 1.86, and 37.34%, respectively (**Table 4**). With the increased inclusion of quinoa flour, the digestion rate of crispy biscuit starch significantly dropped, which was confirmed by the fact that RS increased and RDS and SDS decreased. For patients with type 2 diabetes, obesity, or cardiovascular disease, foods with lower RDS content, higher SDS, and RS contents are healthier (24). Consequently, the decreased RDS and increased RS suggested that crispy biscuits supplemented with quinoa flour should be beneficial, since carbohydrates were digested slowly *in vivo*, and thereby prevented sharp increase of postprandial blood glucose. Amylase was considered to be a key factor in determining starch digestibility (14). Starch digestibility of the crispy biscuits was decreased with the increase of quinoa flour. Wang et al. (60) reported that in the process of digestion, A-type wheat starch gelatinized largely, while B-type wheat starch and quinoa starch granules were wrapped in a protein-sugar-oil film after baking, forming a natural barrier, its digestion rate was slower. In this study, due to the presence of quinoa starch, the content of small starch granules in the reconstituted flour increased, which reduced the starch digestibility. Additionally, reduced starch digestibility may also be attributed to higher phenolic and flavonoid contents restricting the hydrolysis of enzyme (30). As shown in **Figure 3**, the contents of total polyphenol and total flavone of Q20, Q25, and Q30 were significantly higher than those of Q0, and increased with the increase of quinoa content. Therefore, this may also be one of the reasons for the decline in digestibility. In a word, quinoa can greatly reduce starch digestibility and increase the RS content of biscuits, indicating that quinoa can effectively improve the functional attributes of crispy biscuits.

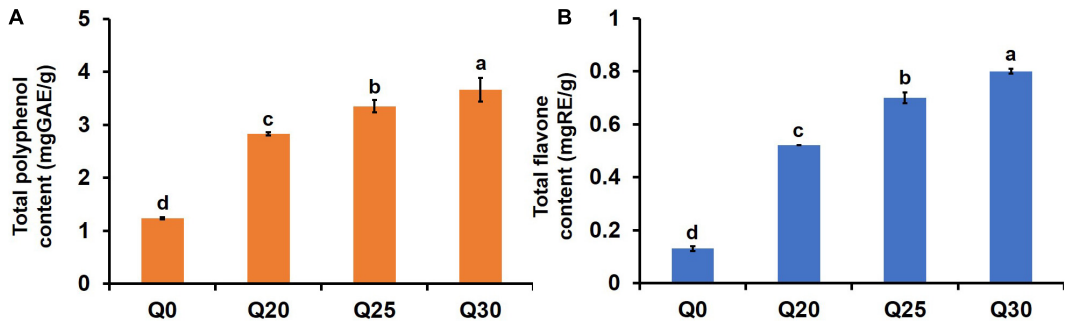

FIGURE 3 | Effects of quinoa addition on functional components in the flour crispy biscuit samples. **(A)** The total polyphenol content in the crispy biscuit samples. **(B)** The total flavone content in the crispy biscuit samples. The letters indicate significant differences ($P < 0.05$).

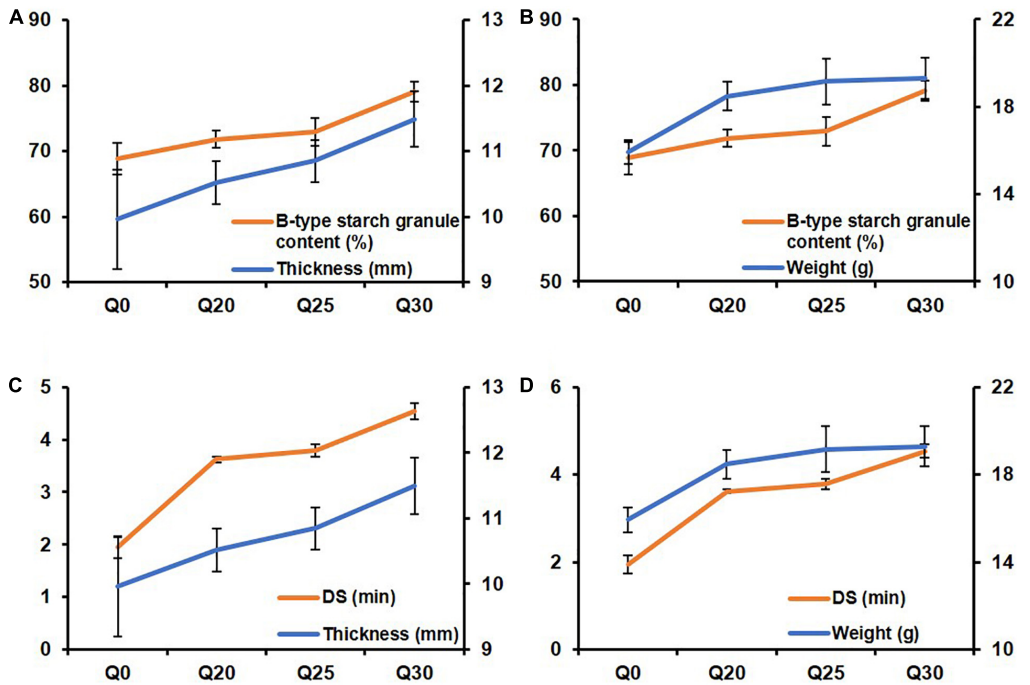

FIGURE 4 | The line charts exhibiting relationship between biscuit properties and starch and rheological properties of quinoa-wheat reconstituted systems. **(A)** The relationship between B-type starch granule content and crispy biscuit thickness. **(B)** The relationship between B-type starch granule content and crispy biscuit weight. **(C)** The relationship between dough stability (DS) and crispy biscuit thickness. **(D)** The relationship between dough stability (DS) and crispy biscuit weight.

The Relationship Between Biscuit Properties and Gluten Composition, Starch and Rheological Properties of Quinoa-Wheat Reconstituted System

To further explore the relationship between the biscuit properties and gluten, starch and rheological properties of the quinoa-wheat reconstituted system, the line graphs were drawn for comparison. The results showed that B-type starch granule content and DS had the same change trend as biscuit thickness and weight with the increase proportion of quinoa flour (**Figure 4**), which is consistent with previous report (61). The possible reason for this trend is that more small starch granules are filled in the gluten network structure. During the dough formation process, the broken network structure is reorganized, thereby improving the dough stability. High-quality dough properties are conducive to volume expansion (62), resulting in increased biscuit thickness and weight.

However, there was no significant relationship between gluten properties and biscuit properties, nor between properties of starch and dough rheology and hardness and toughness of biscuit (**Supplementary Figure 3**), which is consistent with the previous study demonstrating no significant correlation between starch structure and biscuit hardness and fracturability (63). Obviously, there are many factors affecting the quality properties of biscuits, e.g., damage starch, pentosans (64), fiber (65), and

other components in quinoa or wheat, which also requires further research.

CONCLUSION

This study explored the effect of quinoa flour on physiochemical and mixing properties of wheat dough. Moreover, the physical, textural and digestion properties of the formulated crispy biscuits were analyzed. The results of the study showed that although added quinoa flour significantly disrupted the gluten network structure, it increased B-type granule content and gelatinization temperature of doughs. Interestingly, rheological properties of the reconstituted doughs were improved and dough aging was reduced. In addition, quinoa flour significantly improved the textural and digestibility properties of crispy biscuits. The contents of RDS and SDS were significantly reduced, while that of RS was significantly increased, indicating that the formulated biscuits were more beneficial to patients with special diseases (e.g., diabetes). On the whole, quinoa flour at certain levels had a positive effect on biscuit quality: not only improved rheological properties but also yielded promising results on healthy food.

DATA AVAILABILITY STATEMENT

The raw data supporting the conclusions of this article will be made available by the authors, without undue reservation.

AUTHOR CONTRIBUTIONS

YM: investigation, formal analysis, and writing—original draft, review, and editing. DW: methodology, data curation, writing—review, and editing. LG: investigation and data curation. YY, XY, and ZW: resources. KW, XC, and XG: supervision, project administration and writing—review, and editing. All authors contributed to the article and approved the submitted version.

FUNDING

This work was funded by the Open Project of the State Key Laboratory of Plateau Ecology and Agriculture, Qinghai University (Grant No. 2020-KF-003), Science and Technology Transformation Project of Science and Technology Department of Qinghai Province (Grant No. 2022-NK-112), the National Key Research and Development Program of China (Grant No. 2020YFD1001403), Taishan Industrial Experts Program (Grant No. LJNY202006), and Undergraduate Student Innovation and Entrepreneurship Training Program (Grant No. S202110712334).

ACKNOWLEDGMENTS

We thank Yun Jiang for his assistance in language corrections.

SUPPLEMENTARY MATERIAL

The Supplementary Material for this article can be found online at: https://www.frontiersin.org/articles/10.3389/fnut.2022.846808/full#supplementary-material

Supplementary Figure 1 | Gluten protein composition and microstructure of wheat and quinoa reconstituted flours and doughs. **(A)** The UPP% of wheat and quinoa reconstituted flours. **(B–D)** Microstructure indicated by the protein area, protein junctions and lacunarity of the wheat and quinoa reconstituted doughs. The data were derived from five captures of each sample and presented as mean value ± standard deviation.

Supplementary Figure 2 | Image of formulated crispy biscuits appearances and textures with the scale bar of 1 cm.

Supplementary Figure 3 | The line charts exhibiting unobvious relationship between biscuit properties and gluten, starch and rheological properties of quinoa-wheat reconstituted systems.

REFERENCES

1. Yang B, Guo M, Zhao Z. Incorporation of wheat malt into a cookie recipe and its effect on the physicochemical properties of the corresponding dough and cookies. *LWT Food Sci Technol.* (2020) 117:108651. doi: 10.1016/j.lwt.2019.108651
2. Cannas M, Pulina S, Conte P, Del Caro A, Urgeghe PP, Piga A, et al. Effect of substitution of rice flour with quinoa flour on the chemical-physical, nutritional, volatile and sensory parameters of gluten-free ladyfinger biscuits. *Foods.* (2020) 9:808. doi: 10.3390/foods9060808
3. Dakhili S, Abdolalizadeh L, Hosseini SM, Shojaee-Aliabadi S, Mirmoghtadaie L. Quinoa protein: composition, structure and functional properties. *Food Chem.* (2019) 299:125161. doi: 10.1016/j.foodchem.2019.125161
4. Xu X, Luo Z, Yang Q, Xiao Z, Lu X. Effect of quinoa flour on baking performance, antioxidant properties and digestibility of wheat bread. *Food Chem.* (2019) 294:87–95. doi: 10.1016/j.foodchem.2019.05.037
5. Struyf N, Van der Maelen E, Hemdane S, Verspreet J, Verstrepen KJ, Courtin CM. Bread dough and baker's yeast: an uplifting synergy. *Compr Rev Food Sci Food Saf.* (2017) 16:850–67. doi: 10.1111/1541-4337.12282
6. Li S, Liu Y, Tong J, Yu L, Ding M, Zhang Z, et al. The overexpression of high-molecular-weight glutenin subunit Bx7 improves the dough rheological properties by altering secondary and micro-structures of wheat gluten. *Food Res Int.* (2020) 130:108914. doi: 10.1016/j.foodres.2019.108914
7. Liu T, Gao X, Li L, Du D, Cheng X, Zhao Y, et al. Effects of HMW-GS at Glu-B1 locus on the polymerization of glutenin during grain development and on the secondary and micro-structures of gluten in wheat (*Triticum aestivum* L.). *J Cereal Sci.* (2016) 72:101–7. doi: 10.1016/j.jcs.2016.10.007
8. Cooper JK, Stromberger JA, Morris CF, Bai G, Haley SD. End-use quality and agronomic characteristics associated with the Glu-B1al high-molecular-weight glutenin allele in U.S. hard winter wheat. *Crop Sci.* (2016) 56:2348–53. doi: 10.2135/cropsci2015.10.0610
9. Yu L, Ma Y, Zhao Y, Pan Y, Tian R, Yao X, et al. Effect of hulless barley flours on dough rheological properties, baking quality, and starch digestibility of wheat bread. *Front Nutr.* (2021) 8:785847. doi: 10.3389/fnut.2021.785847
10. Ooms N, Delcour JA. How to impact gluten protein network formation during wheat flour dough making. *Curr Opin Food Sci.* (2019) 25:88–97. doi: 10.1016/j.cofs.2019.04.001
11. Bernklau I, Lucas L, Jekle M, Becker T. Protein network analysis – a new approach for quantifying wheat dough microstructure. *Food Res Int.* (2016) 89:812–9. doi: 10.1016/j.foodres.2016.10.012
12. Gao X, Liu T, Ding M, Wang J, Li C, Wang Z, et al. Effects of HMW-GS Ax1 or Dx2 absence on the glutenin polymerization and gluten micro

structure of wheat (*Triticum aestivum* L.). *Food Chem.* (2018) 240:626–33. doi: 10.1016/j.foodchem.2017.07.165
13. Tao H, Huang J-S, Xie Q-T, Zou Y-M, Wang H-L, Wu X-Y, et al. Effect of multiple freezing-thawing cycles on structural and functional properties of starch granules isolated from soft and hard wheat. *Food Chem.* (2018) 265:18–22. doi: 10.1016/j.foodchem.2018.05.065
14. Wang H, Xu K, Liu X, Zhang Y, Xie X, Zhang H. Understanding the structural, pasting and digestion properties of starch isolated from frozen wheat dough. *Food Hydrocoll.* (2021) 111:106168. doi: 10.1016/j.foodhyd.2020.106168
15. Zhang Z, Fan X, Yang X, Li C, Gilbert RG, Li E. Effects of amylose and amylopectin fine structure on sugar-snap cookie dough rheology and cookie quality. *Carbohydr Polym.* (2020) 241:116371. doi: 10.1016/j.carbpol.2020.116371
16. Li G, Zhu F. Quinoa starch: structure, properties, and applications. *Carbohydr Polym.* (2018) 181:851–61. doi: 10.1016/j.carbpol.2017.11.067
17. Cao X, Tong J, Ding M, Wang K, Wang L, Cheng D, et al. Physicochemical properties of starch in relation to rheological properties of wheat dough (*Triticum aestivum* L.). *Food Chem.* (2019) 297:125000. doi: 10.1016/j.foodchem.2019.125000
18. Zi Y, Shen H, Dai S, Ma X, Ju W, Wang C, et al. Comparison of starch physicochemical properties of wheat cultivars differing in bread- and noodle-making quality. *Food Hydrocoll.* (2019) 93:78–86. doi: 10.1016/j.foodhyd.2019.02.014
19. Jiang F, Du C, Guo Y, Fu J, Jiang W, Du S-K. Physicochemical and structural properties of starches isolated from quinoa varieties. *Food Hydrocoll.* (2020) 101:105515. doi: 10.1016/j.foodhyd.2019.105515
20. Li G, Zhu F. Amylopectin molecular structure in relation to physicochemical properties of quinoa starch. *Carbohydr Polym.* (2017) 164:396–402. doi: 10.1016/j.carbpol.2017.02.014
21. Marchini M, Carini E, Cataldi N, Boukid F, Blandino M, Ganino T, et al. The use of red lentil flour in bakery products: how do particle size and substitution level affect rheological properties of wheat bread dough? *LWT Food Sci Technol.* (2021) 136:110299. doi: 10.1016/j.lwt.2020.110299
22. Englyst HN, Kingman SM, Cummings JH. Classification and measurement of nutritionally important starch fractions. *Eur J Clin Nutr.* (1992) 46:S33–50.
23. Reshmi SK, Sudha ML, Shashirekha MN. Starch digestibility and predicted glycemic index in the bread fortified with pomelo (*Citrus maxima*) fruit segments. *Food Chem.* (2017) 237:957–65. doi: 10.1016/j.foodchem.2017.05.138
24. Roman L, Martinez MM. Structural basis of resistant starch (RS) in bread: natural and commercial alternatives. *Foods.* (2019) 8:267. doi: 10.3390/foods8070267
25. Demir B, Bilgicli N. Changes in chemical and anti-nutritional properties of pasta enriched with raw and germinated quinoa (*Chenopodium quinoa* Willd.) flours. *J Food Sci Technol.* (2020) 57:3884–92. doi: 10.1007/s13197-020-04420-7
26. Kahlon TS, Avena-Bustillos RJ, Chiu M-CM. Sensory evaluation of gluten-free quinoa whole grain snacks. *Heliyon.* (2016) 2:e00213. doi: 10.1016/j.heliyon.2016.e00213
27. Tiga BH, Kumcuoglu S, Vatansever M, Tavman S. Thermal and pasting properties of quinoa-wheat flour blends and their effects on production of extruded instant noodles. *J Cereal Sci.* (2021) 97:103120. doi: 10.1016/j.jcs.2020.103120
28. Torbica A, Belović M, Tomić J. Novel breads of non-wheat flours. *Food Chem.* (2019) 282:134–40. doi: 10.1016/j.foodchem.2018.12.113
29. Alvarez-Jubete L, Wijngaard H, Arendt EK, Gallagher E. Polyphenol composition and in vitro antioxidant activity of amaranth, quinoa buckwheat and wheat as affected by sprouting and baking. *Food Chem.* (2010) 119:770–8. doi: 10.1016/j.foodchem.2009.07.032
30. Sharma B, Gujral HS. Influence of nutritional and antinutritional components on dough rheology and in vitro protein & starch digestibility of minor millets. *Food Chem.* (2019) 299:125115. doi: 10.1016/j.foodchem.2019.125115
31. Contreras-Jiménez B, Torres-Vargas OL, Rodríguez-García ME. Physicochemical characterization of quinoa (*Chenopodium quinoa*) flour and isolated starch. *Food Chem.* (2019) 298:124982. doi: 10.1016/j.foodchem.2019.124982
32. Yu L, Guo L, Liu Y, Ma Y, Zhu J, Yang Y, et al. Novel parameters characterizing size distribution of A and B starch granules in the gluten network: Effects on dough stability in bread wheat. *Carbohydr. Polym.* (2021) 257:117623. doi: 10.1016/j.carbpol.2021.117623
33. Wang X-Y, Guo X-N, Zhu K-X. Polymerization of wheat gluten and the changes of glutenin macropolymer (GMP) during the production of Chinese steamed bread. *Food Chem.* (2016) 201:275–83. doi: 10.1016/j.foodchem.2016.01.072
34. Wang J-R, Guo X-N, Xing J-J, Zhu K-X. Revealing the effect mechanism of NaCl on the rheological properties of dough of Chinese traditional hand-stretched dried noodles. *Food Chem.* (2020) 320:126606. doi: 10.1016/j.foodchem.2020.126606
35. Niu M, Hou GG, Kindelspire J, Krishnan P, Zhao S. Microstructural, textural, and sensory properties of whole-wheat noodle modified by enzymes and emulsifiers. *Food Chem.* (2017) 223:16–24. doi: 10.1016/j.foodchem.2016.12.021
36. Toutounji MR Jr, Butardo VM, Zou W, Farahnaky A, Pallas L, Oli P, et al. A high-throughput in vitro assay for screening rice starch digestibility. *Foods.* (2019) 8:601. doi: 10.3390/foods8120601
37. Srichuwong S, Curti D, Austin S, King R, Lamothe L, Gloria-Hernandez H. Physicochemical properties and starch digestibility of whole grain sorghums, millet, quinoa and amaranth flours, as affected by starch and non-starch constituents. *Food Chem.* (2017) 233:1–10. doi: 10.1016/j.foodchem.2017.04.019
38. Hirose Y, Fujita T, Ishii T, Ueno N. Antioxidative properties and flavonoid composition of *Chenopodium quinoa* seeds cultivated in Japan. *Food Chem.* (2010) 119:1300–6. doi: 10.1016/j.foodchem.2009.09.008
39. Pellegrini M, Lucas-Gonzales R, Ricci A, Fontecha J, Fernandez-Lopez J, Perez-Alvarez JA, et al. Chemical, fatty acid, polyphenolic profile, techno-functional and antioxidant properties of flours obtained from quinoa (*Chenopodium quinoa* Willd.) seeds. *Ind Crops Prod.* (2018) 111:38–46. doi: 10.1016/j.indcrop.2017.10.006
40. Chacaliaza-Rodríguez L, Espinoza-Begazo G, Ramos-Escudero F, Servan K. Proximate chemical composition and content of biologically active components in leaves of two quinoa cultivars (Salcedo and Altiplano) produced in Peru. *Res J Med Plants.* (2016) 10:450–6. doi: 10.3923/rjmp.2016.450.456
41. Roman L, de la Cal E, Gomez M, Martinez MM. Specific ratio of A- to B-type wheat starch granules improves the quality of gluten-free breads: optimizing dough viscosity and pickering stabilization. *Food Hydrocoll.* (2018) 82:510–8. doi: 10.1016/j.foodhyd.2018.04.034
42. Li M, Liu C, Zheng X, Hong J, Bian K, Li L. Interaction between A-type/B-type starch granules and gluten in dough during mixing. *Food Chem.* (2021) 358:129870. doi: 10.1016/j.foodchem.2021.129870
43. Li C, Dhital S, Gilbert RG, Gidley MJ. High-amylose wheat starch: structural basis for water absorption and pasting properties. *Carbohydr Polym.* (2020) 245:116557. doi: 10.1016/j.carbpol.2020.116557
44. Li C, Wu A, Yu W, Hu Y, Li E, Zhang C, et al. Parameterizing starch chain-length distributions for structure-property relations. *Carbohydr Polym.* (2020) 241:116390. doi: 10.1016/j.carbpol.2020.116390
45. Tao H, Wang P, Wu F, Jin Z, Xu X. Particle size distribution of wheat starch granules in relation to baking properties of frozen dough. *Carbohydr Polym.* (2016) 137:147–53. doi: 10.1016/j.carbpol.2015.10.063
46. Zeng J, Gao H, Li G. Functional properties of wheat starch with different particle size distribution. *J Sci Food Agric.* (2014) 94:57–62. doi: 10.1002/jsfa.6186
47. Jekle M, Becker T. Wheat dough microstructure: the relation between visual structure and mechanical behavior. *Crit Rev Food Sci Nutr.* (2015) 55:369–82. doi: 10.1080/10408398.2012.656476
48. Dobraszczyk BJ, Morgenstern MP. Rheology and the breadmaking process. *J Cereal Sci.* (2003) 38:229–45. doi: 10.1016/s0733-5210(03)00059-6
49. Yuan C, Sang L, Wang Y, Cui B. Influence of cyclodextrins on the gel properties of kappa-carrageenan. *Food Chem.* (2018) 266:545–50. doi: 10.1016/j.foodchem.2018.06.060
50. Singh S, Singh N. Relationship of polymeric proteins and empirical dough rheology with dynamic rheology of dough and gluten from different wheat varieties. *Food Hydrocoll.* (2013) 33:342–8. doi: 10.1016/j.foodhyd.2013.04.007

51. Gao X, Tong J, Guo L, Yu L, Li S, Yang B, et al. Influence of gluten and starch granules interactions on dough mixing properties in wheat (*Triticum aestivum* L.). *Food Hydrocoll.* (2020) 106:105885. doi: 10.1016/j.foodhyd.2020.105885
52. Hong J, Zeng X-A, Buckow R, Han Z. Structural, thermodynamic and digestible properties of maize starches esterified by conventional and dual methods: differentiation of amylose contents. *Food Hydrocoll.* (2018) 83:419–29. doi: 10.1016/j.foodhyd.2018.05.032
53. Gujral HS, Sharma B, Khatri M. Influence of replacing wheat bran with barley bran on dough rheology, digestibility and retrogradation behavior of chapatti. *Food Chem.* (2018) 240:1154–60. doi: 10.1016/j.foodchem.2017.08.042
54. Adedara OA, Taylor JRN. Roles of protein, starch and sugar in the texture of sorghum biscuits. *LWT Food Sci Technol.* (2021) 136:110323. doi: 10.1016/j.lwt.2020.110323
55. Abdel-Aal E-SM, Hernandez M, Rabalski I, Hucl P. Composition of hairless canary seed oil and starch-associated lipids and the relationship between starch pasting and thermal properties and its lipids. *LWT Food Sci Technol.* (2020) 125:109257. doi: 10.1016/j.lwt.2020.109257
56. Xiao F, Zhang X, Niu M, Xiang XQ, Chang YD, Zhao ZZ, et al. Gluten development and water distribution in bread dough influenced by bran components and glucose oxidase. *LWT Food Sci Technol.* (2020) 137:110427. doi: 10.1016/j.lwt.2020.110427
57. Erukainure OL, Okafor JNC, Ogunji A, Ukazu H, Okafor EN, Eboagwu IL. Bambara-wheat composite flour: rheological behavior of dough and functionality in bread. *Food Sci Nutr.* (2016) 4:852–7. doi: 10.1002/fsn3.356
58. Roman L, Sahagun M, Gomez M, Martinez MM. Nutritional and physical characterization of sugars-nap cookies: effect of banana starch in native and molten states. *Food Funct.* (2019) 10:616–24. doi: 10.1039/c8fo02266f
59. Sazesh B, Goli M. Quinoa as a wheat substitute to improve the textural properties and minimize the carcinogenic acrylamide content of the biscuit. *J Food Process Preserv.* (2020) 44:e14563. doi: 10.1111/jfpp.14563
60. Wang X, Lao X, Bao Y, Guan X, Li C. Effect of whole quinoa flour substitution on the texture and in vitro starch digestibility of wheat bread. *Food Hydrocoll.* (2021) 119:106840. doi: 10.1016/j.foodhyd.2021.106840
61. Wang S, Opassathavorn A, Zhu F. Influence of quinoa flour on quality characteristics of cookie, bread and Chinese steamed bread. *J Texture Stud.* (2015) 46:281–92. doi: 10.1111/jtxs.12128
62. De Bondt Y, Hermans W, Moldenaers P, Courtin CM. Selective modification of wheat bran affects its impact on gluten-starch dough rheology, microstructure and bread volume. *Food Hydrocoll.* (2021) 113:106348. doi: 10.1016/j.foodhyd.2020.106348
63. Zhang Z, Fan X, Yang X, Li C, Gilbert RG, Li E. Effects of amylose and amylopectin fine structure on sugar-snap cookie dough rheology and cookie quality. *Carbohydr Polym.* (2020) 241:108651.
64. Pareyt B, Delcour JA. The role of wheat flour constituents, sugar, and fat in low moisture cereal based products: a review on sugar-snap cookies. *Crit Rev Food Sci.* (2008) 48:824–39. doi: 10.1080/10408390701719223
65. Packkia-Doss PP, Chevallier S, Pare A, Le-Bail A. Effect of supplementation of wheat bran on dough aeration and final bread volume. *J Food Eng.* (2019) 252:28–35. doi: 10.1016/j.jfoodeng.2019.01.014

Conflict of Interest: The authors declare that the research was conducted in the absence of any commercial or financial relationships that could be construed as a potential conflict of interest.

Publisher's Note: All claims expressed in this article are solely those of the authors and do not necessarily represent those of their affiliated organizations, or those of the publisher, the editors and the reviewers. Any product that may be evaluated in this article, or claim that may be made by its manufacturer, is not guaranteed or endorsed by the publisher.

frontiers | Frontiers in Nutrition

BRIEF RESEARCH REPORT
published: 02 May 2022
doi: 10.3389/fnut.2022.887992

Chemical Comparison of Monk Fruit Products Processed by Different Drying Methods Using High-Performance Thin-Layer Chromatography Combined With Chemometric Analysis

Hui-Jie Hong[1†], Qi Yang[1†], Qiao Liu[1], Fong Leong[1] and Xiao-Jia Chen[1,2]*

[1] State Key Laboratory of Quality Research in Chinese Medicine, Institute of Chinese Medical Sciences, University of Macau, Macau, Macao SAR, China, [2] Zhuhai UM Science and Technology Research Institute, Zhuhai, China

OPEN ACCESS

Edited by:
Brian D. Green,
Queen's University Belfast,
United Kingdom

Reviewed by:
Yueliang Zhao,
Shanghai Ocean University, China
Kit Leong Cheong,
Shantou University, China

***Correspondence:**
Xiao-Jia Chen
XiaojiaChen@um.edu.mo

[†] These authors have contributed equally to this work and share first authorship

Specialty section:
This article was submitted to Food Chemistry, a section of the journal Frontiers in Nutrition

Received: 02 March 2022
Accepted: 31 March 2022
Published: 02 May 2022

Citation:
Hong H-J, Yang Q, Liu Q, Leong F and Chen X-J (2022) Chemical Comparison of Monk Fruit Products Processed by Different Drying Methods Using High-Performance Thin-Layer Chromatography Combined With Chemometric Analysis. Front. Nutr. 9:887992. doi: 10.3389/fnut.2022.887992

Monk fruit, also named Luo Han Guo, is the fruit of *Siraitia grosvenorii* (Swingle) C. Jeffrey ex A. M. Lu et Z. Y. Zhang and has been used as both food and traditional Chinese medicine. Due to preservation concerns, monk fruit is usually processed by hot-air drying or using low-temperature techniques after harvest. In this study, high-performance thin-layer chromatography (HPTLC) method was developed for the analysis of 13 mogrosides, 1 flavonoid, and 3 sugars in monk fruit products. Then chemometric analysis was applied to investigate the chemical characteristics in the samples dried by different methods. The results showed that the contents of mogroside V, 11-oxo-mogroside V, isomogroside V, and sucrose in monk fruits dried at low temperature were much higher than those in traditional hot-air drying samples, which was also confirmed by HPTLC-scanning. These findings indicate that HPTLC combined with chemometric analysis provides a reliable tool to understand the chemical differences between the monk fruit products processed by different drying methods, which will be helpful for their quality evaluation.

Keywords: monk fruit, *Siraitia grosvenorii*, high performance thin layer chromatography, drying method, chemical characteristics, chemometric analysis

INTRODUCTION

Monk fruit, also known as Luo Han Guo, is the fruit of *Siraitia grosvenorii* (Swingle) C. Jeffrey ex A. M. Lu et Z. Y. Zhang (1). It is mainly cultivated in Guangxi, China, and has been used as a food ingredient, beverage, and traditional medicine for centuries. Because of its good safety and high sweetness, monk fruit had been approved as a food sweetener by China Food and Drug Administration and awarded the "generally regarded as safe" (GRAS) status by the U.S. Food and Drug Administration (2). It is used as a sugar-free food additive in low-calorie health-promoting drinks, and also as a substitute for sweeteners in health foods for patients with obesity and diabetes

(2). As a traditional Chinese medicine, monk fruit has been used for the treatment of dry cough, sore throat, and constipation (1). Recent pharmacological studies have also shown that monk fruit exhibits anti-diabetic (3–5), anti-cancer (6, 7), anti-inflammatory (8–10), and neuroprotective effects (11–13).

The bioactive and nutritional ingredients in monk fruit include triterpene glycosides, flavonoids, carbohydrates, proteins, fats, vitamins, and minerals. Mogrosides are a group of cucurbitane-type triterpene glycosides that are the major bioactive compounds in monk fruit. The mixture of mogrosides is 300 times sweeter than sucrose (14), but only mogrosides with mogrol aglycone and with more than three sugar moieties possess the sweet taste (15, 16). Flavonoids are also important compounds in monk fruit and exert antibacterial and antioxidant effects (17). In addition, there are various sugars found in monk fruit. In different varieties of monk fruits, the total sugar content accounted for 25–38% of dry weight. Among them, the contents of fructose and glucose were 10–17% and 5–15%, respectively (18).

Monk fruit usually needs a drying process before further use to inhibit microbial growth and extend the shelf life. Traditionally, monk fruit is dried by hot air at 45–70°C for 6–8 days to remove the moisture, after which the outer surface of the monk fruit will turn to dark yellow or brown (**Supplementary Figure 1**), and the taste may be slightly bitter. To obtain better appearance, taste, and quality, low temperature techniques, such as freeze-drying, freeze-vacuum drying, microwave drying, microwave-vacuum drying, microwave-vacuum infrared drying, and freezing followed by microwave-vacuum drying are used for drying monk fruit (19). Currently, both types of monk fruit products are widely available in the market. It is reported that drying methods may greatly affect the bioactive and nutritional components of monk fruit. Lu et al. found that monk fruits dried with freezing contained higher content of mogroside V than those dried under high temperatures (20). In addition, the contents of 10 mogrosides in monk fruits processed by vacuum drying method were markedly higher than those in traditional drying samples (21). Wang et al. indicated that high-temperature drying treatment resulted in a significant decrease in sucrose and glucose concentrations compared with freeze-dried fruit (22). However, these reports employed high-performance liquid chromatography which mainly focused on only mogrosides or sugars due to their different polarity. Simultaneous analysis of multiple components may reflect the quality more comprehensively. Therefore, in this study, 16 compounds in monk fruit products, such as 13 mogrosides [mogroside V (**1**), 11-oxo-mogroside V (**2**), isomogroside V (**3**), mogroside IV (**4**), siamenoside I (**6**), mogroside IV A (**7**), mogroside III A1 (**10**), mogroside III E (**11**), mogroside III (**12**), mogroside II A2 (**14**), mogroside II A1 (**15**) and mogroside II E (**16**)], 1 flavonoid [grosvenorine (**13**)], and 3 sugars [sucrose (**5**), glucose (**8**), and fructose (**9**)] (**Figure 1**) were analyzed by high-performance thin-layer chromatography (HPTLC), which has the advantages of high selectivity for complex components and high efficiency for comparing a large number of samples simultaneously. Then, chemometric analysis was performed to compare the chemical differences in monk fruit products processed by different drying methods.

MATERIALS AND METHODS

Materials and Chemicals

Monk fruit samples of different sizes (S: small; M: medium; L: large; and XL: extra-large) and processed by different drying methods (HT: high temperature and LT: low temperature) were collected at pharmacies from different locations in China. All monk fruit samples were produced in Guilin, Guangxi, and their information is listed in **Supplementary Table 1**. The botanical origin of materials was identified by Dr. Xiao-Jia Chen, one of the authors. All voucher specimens were deposited at the Institute of Chinese Medical Sciences, University of Macau, Macao SAR, China.

All chemicals and solvents were of analytical grade. Ethanol and acetic acid were bought from Xilong Scientific Co., Ltd. (Shantou, China), and sulfuric acid (98%) was acquired from Merck (Darmstadt, Germany). Ethyl acetate was purchased from ACI Lascan Limited (Bangkok, Thailand). Methanol was obtained from Damao Chemical Reagent Factory (Tianjin, China) while *n*-butanol was purchased from Tianjin Fuyu Chemical Reagent Factory (Tianjin, China). All mogrosides (mogroside V, 11-oxo-mogroside V, isomogroside V, mogroside IV, siamenoside I, mogroside IV A, mogroside II A1, mogroside II E, mogroside II A2, mogroside III, mogroside III A1, and mogroside III E) and grosvenorine were purchased from Chengdu Purify Co., Ltd. (Chengdu, China). Glucose, sucrose, and fructose were acquired from Chengdu Pufei De Biotech Co., Ltd. (Chengdu, China). All aqueous solutions were prepared with deionized water purified by the Millipore Milli Q-Plus system (Millipore, Billerica, MA, United States).

Sample Preparation

Dried powdered samples (2.0 g) were sonicated with 40 ml of mill-Q water for 30 min, then the extract was centrifugated at 3,000 rpm for 5 min. The supernatant was collected and extracted with 20 ml of water-saturated *n*-butanol two times. Then, the *n*-butanol fractions were combined and evaporated to dryness in a rotary evaporator. The residue was dissolved in 2.0 ml of methanol and filtered through a 0.22 μm nylon membrane for further experiment.

Standard Solutions Preparation

Separate stock solutions (1 mg/ml) of the 16 compounds were prepared in methanol or water. Then, two mixed standard solutions were prepared, respectively, by mixing equal volumes of the corresponding stock solutions. Mixed standard solution 1 (MS1) was composed of mogroside V, isomogroside V, mogroside IV, siamenoside I, mogroside IV A, mogroside II A1, mogroside II E, mogroside II A2, mogroside III, mogroside III A1, mogroside III E, and glucose at the final concentration of 0.08 mg/ml, while the other components (11-oxo-mogroside V, grosvenorine, fructose and sucrose) were mixed to form the mixed standard solution 2 (MS2) at the final concentration of 0.25 mg/ml.

High-Performance Thin-Layer Chromatography Analysis

A CAMAG TLC system (CAMAG, Switzerland) containing an automatic thin-layer chromatography (TLC) sampler 4 with a 25 μl syringe, an automatic developing chamber, a chromatogram immersion device III, a TLC plate heater III, a TLC visualizer equipped with visionCATS (version 2.5) software, and a TLC scanner 4 was employed for the analyses. To maintain a similar application amount of each standard on the plate, different application volumes were used. MS 1 (22 μl), MS 2 (8 μl), and 28 sample solutions (2 μl) were applied as 8 mm bands and 8 mm from the bottom edge on HPTLC silica gel 60 F_{254} plates (20 cm × 10 cm, Merck, Darmstadt, Germany). After sample application, the plate was pre-saturated with the mobile phase of *n*-butanol - water-ethanol-acetic acid (7:1:1:0.2, v/v/v/v) for 30 min in a glass double-twin trough chamber, then the plate was developed with the same developing agent to 80 mm from the bottom edge. After drying, the plate was then immersed in 10% sulfuric acid in ethanol solution for 1 s and heated at 105°C for 10 min on a TLC plate heater. All plate images were documented under white light and UV 366 nm. Then, the plate was scanned at 290 nm with a scanning speed of 20 mm/s and a slit dimension of 5 × 0.2 mm being employed.

Data Analysis

The obtained HPTLC images were uploaded to the rTLC V.1.0 program[1] for processing (23). The data of every track in the HPTLC images under UV 366 nm were extracted by adjusting the parameters based on sample application. Then, the data matrix of the red channel consisting of sample code, variables ID (R_f

[1]http://shinyapps.ernaehrung.uni-giessen.de/rtlc/

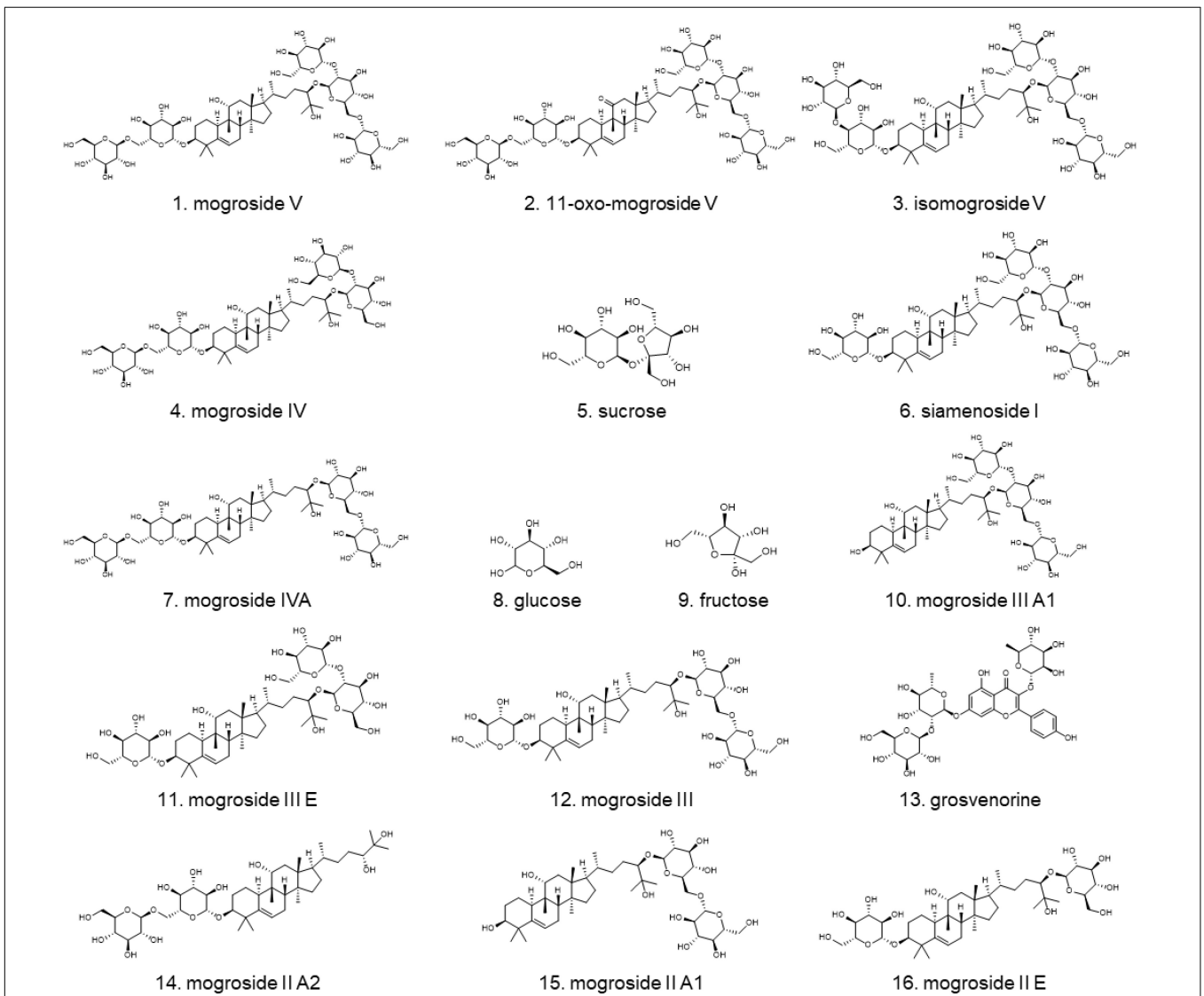

FIGURE 1 | Chemical structures of 16 investigated compounds.

region), and pixel intensity was exported as csv. format and further analyzed using SIMCA software (version 14.1, Umetrics).

RESULTS AND DISCUSSION

Optimization of the High-Performance Thin-Layer Chromatography Conditions

Different developing agents were optimized to achieve good separation. The mobile phase in the Chinese Pharmacopoeia, *n*-butanol-ethanol-water (8:2:3, v/v/v) (1) was first tried, but the mogrosides with the same number of sugar units were hard to be separated. By using the upper layer of *n*-butanol–ethyl acetate-water (4:2:4, v/v/v), the separation of similar mogrosides was greatly improved but the R_f value of mogroside V was too low. With *n*-butanol-water ethanol (7:1:1, v/v/v), the R_f value of mogroside V increased but the chromatographic trailing of mogroside V in samples existed. Finally, a satisfactory result was presented by using *n*-butanol-water-ethanol-acetic acid (7:1:1:0.2, v/v/v/v) as the mobile phase. However, under this condition, mogroside V and 11-oxo-mogroside V, mogroside IV, and sucrose, as well as fructose and glucose were still hard to be separated (**Figure 2**). Therefore, unseparated reference standards were prepared in two different solutions to avoid the overlapping of structural analogs.

Comparison of Monk Fruit Samples Dried at High Temperature and Low Temperature by High-Performance Thin-Layer Chromatography Images Directly

Monk fruit samples of different sizes and dried at different temperatures were analyzed by the developed HPTLC method. As shown in **Figure 2** and **Supplementary Figure 2**, there was no significant difference among the samples of different sizes processed by the same drying method, but the drying method did have influence on the chemical compositions of monk fruit. Mogroside V and 11-oxo-mogroside V, isomogroside V, mogroside IV, siamenoside I, glucose, and fructose were observed in all samples, while sucrose was only detected in LT groups. The major differences between HT and LT samples were in the range of R_f 0.10–0.25, in which the contents of mogroside V, 11-oxo-mogroside V, and isomogroside V in LT groups were much higher than those in HT samples. Moreover, mogroside IV A could be found in HT samples but was hardly detected in most of the LT samples. These results were consistent with the previous reports (20–22).

Comparison of Monk Fruit Samples Dried at High Temperature and Low Temperature by Chemometric Approaches

Although an obvious difference in the HPTLC profiles could be visually inspected between HT and LT monk fruit samples, visual observation was insufficient to discriminate between these two groups. Therefore, chemometric approaches were applied to further explore the chemical characteristics of the two types of monk fruits. The whole HPTLC chromatograms under 366 nm were processed by rTLC program to generate a dataset involving sample code, R_f region, and pixel intensity, and a total of 91 variables were extracted across samples (**Supplementary Table 2**). Principal component analysis (PCA) was first applied to obtain a basic insight into the specific grouping patterns between the monk fruit samples. As shown in **Figure 3A**, the PCA score plot showed a tendency to separate the monk fruit samples in terms of the drying method. The model is composed of five principal components with R^2X value of 0.820 and Q^2 value of 0.646, indicating good fitness and prediction of the constructed PCA model.

To further characterize the differences in monk fruit samples treated with different drying methods, orthogonal partial least square-discriminant analysis (OPLS-DA) was subsequently conducted to sharpen the separation between the groups in PCA. As shown in **Figure 3B**, 28 monk fruit samples were divided into two classes based on different drying methods. All the samples

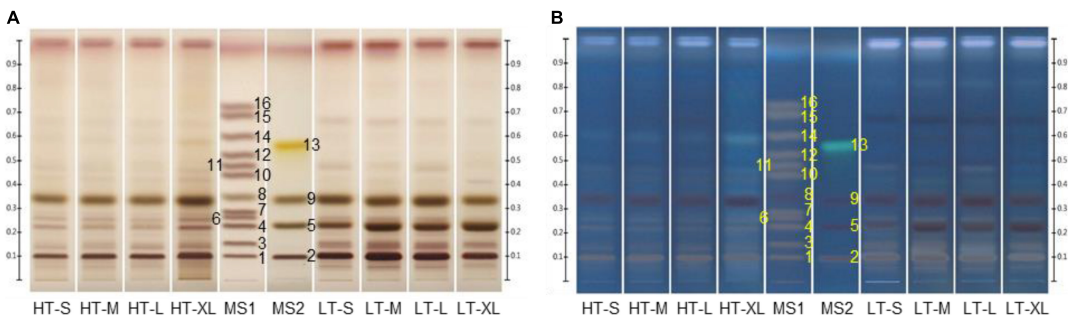

FIGURE 2 | Representative high-performance thin-layer chromatography (HPTLC) chromatograms of mixed standards and monk fruit samples. Plates were immersed into 10% sulfuric acid in ethanol solution for derivatization and photographed under **(A)** white light and **(B)** UV 366 nm. HT, monk fruit dried at high temperature; LT, monk fruit dried at low temperature; S, small; M, medium; L, large; XL, extra-large; MS1 and MS2, mixed standards. (1) Mogroside V (R_f 0.10), (2) 11-oxo-mogroside V (R_f 0.10), (3) isomogroside V (R_f 0.15), (4) mogroside IV (R_f 0.23), (5) sucrose (R_f 0.23), (6) siamenoside I (R_f 0.26), (7) mogroside IV A (R_f 0.29), (8) glucose (R_f 0.35), (9) fructose (R_f 0.34), (10) mogroside III A1 (R_f 0.44), (11) mogroside III E (R_f 0.48), (12) mogroside III (R_f 0.53), (13) grosvenorine (R_f 0.56), (14) mogroside II A2 (R_f 0.60), (15) mogroside II A1 (R_f 0.69), and (16) mogroside II E (R_f 0.73).

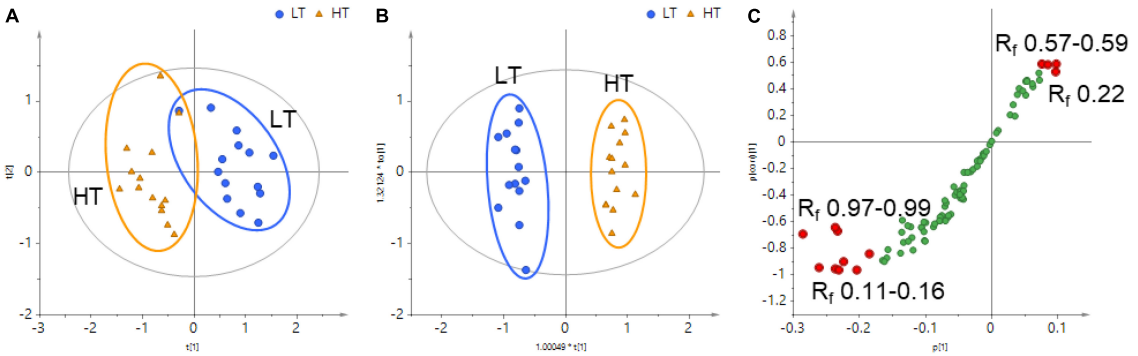

FIGURE 3 | (A) Principal component analysis (PCA) score plot, **(B)** orthogonal partial least square-discriminant analysis (OPLS–DA) score plot, and **(C)** OPLS–DA S-plot of HT and LT samples based on the data extracted from the whole HPTLC chromatograms. The variables contributing most to the differences were highlighted with red-filled circles.

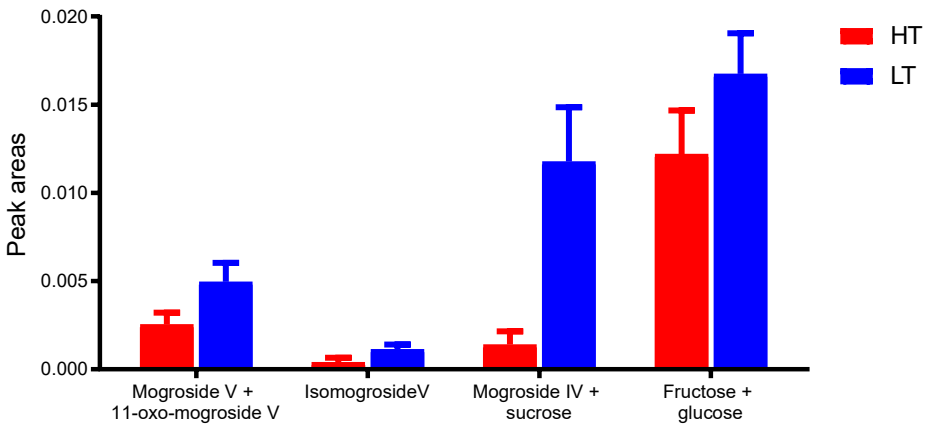

FIGURE 4 | Peak areas of selected mogrosides and sugars in HT and LT samples by HPTLC-scanning.

fell within the Hotelling T2 (0.95) ellipse, where the model fit parameters were 0.699 of R^2X, 0.974 of R^2Y, and 0.929 of Q^2, indicating that the OPLS-DA model established in this study has high goodness-of-fit and predictive ability.

An S-plot was constructed following the OPLS-DA to reveal the chemical components contributing mostly to the differences between the HT and LT groups. In this plot, the data points at the two ends of the S-shaped curve made the greatest contribution to the two-group separation with the highest confidence, which were highlighted in red in **Figure 3C**. The bands of R_f 0.11–0.16 and R_f 0.97–0.99 at the bottom-left corner and the bands of R_f 0.57–0.59 and R_f 0.22 at the top-right corner of the S-shaped curve were considered as the characteristic components contributing most to the distinction of HT and LT groups. Compared with the reference standards, the bands of R_f 0.10, 0.15, and 0.22 contained mogroside V and 11-oxo-mogroside V, isomogroside V, and mogroside IV and sucrose are not separated by the HPTLC method and they correspond to the band of Rf 0.22, respectively.

PCA and OPLS-DA based on the HPTLC data of the 16 compounds with reference standards were also conducted. As shown in **Supplementary Figure 3**, the two types of monk fruit samples were also clearly separated, and mogroside V, 11-oxo-mogroside V, and isomogroside V were the most discriminating between the two groups. Compared with the analysis based on the 16 compounds, the results based on the data from the whole chromatograms could reflect the differences between groups more comprehensively, and more discriminating variables could be found. However, it was difficult to identify the unknown bands under the current HPTLC condition due to the low contents or the poor separation. Further isolation and identification by other chromatographic and detection techniques should be performed in the future.

Semi-Quantification by High-Performance Thin-Layer Chromatography-Scanning

Based on the above results, mogroside V, 11-oxo-mogroside V, isomogroside V, mogroside IV and sucrose were found to be the characteristic compounds to distinguish the two types of monk fruits. Furthermore, fructose and glucose were also important nutritional ingredients in monk fruit. Therefore, these compounds were semi-quantified by HPTLC-scanning to verify

their differences in HT and LT monk fruit samples. Due to the poor resolution, the bands were scanned in four groups, i.e., mogroside V and 11-oxo-mogroside V; isomogroside V; mogroside IV and sucrose were scanned as one group; as well as fructose and glucose. As shown in **Figure 4**, the peak areas of all the investigated compounds in LT samples were significantly higher than those in HT samples, which further confirmed the influence of different drying methods on the chemical components of monk fruit samples.

Possible Factors Affecting the Chemical Compositions of the Processed Monk Fruit

During the drying process, many factors, such as temperature, enzymes, and intermediate products may affect the chemical compositions of the processed monk fruit. It was reported that several enzymes, such as squalene epoxidase, triterpenoid synthases, epoxide hydrolases, cytochrome P450s, and UDP-glucosyltransferases, were involved in the biosynthesis of mogrosides, such as mogroside V, 11-oxo-mogroside V, and isomogroside V (24, 25). These enzymes may be inhibited at high temperature, which may decrease the content of these mogrosides in HT samples (26). While for the sugars, on the one hand, high temperature may lead to the degradation of sucrose, oligosaccharides, and polysaccharides, resulting in a decrease of sucrose levels and an increase in glucose and fructose contents. On the other hand, the Maillard reaction, a type of non-enzymatic browning, may take place between the reducing sugars and amino acids that are rich in monk fruit. The reaction may proceed more rapidly at high temperatures, thus decreasing the levels of glucose and fructose in HT samples (27). Under the influences of these effects, the contents of the glucose and fructose in HT samples were lower than those in LT samples. However, how the drying methods influence the chemical components of monk fruit is still not clear, which needs further exploration in the future.

CONCLUSION

In this study, HPTLC combined with chemometric approaches were used to compare the chemical components of monk fruit products dried at high and low temperatures, respectively. As a result, the contents of mogroside V, 11-oxo-mogroside V, isomogroside V, mogroside IV and sucrose in monk fruits dried at low temperature were higher than those in traditional hot-air drying samples. In the future, laboratory simulated studies should be conducted to explore the relationships between the drying methods and the chemical compositions of monk fruit. In addition, the bioactivities of monk fruit processed by different drying methods should be further studied as well.

DATA AVAILABILITY STATEMENT

The original contributions presented in the study are included in the article/**Supplementary Material**, further inquiries can be directed to the corresponding author/s.

AUTHOR CONTRIBUTIONS

H-JH and QY performed the experiment and prepared the manuscript. QL and FL analyzed the data. X-JC designed the study and finalized the manuscript. All authors read and approved the final manuscript.

FUNDING

This study was funded by the Science and Technology Development Fund, Macau SAR (File No. 0016/2021/A, 0098/2020/A, and SKL-QRCM(UM)-2020-2022), the National Natural Science Foundation of China (File No. 82104354), and the funding grants from University of Macau (File Nos. MYRG2018-00207-ICMS and MYRG2019-00121-ICMS).

SUPPLEMENTARY MATERIAL

The Supplementary Material for this article can be found online at: https://www.frontiersin.org/articles/10.3389/fnut.2022.887992/full#supplementary-material

REFERENCES

1. Chinese Pharmacopoeia Commission. Siraitiae Fructus. In: *Chinese Pharmacopoeia Commission editor. Chinese Pharmacopoeia of the People's Republic of China*. Vol. 1. Beijing: China Medical Science and Technology Press (2020). p. 221–2.
2. Gong X, Chen NMH, Ren K, Jia JY, Wei KH, Zhang L, et al. The fruits of *Siraitia grosvenorii*: a review of a chinese food-medicine. *Front Pharmacol.* (2019) 10:1400. doi: 10.3389/fphar.2019.01400
3. Liu HS, Wang CC, Qi XY, Zou J, Sun ZD. Antiglycation and antioxidant activities of mogroside extract from *Siraitia grosvenorii* (Swingle) fruits. *J Food Sci Technol.* (2018) 55:1880–8. doi: 10.1007/s13197-018-3105-2
4. Zhang YL, Zhou GS, Peng Y, Wang MY, Li XB. Anti-Hyperglycemic and anti-hyperlipidemic effects of a special fraction of Luohanguo extract on obese T2DM rats. *J Ethnopharmacol.* (2020) 247:112273. doi: 10.1016/j.jep.2019.112273
5. Liu HS, Qi XY, Yu KK, Lu AJ, Lin KF, Zhu JJ, et al. AMPK activation is involved in hypoglycemic and hypolipidemic activities of mogroside-rich extract from *Siraitia grosvenorii* (Swingle) fruits on high-fat diet/streptozotocin-induced diabetic mice. *Food Funct.* (2019) 10:151–62. doi: 10.1039/c8fo01486h
6. Liu C, Dai LH, Dou DQ, Ma LQ, Sun YX. A natural food sweetener with anti-pancreatic cancer properties. *Oncogenesis.* (2016) 5:e217. doi: 10.1038/oncsis.2016.28
7. Liu C, Dai LH, Liu YP, Rong L, Dou DQ, Sun YX, et al. Antiproliferative activity of triterpene glycoside nutrient from monk fruit in colorectal cancer and throat cancer. *Nutrients.* (2016) 8:360. doi: 10.3390/nu8060360
8. Shen JK, Shen D, Tang Q, Li ZJ, Jin XM, Li CM. Mogroside V exerts anti-inflammatory effects on fine particulate matter-induced inflammation in porcine alveolar macrophages. *Toxicol Vitro.* (2022) 80:105326. doi: 10.1016/j.tiv.2022.105326
9. Liu YS, Wang J, Guan X, Yu D, Huangfu MJ, Dou T, et al. Mogroside V reduce OVA-induced pulmonary inflammation based on lung and serum

metabolomics. *Phytomedicine.* (2021) 91:153682. doi: 10.1016/j.phymed.2021.153682
10. Sung YY, Kim SH, Yuk HJ, Yang WK, Lee YM, Son E, et al. *Siraitia grosvenorii* residual extract attenuates ovalbumin-induced lung inflammation by down-regulating IL-4, IL-5, IL-13, IL-17, and MUC5AC expression in mice. *Phytomedicine.* (2019) 61:152835. doi: 10.1016/j.phymed.2019.152835
11. Luo HJ, Peng CX, Xu XF, Peng YT, Shi F, Li QH, et al. The protective effects of mogroside V against neuronal damages by attenuating mitochondrial dysfunction via upregulating Sirtuin3. *Mol Neurobiol.* (2022): [Online ahead of print] doi: 10.1007/s12035-021-02689-z
12. Wang H, Meng GL, Zhang CT, Wang H, Hu M, Long Y, et al. Mogrol attenuates lipopolysaccharide (LPS)-induced memory impairment and neuroinflammatory responses in mice. *J Asian Nat Prod Res.* (2020) 22:864–78. doi: 10.1080/10286020.2019.1642878
13. Chen GL, Liu CH, Meng GL, Zhang CT, Chen F, Tang SS, et al. Neuroprotective effect of mogrol against $A\beta_{1-42}$ induced memory impairment neuroinflammation and apoptosis in mice. *J Pharm Pharmacol.* (2019) 71:869–77. doi: 10.1111/jphp.13056
14. Fang CN, Wang QQ, Liu XY, Xu GW. Metabolic profiling analysis of *Siraitia grosvenorii* revealed different characteristics of green fruit and saccharified yellow fruit. *J Pharm Biomed Anal.* (2017) 145:158–68. doi: 10.1016/j.jpba.2017.06.046
15. Cicek SS, Esposito T, Girreser U. Prediction of the sweetening effect of *Siraitia grosvenorii* (Luo Han Guo) fruits by two-dimensional quantitative NMR. *Food Chem.* (2021) 335:127622. doi: 10.1016/j.foodchem.2020.127622
16. Li C, Lin LM, Sui F, Wang ZM, Huo HR, Dai L, et al. Chemistry and pharmacology of *Siraitia grosvenorii*: a review. *Chin J Nat Med.* (2014) 12:89–102. doi: 10.1016/S1875-5364(14)60015-7
17. Wang MY, Xing SH, Luu T, Fan M, Li XB. The gastrointestinal tract metabolism and pharmacological activities of grosvenorine, a major and characteristic flavonoid in the fruits of *Siraitia grosvenorii*. *Chem Biodivers.* (2015) 12:1652–64. doi: 10.1002/cbdv.201400397
18. Xu WK, Meng LS. Analysis of sugar content in Siraitiae Fructus. *Guangxi Agric Sci.* (1980) 29.
19. Ji L. *Effects of Different Drying and Processing Methods on Vitamin C, Color, Phenolics, Antioxidant Activity, and Mogroside V of Luo Han Guo (Siraitia Grosvenorii) Drink*. Master's tehsis. New Brunswick, NJ: Rutgers, The State University of New Jersey (2016).
20. Lu FL, Li DP, Liu JL, Huang YL. Chromatographic fingerprinting analysis on chemical compositions of *Siraitia grosvenorii* fruit with different drying treatments. *Guangxi Agric Sci.* (2009) 40:625–8.
21. Zhou L, Zhu YY. The effect of vacuum drying method on the content of ten mogrol glycosides in Siraitiae Fructus by HPLC-MS. *Chin J Pharm Anal.* (2014) 34:275–80. doi: 10.16155/j.0254-1793.2014.02.009
22. Wang HY, Ma XJ, Mo CM, Zhao H, Tu DP, Bai LH, et al. Determination of sugar components and contents in fruit flesh of *Siraitia grosvenorii*. *Guihaia.* (2015) 35:775–81.
23. Fichou D, Ristivojević P, Morlock GE. Proof-of-Principle of rTLC, an open-source software developed for image evaluation and multivariate analysis of planar chromatograms. *Anal Chem.* (2016) 88:12494–501. doi: 10.1021/acs.analchem.6b04017
24. Itkin M, Davidovich-Rikanati R, Cohen S, Portnoy V, Doron-Faigenboim A, Oren E, et al. The biosynthetic pathway of the nonsugar, high-intensity sweetener mogroside V from *Siraitia grosvenorii*. *Proc Natl Acad Sci U S A.* (2016) 113:E7619–28. doi: 10.1073/pnas.1604828113
25. Zhang J, Dai L, Yang J, Liu C, Men Y, Zeng Y, et al. Oxidation of cucurbitadienol catalyzed by CYP87D18 in the biosynthesis of mogrosides from *Siraitia grosvenorii*. *Plant Cell Physiol.* (2016) 57:1000–7. doi: 10.1093/pcp/pcw038
26. Wang HY, Ma XJ, Mo CM, Zhao H, Tu DP, Bai LH, et al. Effects of shading on contents of mogrosides and sugars in fruit flesh of *Siraitia grosvenorii*. *Guihaia.* (2016) 36:1344–52.
27. Ames JM. The maillard reaction. In: Hudson BJF editor. *Biochemistry of Food Proteins*. Boston, MA: Springer (1992). p. 99–153.

Conflict of Interest: The authors declare that the research was conducted in the absence of any commercial or financial relationships that could be construed as a potential conflict of interest.

Publisher's Note: All claims expressed in this article are solely those of the authors and do not necessarily represent those of their affiliated organizations, or those of the publisher, the editors and the reviewers. Any product that may be evaluated in this article, or claim that may be made by its manufacturer, is not guaranteed or endorsed by the publisher.

frontiers | Frontiers in Nutrition

MINI REVIEW
published: 11 May 2022
doi: 10.3389/fnut.2022.888245

Application of Machine Vision System in Food Detection

Zhifei Xiao, Jilai Wang, Lu Han*, Shubiao Guo and Qinghao Cui*

Key Laboratory of High Efficiency and Clean Mechanical Manufacture of Ministry of Education, School of Mechanical Engineering, National Demonstration Center for Experimental Mechanical Engineering Education, Shandong University, Jinan, China

Food processing technology is an important part of modern life globally and will undoubtedly play an increasingly significant role in future development of industry. Food quality and safety are societal concerns, and food health is one of the most important aspects of food processing. However, ensuring food quality and safety is a complex process that necessitates huge investments in labor. Currently, machine vision system based image analysis is widely used in the food industry to monitor food quality, greatly assisting researchers and industry in improving food inspection efficiency. Meanwhile, the use of deep learning in machine vision has significantly improved food identification intelligence. This paper reviews the application of machine vision in food detection from the hardware and software of machine vision systems, introduces the current state of research on various forms of machine vision, and provides an outlook on the challenges that machine vision system faces.

Keywords: machine vision system, deep learning, food detection, food classification, food Image analysis

OPEN ACCESS

Edited by:
Qiang Xia,
Ningbo University, China

Reviewed by:
Yang Tao,
Nanjing Agricultural University, China

****Correspondence:***
Jilai Wang
jlwang@sdu.edu.cn
Lu Han
jl.wang@connect.polyu.hk

Specialty section:
This article was submitted to Food Chemistry, a section of the journal Frontiers in Nutrition

Received: *02 March 2022*
Accepted: *22 April 2022*
Published: *11 May 2022*

Citation:
Xiao ZF, Wang JL, Han L, Guo SB and Cui QH (2022) Application of Machine Vision System in Food Detection. Front. Nutr. 9:888245. doi: 10.3389/fnut.2022.888245

INTRODUCTION

The food industry is becoming more competitive and dynamic, and consumers' awareness of what they are eating is increasing (1). Consumers' desires for diversified functions of food have gradually increased over the last few years (2). This is due to new demands not only for food's nutritional needs but also for its health and quality (3). In order to improve the efficiency and quality of food production, efficient and advanced food processing detection methods need to be developed (4).

Food quality and safety are the foundations of food processing and human health, thus classification and inspection of food are critical in the food processing (5). Traditionally, the quality of ingredients was mainly determined by human sensory testing, which is inefficient and subjective (6). The machine vision system can capture various information of food including size and dimensions, appearance and shape, and surface color, etc. It can accurately capture the detailed information of food products, improve the accuracy of monitoring and monitor food processing with limited human errors (7). Because of the advancement of computer technology, machine vision system has been applied in industrial applications, including the food processing industry (8).

The main function of computer vision is to simulate the video and graphic information seen by human eyes and to monitor and process existing data image information, which can facilitate technicians to quickly capture sensitive detection indicators in the process of data entry, information integration, data analysis and data labeling (9). Machine vision systems usually include two parts: image information capture and image information

sprocessing. Image information capture is mainly through a variety of hardware devices for real-time acquisition of food image information. Information processing is through the setting of scientific operating procedures, the core stored information for secondary evaluation, to facilitate the technical staff to timely probe, receive, and understand the actual state of low level visual inspection information (10). computer technology is primarily used for food material classification and defect analysis (11). Through machine vision and deep learning, computer technology provides an accurate, efficient, and non-destructive method for detecting and grading agricultural products (12). The computer vision system and deep learning framework are shown in **Figure 1**.

The purpose of this review is to review the impact of computer technology on food detection and assortment, and to provide a reliable reference for further research on the intelligence and efficiency of the food industry.

COLLECTION OF TESTED FOOD INFORMATION

Machine vision system consists of an image acquisition equipment and an image information processing system. Among them, the image acquisition equipment has a variety of acquisition forms, including X-ray, thermal imaging, remote sensing imaging, magnetic resonance imaging, and other acquisition equipment in addition to the common high definition camera (14). Image information processing is the analysis of the acquired food information, mainly extracting and identifying the

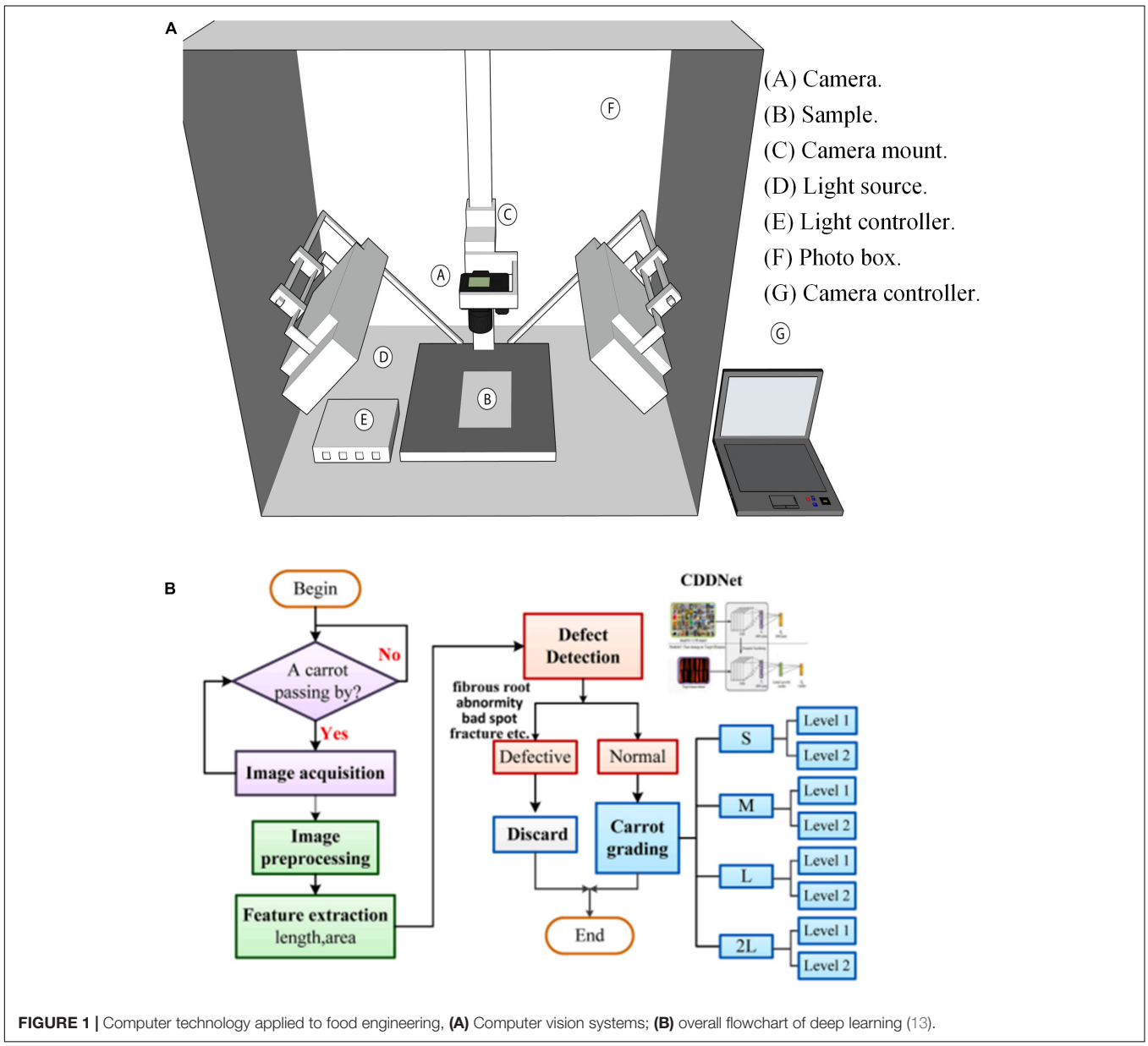

FIGURE 1 | Computer technology applied to food engineering, **(A)** Computer vision systems; **(B)** overall flowchart of deep learning (13).

acquired image information. This process of image acquisition can be seen as the acquisition of image signals and does not involve changes in the interpretation of the image content or meaning (15).

High Definition Camera Acquisition Equipment

Machine vision for recognizing food information is becoming increasingly popular, such as food defect recognition and ripeness analysis (16). For food defect detection, Patel et al. (17) developed a method using monochrome cameras for automatic mango sorting, and result showed that the system's detection efficiency and accuracy reached 97.88% and 88.75%, respectively. Noor Fatima et al. (18) used industrial cameras combined with deep learning to develop a device for tracking the adulteration of papaya seeds in black pepper. Furthermore, machine vision can identify and classify food products based on their color. Burce Atac et al. (19) proposed a method to extract average or characteristic color information from digital images of food products, and discussed specific applications for different food products. Ayustaningwarno et al. (20) used computer image analysis to quantify the color distribution of fried mangoes. To verify the efficiency of machine vision, Fitriyono Ayustaningwarno et al. (21) experimentally compared the ability of sensory testing, Hunterlab colorimeter, a commercial machine vision system (IRIS-Alphasoft), and the custom-made machine vision system (Canon) techniques to discriminate among nine vacuum-fried fruit samples.

With the increasingly widespread use of machine vision, it becomes increasingly common to use stereo systems to collect depth information about the environment for object recognition and environmental modeling. To increase the accuracy and authenticity of image information collection, 3D stereo cameras are used in food inspection (22). Stereo camera prototypes are used to capture pairs of images for estimating the size of target foods (23). Su et al. (24) used a depth camera based on machine vision technique to successfully assess the sample quality in 3D space of potatoes. Sepehr Makhsous et al. (25) stated that 3D detection system can monitor food volume for accurate monitoring of diabetic patients' dietary intake. Yao et al. (26) proposed a potato volume measurement method based on RGB-D camera to achieve automatic monitoring of potato volume. The prediction errors were found to be 9% for regular potatoes and 30% for irregular potatoes through experiments.

Due to the diversity and complexity of the food industrial identification objectives, high definition camera has a number of problems in its application (27). Firstly, high definition camera requires high working conditions and cannot handle image information with high noise and low brightness. In addition, when the quality characteristics are mainly determined by the inherent properties of the sample (composition and internal physical properties), computer vision techniques appear less effective because they are not easily detected from the surface. Furthermore, high definition cameras has limitations in recognizing defects with high color similarity. To improve the recognition ability of machine vision, some corresponding acquisition devices have been developed for the application in food inspection.

Other Information Collection Equipments

Due to the development and maturity of imaging spectroscopy technology, hyperspectral imaging sensors are used for the accurate detection of food appearance (28). Xi et al. (29) investigated the effect of different peel colors on soluble solids content using hyperspectral imaging and developed a prediction model for soluble solids content. To improve identification efficiency, Li et al. (17) developed an improved watershed segmentation algorithm with morphological gradient reconstruction and marker extraction, which is different from the traditional segmentation algorithm, and applied it to analyze multispectral images. The test results showed that the recognition accuracy of the algorithm was found to be 100%. Zhang et al. (30) developed a multispectral image classification algorithm for the detection of common citrus defects based on visible-NIR hyperspectral imaging technology, and successfully applied it to the detection of citrus defects. For internal food inspection, the information acquisition equipment can use X-ray and magnetic resonance imaging. X-ray devices are used to detect foreign objects inside food by using X-rays through the food surface, and Kazuya Urazoe et al. (31) used X-rays combined with deep learning to successfully apply them to the detection of fish bones.

Magnetic resonance imaging can non-destructively detect and image the structure of food (32). Nakashima (33) developed a set of handheld magnetic resonance sensors consisting of a planar RF coil and a single-sided magnetic circuit for the measurement of the internal fat content of tuna. The temperature of food is one of the key factors affecting the quality of food, and thermal imaging can monitor and control the temperature of food at various points in the process (34). Zeng et al. (35) built a thermal imaging system for pear detection and used an improved deep learning algorithm based on a small sample dataset of thermal images to classify pears with or without bruises. For large-scale agri-food detection, remote sensing technology is used to increase agricultural yields and reduce input losses (36). Romanko and Matthew (37) assessed the effectiveness of remote sensing technology in modeling several important agrochemical parameters, noting that remote sensing technology can promote modern agriculture, improve the efficiency of agrochemical use and reduce environmental pollution. Lin et al. (38) used high resolution (6 m) multispectral satellite imagery SPOT-6 for monitoring powdery mildew in winter wheat in areas with severe disease infection and pointed out the great potential of high resolution multispectral satellite imagery data for crop disease monitoring.

IMAGE INFORMATION PROCESSING BASED ON DEEP LEARNING

In the food inspection process, image information processing and analysis is at the core of computer vision inspection. The purpose of image processing is to improve picture quality and to address defects such as picked geometric distortion, incorrect

focus, picture noise, uneven illumination and camera motion. Image analysis is the process of distinguishing objects (objects to be detected) from the background and generating quantitative information that is used in the subsequent control system for decision making. The processing of image information can be divided into three levels: low level processing (image acquisition and pre-processing), mid-level processing (image segmentation and description) and high level processing (recognition and interpretation).

Low Level Processing

Computer processing can only process data in digital form, so it is necessary to transform the food information acquired by various collection devices. The relevant information acquired through hardware has certain defects due to the acquisition environment (light, humidity) as well as the equipment (device motion, transmission distance). In order to improve the recognition accuracy of machine vision, pre-processing of the information, including noise reduction, contrast adjustment, etc., is required. Among them, Che et al. (39) performed low order processing of the acquisition information and reflection calibration of the image information in order to reduce the effects of different configurations of camera quantum efficiency and hyperspectral imaging systems, thus improving the subsequent recognition accuracy. Fan et al. (40) corrected the original hyperspectral images using white and dark reference images in order to improve the recognition rate of internal bruises in blueberries, thus eliminating current-induced image noise and errors caused by non-uniform illumination.

Mid-Level Processing

Intermediate processing focuses on image segmentation, image representation and description. Its main purpose is to select the overall information collected to detect the object region. Image segmentation is one of the most important steps in the whole image processing technique, which can improve the accuracy and recognition efficiency of the subsequent advanced processing. Intermediate level processing has important applications in machine vision. Li et al. (41) proposed an improved watershed segmentation algorithm based on morphological filtering and morphological gradient reconstruction and marker constraints for segmenting rotten points on apples in order to achieve fast automatic recognition of whether a fruit is rotten or not. Che et al. (39) built and compared different bruise extraction models after selecting the region of interest by certain rules. The comparison revealed that the random model algorithm was more suitable than other algorithms for classifying bruises on apples. Luo et al. (42) used an improved watershed segmentation algorithm for bruise detection analysis on multispectral principal component analysis images and obtained an overall detection accuracy of 99.5%. Li et al. (43) used bi-dimensional empirical pattern decomposition for removing noise from multispectral images and further reconstructing the images. And an improved watershed segmentation method with morphological gradient reconstruction, marker extraction and image correction is proposed to segment the decayed regions in fruits using the reconstructed multispectral images.

High Level Processing (Deep Learning Image Processing)

Common techniques for evaluating food quality include deep learning techniques, statistical learning, fuzzy logic and genetic algorithms. In the last few years, deep learning methods have shown excellent computational performance in several fields, among which the field of computer vision is one of the most prominent application areas of deep learning. Among the various deep learning neural networks, convolutional neural networks have been applied to computer vision, which is particularly suitable for handling various tasks in the field of computer vision, such as image classification, object detection, and semantic segmentation. With the advancement of machine learning, especially the development of convolutional neural networks, the collected food pictures can be further processed to classify the food (44). A CNN model of image recognition is shown in **Figure 2**. Deep learning automatically extract the features of food shape through neural grid learning, which has the advantage of intelligent recognition compared with traditional image processing methods (45).

Researchers are currently conducting extensive studies on the applications of deep learning in food safety and quality assessment. The recognition steps of conventional deep learning are to collect a large number of required building datasets, then use the datasets to train a network model, and finally use

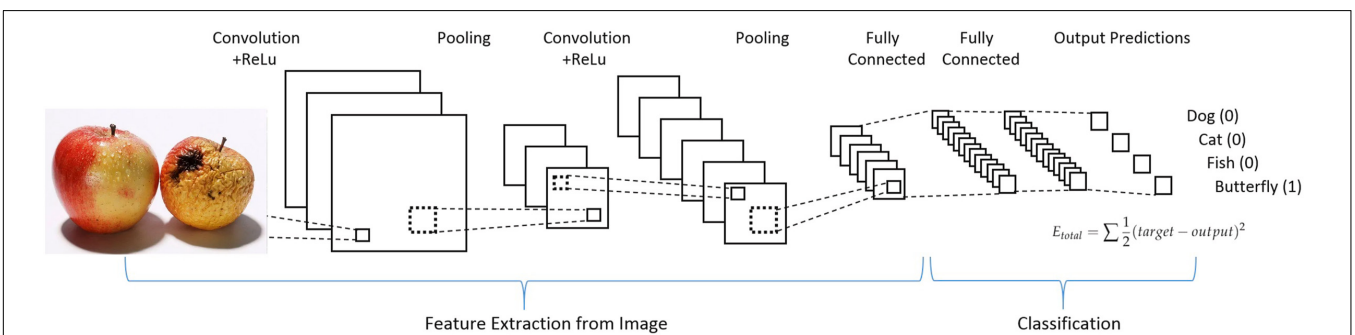

FIGURE 2 | The architecture of a typical CNN.

the training model for the detection and recognition of food images (46). Xie et al. (47) used five classical CNN (Densenet-121, ResNet-50, Inception-V3, VGG-16 and VGG-19) models to identify defective carrots and found that CNN models can be an effective method to identify defective carrots through experiments. As an upgrade to machine vision systems, Deng et al. (48) used machine vision combined with deep learning to achieve automatic grading of carrots and improve the intelligence of recognition. Zhu et al. (49) proposed an improved dense capsule network model (Modified-DCNet) for carrot appearance quality detection. This modified model introduces a self-attention layer, which reduces the interference of background information on the recognition task. Moreover, the capsule layer of the modified model uses a locally constrained dynamic routing algorithm to reduce the size of the network parameters and the training load of the network. To improve the accuracy of identification, Rong et al. (50) used deep learning to detect peach varieties and established a VIS-NIR spectral database containing five peach varieties to achieve accurate identification of peach varieties. After testing, it was found that the deep learning-based model achieved the accuracy of 100% in the validation dataset and the accuracy of 94.4% in the test dataset. To improve the recognition efficiency of deep learning, Muoz et al. (51) used different deep learning networks to detect the intramuscular fat content in dry cured ham and found that CNNs can accurately identify and takes less time on the network development by comparison.

Despite its accuracy in image recognition, deep learning has some inherent disadvantages: (1) it requires a large number of food images for input training when performing grid training, (2) deep learning requires high computing performance of the computer, and (3) it takes a lot of time during training.

CONCLUSION AND FUTURE PERSPECTIVES

By summarizing the basic concepts and technologies of machine vision systems, as well as the latest developments and applications of systems in the food detection industry, the following conclusions have been drawn.

(1) The application of computer vision technology in food detection has greatly improved the efficiency of food inspection and promoted the development of food safety, which is an important part of the intelligent process of food engineering. The use of computer vision systems enables automated, objective, rapid and hygienic inspection of a wide range of raw and processed foods.
(2) Machine vision has high recognition accuracy, however, under low light, high humidity, and high noise conditions, there are corresponding detection errors. Therefore, it is necessary to develop high-resolution acquisition devices to improve the quality/accuracy of inspection.
(3) Image processing is considered to be the core of computer vision. With same acquired information, advanced processing software can improve processing efficiency and recognition accuracy. Therefore, it is significant to develop more efficient algorithms to make machine vision more suitable for food inspection.

AUTHOR CONTRIBUTIONS

ZX: information collection and writing. JW: figure preparation and proofreading. LH: manuscript framework and writing. SG and QC: writing. All authors contributed to the article and approved the submitted version.

FUNDING

This study was supported by the Young Scholars Program of Shandong University, the Undergraduate Education Teaching Reform and Research Programs of Shandong University (2021Y220), and the Shandong Provincial Natural Science Foundation (ZR2019BEE062).

REFERENCES

1. Xun S, Shuai L, Zhang XY, Yang T, Grzegorz B, Joon YY, et al. Recent advances in hydrodynamic cavitation-based pretreatments of lignocellulosic biomass for valorization. *Bioresour Technol.* (2021) 345:126251. doi: 10.1016/j.biortech.2021.126251
2. Knorr D, Augustin MA. Food processing needs, advantages and misconceptions. *Trends Food Sci Technol.* (2020) 108:103–10. doi: 10.1016/j.tifs.2020.11.026
3. Li CJ, Zhu HM, Li CY, Qian H, Yao WR, Guo YH. The present situation of pesticide residues in China and their removal and transformation during food processing. *Food Chem.* (2021) 354:129552. doi: 10.1016/j.foodchem.2021.129552
4. Xu L, Zheng Y, Zhou C, Pan DD, Geng F, Cao JX, et al. Kinetic response of conformational variation of duck liver globular protein to ultrasonic stimulation and its impact on the binding behavior of n-alkenals. *LWT.* (2021) 150:111890. doi: 10.1016/j.lwt.2021.111890
5. Bei M, Domua C, Jude E, Osvat M, Dragoi AE, Mitrica B. The impact of food quality and safety on consumer perception and attitude to food choices in Romania. Opportunities under Green Deal. *Glob Econ Observer.* (2021) 9:156–65.
6. Pedreschi F, Mery D, Bunger A, Yanez V. Computer vision classification of potato chips by color. *J Food Process Eng.* (2011) 34:1714–28. doi: 10.1111/j.1745-4530.2009.00540.x
7. Zhu LL, Spachos P, Pensini E, Plataniotis KN. Deep learning and machine vision for food processing: a survey. *Curr Res Food Sci.* (2021) 4:233–49. doi: 10.1016/j.crfs.2021.03.009
8. Bhargava A, Bansal A, Goyal V. Machine learning - based detection and sorting of multiple vegetables and fruits. *Food Anal Meth.* (2021) 15:228–42. doi: 10.1007/10_2016_51
9. Bi X. Machine vision. In: Bi X editor. *Environmental Perception Technology for Unmanned Systems*. Singapore: Springer Singapore (2021). p. 105–41.
10. Patel KK, Kar A, Jha SN, Khan MA. Machine vision system: a tool for quality inspection of food and agricultural products. *J Food Sci Technol.* (2012) 49:123–41. doi: 10.1007/s13197-011-0321-4
11. Bhargava A, Bansal A. Fruits and vegetables quality evaluation using computer vision: a review. *J King Saud Univ Comput Inf Sci.* (2021) 33:243–57. doi: 10.1080/10408398.2013.777020

12. Zhang B, Huang W, Li J, Zhao C, Fan S, Wu J, et al. Principles, developments and applications of computer vision for external quality inspection of fruits and vegetables: a review. *Food Res Int.* (2014) 62:326–43. doi: 10.1016/j.foodres.2014.03.012
13. Li S, Zhang R, Lei D, Huang YQ, Cheng SY, Zhu ZZ, et al. Impact of ultrasound, microwaves and high-pressure processing on food components and their interactions. *Trends Food Sci Technol.* (2021) 109:1–15. doi: 10.1016/j.tifs.2021.01.017
14. Xie J, Zheng Y, Du R, Xiong WY, Cao YF, Ma ZY, et al. Deep learning-based computer vision for surveillance in ITS: evaluation of state-of-the-art methods. *IEEE Trans Veh Technol.* (2021) 70:3027–42. doi: 10.3390/s21227543
15. Zhang B, Gu B, Tian GZ, Zhou J, Huang JC, Xiong YJ. Challenges and solutions of optical-based nondestructive quality inspection for robotic fruit and vegetable grading systems: a technical review. *Trends Food Sci Technol.* (2018) 81:213–31. doi: 10.1016/j.tifs.2018.09.018
16. Gila A, Bejaoui MA, Beltrán G, Marquez AJ. Rapid method based on computer vision to determine the moisture and insoluble impurities content in virgin olive oils. *Food Control.* (2020) 113:107210. doi: 10.1016/j.foodcont.2020.107210
17. Li JB, Chen LP, Huang WQ. Detection of early bruises on peaches (Amygdalus persica L.) using hyperspectral imaging coupled with improved watershed segmentation algorithm. *Postharvest Biol Technol.* (2018) 135:104–13. doi: 10.1016/j.postharvbio.2017.09.007
18. Fatima N, Areeb QM, Khan IM, Khan MM. Siamese network-based computer vision approach to detect papaya seed adulteration in black peppercorns. *J Food Process Preserv*. (2021). doi: 10.1111/jfpp.16043
19. Mogol BA, Kmen V. Computer vision-based analysis of foods: a non-destructive colour measurement tool to monitor quality and safety. *J Sci Food Agric.* (2014) 94:1259–63. doi: 10.1002/jsfa.6500
20. Ayustaningwarno F, Ginkel EV, Vitorino J, Dekker M, Verkerk R. Nutritional and physicochemical quality of vacuum-fried mango chips is affected by ripening stage, frying temperature, and time. *Front Nutr.* (2020) 7:95. doi: 10.3389/fnut.2020.00095
21. Ayustaningwarno F, Fogliano V, Verkerk R, Dekker M. Surface color distribution analysis by computer vision compared to sensory testing: vacuum fried fruits as a case study. *Food Res Int.* (2021) 143:110230. doi: 10.1016/j.foodres.2021.110230
22. Vázquez-Arellano M, Griepentrog HW, Reiser D, Paraforos DS. 3-D imaging systems for agricultural applications—a review. *Sensors.* (2016) 16:618. doi: 10.3390/s16050618
23. Smith LN, Zhang W, Hansen MF, Hales LJ, Smith ML. Innovative 3D and 2D machine vision methods for analysis of plants and crops in the field. *Comput Ind.* (2018) 97:122–31. doi: 10.1016/j.compind.2018.02.002
24. Su Q, Naoshi K, Li M, Sun H, Firmanda A, Harshana H. Potato quality grading based on machine vision and 3D shape analysis. *Comput Electron Agric.* (2018) 152:261–8. doi: 10.1016/j.compag.2018.07.012
25. Makhsous S, Mohammad HM, Schenk JM, Mamishev A, Kristal AA. Novel mobile structured light system in food 3D reconstruction and volume estimation. *Sensors.* (2019) 19:564. doi: 10.3390/s19030564
26. Long Y, Wang YH, Zhai ZM, Wu L, Li MZ, Sun H, et al. Potato volume measurement based on RGB-D camera. *IFAC-PapersOnLine.* (2018) 51:515–20. doi: 10.1016/j.ifacol.2018.08.157
27. Fan S, Li J, Zhang YH, Tian X, Wang QY, He X, et al. On line detection of defective apples using computer vision system combined with deep learning methods. *J Food Eng.* (2020) 286:110102. doi: 10.1016/j.jfoodeng.2020.110102
28. Behmann J, Mahlein AK, Paulus S, Dupuis J, Kuhlmann H, Oerke E, et al. Generation and application of hyperspectral 3D plant models: methods and challenges. *Mach Vis Appl.* (2016) 27:611–24. doi: 10.1007/s00138-015-0716-8
29. Tian X, Li J, Wang Q, Fan SX. A bi-layer model for nondestructive prediction of soluble solids content in apple based on reflectance spectra and peel pigments. *Food Chem.* (2018) 239:1055–63. doi: 10.1016/j.foodchem.2017.07.045
30. Zhang H, Zhang S, Dong W, Wei L, Huang YF, Zhan BS, et al. Detection of common defects on mandarins by using visible and near infrared hyperspectral imaging. *Infrared Phys. Technol.* (2020) 108:103341. doi: 10.1016/j.infrared.2020.103341
31. Urazoe K, Kuroki N, Maenaka A, Tsutsumi H, Iwabuchi M, Fuchuya K, et al. Automated fish bone detection in X-Ray images with convolutional neural network and synthetic image generation. *IEEJ Trans Electr Electron Eng.* (2021) 16:1510–7. doi: 10.1002/tee.23448
32. Ebrahimnejad H, Ebrahimnejad H, Salajegheh A, Barghi H. Use of magnetic resonance imaging in food quality control: a review. *J Biomed Phys Eng.* (2018) 8:127–32.
33. Nakashima Y. Development of a hand-held magnetic resonance sensor for the nondestructive quantification of fat and lean meat of fresh tuna. *J. Food Meas. Charact.* (2020) 14:2947–55. doi: 10.1007/s11694-020-00539-5
34. Vadivambal R, Jayas DS. Thermal imaging in agriculture and food industry-a review. *Food Bioprocess Technol*. (2011) 4:186–99.
35. Zeng XY, Miao Y, Ubaid S, Gao XM, Zhang SL. Detection and classification of bruises of pears based on thermal images. *Postharvest Biol. Technol.* (2020) 161:111090. doi: 10.1016/j.postharvbio.2019.111090
36. Sishodia RP, Ray RL, Singh SK. Applications of remote sensing in precision agriculture: a review. *Remote Sens.* (2020) 12:3136. doi: 10.3390/rs12193136
37. Romanko M. *Remote Sensing in Precision Agriculture: Monitoring Plant Chlorophyll, and Soil Ammonia, Nitrate, and Phosphate in Corn and Soybean Fields*. Bowling Green, OH: Bowling Green State University (2017).
38. Yuan L, Pu R, Zhang J, Wang JH, Yang H. Using high spatial resolution satellite imagery for mapping powdery mildew at a regional scale. *Precision Agric.* (2016) 17:332–48. doi: 10.1007/s11119-015-9421-x
39. Che WK, Sun LJ, Zhang Q, Tan WY, Ye DD, Zhang D, et al. Pixel based bruise region extraction of apple using Vis-NIR hyperspectral imaging. *Comput Electron Agric.* (2018) 146:12–21. doi: 10.1016/j.compag.2018.01.013
40. Fan SX, Li CY, Huang WQ, Chen LP. Detection of blueberry internal bruising over time using NIR hyperspectral reflectance imaging with optimum wavelengths. *Postharvest Biol Technol.* (2017) 134:55–66. doi: 10.1016/j.postharvbio.2017.08.012
41. Li JB, Luo W, Wang Z, Fan SX. Early detection of decay on apples using hyperspectral reflectance imaging combining both principal component analysis and improved watershed segmentation method. *Postharvest Biol Technol.* (2019) 149:235–46. doi: 10.1016/j.postharvbio.2018.12.007
42. Luo W, Zhang H, Liu X. Hyperspectral/Multispectral reflectance imaging combining with watershed segmentation algorithm for detection of early bruises on apples with different peel colors. *Food Analytical Methods.* (2019) 12:1218–28. doi: 10.1007/s12161-019-01456-0
43. Li J, Zhang RY, Li JB, Wang ZL, Zhang HL, Zhan B, et al. Detection of early decayed oranges based on multispectral principal component image combining both bi-dimensional empirical mode decomposition and watershed segmentation method. *Postharvest Biol Technol.* (2019) 158:110986. doi: 10.1016/j.postharvbio.2019.110986
44. Sun Y, Lu R, Lu YF, Lu YZ, Pan LQ. Detection of early decay in peaches by structured-illumination reflectance imaging. *Postharvest Biol. Technol.* (2019) 151:68–78. doi: 10.1016/j.postharvbio.2019.01.011
45. Barrowclough OJD, Muntingh G, Nainamalai V, Stangeby I. Binary segmentation of medical images using implicit spline representations and deep learning. *Comput Aided Geom Des.* (2021) 85:101972. doi: 10.1016/j.cagd.2021.101972
46. Potka S, Wlodarczyk T, Szczerba R, Pokita P, Komisarek O, Matthews BA, et al. Convolutional neural networks in orthodontics: a review. *arXiv [Preprint]* (2021):doi: 10.48550/arXiv.2104.08886
47. Xie WJ, Wei S, Zheng ZH, Jiang Y, Yang DY. Recognition of defective carrots based on deep learning and transfer learning. *Food Bioprocess Technol.* (2021) 14:1–14.
48. Deng L, Li J, Han Z. Online defect detection and automatic grading of carrots using computer vision combined with deep learning methods. *LWT-Food Sci. Technol.* (2021) 149:111832. doi: 10.1016/j.lwt.2021.111832
49. Zhu HF, Yang LH, Sun YX, Han ZZ. Identifying carrot appearance quality by an improved dense CapNet. *Trends Food Sci Technol.* (2020) 44:e13586.

50. Rong D, Wang HY, Ying YB, Zhang ZY, Zhang YS. Peach variety detection using VIS-NIR spectroscopy and deep learning. *Comput Electron Agric.* (2020) 175:105553. doi: 10.1016/j.compag.2020.105553
51. Chen GW, Chen YA, Chang HY, Huang TC, Chen TY. Combined impact of high-pressure processing and slightly acidic electrolysed water on Listeria monocytogenes proteomes. *Food Res Int.* (2021) 147:110494. doi: 10.1016/j.foodres.2021.110494

Conflict of Interest: The authors declare that the research was conducted in the absence of any commercial or financial relationships that could be construed as a potential conflict of interest.

Publisher's Note: All claims expressed in this article are solely those of the authors and do not necessarily represent those of their affiliated organizations, or those of the publisher, the editors and the reviewers. Any product that may be evaluated in this article, or claim that may be made by its manufacturer, is not guaranteed or endorsed by the publisher.

frontiers | Frontiers in Nutrition

MINI REVIEW
published: 13 May 2022
doi: 10.3389/fnut.2022.884835

Research Status and Prospect for Vibration, Noise and Temperature Rise-Based Effect of Food Transport Pumps on the Characteristics of Liquid Foods

*XiaoQi Jia[1], Songyu Li[1], Bo Li[2], Li Zhang[3], Qiangmin Ding[4], Panlong Gao[4] and ZuChao Zhu[1]**

[1] Key Laboratory of Fluid Transmission Technology of Zhejiang, Zhejiang Sci-Tech University, Hangzhou, China, [2] Hangzhou Weiguang Electronic Co., Ltd., Hangzhou, China, [3] Department of Application and Engineering, Zhejiang Economic & Trade Polytechnic, Hangzhou, China, [4] Hefei General Machinery Research Institute, Hefei, China

OPEN ACCESS

Edited by:
Qiang Xia,
Ningbo University, China

Reviewed by:
Jasenka Gajdoš Kljusurić,
University of Zagreb, Croatia
Kaavya Rathnakumar,
University of Wisconsin-Madison, United States

***Correspondence:**
ZuChao Zhu
zhuzuchao01@163.com

Specialty section:
This article was submitted to Food Chemistry, a section of the journal Frontiers in Nutrition

Received: 27 February 2022
Accepted: 07 April 2022
Published: 13 May 2022

Citation:
Jia X, Li S, Li B, Zhang L, Ding Q, Gao P and Zhu Z (2022) Research Status and Prospect for Vibration, Noise and Temperature Rise-Based Effect of Food Transport Pumps on the Characteristics of Liquid Foods. Front. Nutr. 9:884835. doi: 10.3389/fnut.2022.884835

In the field of food processing, the processing of liquid foods has always played an important role. Liquid foods have high requirements for the processing environment and equipment. As the core equipment in liquid foods processing, food transport pumps are widely used in liquid foods production, processing and transportation. Most liquid foods are non-Newtonian and vulnerable to vibration, noise, and temperature rise produced by rotary motions of food transport pumps in operation, which can finally affect foods safety. Therefore, this review summarizes the impact of mechanical vibration, noise, and temperature rise on liquid food products, with the aim of ensuring food safety while designing a cleaner, safer and more reliable food transport pumps in the future.

Keywords: vibration, noise, temperature rise, food transport pump, liquid foods

INTRODUCTION

With the continuous development of economy and society, food safety is not only a major public health safety issue (1), but also a major issue related to people's survival and development and nutritional health (2–4). The impact of all links of food production on food safety cannot be ignored, especially in food processing and transportation (5–7). The processing of liquid foods such as peanut butter, beer, and milk makes enormous demands on delivering equipment. Due to the different molecular structures and physical parameters of various liquids, the impact of physical parameters of various equipment operation (mainly including vibration, noise and temperature rise) on liquid foods should be considered during the transportation of liquid foods (8–11). Food transport pumps accelerate the output of liquid food under pressure, thus realizing efficient and stable conveyance of liquid foods. It is the core delivering equipment in the production process of liquid foods. The most used two types of food transport pumps are vane pumps and positive displacement pumps (12–14). Vibration, noise and temperature rise caused by long-term operation are ubiquitous in the use of food transport pumps (15–19).

When delivering liquid foods, pressure pulsation exists in the flow field due to the rotor–stator interaction between the vanes and volutes of the pump. Such pressure pulsations will result in the vibration and noise of the pump (20–23). In addition, local temperature rise of liquid foods in pump impeller and volute will occur during operation of food transport pumps, which will affect the safety of liquid foods (24, 25). Vibration, noise, and temperature rise of liquid foods are inevitable in the process of transfer. Extensive research efforts have been made to investigate the effect of such factors on the quality of liquid foods. This review focuses on the impact of liquid foods in the transfer process in terms of mechanical vibration, noise, and temperature rise.

EFFECT OF VIBRATION-INDUCED FACTORS ON LIQUID FOODS

Vibration in the process of transfer can negatively affect liquid foods (milk, liquor, yogurt, juice, etc.). For example, during yogurt fermentation, the vibration caused by large yogurt transfer pumps will spread to the fermenter (26), and the characteristic frequency of vibrations can affect pH and disturb protein network formation, which can lead to defects in yogurt texture (27). Körzendörfer et al. (28) tested the effect of vibration on the fermentation process of yogurt, and showed that mechanical vibration causes yogurt to produce large particles on the millimeter scale during stirring, while this particle formation is mainly induced by changes in yogurt pH (29). According to particle image velocimetry results, vibration forces the yogurt to undergo vertical back and forth movements, which leads to local protein breakage during aggregation and gelation, making the yogurt more susceptible to syneresis during storage (30). Richmond et al. (31) studied the stability of yogurt during simulated transport in different secondary packaging. Textural defects caused by vibration include whey and cracked or completely destroyed coagulum. In contrast, agitated yogurt might suffer from structural losses (such as hardness) and phase separation in the process of transfer (32, 33). In addition, the vibration can affect the concentration of aldehydes, especially at higher storage temperatures (34). Jaskula-Goiris et al. (10) have studied the beer production process, and found that vibration can lead to intensified collisions between fluid molecules, which can cause beer to undergo oxidative reactions and thus become turbid.

However, studies also have showed that mechanical vibration also positively affects liquid foods. Stoforos et al. (35) examined the effect of vibration on thermal mixing of liquid foods during cooling of several highly viscous foods, potato puree, banana puree, applesauce, and cheese sauce was investigated, and the results showed that thermal mixing of liquid foods was improved under low frequency lateral vibration. Low frequency lateral vibrations can homogenize the temperature distribution of liquid foods while also accelerating food cooling. Kim et al. (36) found that resonance vibration could alleviate the membrane fouling problem of whole milk during filtration process, and resonance vibration could more effectively alleviate the fouling phenomenon of milk. Salek et al. (37) concluded that mechanical vibration can convert mechanical energy into thermal energy and enhance the hardness, storage modulus, and viscosity of cheese sauce. Warmińska et al. (38) studied the effect of vertical vibration (10–60 Hz, 0.5–2 h) on raw milk, and found that vibration increases electrical conductivity, while also altering the heat and clotting behavior of chymosin. Czerniewicz et al. (39) revealed that vibration decreased the pH of raw milk while increasing the amount of free fatty acids (40).

EFFECT OF NOISE-INDUCED FACTORS ON LIQUID FOODS

Both noise and acoustic wave characteristics have a significant effect on food safety (41–43). Ultrasound has a more pronounced physical effect on milk and dairy products, and related studies have shown that ultrasound has a distinct effect on the degree of emulsification and overall homogenization of milk and dairy products (44, 45). According to this research phenomenon, related researchers made low-fat dairy products by using ultrasound for separating emulsion and removing the fat layer (46, 47). Ultrasound has also been used to enhance the milk curding ability (48). O'Sullivan et al. (49) found that Ultrasound has been found to reduce micelle size and hydrodynamic volume of sodium caseinate, whey and milk protein isolates. Shanmugam et al. (44) studied flaxseed oils/milk emulsion composition, and found that ultrasound treatment improved the gel properties, gel strength, and elasticity, while reducing the gelation time of emulsions. Gursoy et al. (50) showed that ultrasound can postpone the separation of serum from milk and increase the viscosity of milk. Chandrapala et al. (51) concluded that ultrasound could accelerate the dissolution of powder in milk and the release of individual casein micelles into solution. Sfakianakis et al. (52) found that ultrasonicated milk samples also showed an increase in gel stiffness, clotting strength, final storage modulus, cohesiveness, and water holding capacity.

Aadi (53) found that ultrasound could improve turbidity values, antioxidant capacity, free radical scavenging activity, ascorbic acid of liquid foods such as phenolics, flavonoids and flavonols. Abid (54) found that ultrasound could enhance the concentration values of inactivated polyphenolic compounds and sugars in enzymes (polyphenolase, peroxidase, and pectin methylesterase) and microbial communities. Ultrasound could also effectively reduce the number of microbes in juice (55). Jiang et al. (56) found that ultrasound could enhance the antioxidant activity of fliud foods. Tomadoni et al. (57) found that ultrasound could effectively reduce the number of yeasts and molds in strawberry and kiwifruit juices.

EFFECT OF TEMPERATURE RISE INDUCED FACTORS ON LIQUID FOODS

For most foods, temperature rise implies a deterioration of food quality. Temperature significantly affects microbial reproduction and speeds up food spoilage under appropriate humidity and oxygen conditions (58). Generally, within a certain range of

TABLE 1 | A summary table of all mentioned papers outcomes.

Characteristics	Product	References	Outcomes
Vibration	Yogurt	(28)	Produce large millimeter-sized particles
	Yogurt	(31)	Cause texture defects
	Beer	(10)	Oxidation of beer
	Mashed Potatoes et al.	(35)	Improve thermal mixing of foods
	Whole milk	(36)	Reduce milk scaling
	Cheese sauce	(37)	Increase hardness, storage modulus and viscosity
	Raw milk	(38)	Alter heat and rennet coagulation behavior
	Raw milk	(39)	Decrease pH and increase the amount of free fatty acid
Noise	Milk	(49)	Reduce micelle size and hydrodynamic volume of sodium caseinate, whey and milk protein isolate
	Flaxseed Oil/Milk	(44)	Improve gel properties, gel strength and elasticity
	Milk	(50)	Delay serum separation and increased viscosity
	Milk	(51)	Accelerate the dissolution of powders
	Milk	(52)	Increase gel hardness, coagulation strength, final storage modulus, cohesion and water holding capacity
	Phenols and flavonoids	(53)	Improve food turbidity value, antioxidant capacity, free radical scavenging activity, ascorbic acid
	Enzyme	(54)	Enhance concentration values of inactive polyphenolic compounds and sugars
	Mulberry juice	(56)	Enhance antioxidant activity
	Strawberry and kiwifruit Juice	(57)	Reduce yeast and mold counts
Temperature rise	Yogurt	(63)	accelerate spoilage
	Milk	(64)	Maillard reaction
	Milk	(67)	Produce bad odor components
	Yogurt	(68)	Reduce viscosity and smoothness
	Yogurt	(71)	Negative effects of nutrition, physical properties, and flavor

temperature, when the temperature of foods rises by 10°C under constant moisture conditions, the enzymatic and non-enzymatic chemical reaction rate will double, and the rate of food spoilage will increase by 4–6 times (59). The increase in temperature also damages the internal organizational structure of food, thus seriously worsening the quality. Excessive heat can also denature proteins in foods, disrupt vitamins especially vitamin C in watery foods, or change the properties due water loss and deform foods (60). Therefore, the temperature rise of food transport pumps should be strictly controlled during the operation of liquid foods (61). High-protein foods such as milk and soybean milk are highly sensitive to temperature and greatly affected by temperature in the process of production. During yogurt transfer, the temperature should be controlled at around 5°C to avoid spoilage (62, 63). Al-Attabi (64) found that the physical and chemical reactions in heat treatment resulted in changes in milk flavor, which is different from the flavor of raw milk. The temperature increase of milk results in Maillard reaction, lipid degradation and thermal denaturation of whey proteins and milk fat globule membranes (65). In addition, some by-products of Maillard reaction are harmful to human health and can cause allergic reactions when severe (66). Zhang et al. (67) found that the longer the heat treatment time, the higher the heating temperature of milk, and the more extensive the Maillard reaction, which resulted in various unacceptable odor components. Wu et al. (68) found that the yogurt fermentation temperature might degrade yogurt quality with the growth of microbes, and that culture temperature during production had a significant effect on the physical characteristics of the final product. Higher temperatures exacerbated yogurt whey separation (69), which would result in a weak protein network with coarser microstructures and reduce the viscosity and smoothness of yogurt (70). Yang et al. (71) studied the effect of different fermentation temperatures on the quality of yogurt and metabolites, found that temperature rise caused different degrees of negative effects on the nutritional, physical characteristics and flavor of yogurt. Finally, all the above mentioned papers outcomes are shown in **Table 1**.

CONCLUSION AND PERSPECTIVE

Food safety has been a hotspot and sticking point in research. This review summarized the effect of vibration, noise, and temperature rise in the operation of food transport pumps on the physical, chemical, and structural characteristics of liquid foods. However, machinery vibration and ultrasound are also used for improving the taste of liquid foods, but other hazardous materials will also come with temperature rise. In general, machinery vibration, noise, and temperature rise have both positive and negative effects on liquid foods. Therefore, further research should proceed. At the beginning of food transport pumps

design, it is necessary to take full account of its impact on specific food, such as milk, yogurt, wine, fruit juice, etc., to develop a more adjustable multi-scene food transport pump, which can adjust the rotating speed, flow rate and blade structure according to different liquid foods. Such multi-functional food transport pumps are also the main research and development direction of food machinery in the future. It is also necessary to take into account the material characteristics of food transport pumps, and introduce new technologies and materials, such as carbon nanomaterials, coating technology, which can improve the food transport pumps' damping capacity, sound and vibration absorption capacity, and environmental friendliness. All of this technology will reduce vibration, reduce temperature rise and protect food more safely, when liquid foods are transferred by food transport pumps.

AUTHOR CONTRIBUTIONS

XJ: methodology and writing-review and editing. SL: formal analysis, data curation, visualization, and original draft. BL: supervision. QD and PG: polish the article. ZZ: conceptualization. All authors contributed to the article and approved the submitted version.

FUNDING

This work was supported by the National Natural Science Foundation of China (Grant No. 51906221), the Key Research and Development Program of Zhejiang Province (Grant No. 2022C01148), and the Joint Fund of Zhejiang Natural Science Foundation (Grant No.LZY21E060002).

REFERENCES

1. Xu L, Zheng Y, Zhou C, Pan D, Geng F, Cao J, et al. Kinetic response of conformational variation of duck liver globular protein to ultrasonic stimulation and its impact on the binding behavior of n-alkenals. *LWT*. (2021) 150:111890. doi: 10.1016/j.lwt.2021.111890
2. Shi Y, Zhou K, Li S, Zhou M, Liu W. Heterogeneous graph attention network for food safety risk prediction. *J Food Eng.* (2022) 323:111005. doi: 10.1016/j.jfoodeng.2022.111005
3. Silva VL, Sanjuan N. Opening up the Black Box: A Systematic Literature Review ofLife Cycle Assessment in Alternative Food Processing Technologies. *J Food Eng.* (2019) 250:33–45. doi: 10.1016/j.jfoodeng.2019.01.010
4. Chen X, Voigt T. Implementation of the Manufacturing Execution System in the food and beverage industry—ScienceDirect. *J Food Eng.* (2020) 278:109932. doi: 10.1016/j.jfoodeng.2020.109932
5. Silva VL, Sereno AM, José DASP. Food industry and processing technology: on time to harmonize technology and social drivers. *Food Eng Rev*. (2018) 10:1–13. doi: 10.1007/s12393-017-9164-8
6. Boye JI, Arcand Y. Current trends in green technologies in food production and processing. *Food Eng Rev.* (2013) 5:1–17. doi: 10.1007/s12393-012-9062-z
7. Dagdelen C, Aday MS. The effect of simulated vibration frequency on the physico-mechanical and physicochemical properties of peach during transportation. *J LWT—Food Sci Technol.* (2020) 137:110497. doi: 10.1016/j.lwt.2020.110497
8. Zachwieja J. Stress analysis of vibrating pipelines. *AIP Conf Proc.* (2017) 1822:020017. doi: 10.1063/1.4977691
9. Zeng L, Jansson LG, Borjesson A. Piping vibration and vibration damage prevention through screening of dynamic susceptibility. In: *Proceedings of the 2017 25th International Conference on Nuclear Engineering.* (2017). p. 2. doi: 10.1115/ICONE25-66658
10. Jaskula-Goiris B, Causmaecker BD, Rouck GD, Aerts G, Paternoster A, Braet J, et al. Influence of transport and storage conditions on beer quality and flavour stability. *J Inst Brew.* (2018) 125:60–8. doi: 10.1002/jib.535
11. Sun X, Liu S, Zhang X, Tao Y, Boczkaj G, Yoon JY, et al. Recent advances in hydrodynamic cavitation-based pretreatments of lignocellulosic biomass for valorization. *Bioresour Technol.* (2022) 345:126251. doi: 10.1016/j.biortech.2021.126251
12. Tamime AY, Robinson RK. *Tamime and Robinson's Yoghurt: Science and Technology.* 3rd ed. Woodhead Publishing Limited (2007). p. 1–791. doi: 10.1533/9781845692612
13. Shigemitsu T, Nakaishi E, Maeda M, Araki Y. Influence of blade number on performance and internal flow condition of centrifugal pump for low viscous liquid food. *Int J Fluid Machin Syst.* (2021) 14:132–41. doi: 10.5293/IJFMS.2021.14.1.132
14. Wang L. Energy efficiency technologies for sustainable food processing. *Energy Efficiency.* (2014) 7:791–810. doi: 10.1007/s12053-014-9256-8
15. Ca OY, Dou Y, Huang Y, Cheng J. Study on vibration characteristics of fracturing piping in pump-starting and pump-stopping water hammer. *J Fail Anal Preven.* (2019) 19:1093–104. doi: 10.1007/s11668-019-00699-7
16. Vasil'ev VA, Chegurko LE. Rotor vibration and liquid pressure pulsation in a centrifugal pump. *Chem Petrol Eng.* (1979) 15:334–6. doi: 10.1007/BF01155700
17. Zeng G, Li Q, Wu P, Qian B, Huang B, Li S, et al. Investigation of the impact of splitter blades on a low specific speed pump for fluid-induced vibration. *J Mech Sci Technol.* (2020) 34:2883–93. doi: 10.1007/s12206-020-0620-7
18. Wu J, Zheng S, Wang C, Yu Z. Study on pipeline self-excited vibration using transient fluid-structure coupling method. *Int J Adv Manuf Technol.* (2020) 107:4055–68. doi: 10.1007/s00170-020-04983-x
19. Sun X, Yang Z, Wei X, Tao Y, Boczka G, Yoon JY, et al. Multi-objective optimization of the cavitation generation unit structure of an advanced rotational hydrodynamic cavitation reactor. *Ultrason. Sonochem.* (2021) 80:105771. doi: 10.1016/j.ultsonch.2021.105771
20. Jia XQ, Cui BL, Zhu ZC, Zhang YL. Experimental Investigation of Pressure Fluctuations on Inner Wall of a Centrifugal Pump. *Int J Turbo Jet-Eng.* (2017) 36:401–10. doi: 10.1515/tjj-2016-0078
21. Cui B, Zhang Y, Huang Y. Analysis of the pressure pulsation and vibration in a low-specific-speed centrifugal pump. *J Fluids Eng.* (2021) 143:021201. doi: 10.1115/1.4048691
22. Huang WX, Alben S. Fluid–structure interactions with applications to biology. *Acta Mech Sin.* (2016) 32:977–9. doi: 10.1007/s10409-016-0608-9
23. Xuan X, Wang M, Zhang M, Kaneti YV, Xu X, Sun X, et al. Nanoarchitectonics of low-dimensional metal-organic frameworks toward photo/electrochemical CO2 reduction reactions. *J CO2 Utill.* (2022) 57:101883. doi: 10.1016/j.jcou.2022.101883
24. Yuan M, Tan D. Quantitative analysis of the influence of eccentricity on the thermal characteristics of in-wheel motor. *J Mech Sci Technol.* (2022) 36:991–1002. doi: 10.1007/s12206-022-0145-3
25. Mercy A, Umamaheswari B, Latha K. Reduced-order thermal behavior of universal motor-driven domestic food mixers/grinders using AC and DC supplies. *J Power Electron.* (2021) 21:1322–32. doi: 10.1007/s43236-021-00268-y
26. Pt A, Ak B, Jh B, Es A. Vibrations as a cause of texture defects during yogurt manufacturing–Formation of vibrations and their propagation in dairy production lines. *J Food Eng.* (2020) 293:110369. doi: 10.1016/j.jfoodeng.2020.110369
27. Walstra P, Wouters J, Geurts TJ. *Dairy Science and Technology, Second Edition.* (2006). doi: 10.1201/9781420028010
28. Koerzendoerfer A, Temme P, Noebel S, Schluecker E, Hinrichs J. Vibration-induced particle formation during yogurt fermentation—Industrial vibration measurements and development of an experimental setup. *J Food Res Int.* (2016) 85:44–50. doi: 10.1016/j.foodres.2016.04.004
29. Krzendrfer A, Temme P, Schlücker E, Hinrichs J. Vibration-induced particle formation during yogurt fermentation—effect of frequency and amplitude. *J Dairy Sci.* (2018) 101:3866–77. doi: 10.3168/jds.2017-13905

30. Ak A, Pt B, Al B, Jh A. Vibrations as a cause of texture defects during the acid-induced coagulation of milk—fluid dynamic effects and their impact on physical properties of stirred yogurt. *J Food Eng.* (2020) 292:110254. doi: 10.1016/j.jfoodeng.2020.110254
31. Richmond ML, Harte BR, Gray JI, Stine CM. Physical damage of yogurt. *The role of secondary packaging on stability of yogurt. J food protection.* (1985) 48:482–6. doi: 10.4315/0362-028X-48.6.482
32. Anna L, Xinxin W, Ruikang C, Shujun X. Modeling the effect of vibration on the quality of stirred yogurt during transportation. *J Food Sci Biotechnol.* (2020) 29:889–96. doi: 10.1007/s10068-020-00741-7
33. Tamime AY, Robinson RK. *RobinsonYoghurt: Science and Technology* (third ed.), Woodhead Publishing Limited, Cambridge, UK (2007).
34. Paternoster A, Jaskula-Goiris B, Causmaecker BD, Vanlanduit S, Springael J, Braet J, et al. The interaction effect between vibrations and temperature simulating truck transport on the flavor stability of beer. *J Science Food Agricult.* (2019) 99:2165–74. doi: 10.1002/jsfa.9409
35. Stoforos GN, Farkas BE, Simunovic J. Thermal mixing via acoustic vibration during continuous flow cooling of viscous food products. *J Food Bioprod Process.* (2016) 100:551–9. doi: 10.1016/j.fbp.2016.07.008
36. Kim SH, Min CS. Fouling reduction using the resonance vibration in membrane separation of whole milk. *J Indus Eng Chem.* (2019) 75:123–9. doi: 10.1016/j.jiec.2019.03.011
37. Salek RN, Vašina M, Lapčík L, Cerníková M, Lorencová E, Li P, et al. Evaluation of various emulsifying salts addition on selected properties of processed cheese sauce with the use of mechanical vibration damping and rheological methods. *J LWT Food Sci Technol.* (2019) 107:178–84. doi: 10.1016/j.lwt.2019.03.022
38. Warminska M, Kruk A, Brandt W. Effect of vibration frequency and exposure time on the technological usability of fresh milk. *Polish J Food Nutr Sci.* (2006) 15–56:247–51. Available online at: http://journal.pan.olsztyn.pl/pdf-98706-30519?filename=30519.pdf
39. Czerniewicz M, Kruk A, Kielczewska K. Storage stability of raw milk subjected to vibration. *Polish J Food Nutr Sci.* (2006) 15–56:65–70. Available online at: http://journal.pan.olsztyn.pl/pdf-98675-30488?filename=STORAGE%20STABILITY%20OF%20RAW.pdf
40. Kamath S, Wulandewi A, Deeth H. Relationship between surface tension, free fatty acid concentration and foaming properties of milk. *J Food Res Int.* (2008) 41:623–9. doi: 10.1016/j.foodres.2008.03.014
41. Mason TJ, Peters D. *Practical Sonochemistry: Power Ultrasound Uses and Applications* (second ed.), Elsevier, London (2003). p. 1–155. doi: 10.1533/9781782420620.1
42. Mason TJ, Chemat F, Ashokkumar M. Power ultrasonics for food processing. In: Gallego-Juarez JA, Graff KF, editors. *Power Ultrasonics: Applications of High Intensity Ultrasound*. Cambridge: Woodhead Publishing (2015). p. 815–43. doi: 10.1016/B978-1-78242-028-6.00027-2
43. Tiwari BK, Mason TJ. Ultrasound processing of liquid foods. *Novel Thermal Non-Thermal Technol Liquid Foods.* (2012) 6:135–65. doi: 10.1016/B978-0-12-381470-8.00006-2
44. Shanmugam A, Ashokkumar M. Functional properties of ultrasonically generated flaxseed oil-dairy emulsions. *Ultrason Sonochem.* (2014) 21:1649–57. doi: 10.1016/j.ultsonch.2014.03.020
45. O'Sullivan J, Beevers J, Park M, Greenwood R, Norton I. Comparative assessment of the effect of ultrasound treatment on protein functionality pre-and post-emulsification. *Colloids Surf A Physicochem Eng Aspects.* (2015) 484:89–98. doi: 10.1016/j.colsurfa.2015.07.065
46. Leong T, Juliano P, Johansson L, Mawson R, McArthur S, Manasseh R. Temperature effects on the ultrasonic separation of fat from natural whole milk. *Ultrason Sonochem.* (2014) 21:2092–8. doi: 10.1016/j.ultsonch.2014.02.003
47. Leong T, Johansson L, Juliano P, Mawson R, Mcarthur S, Manasseh R. Design parameters for the separation of fat from natural whole milk in an ultrasonic litre-scale vessel. *Ultrason Sonochem.* (2014) 21:1289–98. doi: 10.1016/j.ultsonch.2014.01.007
48. Zhao L, Zhang S, Uluko H, Liu L, Lv J. Effect of ultrasound pretreatment on rennet-induced coagulation properties of goat's milk. *Food Chem.* (2014) 165:167–74. doi: 10.1016/j.foodchem.2014.05.081
49. O'Sullivan J, Arellano M, Pichot R, Norton I. The effect of ultrasound treatment on the structural, physical and emulsifying properties of dairy proteins. *Food Hydrocoll.* (2014) 42:386–96. doi: 10.1016/j.foodhyd.2014.05.011
50. Gursoy O, Yilmaz Y, Gokce O, Ertan K. Effect of ultrasound power on physicochemical and rheological properties of yoghurt drink produced with thermosonicated milk. *Emir J Food Agricult.* (2016) 28:235–41. doi: 10.9755/ejfa.2015-09-719
51. Chandrapala J, Martin G, Kentish SE, Ashokkumar M. Dissolution and reconstitution of casein micelle containing dairy powders by high shear using ultrasonic and physical methods. *Ultrason Sonochem.* (2014) 21:1658–65. doi: 10.1016/j.ultsonch.2014.04.006
52. Sfakianakis P, Tzia C. Flavor and sensory characteristics of yogurt derived from milk treated by high intensity ultrasound. Ho CT, Mussinan C, Shahidi F, Contis ET, editors. *Nutrition, Functional and Sensory Properties of Foods*. UK: RSC publishing (2013). p. 92–97. doi: 10.1039/9781849737685-00092
53. Aadil RM, Zeng XA, Han Z, Sun DW. Effects of ultrasound treatments on quality of grapefruit juice. *Food Chem.* (2013) 141:3201–6. doi: 10.1016/j.foodchem.2013.06.008
54. Abid M, Jabbar S, Hu B, Hashim MM, Hu B, Lei S, et al. Thermosonication as a potential quality enhancement technique of apple juice. *Ultrason Sonochem.* (2014) 21:984–90. doi: 10.1016/j.ultsonch.2013.12.003
55. Abid M, Jabbar S, Wu T, Hashim MM, Hu B, Lei S, et al. Sonication enhances polyphenolic compounds, sugars, carotenoids and mineral elements of apple juice. *Ultrason Sonochem.* (2014) 21:93–7. doi: 10.1016/j.ultsonch.2013.06.002
56. Jiang B, Mantri N, Hu Y, Lu J, Jiang W, Lu H. Evaluation of bioactive compounds of black mulberry juice after thermal, microwave, ultrasonic processing, and storage at different temperatures. *Food Sci Technol Int.* (2014) 21:92–399. doi: 10.1177/1082013214539153
57. Tomadoni B, Cassani L, Ponce A, Moreira MR, Agero MV. Optimization of ultrasound, vanillin and pomegranate extract treatment for shelf-stable unpasteurized strawberry juice. *LWT Food Sci Technol.* (2016) 72:475–84. doi: 10.1016/j.lwt.2016.05.024
58. Aviara NA, Haque MA. Moisture dependence of thermal properties of sheanut kernel. *J Food Eng.* (2001) 47:109–13. doi: 10.1016/S0260-8774(00)00105-9
59. Sablani SS, Kasapis S, Rahman MS. Evaluating water activity and glass transition concepts for food stability. *J Food Eng.* (2007) 78:266–71. doi: 10.1016/j.jfoodeng.2005.09.025
60. Chowdhury S, Roy R, Mandal BK. A review on energy and exergy analysis of two-stage vapour compression refrigeration system. *J Int J Air Conditioning Refrig.* (2019) 27:1930001.1–9. doi: 10.1142/S2010132519300015
61. AlbayatiO AZ, Kumar R, Chauhan G. Forced air precooling studies of perishable food products. *Int J Food Eng.* (2007) 3:8. doi: 10.2202/1556-3758.1119
62. Igaa B, Ah A, Vg A. Lactose hydrolysis and protein fortification pose an increased risk for the formation of Maillard reaction products in UHT treated milk products. *J Food Composition Anal.* (2019) 84:103308. doi: 10.1016/j.jfca.2019.103308
63. Elliott AJ, Deeth HC, Datta N, Amenu B. Heat-induced and other chemical changes in commercial UHT milks. *J Dairy Res.* (2005) 72:442. doi: 10.1017/S002202990500138X
64. Al-Attabi Z, D'Arcy BR, Deeth HC. Volatile sulfur compounds in pasteurised and UHT milk during storage. *Dairy Sci Technol.* (2014) 94:241–53. doi: 10.1007/s13594-013-0157-y
65. Lee AP, Barbano DM, Drake MA. The influence of ultra-pasteurization by indirect heating versus direct steam injection on skim and 2% fat milks. *J Dairy Sci.* (2017) 100:1688–701. doi: 10.3168/jds.2016-11899
66. Lee CH, Chen KT, Lin JA, Chen YT, Hsieh CW. Recent advances in processing technology to reduce 5-hydroxymethylfurfural in foods. *J Trends Food Sci Technol.* (2019) 93:271–80. doi: 10.1016/j.tifs.2019.09.021
67. Zhang Y, Yi S, Lu J, Pang X, Xu X, Lv J, et al. Effect of different heat treatments on the Maillard reaction products, volatile compounds and glycation level of milk. *J Int Dairy J.* (2021) 123:05182–105182. doi: 10.1016/j.idairyj.2021.105182
68. Wu S, Li D, Li S. J., Bhandari, Bhesh, Yang, B. L., et al. Effects of incubation temperature, starter culture level and total solids content on the rheological properties of yogurt. *Int J Food Eng.* (2009) 5:1–17. doi: 10.2202/1556-3758.1436
69. Ceja B, Rka B, Eor B, Tkh A, Agja B, Sbs B. Processing of high-protein yoghurt—a review. *Int Dairy J.* (2019) 88:42–59. doi: 10.1016/j.idairyj.2018.08.002

70. Rpl A, Mjm A, Cap A, Ss B, Jalds A, Amg B, et al. Physicochemical and microbial changes in yogurts produced under different pressure and temperature conditions–ScienceDirect. *J LWT.* (2019) 99:423–30. doi: 10.1016/j.lwt.2018.09.074
71. Yang S, Yan D, Zou Y, Mu D, Wu J. Fermentation temperature affects yogurt quality: a metabolomics study. *J Food Biosci.* (2021) 42:101104. doi: 10.1016/j.fbio.2021.101104

Conflict of Interest: BL was employed by Hangzhou Weiguang Electronic Co., Ltd., Hangzhou, China.

The remaining authors declare that the research was conducted in the absence of any commercial or financial relationships that could be construed as a potential conflict of interest.

Publisher's Note: All claims expressed in this article are solely those of the authors and do not necessarily represent those of their affiliated organizations, or those of the publisher, the editors and the reviewers. Any product that may be evaluated in this article, or claim that may be made by its manufacturer, is not guaranteed or endorsed by the publisher.

frontiers | Frontiers in Nutrition

MINI REVIEW
published: 19 May 2022
doi: 10.3389/fnut.2022.888047

Photolysis for the Removal and Transformation of Pesticide Residues During Food Processing: A State-of-the-Art Minireview

Qian Xiao[2,3], Xiaoxu Xuan[1], Grzegorz Boczkaj[4], Joon Yong Yoon[5] and Xun Sun[1,6]**

[1] Key Laboratory of High Efficiency and Clean Mechanical Manufacture, Ministry of Education, School of Mechanical Engineering, Shandong University, Jinan, China, [2] State Key Laboratory of Pollution Control and Resource Reuse, College of Environmental Science and Engineering, Tongji University, Shanghai, China, [3] Department of Civil Engineering, The University of Hong Kong, Pokfulam, Hong Kong SAR, China, [4] Department of Process Engineering and Chemical Technology, Faculty of Chemistry, Gdańsk University of Technology, Gdańsk, Poland, [5] Department of Mechanical Engineering, Hanyang University, Ansansi, South Korea, [6] Department of Mechanical Engineering, The University of Hong Kong, Pokfulam, Hong Kong SAR, China

Pesticide residues are of great significant issue that exerted adverse effects on humans. There is a need for effective and non-toxic decontamination of pesticide residues during food processing. In this minireview, the recent advances in the degradation of pesticide residues by photolysis have been firstly described during food processing. The mechanisms of pesticide residues destruction by photolysis were discussed accordingly. Finally, applications of photolysis in the degradation of pesticide residues from beverages, fresh produce, and food rinse waste were also summarized.

Keywords: food processing, photolysis, pesticide residues, pollutant decontamination, transformation

OPEN ACCESS

Edited by:
Qiang Xia,
Ningbo University, China

Reviewed by:
Liliana Silva,
LAQV Network of Chemistry and Technology, Portugal
Emel Oz,
Atatürk University, Turkey

****Correspondence:***
Qian Xiao
2015xiaoqian@tongji.edu.cn
Xun Sun
xunsun@sdu.edu.cn

Specialty section:
This article was submitted to Food Chemistry, a section of the journal Frontiers in Nutrition

Received: *02 March 2022*
Accepted: *29 March 2022*
Published: *19 May 2022*

Citation:
Xiao Q, Xuan X, Boczkaj G, Yoon JY and Sun X (2022) Photolysis for the Removal and Transformation of Pesticide Residues During Food Processing: A State-of-the-Art Minireview. Front. Nutr. 9:888047. doi: 10.3389/fnut.2022.888047

INTRODUCTION

Global food supply should be enhanced by 70–100% by 2050 in order to meet the demand for the improvement in population size (1). The pesticide has been widely applied to control insects, fungus, and weeds for increased food production in the world (2, 3). Some amounts of pesticide residues could remain on foods such as vegetables and fruits that accounted for 30% of an individual's diet, which is frequently transferred to markets and consumed by humans without proper washing or with minimal processing (4). Unfortunately, pesticides have been identified as a major problem by a variety of countries because of their persistence in environments and adverse effects on human health, including the destruction of biodiversity, and dermatological, gastrointestinal, neurological, carcinogenic, respiratory, reproductive, and endocrine effects (5–7). Therefore, it is of great significance for the degradation of pesticide residues during food processing.

Pesticide residues have been categorized as insecticides, herbicides, and other pesticides by the United States Environmental Protection Agency (US EPA) (8). Several methods have been utilized to degrade pesticide residues during food processing, including conventional techniques, and advanced treatment techniques, i.e., non-thermal physical methods (4), and chemical methods (9). Conventional techniques mainly fall into cleaning with various reagents, peeling, drying, heating, and other processes (10, 11). Chemical methods mainly include ozone (9), and photocatalytic oxidation (12–14); non-thermal physical methods primarily contain cold plasma, photolysis, electron beam, electrolyzed water, etc. (14–17). Conventional techniques, i.e., cleaning in water, had limited effects on pesticide removal based on that most pesticides are hydrophobic in nature

(9, 18, 19). Cleaning and peeling, drying, concentration, fermentation, and other processes easily transform pesticides into toxic products, which showed the limited applications during food processing (9, 20). Moreover, ozone can cause negative alternations on food components: loss of some vitamins, phenolic compounds, ascorbic acids, and carotenoids, changes in color, sensory characteristics, and other adverse effects (21–23). Also, degradation products of pesticide residues after ozone treatment were demonstrated to be more toxic than the parent compounds (24, 25). These further have retarded the development of ozone-based technologies. Similarly, although photocatalytic oxidation did show high pesticide degradation performance, they significantly increased the toxicity of the treated solutions, inhibiting their further applications in food processing. This together led to the development of non-thermal physical methods.

Non-thermal physical methods showed numerous characteristics of the non-thermal treatment, economic friendliness, low costs, high efficiency, and low reaction time (4, 26). Amongst them, the photolytic techniques have been reported to be an effective, non-chemical, and residue-free approach (27–29), indicating their good prospects in food processing, such as beverages, fresh products including honey, and dairy products, and rinse wastewater. Therefore, it is necessary to comprehensively review the available and newest literature associated with pesticide degradation by photolysis. Also, this minireview article is important and useful to readers in the areas for understanding the mechanism, most updated progress, and the primary application of this technology. To the best of our knowledge, there is no comprehensive review of the application of photolysis.

In this minireview, our aim is to present recent advances in photolysis for the degradation of pesticide residues during food processing. The mechanisms of pesticide residues destruction by photolysis were discussed accordingly. Finally, applications of photolysis have been summarized in the degradation of pesticide residues in beverages, fresh products, and food rinse waste.

THE MECHANISM OF PHOTOLYSIS FOR THE DEGRADATION AND TRANSFORMATION OF PESTICIDE RESIDUES

Photolysis mainly includes ultraviolet (UV) light irradiation (27, 30–34), pulsed light (PL) technology (4, 35, 36), as well as visible light illumination (37, 38). The UV spectrum falls into UV-A (380–315 nm), UV-B (315–280 nm), UV-C (280–200 nm), vacuum-UV (VUV) (200–100 nm), and extreme UV (100–1 nm). The low-pressure mercury vapor lamps emitting at 185 and 254 nm, and xenon excimer lamps emitting at 172 nm have been often utilized for applications in food processing (2). Photolysis was first proposed for the degradation of pesticide residues (i.e., organochlorine insecticides) in fluid milk and butter oil by Li and Bradley (39, 40). Since then, the development and applications of photolysis for different pesticide decontamination purposes were extensively carried out (41). Fundamentals of photolysis have been proposed in the literature.

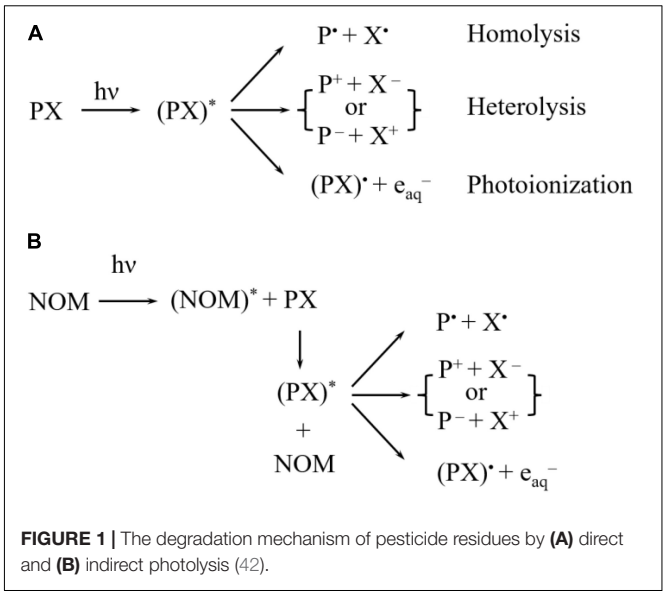

FIGURE 1 | The degradation mechanism of pesticide residues by **(A)** direct and **(B)** indirect photolysis (42).

Photodegradation of pesticide residues could be achieved *via* two mechanisms: direct photolysis and indirect photolysis. On the one hand, in the direct photolysis, pesticides that absorb energy from the UV light can trigger chemical reactions upon the irradiation of UV light: the chemical structure of a pesticide can be transformed into an excited state and then into a triple-state, which would finally undergo *via* homolysis, heterolysis, and photoionization, which could be seen in **Figure 1A** (42). On the other hand, in indirect photolysis, sensitizers such as natural organic matters (NOM) (30) (**Figure 1B**), absorbing photos would result in the production of highly active species (i.e., NOM*) through the excitement of UV light, which would react with pesticide residues. Just as stated above, pesticide residues could further decompose through three main pathways including homolysis, heterolysis, and photoionization. It has been reported that immediate products were generated after photodegradation by involving structural changes such as dehalogenation, desulfuration, dealkylation, and oxidation of the alkyl chains (4), which could be identified through mass spectrometry (MS) analysis. Degradation pathways include multiple successive and competitive steps with the later destruction processes being involved in the earlier formation of degraded processes (4). In addition, solution pH could exert an effect on the formation of immediate species of pesticide residues, and the degradation pathways accordingly (43). Understanding the degradation and transformation of pesticide residues during food processing not only can help to design and optimize the decontamination process, but also provide important information for further reducing food safety risks.

TABLE 1 | The degradation of pesticide residues in beverages.

Pesticides	Processes	Reaction conditions	Efficiency	References
Patulin	Ultraviolet (UV-C) irradiation	∼ 0.2 ppm patulin, UV-C dose of 0.4 J/cm^2	69.47 (± 0.69)%	Chandra et al. (44)
Patulin	UV-C irradiation	1 ppm patulin, UV-C dose of 5.6 J/cm^2	89%	Tikekar et al. (45)
Patulin	UV-C irradiation	1 ppm patulin, UV-C doses of 7.2 J/cm^2	94.8% for 40 min	Zhu et al. (46)
Patulin	UV multi-wavelength emitting lamp	0.5 ppm patulin, pH 4.0, 25°C	∼100% in 60 min	Ibarz et al. (47)
Cartap	UV-light irradiation	1 ppm cartap, 200 W mercury lamp	98.5% at 2 h	Dai et al. (27)
Nereistoxin	UV-light irradiation	1 ppm nereistoxin, 200 W mercury lamp	100.0% in 0.5 h	Dai et al. (27)
Dichlorvos	Sunlight irradiation	4.5 μM dichlorvos at pH 3 and pH 7	0.040–0.064 h^{-1}	Bustos et al. (48)
Dichlorvos	254 nm UV irradiation	4.5 μM dichlorvos, 0.1 Einstein/L	97% in 6 h	Bustos et al. (48)
Epicatechin (EC)	Blue light illumination at 438 nm	1 mM EC, 2.0 mW/cm^2, in the presence of epigallocatechin gallate	57.9% in 3 h (epigallocatechin gallate), 64.5% in 3 h (gallic acid)	Huang et al. (49)

APPLICATIONS OF PHOTOLYSIS DURING FOOD PROCESSING

The Decontamination of Beverages

As reported, significant degradation of patulin could be achieved in apple juice, which was attributable to its absorption of photons in the UV-C range in **Table 1** (45–47). Similarly, Chandra et al., found that patulin could not be degraded in water, but would be very efficiently decomposed in apple juice at the same conditions with UV illumination as shown in **Table 1** (44). The authors demonstrated that riboflavin in apple juice played a significant role in the photodegradation of patulin. This inspired other scholars to further investigate the effect of matrix components in food and their importance on the photodegradation of pesticides and metabolites. Dai et al. conducted the degradation of pesticide residues such as cartap and nereistoxin in tea beverages by photolysis in **Table 1** (27). The authors reported that water-soluble components in beverages did affect the degradation of pesticide residues. As known, tea samples comprise various types of water-soluble chemical components, such as total sugar, caffeine, and tea polyphenols. Catechins with hydroxyl groups, one type of polyphenol, in green tea, could complex with cartap through amide bonds, further accelerating cartap degradation (50). Reportedly, catechins in black tea firstly transformed into theaflavin and thearubigin, then complexed with caffeine, and finally precipitated, which resulted in reduced hydroxyl groups. Accordingly, compared to green tea beverages, cartap was less affected in black tea beverages. Taking together, the water-soluble components in tea mainly played an inhibitive role in the photolytic process of pesticide residues (27). This was primarily attributable to the presence of polyphenols in tea beverages that could compete with pesticides for the light and quench free radicals, and thus slow down the photodegradation of cartap and nereistoxin.

As stated before, irradiation absorption by a compound could lead to its degradation and transformation by direct photolysis (48). The degradation of cartap and nereistoxin in water and tea beverages reached 81.8–100% after 6 h with 200 W of UV illumination, which was mainly ascribed to the easy destruction of disulfide bonds of nereistoxin by UV irradiation (51). This could be evidenced by cartap and nereistoxin showing a maximum UV absorption at 190 nm with pH 7.21, and at 196 nm with pH 3.04, respectively, as shown in **Table 1**, substantiating their ability to absorb UV light (27). Additionally, different degradation behaviors were observed in a variety of tea beverages, i.e., green tea beverages and black tea beverages. Huang et al. found that the photodegradation of nereistoxin in green tea beverages was lower than that in black tea beverages (**Table 1**), which was attributable to the inhibitory effect of high concentrations of catechins in the former (49). Therefore, it is urgent to investigate and compare the decontamination of pesticide residues in realistic beverages.

The Decontamination of Fresh Produce

Reportedly, the temperature played a minor role in the photolysis, whereas light intensity, irradiation time, types of pesticide residues, and UV light sources are important in the decomposition of pesticide residues by photolysis (52). Yuan et al. demonstrated the photodegradation of organophosphorus pesticides (OPs) in the honey medium, including coumaphos, methyl parathion, and fenitrothion under three different intensities (37). For instance, the degradation of coumaphos was 93.38, 96.52, and 97.02%, respectively, after 1 h with 250, 500, and 750 W/m^2 sunlight irradiation. As a result, there was a positive relationship between sunlight intensity and the degradation of pesticide residues in the honey medium. Meanwhile, the longer the reaction time is, the faster the degradation of pesticide residues is and the lower the residual concentration of pesticide residues is. The decontamination efficiency of coumaphos reached 90% within 15 min, which was lower than that after 1 h

(97.02%) under 750 W/m^2 sunlight irradiation. Moreover, types of pesticide residues could also exert an effect on the degradation of pesticides. Amongst them, coumaphos exhibited the best degradation performance (90% of degradation after 15 min); the removal percentage of fenitrothion and methyl parathion reached 83.3, and 73.11%, respectively, within 1 h under 750 W/m^2 sunlight illumination (37).

The effect of UV light sources on the degradation of pesticides was further investigated, including VUV, and UVC. Results demonstrated that VUV (185 nm) was more effective than UVC (254 nm) in the degradation of pesticides such as pyraclostrobin, boscalid, fludioxonil, and azoxystrobin under the same reaction condition (53). It was mainly due to VUV at 185 nm could produce more energetic photons. Additionally, Yang et al. investigated the removal of five typical pesticides from water by VUV/UV at both bench- and pilot-scale studies (5). Results showed that VUV/UV showed much more effective and energy-efficient than UV and all pesticides could be removed with an efficiency of >90% at a VUV fluence of 12 mJ/cm^2. Furthermore, pilot-scale studies revealed that VUV/UV processes had a stable performance with acceptable energy consumption of 0.27–1.52 kWh/(m^3order). As a result, photolysis showed the potential for the degradation of pesticides as an energy-efficient and high-efficiency technology for surface decontamination of fresh produce.

Applications of Photolysis in Food Rinse Waste

Several photodegradation techniques by UV have been utilized for the degradation of pesticide residues from wastewater (27, 47). The pulsed light (PL) technology serves as a novel tool for the degradation of several herbicides in food rinse waste. As known, PL technology contains a successive repetition of short duration (325 μs) and high power flashes emitted by xenon lamps that range from ∼200 to 1,000 nm with a considerable amount of light in the short-wave UV spectrum. Baranda et al. investigated the photodegradation of several triazidic and organophosphorus pesticides in aqueous solutions by PL technology (35). The most studied pesticide residues were degraded very fastly, and their degradation was greater than 50% in a short period of time (milliseconds). However, there is a lack of studies on the toxicity of photodegradation products in the process. Considering that the PL technology (xenon flashlamp) had the characteristics of a mercury-free system, it could be therefore considered as a promising environmentally friendly photolytic approach for the decontamination of pesticide residues from rinse wastewater.

Moreover, the degradation kinetics of pesticide residues in wastewater could be fitted using a pseudo-first-order kinetics model by using UV irradiation (54, 55). Cunha and Teixeira (54) reported that the pseudo-first-order reaction rate constant for azoxystrobin, difenoconazole, and imidacloprid was in the ranges of 0.128–0.249 s^{-1}, 0.019–0.048 s^{-1}, and 0.129–0.266 s^{-1}, respectively, in tomato rinse water by photolysis. In addition, the degradation of chlorpyrifos in water was carried out with sunlight illumination to extend the light spectrum to visible light. Results showed that the highest degradation rate was 4.2% per day in distilled water at the light intensity of 43,400 lx and 7.4% per day in lake water at the light intensity of 42, 200 lx (56). The faster degradation was achieved in natural water than distilled water (56, 57), demonstrating a greater application potential of solar irradiation. The enhanced degradation could be ascribed to the presence of components such as natural organic matters and thus greater formation of active species during the process (56). Admittedly, there was a slower degradation of malathion by UV alone than photocatalytic treatment processes including UV/H_2O_2, UV/TiO_2, and UV/Fenton systems (43). However, it was interesting to find that no increase in toxicity was observed for the malathion aqueous solution with UV irradiation alone, whereas the toxicity of the malathion aqueous solution was increased sharply with photocatalytic processes (43). These findings indicate that photolysis, instead of photocatalytic treatment technologies, showed greater potential applications in food rinse wastewater in terms of both treatment efficiency and the toxicity of intermediate products. It needs to be noted that most research was carried out in bench- and pilot-scale studies. Future research should be paid more attention to improving pesticide residues degradation in industrial-scale studies.

CONCLUSION

The photolytic technique, a promising water treatment technology, has attracted increasing attention due to improved performance, such as no chemical required, and more safety, and could be widely implemented for various foods decontamination purposes. In photolysis, the chemical reaction would occur when the light energy absorbed by pesticides is higher than the bond energy of a chemical bond in the pesticide molecule. The application potential of photolysis indicated that the photolytic technique could work in various complex environments, including beverages, fresh produce, and natural food rinse wastewater. Although some achievements have been made, there possess still many challenges before photolysis has been applied in food processing, primarily including large energy input, sequential maintenance required, as well as thus increased cost. Assessing health risks and socioeconomic impacts of immediate products in the degradation of pesticide residues should be extremely important future work.

AUTHOR CONTRIBUTIONS

QX: investigation, resources, writing – original draft, review, and editing, conceptualization, and supervision. XX, GB, and JY: writing – review and editing. XS: writing – review and editing, conceptualization, and supervision. All authors contributed to the article and approved the submitted version.

FUNDING

This work was supported by the National Natural Science Foundation of China (Grant Nos. 51906125 and 52111540266) and Hong Kong Scholars Program (Grant Nos. XJ2021035 and XJ2021030).

REFERENCES

1. Kashyap PL, Xiang X, Heiden P. Chitosan nanoparticle based delivery systems for sustainable agriculture. *Int J Biol Macromol.* (2015) 77:36–51. doi: 10.1016/j.ijbiomac.2015.02.039
2. Misra NN. The contribution of non-thermal and advanced oxidation technologies towards dissipation of pesticide residues. *Trends Food Sci Technol.* (2015) 45:229–44. doi: 10.1016/j.tifs.2015.06.005
3. Stöckelhuber M, Muller C, Vetter F, Mingo V, Lotters S, Wagner N, et al. Determination of pesticides adsorbed on arthropods and gastropods by a Micro-QuEChERS approach and GC–MS/MS. *Chromatographia.* (2017) 80:825–9. doi: 10.1007/s10337-017-3280-8
4. Abedi-Firoozjah R, Ghasempour Z, Khorram S, Khezerlou A, Ehsani A. Non-thermal techniques: a new approach to removing pesticide residues from fresh products and water. *Toxin Rev.* (2020) 40:562–75. doi: 10.1080/15569543.2020.1786704
5. Yang L, Li M, Li W, Jiang Y, Qiang Z. Bench- and pilot-scale studies on the removal of pesticides from water by VUV/UV process. *Chem Eng J.* (2018) 342:155–62. doi: 10.1016/j.cej.2018.02.075
6. Lopez-Alvarez B, Villegas-Guzman P, Peñuela GA, Torres-Palma RA. Degradation of a toxic mixture of the pesticides carbofuran and iprodione by UV/H2O2: evaluation of parameters and implications of the degradation pathways on the synergistic effects. *Water Air Soil Pollut.* (2016) 227:215.
7. Nicolopoulou-Stamati P, Maipas S, Kotampasi C, Stamatis P, Hens L. Chemical pesticides and human health: the urgent need for a new concept in agriculture. *Front Public Health.* (2016) 4:148. doi: 10.3389/fpubh.2016.00148
8. Gavahian M, Sarangapani C, Misra NN. Cold plasma for mitigating agrochemical and pesticide residue in food and water: similarities with ozone and ultraviolet technologies. *Food Res Int.* (2021) 141:110138. doi: 10.1016/j.foodres.2021.110138
9. Pandiselvam R, Kaavya R, Jayanath Y, Veenuttranon K, Lueprasitsakul P, Divya V, et al. Ozone as a novel emerging technology for the dissipation of pesticide residues in foods–a review. *Trends Food Sci Technol.* (2020) 97:38–54. doi: 10.1016/j.tifs.2019.12.017
10. Lozowicka B, Jankowska M, Hrynko I, Kaczynski P. Removal of 16 pesticide residues from strawberries by washing with tap and ozone water, ultrasonic cleaning and boiling. *Environ Monit Assess.* (2016) 188:51–51. doi: 10.1007/s10661-015-4850-6
11. Li C, Zhu H, Li C, Qian H, Yao W, Guo Y. The present situation of pesticide residues in China and their removal and transformation during food processing. *Food Chem.* (2021) 354:129552. doi: 10.1016/j.foodchem.2021.129552
12. Vaya D, Surolia PK. Semiconductor based photocatalytic degradation of pesticides: an overview. *Environ Technol Innovat.* (2020) 20:101128. doi: 10.3390/ma13061338
13. Bano K, Kaushal S, Singh PP. A review on photocatalytic degradation of hazardous pesticides using heterojunctions. *Polyhedron.* (2021) 209:115465. doi: 10.1016/j.poly.2021.115465
14. Xiao Q, Yu S. The role of dissolved oxygen in the sulfite/divalent transition metal ion system: degradation performances and mechanisms. *Chem Eng J.* (2021) 417:129115. doi: 10.1016/j.cej.2021.129115
15. Xiao Q, Yu S. Reduction of bromate from drinking water by sulfite/ferric ion systems: efficacy and mechanisms. *J Hazard Mater.* (2021) 418:125940. doi: 10.1016/j.jhazmat.2021.125940
16. Gao X, Li P, Gu Z, Xiao Q, Yu S, Hou LA. Preparation of poly(piperazine-amide) nanofilms with micro-wrinkled surface via nanoparticle-templated interfacial polymerization: performance and mechanism. *J Membrane Sci.* (2021) 638:119711. doi: 10.1016/j.memsci.2021.119711
17. Sun X, Yang Z, Wei X, Tao Y, Boczkaj G, Yong Yoon J, et al. Multi-objective optimization of the cavitation generation unit structure of an advanced rotational hydrodynamic cavitation reactor. *Ultrason Sonochem.* (2021) 80:105771. doi: 10.1016/j.ultsonch.2021.105771
18. Dhananjayan V, Jayakumar S, Ravichandran B. Conventional methods of pesticide application in agricultural field and fate of the pesticides in the environment and human health. In: Rakhimol KR, Sabu T, Tatiana V editors. *Controlled Release of Pesticides for Sustainable Agriculture*. Cham: Springer International Publishing (2020). p. 1–39. doi: 10.3390/ijerph18020468
19. Bajwa U, Sandhu KS. Effect of handling and processing on pesticide residues in food- a review. *J Food Sci Technol.* (2014) 51:201–20. doi: 10.1007/s13197-011-0499-5
20. Sun X, Liu S, Zhang X, Tao Y, Boczkaj G, Yong JY, et al. Recent advances in hydrodynamic cavitation-based pretreatments of lignocellulosic biomass for valorization. *Bioresour Technol.* (2022) 345:126251. doi: 10.1016/j.biortech.2021.126251
21. Patil S, Torres B, Tiwari BK, Wijngaard HH, Bourke P, Cullen PJ, et al. Safety and quality assessment during the ozonation of cloudy apple juice. *J Food Sci.* (2010) 75:M437–43. doi: 10.1111/j.1750-3841.2010.01750.x
22. Chauhan OP, Raju PS, Ravi N, Singh A, Bawa AS. Effectiveness of ozone in combination with controlled atmosphere on quality characteristics including lignification of carrot sticks. *J Food Eng.* (2011) 102:43–8. doi: 10.1016/j.jfoodeng.2010.07.033
23. Meijers RT, derwald-Muller EO, Nuhn PANM, Kruithof JC. Degradation of pesticides by ozonation and advanced oxidation. *Ozone Sci Eng.* (1995) 17:673–86. doi: 10.1080/01919512.1995.10555778
24. Velioglu YS, Ergen SF, Aksu P, Altındag A. Effects of Ozone treatment on the degradation and toxicity of several pesticides in different grou. *J Agric Sci.* (2018) 24:245–55. doi: 10.15832/ankutbd.446448
25. Wu J, Luan T, Lan C, Hung Lo TW, Chan GYS. Removal of residual pesticides on vegetable using ozonated water. *Food Control.* (2007) 18:466–72. doi: 10.1016/j.foodcont.2005.12.011
26. Sun X, You W, Xuan X, Ji L, Xu X, Wang G, et al. Effect of the cavitation generation unit structure on the performance of an advanced hydrodynamic cavitation reactor for process intensifications. *Chem Eng J.* (2021) 412:128600. doi: 10.1016/j.cej.2021.128600
27. Dai J, Jiang C, Chai Y, Wang C, Chen H, Liu X. Photolysis kinetics of cartap and nereistoxin in water and tea beverages under irradiation of simulated sunlight and ultraviolet under laboratory conditions. *Food Chem.* (2021) 355:129595. doi: 10.1016/j.foodchem.2021.129595
28. Bintsis T, Litopoulou-Tzanetaki E, Robinson RK. Existing and potential applications of ultraviolet light in the food industry – a critical review. *J Sci Food Agric.* (2000) 80:637–45. doi: 10.1002/(SICI)1097-0010(20000501)80:6<637::AID-JSFA603>3.0.CO;2-1
29. Xuan X, Wang M, Zhang M, Kaneti YV, Xu X, Sun X, et al. Nanoarchitectonics of low-dimensional metal-organic frameworks toward photo/electrochemical CO2 reduction reactions. *J CO2 Utilizat.* (2022) 57:101883. doi: 10.1016/j.jcou.2022.101883
30. Pinna MV, Pusino A. Direct and indirect photolysis of two quinolinecarboxylic herbicides in aqueous systems. *Chemosphere.* (2012) 86:655–8. doi: 10.1016/j.chemosphere.2011.11.016
31. Xiao Q, Yu S, Li L, Zhang Y, Yi P. Degradation of bromate by Fe(II)-Ti(IV) layered double hydroxides nanoparticles under ultraviolet light. *Water Res.* (2019) 150:310–20. doi: 10.1016/j.watres.2018.11.067
32. Xiao Q, Ren Y, Yu S. Pilot study on bromate reduction from drinking water by UV/sulfite systems: economic cost comparisons, effects of environmental parameters and mechanisms. *Chem Eng J.* (2017) 330:1203–10. doi: 10.1016/j.cej.2017.08.071
33. Xiao Q, Wang T, Yu S, Yi P, Li L. Influence of UV lamp, sulfur(IV) concentration, and pH on bromate degradation in UV/sulfite systems: mechanisms and applications. *Water Res.* (2017) 111:288–96. doi: 10.1016/j.watres.2017.01.018
34. Xiao Q, Yu S, Li L, Wang T, Liao X, Ye Y. An overview of advanced reduction processes for bromate removal from drinking water: reducing agents, activation methods, applications and mechanisms. *J Hazard Mater.* (2017) 324:230–40. doi: 10.1016/j.jhazmat.2016.10.053
35. Baranda AB, Fundazuri O, Martínez de Marañón I. Photodegradation of several triazidic and organophosphorus pesticides in water by pulsed light technology. *J Photochem Photobiol A Chem.* (2014) 286:29–39. doi: 10.1016/j.jphotochem.2014.03.015
36. Baranda AB, Lasagabaster A, de Marañón IM. Static and Continuous flow-through pulsed light technology for pesticide abatement in water. *J Hazardous Mater.* (2017) 340:140–51. doi: 10.1016/j.jhazmat.2017.07.012
37. Yuan Z, Yao J, Liu H, Han J, Trebše P. Photodegradation of organophosphorus pesticides in honey medium. *Ecotoxicol Environ Safety.* (2014) 108:84–8. doi: 10.1016/j.ecoenv.2014.06.032

38. Cheng W, Zheng Z, Yang J, Chen M, Yao Q, Chen Y, et al. The visible light-driven and self-powered photoelectrochemical biosensor for organophosphate pesticides detection based on nitrogen doped carbon quantum dots for the signal amplification. *Electrochimica Acta.* (2019) 296:627–36. doi: 10.1016/j.electacta.2018.11.086
39. Li CF, Bradley R. Degradation of chlorinated hydrocarbon pesticides in milk and butteroil by ultraviolet energy. *J Dairy Sci.* (1969) 52:27–30.
40. Li CF, Bradley RL. Degradation of chlorinated hydrocarbon pesticides in milk and butteroil by ultraviolet Energy1. *J Dairy Sci.* (1969) 52:27–30. doi: 10.3168/jds.S0022-0302(69)86495-7
41. Falguera V, Pagán J, Garza S, Garvín A, Ibarz A. Ultraviolet processing of liquid food: a review. Part 1: fundamental engineering aspects. *Food Res Int.* (2011) 44:1571–9. doi: 10.1016/j.foodres.2011.02.056
42. Burrows HD, Canle L M, Santaballa JA, Steenken S. Reaction pathways and mechanisms of photodegradation of pesticides. *J Photochem Photobiol B Biol.* (2002) 67:71–108. doi: 10.1016/s1011-1344(02)00277-4
43. Li W, Zhao Y, Yan X, Duan J, Saint CP, Beecham S. Transformation pathway and toxicity assessment of malathion in aqueous solution during UV photolysis and photocatalysis. *Chemosphere.* (2019) 234:204–14. doi: 10.1016/j.chemosphere.2019.06.058
44. Chandra S, Patras A, Pokharel B, Bansode RR, Begum A, Sasges M. Patulin degradation and cytotoxicity evaluation of UV irradiated apple juice using human peripheral blood mononuclear cells. *J Food Process Eng.* (2017) 40:e12586.
45. Tikekar RV, Anantheswaran RC, LaBorde LF. Patulin degradation in a model apple juice system and in apple juice during ultraviolet processing. *J Food Process Preservat.* (2014) 38:924–34. doi: 10.1111/j.1750-3841.2010.02015.x
46. Zhu Y, Koutchma T, Warriner K, Shao S, Zhou T. Kinetics of patulin degradation in model solution, apple cider and apple juice by ultraviolet radiation. *Food Sci Technol Int.* (2013) 19:291–303. doi: 10.1177/1082013212452414
47. Ibarz R, Garvín A, Falguera V, Pagán J, Garza S, Ibarz A. Modelling of patulin photo-degradation by a UV multi-wavelength emitting lamp. *Food Res Int.* (2014) 66:158–66. doi: 10.1016/j.foodres.2014.09.006
48. Bustos N, Cruz-Alcalde A, Iriel A, Fernández Cirelli A, Sans C. Sunlight and UVC-254 irradiation induced photodegradation of organophosphorus pesticide dichlorvos in aqueous matrices. *Sci Total Environ.* (2019) 649:592–600. doi: 10.1016/j.scitotenv.2018.08.254
49. Huang S-T, Hung Y-A, Yang M-J, Chen I-Z, Yuann J-MP, Liang J-Y. Effects of epigallocatechin gallate on the stability of epicatechin in a photolytic process. *Molecules.* (2019) 24:787. doi: 10.3390/molecules24040787
50. Burns SE, Hassett JP, Rossi MV. Binding effects on humic-mediated photoreaction:? intrahumic dechlorination of mirex in water. *Environ Sci Technol.* (1996) 30:2934–41. doi: 10.1021/es950906i
51. Abaskharon RM, Gai F. Direct measurement of the tryptophan-mediated photocleavage kinetics of a protein disulfide bond. *Phys Chem Chem Phys.* (2016) 18:9602–7. doi: 10.1039/c6cp00865h
52. Tomer V. Vegetable processing at household level: effective tool against pesticide residue exposure. *IOSR J Environ Sci Toxicol Food Technol.* (2013) 6:43–53. doi: 10.9790/2402-0624353
53. Choi SW, Shahbaz HM, Kim JU, Kim D-H, Yoon S, Jeong SH, et al. Photolysis and TiO2 photocatalytic treatment under UVC/VUV irradiation for simultaneous degradation of pesticides and microorganisms. *Appl Sci.* (2020) 10:4493. doi: 10.3390/app10134493
54. Cunha ILC, Teixeira A. Degradation of pesticides present in tomato rinse water by direct photolysis and UVC/H2O2: optimization of process conditions through sequential Doehlert design. *Environ Sci Pollut Res Int.* (2021) 28:24191–205. doi: 10.1007/s11356-021-13387-7
55. Jafari SJ, Moussavi G, Hossaini H. Degradation and mineralization of diazinon pesticide in UVC and UVC/TiO2 process. *Desalination Water Treat.* (2016) 57:3782–90. doi: 10.1080/19443994.2014.987171
56. Hossain MS, Fakhruddin ANM, Chowdhury MAZ, Alam MK. Degradation of chlorpyrifos, an organophosphorus insecticide in aqueous solution with gamma irradiation and natural sunlight. *J Environ Chem Eng.* (2013) 1:270–4. doi: 10.1016/j.jece.2013.05.006
57. Sakkas VA, Lambropoulou DA, Albanis TA. Study of chlorothalonil photodegradation in natural waters and in the presence of humic substances. *Chemosphere.* (2002) 48:939–45. doi: 10.1016/s0045-6535(02)00121-2

Conflict of Interest: The authors declare that the research was conducted in the absence of any commercial or financial relationships that could be construed as a potential conflict of interest.

frontiers | Frontiers in Nutrition

MINI REVIEW
published: 27 May 2022
doi: 10.3389/fnut.2022.925846

Advanced Lipidomics in the Modern Meat Industry: Quality Traceability, Processing Requirement, and Health Concerns

Chengliang Li[1†], Burcu Ozturk-Kerimoglu[2], Lichao He[1], Min Zhang[1,3], Jiajing Pan[1,3], Yuanyi Liu[1], Yan Zhang[1], Shanfeng Huang[4], Yue Wu[5] and Guofeng Jin[1]*

[1] School of Food and Health, Beijing Technology and Business University, Beijing, China, [2] Ege University, Engineering Faculty, Food Engineering Department, İzmir, Turkey, [3] College of Food Science and Technology, Huazhong Agricultural University, Wuhan, China, [4] School of Biology and Food Engineering, Chuzhou University, Chuzhou, China, [5] Sonochemistry Group, School of Chemistry, The University of Melbourne, Parkville, VIC, Australia

OPEN ACCESS

Edited by:
Qiang Xia,
Ningbo University, China

Reviewed by:
Haizhou Wu,
Chalmers University of Technology, Sweden
Daoying Wang,
Jiangsu Academy of Agricultural Sciences (JAAS), China

***Correspondence:**
Guofeng Jin
jgf@mail.hzau.edu.cn

†Present address:
Chengliang Li,
Instituto de Agroquímica y Tecnología de Alimentos (IATA-CSIC), Paterna, Spain

Specialty section:
This article was submitted to Food Chemistry, a section of the journal Frontiers in Nutrition

Received: 22 April 2022
Accepted: 02 May 2022
Published: 27 May 2022

Citation:
Li C, Ozturk-Kerimoglu B, He L, Zhang M, Pan J, Liu Y, Zhang Y, Huang S, Wu Y and Jin G (2022) Advanced Lipidomics in the Modern Meat Industry: Quality Traceability, Processing Requirement, and Health Concerns. Front. Nutr. 9:925846. doi: 10.3389/fnut.2022.925846

Over the latest decade, lipidomics has been extensively developed to give robust strength to the qualitative and quantitative information of lipid molecules derived from physiological animal tissues and edible muscle foods. The main lipidomics analytical platforms include mass spectrometry (MS) and nuclear magnetic resonance (NMR), where MS-based approaches [e.g., "shotgun lipidomics," ultra-performance liquid chromatography-tandem mass spectrometry (UPLC-MS/MS), matrix-assisted laser desorption and ionization time-of-flight mass spectrometry (MALDI-TOF-MS)] have been widely used due to their good sensitivity, high availability, and accuracy in identification/quantification of basal lipid profiles in complex biological point of view. However, each method has limitations for lipid-species [e.g., fatty acids, triglycerides (TGs), and phospholipids (PLs)] analysis, and necessitating the extension of effective chemometric-resolved modeling and novel bioinformatic strategies toward molecular insights into alterations in the metabolic pathway. This review summarized the latest research advances regarding the application of advanced lipidomics in muscle origin and meat processing. We concisely highlighted and presented how the biosynthesis and decomposition of muscle-derived lipid molecules can be tailored by intrinsic characteristics during meat production (i.e., muscle type, breed, feeding, and freshness). Meanwhile, the consequences of some crucial hurdle techniques from both thermal/non-thermal perspectives were also discussed, as well as the role of salting/fermentation behaviors in *postmortem* lipid biotransformation. Finally, we proposed the inter-relationship between potential/putative lipid biomarkers in representative physiological muscles and processed meats, their metabolism accessibility, general nutritional uptake, and potency on human health.

Keywords: meat lipidomics, mass spectrometry, nuclear magnetic resonance, lipid biomarkers, lipolysis, biosynthesis, meat processing, nutritional value

INTRODUCTION

The global meat industry is a continuously growing sector with an ever-increasing demand. The Organization for Economic Co-operation and Development (OECD) and the Food and Agriculture Organization of the United Nations (FAO) have recently stated that worldwide meat production is projected to expand by approximately 44 million tons by 2030, despite the detrimental impacts of the coronavirus disease 2019 (COVID-19) pandemic and other possible restrictions (1). Meat is considered a unique animal-derived food providing high biological value proteins with all essential amino acids and various micronutrients (2). Alongside proteins, lipids are abundant constituents in meat and meat products that play critical roles in providing desirable mouth-feel perception, characteristic flavor, favorable texture, juiciness, and enhanced cooking yield (3). According to the complexity of structure and biosynthesis, lipids are divided into eight categories, depending on their differences in the level of unsaturation, the type of the covalent bond, the fatty acyl chain length, double bond location, the head groups, Z/E geometric isomerism, and the branched functional groups (4, 5). Specifically, these muscle-derived lipid species mainly include non-esterified/free fatty acids (FFAs), glycerolipids (GLs), glycerophospholipids (GPs), sphingolipids (SLs), sterol lipids, prenol lipids, saccharolipids, and polyketides (6). Among them, triglycerides (TGs) or triacylglycerols (TAGs) and phospholipids (PLs), two common and most abundant categories of lipids, are highly associated with health and nutritional functions in the body (7, 8). TGs are mainly composed of FAs, such as capric acid (Ca) and lauric acid (La), but their contents can vary greatly among different breeds and muscle tissues (9). Membrane phospholipid composition may play a critical role in subsequent lipid oxidation development in raw and cooked meats (10, 11), while SLs and glycolipids contribute more functions to human health, such as increasing anti-inflammatory and anticarcinogenic activities and alleviating the risk of cardiovascular diseases and cholesterol absorption (7, 12). Traditional studies utilize gas chromatography (GC) with known standards or mass spectrometry (MS) to detect and identify total fatty acids in the samples, where saponification and derivatization protocols are usually required to generate the volatile fatty acid analytes and may result in the loss of information about the original esterified structure (neutral or polar lipids) (9, 13). Thus, the modern meat industry deserves the exploration of lipid composition from different biological sources through global profiling for the qualitative and quantitative characterization of individual lipid species (11).

During the latest decade, scientific expertise and technologies are constantly being developed with commercial or industrial aspects to advance the traceability and authentication of meat products and to address the safety concerns of the public, and for economic and quality reasons as well (14). Although meat from different species can be easily detected using deoxyribonucleic acid (DNA)-based techniques, the mixing of meat from different biological sources (e.g., geographical origins) is more difficult to detect. In this regard, MS- and nuclear magnetic resonance (NMR)-based lipidomics, such as both untargeted and targeted approaches, have been suggested as a promising strategy for this detection (15–17). The high-throughput untargeted analysis has the advantage of detecting lipid metabolites as comprehensively as possible by emphasizing the changes in quantity in biological importance (14, 15). Additionally, the targeted approach focuses on identifying and acquiring a number of specific fractions of known lipid species, for instance, FFAs, PLs, and cholesterol, in the presence of external chemical standards or available databases (18, 19). To achieve more persuasive results, the sample/lipid-extract preparation, chromatographic separation or direct-infusion MS (DI-MS, "shotgun lipidomics"), method validation, multivariate data processing, and bioinformatics evaluation have been well considered in the entire analytical platform (4, 15).

Exploratory analysis, classification/discriminant analysis, and regression analysis/prediction models have been proven to be useful in lipidomics data analysis. Apart from these chemometric tools or machine learning methods, however, bioinformatic validation should be crucial for determining the potential biomarkers of lipid species present in a biological system and providing molecular insights into alterations in energetic/metabolic pathways of lipid biosynthesis (4). Hence, in this short review, we examined the mainstream of recently published investigation available with discussions regarding the applications of MS-/NMR-based lipidomics in muscle foods, such as meat origin and adulteration identification, meat safety assessment, and dietary lipid nutrition during representative processing conditions and/or *in vitro* treatment.

MEAT LIPIDOMICS IN TRACEABILITY AND MICROBIAL SAFETY

Meat is originally skeletal muscles of livestock and thereby suffers from some factors in the livestock production system, mainly such as animal genetic/breed background, feeding types, geographical location, and environmental stress, particularly associated with spoilage developed by microbiological activity (20). As highlighted in literature evidence (**Table 1**), different efforts have been undertaken to achieve lipid-label validation depending on diagnostic and reliable features that can reflect the origins/authenticity of suspected muscles and their freshness status through the lipidomics strategy. The consequent lipid molecules that are inherently from muscle tissues or result from the metabolism of indigenous microorganisms vary among different species, such as beef (14, 18, 21–24), pork (24–27), sheep/goat (28), poultry (16), and marine products (29–32). To investigate the effect of genetic background, MALDI-TOF-MS and Phosphorus-31 NMR (^{31}P NMR)-based lipidomics were successfully applied to capture the differences in fatty acid biosynthesis among German Simmental bulls fed with different diets. Consequently, TGs, phosphatidylethanolamines (PEs), phosphatidylcholine (PCs), phosphatidylinositol (PIs), cardiolipins (CLs), and cholesterol were identified as potential biomarkers (22). Furthermore, untargeted and targeted MS-based lipidomics based on the use of ultra-performance liquid chromatography (UPLC) coupled with high-resolution MS

(HRMS) has shown good discriminative power between different species/breeds and feeding conditions toward extended global lipid information with appropriate multivariate data analysis (**Table 1**). A panel of lipids, particularly GLs [diacylglycerols (DAGs) and TAGs], lysophosphatidylcholines (LPCs), lysophosphatidylethanolamines (LPEs), and n-6 polyunsaturated fatty acids (PUFAs) have been screened out as specific markers for differentiation of animal diets (18, 21, 25, 28, 29). More intermuscular differences traceable properties in lipidomics can be evaluated as a function of geographical origin and for adulteration (**Table 1**). For instance, GLs [TGs and diglycerides (DGs)] and GPs were screened as main lipid biomarkers by principal component analysis (PCA) and partial least squares-discriminant analysis (PLS-DA) modeling through UPLC-Q-TOF-MS/MS approach for China's domestic pork (from Tibetan, Jilin, and Sanmenxia black pigs), suggesting the difference in production systems, feeds and genetic backgrounds (26).

It is also noticeable that exposure to microbes may significantly influence the lipid compositions during meat production where other indicators are usually involved, e.g., isotopic ratios and feeding (23). Particularly for marine products, such as fish, fatty acids, and GPs, metabolism is identified as the major pathway through microbial contamination during cutting, storage, and distribution processes after slaughter. A study was conducted to evaluate the spoilage of farmed Atlantic salmon (*Salmo salar L.*) during storage at 4°C for up to 15 days by adopting the UPLC-Q-Exactive-MS with high sensitivity (30). According to the results, the increase of LPC (C17:0) and LPC (C18:0) could result from the hydrolysis of PC (C18:4/C16:1) as a major freshness index. Assisted by "shotgun lipidomics," PCs, PEs, PIs, phosphatidylserines (PSs), and sphingomyelins (SMs) were profiled as the lipid biomarkers of interest for the naturally spoiled muscle from *Ctenopharyngodon idellus* during room-temperature storage. UPLC-HRMS-based lipidomics has also shown good strength in identifying PCs, ceramides (CERs), and SLs metabolism as differentiated by pork and beef ground meat from different grades or due to death from diseases/abnormalities (24, 27). However, NMR-based lipidomics can screen more polar lipid metabolites and thus provides characteristic information on the metabolic profile of adulterated muscle. The presence of o-phosphocholine and a reduced level of Myo-inositol in turkey breast muscle injected with protein hydrolysates were observed through Proton NMR (^{1}H NMR) untargeted lipidomics, suggesting the possible role of Myo-inositol deficiency in enhanced lipolysis (16, 33).

MEAT LIPIDOMICS AS AFFECTED BY PROCESSING FACTORS

Up to date, various meat processing strategies, such as castration (34), thermal/non-thermal techniques (8, 17, 19, 35–38), freezing/thawing intervention (39), *in vitro* oxidation (40, 41), *postmortem* aging/storage (11, 42), modified atmosphere packaging (MAP) (42), and brining/drying-curing/preservatives treatments (43–47) have been implicated to improve the microbiological safety, color, flavor, and texture for the development of favorable meat products (**Table 2**). Accordingly, DI-MS and/or a combination of GC and liquid chromatography (GC/LC) and MS techniques have been utilized in the application of thermal processing to identify dozens of different lipids as potential biomarkers. Consequently, the lipolysis of TGs and PLs was noted as a strong flavor-binding precursors through different thermal degradation (boiling, steaming, and roasting) and showed specific losses of representative lipids (19, 35). It is worthwhile to note that fresh fish fillets, particularly *Pleuronectes platessa* upon high-pressure processing (HPP) were characterized by a distinctly high level of lipid-derived polar metabolites, serine-phosphoethanolamine species (Ser-PETA) (36). Specifically, studies on the discrimination of untreated/irradiated raw/ground meat from commercially produced goat, chicken, turkey, and pork through global lipid profile using UPLC-Q-Exactive-Orbitrap-MS/MS, targeted GC-resolved fatty acids composition, and chemometric tools (PCA and PLS-DA) have been recently reported (8, 37, 38). These authors observed γ-ray irradiation dose-dependent increase in docosahexaenoic acid (DHA)-enriched PC (C18:4/C22:6) + H in goat meat, while X-ray irradiation tended to result in n-3 PUFA-enriched lipids in chicken and turkey meat, accompanied with a noticeable accumulation of PLs and oxidized short- and long-chain FFAs. Comprehensive lipidomics based on GC-technique and phosphorus-31/carbon-13 NMR (^{31}P/^{13}C NMR) spectroscopy was devoted for hoki co-product (i.e., roe) treated with a pulsed electric field (PEF), where abundant PLs and a high level of lyso-diphosphatidylglycerols (LDPGs), LPEs, lysophosphatidylserines (LPSs), and LPCs were finally characterized, and PEF transformed more *sn*-2 phospholipid eicosapentaenoic acid (EPA) and DHA into *sn*-1,3 positions with potentially compromised bioavailability in terms of re-esterified structures (17). Additionally, when frozen Atlantic salmon and bullet tuna were thawed, an untargeted MS-based lipidomics approach detected abundant water-soluble phospholipid metabolites (i.e., L-α-glyceryl-phosphoryl-choline and *N*-methyl-ethanolamine phosphate) (39). However, hydroxyl radical (·OH) attacks can significantly alter the lipidomics profiles of shrimp and yak muscle to a large extent. PEs enriched in PUFAs were highly vulnerable to *in vitro* oxidation but both GPs metabolism and fatty acid biosynthesis were enriched during the subsequent deterioration and spoilage process of oxidized yak hindquarter meat (40, 41). On the other hand, PLs in porcine meat can undergo enzymatic hydrolysis during *postmortem* aging. For example, by employing targeted UPLC-TQ-MS/MS (with PLs as internal standards) to determine the PLs lipolysis tendency, researchers found that *postmortem* porcine loin (*M. Longissimus*) up to 21 days at 4°C was rich in PIs, PSs, and PAs, particularly C38:4 and C36:2 lipid species. Phospholipase A_2 (PLA_2) can be activated by *postmortem* calcium influx from the sarcoplasmic reticulum (SR) with a surge of LPCs in aging muscles (11). Apart from the targeted MS approach, untargeted "shotgun lipidomics" [electrospray ionization (ESI)-QTrap-MS/MS] became useful in identifying the lipid biomarkers derived from water-boiled dry-cured Pekin duck as a function of salting and ripening times (43, 44). In

TABLE 1 | Representative applications of MS-/NMR-based lipidomics in meat origin/adulteration identification, nutritional/microbial quality, and biological function.

Type of origin	Species and muscle tissues	Sample preparation/lipid extraction methods	Analytical techniques	Data processing	Identified lipids and potential biomarkers	Possible biological functions and/or bioinformatics evaluation	References
Breed	Cattle-yak, yak, and cattle (*Longissimus thoracis*)	Extraction with methyl tertbutyl ether/methanol/water (2.6:2.0:2.4, v/v/v) with reconstitution in acetonitrile solution containing 0.04% acetic acid	UPLC-QTrap-MS/MS, untargeted	ANOVA, PCA, OPLS-DA, VIP	Phospholipids containing long-chain PUFAs, PAs, PCs, PEs, as well as SMs, CARs, FFAs, LPCs, CERs, TGs, DGs, MGs, long-chain acylcarnitines	Difference in energy metabolism and lipid nutrition quality, biomarkers of β-oxidation of fatty acids using KEGG database and enrichment	Gu et al. (21)
	Luchuan and Duroc boar pigs (*Longissimus* muscle)	Extraction with 70% aqueous methanol 4°C overnight	UPLC-QTrap-MS/MS, untargeted	ANOVA, *t*-test, PCA, OPLS-DA, HCA, VIP	TGs, PCs, PEs, DGs, and CERs	Regulation of lipolysis in adipocytes, fat digestion and absorption, and cholesterol metabolism enriched by KEGG database	Zhang et al. (25)
Feeding condition	Sheep/goat (*Biceps femoris*)	Aqueous/organic extraction by methanol/water (1:1, v/v) solution, dichloromethane/methanol (3:1, v/v) with resuspension of the dried extracts in isopropanol/acetonitrile (9:1, v/v)	UPLC-Q-TOF-MS, untargeted	ANOVA, PCA, OPLS-DA, VIP, permutation test, SVM	Glycerolipids (DAGs, TAGs), PCs, LPCs, PEs and SMs, acylcarnitines, n-6 PUFAs (arachidonic acid)	Functional components of membrane bilayers, energy storage, nutritional and physiological properties	Wang et al. (28)
	Beef steers tissues (Duodenum, liver, subcutaneous adipose, and *Longissimus dorsi*)	Phospholipids and cholesterol extraction by Bligh and Dyer's liquid–liquid extraction (LLE) method	UPLC-TQ-MS, targeted	FDR *p*-adjustment, *t*-test, ROC, Pearson's correlation analysis	PCs, PEs, LPCs, LPEs, cholesterol	Linoleic/α-linolenic acids metabolism and biosynthesis, metabolic crossroad induced by gain-to-feed ratios	Artegoitia et al. (18)
	German Simmental bulls fed with different diets (*Longissimus* muscle)	Homogenization in chloroform/methanol (2:1, v/v) followed by lipid isolation. Dried lipids restabilized in 50 mM Tris buffer (pH 7.65)	TLC separation, MALDI-TOF MS, ^{31}P NMR spectroscopy (242.88 MHz)	PSD experiment (precursor ions), spectra deconvolution	TAGs, PEs, PCs, PIs, CLs, cholesterol	Regulating fatty acid biosynthesis in beef cattle under different dietary regimes	Dannenberger et al. (22)
	Hepatopancreas of mud crab (*Scylla paramamosain*) fed with DHA/EPA diets	Extraction with dichloromethane/methanol (3:1, v:v) followed by resuspension in isopropanol/acetonitrile/H_2O (2:1:1, v:v:v)	UPLC-Q-Exactive-Orbitrap-MS, untargeted	*t*-test, PCA, PLS-DA, HCA, VIP	PCs, PEs, PSs, PIs, LPCs, SMs, TGs, and FFAs	Association with fatty acid transport/deposition, β-oxidation, long-chain PUFAs (DHA) biosynthesis using GO analysis, KEGG pathway enrichment	Wang et al. (29)
Geographical origin	Beef (from United States (US), Japan and Australia)	Homogenization with chloroform/methanol (1:1, v/v) followed by Bligh and Dyer's liquid–liquid extraction (LLE) method	UPLC-Orbitrap-MS, untargeted	ANOVA, PCA, PLS-DA, OPLS-DA, VIP, LOO-CV, jackknife confidence intervals test	PCs, PEs and n-6/n-3 FFAs, MUFAs and particularly n-3 PUFAs	Nutritional quality and differential human diet	Man et al. (14)
	China's domestic pork (from Tibetan, Jilin and Sanmenxia black pigs)	Homogenization and extraction with isopropanol	UPLC-Q-TOF-MS/MS, untargeted	ANOVA, PCA, PLS-DA, VIP	Glycerolipids (TGs, DGs), glycerophospholipids, sterol lipids, sphingolipids, polyketides, fatty acyls and prenol lipids	Main causes possibly including the difference in production systems, feeds and genetic backgrounds	Mi et al. (26)
	Beef (from six countries including Argentina, Australia, Brazil, Canada, New Zealand and Uruguay)	Homogenization with Folch solution [chloroform/methanol (2:1, v/v)] followed by dryness and re-solubilization	LC-Q-TOF-MS (comparison between DuoSpray and DART ion source), untargeted	RSD examination, PCA, fold change with *p*-adjustment of ANOVA, SVM	Glyceride (monoglyceride, diglyceride and triglyceride), FFAs, PIs, PEs, LPEs, LPCs, CARs, SMs, NAEs	Some indicators involved in lipid compositions, such as isotopic ratios, animal growth, production systems (feeding and exposure to microbials)	Wang et al. (23)

(Continued)

TABLE 1 | (Continued)

Type of origin	Species and muscle tissues	Sample preparation/lipid extraction methods	Analytical techniques	Data processing	Identified lipids and potential biomarkers	Possible biological functions and/or bioinformatics evaluation	References
Freshness or microbial diversity	Farmed Atlantic salmon (*Salmo salar L.*) during storage at 4°C for up to 15 days	Extraction with methanol/water (2:5, v/v) and methyl tertary butyl ether followed by resuspension in isopropanol:acetonitrile (1:1, v/v)	UPLC-Q-Exactive-MS, untargeted	PCA, *t*-test, fold change with *p*-adjustment of ANOVA	LPCs and PCs	KEGG pathway showed linoleic acid metabolism, arachidonic acid metabolism and glycerophospholipid metabolism. The increase in LPC (C17:0) and LPC (C18:0) could result from the hydrolysis of PC (18:4/16:1) as a major freshness index.	Chen et al. (30)
	Large yellow croaker (*Larimichthys crocea)* fillets affected by cold treatment (−1°C and −3°C) during up to 35 days of storage	Homogenization in chloroform/methanol (2:1, v/v) followed by resuspension with isopropanol	UPLC-Q-Exactive-Orbitrap-MS, untargeted	ANOVA, Pearson's correlation analysis, PCA, PLS-DA, VIP	CERs, CLs, DGs, HexCer, LPCs, LPEs, PCs, PEs, PGs, PIs, PSs, SMs, and TGs	Autophagy-animal, glycerophospholipid metabolism, linoleic/α-linolenic metabolism, arachidonic acid metabolism, and glycosylphosphatidylinositol (GPI)-anchor biosynthesis enriched by KEGG database	Chen et al. (31)
	Muscle from *Ctenopharyngodon idellus* during room-temperature storage for 72 h	Homogenization with chloroform/methanol (2:1, v/v) followed by Bligh and Dyer's liquid–liquid extraction (LLE) method, dryness and re-solubilization	ESI-MS/MS (shotgun lipidomics), untargeted	Peak intensity screening, signal-to-noise ratio (SN) optimization, monitoring of precursor ion scan	Tracking phospholipid profiling including PCs, PEs, PIs, PSs, SMs	Oxidation and hydrolysis were mentioned as the two main causes for the deterioration of phospholipid in fish muscle during storage. PE molecular species may result from the microbe bred in the muscle.	Wang and Zhang (32)
Adulteration	Pork meat (hindquarter) from live pigs conventionally butchered versus dead pigs butchered immediately after death from diseases/abnormalities	Dual-phase extraction by methyl tert–butyl ether/methanol/H_2O system, lipids redissolved in acetonitrile/isopropanol/H_2O (65:30:5, v/v/v)	UPLC–TripleTOF–MS/MS, UPLC-QTrap-MS/MS, untargeted/ pseudotargeted	Welch *t*-test, PCA, and HCA	PCs and TGs	The lower PCs content in dead pork implied the conversion into other metabolites, such as PEth.	Cao et al. (27)
	Different grades of beef mince and pork mince purchased from a national retail outlet	Homogenization in chloroform/methanol (1:1, v/v), lyophilised lipids redissolved in chloroform/methanol/water (1:4:4, v/v)	UPLC-LTQ Orbitrap-MS, untargeted	Kruskal–Wallis ANOVA, PLS-DA, Spearman's correlation analysis, VIP	CERs, sphingolipids, PGs, TGs	Ceramide in sphingolipids metabolism by KEGG pathway analysis. Excessive irradiation may increase the content of free fatty acids, particularly in pork.	Trivedi et al. (24)
	Adulterated turkey breast muscle with protein hydrolysates	Homogenization first in ice-cold methanol, then ice-cold chloroform and finally ice-cold water. Storage at 4°C overnight and dried matter resuspended in an aqueous solution containing 0.05% TSP	^{1}H NMR Spectroscopy (400 MHz), untargeted	ANOVA, PCA	o-phosphocholine, myo-inositol	The possible mechanism of lipolysis due to myo-inositol deficiency	Wagner et al. (16)

TSP, sodium trimethylsilyl-2,2,3,3-tetradeuteroproprionate; DHA, docosahexaenoic acid; EPA, eicosapentaenoic acid; GC-FID, capillary gas chromatography coupled with flameionization detection; UPLC-Q-TOF-MS, ultraperformance liquid chromatography-quadrupole, time-of-flight mass spectrometry; UPLC-TQ-MS, ultraperformance liquid chromatography-triple quadrupole mass spectrometry; UPLC-TripleTOF-MS, ultraperformance liquid chromatography-triple time-of flight mass spectrometry; UPLC-QTrap-MS/MS, ultraperformance liquid chromatography-hybrid triple quadrupole-linear ion trap, tandem mass spectrometry; UPLC-LTQ Orbitrap-MS, ultraperformance liquid chromatography-hybrid linear ion trap-orbitrap, mass spectrometry; UPLC-Orbitrap-MS, ultraperformance liquid chromatography coupled with high-resolution orbitrap mass spectrometry; UPLC-Q-Exactive-Orbitrap-MS, ultraperformance liquid chromatography coupled to quadrupole exactive orbitrap high resolution mass spectrometry; TLC, thin-layer chromatography; MALDI-TOF MS, matrix-assisted laser desorption and ionization time-of-flight mass spectrometry; DART, direct-analysis-in-real-time ionization; ESI-QTrap-MS/MS: direct-infusion electrospray ionization-hybrid triple quadrupole-linear ion trap tandem mass spectrometry; NMR, nuclear magnetic resonance spectroscopy; ANOVA, analysis of variance; PCA, principal component analysis; PLS-DA, partial least squares discriminant analysis; OPLS-DA, orthogonal partial least squares discriminant analysis; HCA, hierarchical cluster analysis; VIP, variable importance in projection; LOO-CV, leave-one-out cross-validation; SVM, support vector machine; FDR, fold discovered rate; ROC, receiver-operator characteristic curve analysis; PSD, post source decay; RSD, relative standard deviations; TGs, triglycerides; DGs, diglycerides; MGs, monoglycerides; DAGs, diacylglycerols; TAGs, triacylglycerols; PAs, phosphatidic acids; PCs, phosphatidylcholines; PEs, phosphatidylethanolamines; PGs, phosphatidylglycerols; PSs, phosphatidylserines; PIs, phosphatidylinositols; LPCs, lysophosphatidylcholines; LPEs, lysophosphatidylethanolamines; SMs, sphingomyelines; CERs, ceramides; CARs, carnitines; NAEs, N-acyl ethanol-amines; HexCer, hexosylceramide; CLs, cardiolipins; FFAs, free fatty acids; MUFAs, monounsaturated fatty acids; PUFAs, polyunsaturated fatty acids; PEth, phosphatidylethanol; FAMEs, fatty acid methyl esters; GO, gene Ontology; KEGG, service of Kyoto Encyclopedia of Genes and Genomes.

those studies, the findings pointed out that low-salt (< 6%) dry-cured duck significantly promoted the degradation of individual PLs (e.g., PCs, PGs, PEs, PSs, and PIs) probably resulting from a robust release of phospholipase, though some LPCs were damaged possibly due to oxidation and thermal degradation provided by boiling. In other cases, by combining the GC-system and untargeted hydrophilic interaction liquid chromatography (HILIC) coupled to QTrap-MS, saturated fatty acids (SFAs) (C16:0), monounsaturated fatty acids (MUFAs) (C18:1), and PUFAs (C18:2) were observed to be important lipid-derived flavor precursors in low-salted salmon and PCs content was kept at a high level even at 30% NaCl replacement rather than PSs (45). Following untargeted UPLC-QTrap-MS/MS lipidomics, salting/preservatives treatment of goat meat led to decrements in TGs concentration (47) while dry-curing of mutton ham (M. *biceps femoris*) significantly contributed to GLs, DGs, and specifically C20:3 and C18:4 FFAs released, showing characteristic metabolisms of GPs and SLs (46).

DISCUSSION ON POSSIBLE MECHANISMS AND FUTURE REMARKS

Lipids are inherently abundant in muscle tissues, which play critical roles in a series of cellular processes and physiological/biological activities (e.g., cell membrane architecture, cell signaling and energy-storing) (48). Breeds and feeding conditions, which usually have a large impact on animal physiology, determine the skeletal muscle growth and maturation, the final meat yield, and nutritional/flavor quality (21, 28, 29). NMR-/MS-based approaches have been attempted to obtain lipid-metabolite signatures and their relationship to physiological alteration in tissues as well as the potency in meat production. Differences in muscle energy metabolism, lipolysis in adipocytes, fat digestion/absorption, and cholesterol metabolism, β-oxidation of fatty acids, in particular, would offer the dynamics of redox status, oxidative stability, and consumer acceptability as influenced by the nutrients and ingredients in the animal feeds (20). For instance, concentrate-fed sheep are generally more obese compared with pasture-grazing sheep. High-fat diets may thereby promote the levels of isoleucine, lipids, glutamate, and 3-methylhistidine and lead to decreased citrate and glycerophosphorylcholines (GPCs) in animals (28). Consequently, as putatively revealed from lipidomics analysis, DAGs tend to accumulate in meat from concentrate-fed sheep/goats due to fat deposition, while some saturated TGs (e.g., C40:0, C42:0, and C44:0) in meats can be favored by pasture-grazing feeding strategy, showing a positive biological function of energy storage (28). PLs are the primary structural constituents of biological membranes and serve as critical nutrients owing to their physiological and nutritional properties. Following lipidomics, some species of fatty acid components and PLs have been useful markers in muscle tissues for differentiating breeds/dietary supplementation (21, 28, 29), detecting adulteration (27), and monitoring microbial accessibility (30–32). For instance, n-3 long-chain PUFA, such as EPA (C20:5n-3) and DHA (C22:6n-3) are essential fatty acids (EFA) for marine fish and crustaceans. An appropriate ratio of DHA/EPA feeding diet can improve the lipogenesis, integrity of membrane PLs, and DHA biosynthesis/deposition, meanwhile, inhibiting the mitochondrial β-oxidation of fatty acid and supporting growth performance in the hepatopancreas of *S. paramamosain* (29).

Lipids in the meat matrix are usually involved in thousands of metabolites that may be affected by species, nutrients, microbial diversity, production, and storage. These muscle-derived lipid metabolites are not only the phenotypic consequences of physiological muscle metabolism but also the major molecular basis for characterizing organoleptic components following different processing conditions (20, 49–51). For dry-cured meats, lipolysis usually involves a set of endogenous adipose tissue TGs lipases [e.g., neutral and basic ones including hormone-sensitive lipases (HSL) and lipoprotein lipases (LPL)] and some phospholipases (classified as A_1, A_2, C, and D) responsible for PLs degradation followed by auto-oxidation, which contributes to the formation of aromatic volatile compounds (10, 52, 53). However, we should note that the identification efficacy of bioactive lipid species through classical MS-based lipidomics approaches would be significantly affected by the applied lipid extraction protocols [e.g., liquid–liquid extraction (LLE), some alternative methods, such as methyl tert-butyl ether (MTBE)] mainly due to the characteristic amphipathic properties of lipids to achieve a differential partition (54, 55). In particular, the good recovery, ionization efficiency, and identification of global phospholipid species by LC-MS are still difficult to achieve, arising from their complexity in molecular structures (i.e., the length of the fatty acid chains and the difference in fatty acyl substitution at the glycerol backbone), and hydrophilicity across the entire chromatographic separation (28, 45, 56). Regarding the MS instruments showing high sensitivity, multi-sourced trace impurities that could result from biological matrices (e.g., remaining proteins in muscle tissues), solvents used for lipid extraction, preparation devices, such as siloxenes and phthalates, and even sample containers, such as plasticizers could be detected when they are carried to the lipid extract and thus these impurities may influence the reproducibility of the lipidomics profile (54). So, the extension of GC-system and NMR-based lipidomics and their combination with LC-resolved MS would exert unique superiority to enrich the entire lipid metabolism pathway (e.g., biosynthesis, oxidative decomposition, and enzymatic lipolysis) by detecting FAs, TGs, and sterols as well as some specific short and polar secondary lipid-metabolites (8, 16, 17, 19, 22). Indeed, during non-thermal processing, such as HPP, some important water-soluble lipid-metabolites (e.g., Ser-PETA) might be active in fatty acid transformation and participate in GPs metabolism (36). Overall, the lipolysis of TGs and PLs in meats are closely related to some relevant factors, mainly including (i) the feeding processes of animals (28, 29), (ii) circumstances in slaughtering (30, 31), (iii) *postmortem* aging (11, 42), (iv) thermal/non-thermal processing (8, 13, 17, 19, 35, 37, 57), and (v) brining/dry-ripening processes (45–47, 58). As a result, the physical/redox status of muscle/adipose tissues can be changed with the difference in bioavailability and bioactivity of endogenous and microbial lipases/phospholipases

TABLE 2 | The implications of MS-/NMR-based lipidomics in processed meat, quality control, and metabolism monitoring.

Processing factors	Species and muscle tissues and/or co-product	Sample preparation/lipid or metabolites extraction methods	Analytical techniques	Data processing	Identified lipids and potential biomarkers	Main results/possible biological functions and/or bioinformatics evaluation	References
Castration	Psoas major muscle of lambs	Homogenization with chloroform/methanol (2:1, v/v) followed by liquid–liquid extraction (LLE), dryness, and resuspension in chloroform/methanol (2:1, v/v)	UPLC-Q-Exactive-Orbitrap-MS/MS, untargeted	ANOVA, Student's two-tailed *t*-test, PCA, HCA	Major lipid species identified as PCs, PEs, SMs, TGs, FFAs, DGs, particularly in the castration group	Castration could increase IMF content and modify the intramuscular TGs/phospholipids ratio and the PUFAs/SFAs ratio.	Li et al. (34)
Thermal processing	Boiled, steamed and roasted Tan sheep meat (M. *longissimus dorsi*)	Lipid extraction with 100% isopropanol alcohol followed by protein precipitation, centrifugation, and collection of the supernanant	UPLC-Q-Exactive-Orbitrap-MS/MS, untargeted	p-adjustment, RSD examination, PCA, PLS-DA, VIP, HCA	SMs, CERs, LPCs, PCs, PEs, TAGs	The boiled approach was representative of more losses of SMs than CERs in meat, while the steamed one contributes to losses of PCs and LPCs in glycerophospholipid metabolism. These processed diets provided different options to the patients with atherosclerosis and cancer, the elderly, and infants.	Jia et al. (35)
	Roasted mutton (M. *back strap*) from 6-month-old sheep	Fatty acids in lipids extracted with dichloromethane/methanol solution (2:1, v/v) followed by phase-separation, restabilized in butylated hydroxytoluene/ hexane (0.02%, w: v) and methylation. Lipid extraction for lipidome analysis using isopropanol followed by centrifugation, and collection of the supernanant.	GC-FID, targeted (with FAMEs external standards); UPLC-Q-TOF-MS/MS, untargeted	ANOVA, OPLS-DA, VIP, Correlation analysis	TGs (e.g., C16:0/C18:1/C18:1, C18:0/C18:0/C18:1), PCs (C30:6, C28:3), and PEs. FFAs such as C16:0, C18:0 and C18:1.	TGs should be predominant lipids relevant to the aroma binding stability during roasting times. Phospholipids content showed a negative correlation with characteristic aroma, e.g., pentanal, hexanal, and heptanal, suggesting lipolysis and oxidative degradation.	Liu et al. (19)
High pressure processing (HPP)	Fresh fish fillets (*Salmo salar* and *Pleuronectes platessa*)	Homogenization with perchloric acid (0.1 mol/L) to extract polar metabolites followed by centrifugation and supernatant separation	UPLC-Q-Exactive-Orbitrap-MS/MS, untargeted	ANOVA, HCA, Volcano Plot (VP)	High concentration of lipid-derived serine-phosphoethanolamine species (Ser-PETA), particularly in *Pleuronectes platessa* group regardless of HPP	Some specific polar lipid-metabolites (e.g., Ser-PETA) might be active in fatty acid transformation and participate in glycerophospholipid metabolism.	Castrica et al. (36)
Pulsed electric field (PEF)	Hoki roe treated with PEF at different field strengths (0.62, 1.25, 1.875 kV/cm) and frequencies (25, 50, 100 Hz)	Total lipid extracted with hexane/methanol (1:2, v/v) using ETHEX partition method followed by homogenization, filtration and evaporation	GC-FID, targeted (with FAMEs external standards); ^{31}P NMR spectroscopy (162 MHz, to analyze phospholipid composition), ^{13}C NMR spectroscopy (100 MHz, to analyze the ratio of positional distribution of EPA and DHA on TAGs)	Semi-quantification in the abundance of each lipid using the integrated response of the NMR spectra, two-way and one-way ANOVA	PAs, PEs, PSs, PIs, PCs, LDPGs, LPEs, LPSs, LPCs, CLs, and SMs; n-3 fatty acids, i.e., DHA/EPA esterified at *sn*-2/*sn*-1,3	High PEF input resulted in abundant phospholipids without affecting n-3 fatty acid content, and generated LDPGs, LPEs, LPSs and LPCs. PEF transformed more *sn*-2 phospholipid EPA and DHA into *sn*-1,3 positions, indicating a negative change in re-esterified structures to phospholipids and decreased bioavailability of hoki roe lipids.	Ahmmed et al. (17)
γ-ray irradiation	Goat meat (uncastrated, from *Longissimus dorsi*) irradiated at different doses (0, 1, 2, 4 and 6 kGy)	Extraction with methanol and MTBE, dried lipids restabilized in acetonitrile/isopropanol/H_2O (65:30:5, v/v/v)	UPLC-Q-Exactive-Orbitrap-MS/MS, untargeted	RSD examination, ANOVA, PCA, PLS-DA, VIP	Increased content in TGs, PCs, PEs, LPEs, CERs, LPCs and SPHs; decreased level of DGs, PSs, PGs, PIs and SMs after irradiation	Lipid variables were involved in the major pathways of glycerophospholipid and sphingolipid metabolism. DHA-enriched PC (C18:4/C22:6) + H exhibit an increase upon irradiation.	Jia et al. (37)

(Continued)

TABLE 2 | (Continued)

Processing factors	Species and muscle tissues and/or co-product	Sample preparation/lipid or metabolites extraction methods	Analytical techniques	Data processing	Identified lipids and potential biomarkers	Main results/possible biological functions and/or bioinformatics evaluation	References
X-ray irradiation	Chicken, turkey and mixed (chicken, turkey and pork) ground meat irradiated at different doses (0, 0.5, 1, 3 and 5 kGy)	Homogenization with chloroform/methanol (1:2, v/v) followed by Bligh and Dyer's liquid–liquid extraction (LLE) and resuspension in 95% hexane and dryness. Additional methylation for the extracted fatty acids.	GC-FID, targeted (with FAMEs external standards); UPLC-Q-Exactive-Orbitrap-MS/MS, untargeted	ANOVA, PCA, Volcano Plot (VP)	DGs, TGs, SMs, CERs, LPGs, LPIs, LPEs, LPCs, PIs, PEs, PCs. PSs, and PGs. Phospholipids increased in a dose dependent manner with enriched level of PUFAs	The content of n-3 PUFA-enriched lipids in irradiated chicken and turkey meat reflected the meat's nutritional value. Oxidized phospholipids (OxPLs) were identified in low abundance as a potential new biomarker.	Chiesa et al. (8)
	Chicken, turkey and mixed (chicken, turkey and pork) ground meat irradiated at different doses (0, 0.5, 1, 3 and 5 kGy)	Extraction with cold mixture (0.1% formic acid, H_2O/methanol (20:80, v/v)	UPLC-Q-Exactive-Orbitrap-MS/MS, untargeted	ANOVA, HCA, Box-Whisker charts (BWC), Volcano Plot (VP), paired *t*-test	Short and long-chain fatty acids (e.g., oxidized *cis*, *cis*-1,4-pentadiene fatty acids)	PUFA and their oxidative derivatives should be good biomarkers to speculate lipid oxidation pathway in ground meat triggered by irradiation	Panseri et al. (38)
Freezing/ thawing processing	Atlantic salmon (*Salmo salar*) and bullet tuna (*Auxis rochei*) during freeze (−20°C/−35°C and −18°C, respectively)/thaw processing	Homogenization with perchloric acid (0.1 M) to extract polar metabolites followed by centrifugation, supernatant collection and dilution	UPLC-Q-Exactive-Orbitrap-MS/MS, untargeted	ANOVA, fold change with p-adjustment, PCA, Volcano Plot (VP), Box-Whisker charts (BWC) with descriptive statistics	L-α-glyceryl-phosphoryl-choline, *N*-methyl-ethanolamine phosphate	These two water-soluble phospholipid metabolites increase upon thawing of frozen samples regardless of the storage period, suggesting an impaired phospholipid membrane integrity, and enhanced phospholipid catabolism and lipid oxidation	Chiesa et al. (39)
In vitro oxidation	Whiteleg shrimp (M. *Litopenaeus vannamei*) upon H_2O_2/ascorbate-based hydroxyl radical (˙OH)-generating system (1, 2 and 4 mM H_2O_2)	Homogenization with cold chloroform/methanol (2:1, v/v) followed by liquid–liquid extraction (LLE), concentration, and resuspension in isopropanol	UPLC-TripleTOF-MS/MS, untargeted	ANOVA, PCA, OPLS-DA, permutation test, VIP	PCs (C38:3), CLs (C62:2), and PEs (C34:9)	Hydroxyl radical attack can alter the lipidomics profiles of shrimp muscle to a large extent. High concentration of oxidizing conditions exacerbated lipid peroxidation. PEs enriched in PUFAs are more susceptible to oxidation *via* radical attack than PCs molecules.	Tu et al. (40)
	Yak hindquarter meat in a Fenton oxidation system ($FeCl_3$/ascorbate/10 mM H_2O_2) followed by refrigerated storage at 4°C for 2 h	Tissue extract mixed with cold 75% chloroform/methanol (1:9, v/v) and 25% H_2O by two-step extraction toward metabolite optimal recovery	UPLC-Q-Exactive-Orbitrap-MS/MS, untargeted	ANOVA, PCA, PLS-DA, OPLS-DA, HCA	FFAs (e.g., stearic acid, linoleic acid, arachidonic acid)	Notable glycerophospholipid metabolism in oxidized yak meat indicated deterioration and spoilage process. 2-hydroxy-3-oxoadipate was assumed to promote fatty acid oxidation, while arachidonic acid could be involved in fatty acid biosynthesis as revealed by KEGG enrichment	Huang et al. (41)
Postmortem aging/ Packaging/ Storage	*Postmortem* porcine loin (Longissimus) during aging for 1, 8 and 21 days at 4°C	Homogenization with chloroform/methanol (1:1, v/v) followed by liquid–liquid extraction (LLE), dryness, and resuspension in chloroform	UPLC-TQ-MS/MS, targeted (with phospholipid internal standards)	ANOVA, Tukey and Tukey-Kramer *p*-adjustments	PIs (e.g., C38:4), PSs (e.g., C36:2), LPCs, and PAs	Phospholipids underwent enzymatic hydrolysis during aging (except for C18:2 or C20:4 within PI and PS). Phospholipase A2 (PLA2) could be activated by postmortem calcium influx from the sarcoplasmic reticulum (SR) with a surge of LPCs	Chao, Donaldson et al. (11)
	Postmortem bovine muscle, M. *longissimus dorsi lumborum* by different packaging methods, i.e., under high oxygen modified atmosphere, oxygen permeable film, and vacuum-packaging during up to 14 days	Extraction of lipids by Folch's method, homogenization with chloroform/methanol (2:1, v/v) followed by standing overnight at 4°C and separation of organic layer	MALDI-TOF-MS, MALDI–MSI, targeted (phospholipids, triglycerides and sterols)	Semi-quantification in the abundance of each marker lipid (with targeted m/z)	PCs, LPCs, PEs, LPEs, TAGs and sterols	PCs (except for C18:1/C18:0) were sensitive to oxidative degradation while cholesterol showed relatively high stability to oxidation.	Dyer et al. (42)

(Continued)

TABLE 2 | (Continued)

Processing factors	Species and muscle tissues and/or co-product	Sample preparation/lipid or metabolites extraction methods	Analytical techniques	Data processing	Identified lipids and potential biomarkers	Main results/possible biological functions and/or bioinformatics evaluation	References
Salting/Drying-curing/ Preservatives treatment	Water-boiled dry-cured Pekin duck at 6% saute-salt (w/w) following 3 days of ripening	Phospholipid extraction with chloroform/methanol (1:2, v/v) followed by Bligh and Dyer's liquid–liquid extraction (LLE), centrifugation, dryness and dilution	ESI-QTrap-MS/MS (shotgun lipidomics), untargeted	ANOVA, PCA, PLS-DA, VIP	LPLs (C18:2), PEs, PCs [C34:2 (C16:0/C18:2)], PGs, PIs, and PSs	Processing decreased most of the phospholipid molecular species but increased LPLs content until extended ripening (2 days). Boiling resulted in loss in some of the LPLs suggesting an oxidative thermal-degradation and decomposition.	Li et al. (43)
	Water-boiled dry-cured Pekin duck with three different salt contents: 4% (low-salt), 6% (medium-salt) and 8% (high-salt)	Phospholipid extraction with chloroform/methanol (1:2, v/v) followed by liquid–liquid extraction (LLE), centrifugation, dryness and dilution	ESI-QTrap-MS/MS (shotgun lipidomics), untargeted	ANOVA, PLS-DA, VIP	PCs, PGs, PEs, PSs, and PIs	Low-salt (< 6%) dry-cured duck had a significant effect on total phospholipid content and promoted the degradation of individual phospholipids (especially those containing unsaturated fatty acids) probably due to a robust release of phospholipase.	Li et al. (44)
	Low-salted salmon treated with sodium replacers (KCl, $CaCl_2$) and flavor enhancers (yeast extract, lysine, taurine)	Homogenization with Folch solution [chloroform/methanol (2:1, v/v)] followed by phase-separation and dryness. Methylation for the extracted fatty acids. Crude lipids re-stabilized in chloroform toward phospholipids analysis	GC-FID, targeted (with FAMEs external standards); HILIC-QTrap-MS, untargeted	ANOVA, *post hoc* Duncan multiple range tests, PCA, OPLS-DA, HCA, VIP	SFAs (C16:0), MUFAs (C18:1), PUFAs (C18:2), PCs, PEs, PSs, and PIs	PCs content remained high even at 30% NaCl replacement rather than PSs. The addition of flavor enhancers increased the total content of phospholipids.	Wang et al. (45)
	Dry-cured mutton ham (M. *biceps femoris*) from Xinjiang fine-wool sheep processed through 105 days of fermentation and 60 days of ripening	Lipid extraction with MTBE/methanol (3:1, v/v) followed by liquid–liquid extraction (LLE), centrifugation and concentration	UPLC-QTrap-MS/MS, untargeted	ANOVA, PCA, OPLS-DA, VIP, fold change with *p*-adjustment, permutation test, Volcano Plot (VP)	PCs, PEs, PSs, LPCs, and LPEs	FFAs content increased during ham processing. Glycerophospholipid metabolism and sphingolipid metabolism were mentioned as the most important metabolic pathways using KEGG database and MSEA analysis.	Guo et al. (46)
	Four treatments of Hengshan goat meat sausages (preservative-free, natamycin, potassium sorbate and sodium diacetate)	Lipid extraction with 100% isopropanol alcohol followed by protein precipitation, centrifugation and organic-phase separation	UPLC-Q-Exactive-Orbitrap-MS/MS, untargeted	RSD examination, fold change with *p*-adjustment, PCA, PLS-DA, VIP	CERs, DGs, LPCs, PCs, PEs, PIs, PSs, SMs, TGs	Preservative treatments decrease of TGs concentration in goat meat. Significant lipid variables are related to glycerophospholipid, and sphingolipid metabolism as explained by KEGG pathway.	Jia et al. (47)

MTBE, methyl tert-butyl ether; ETHEX, ethanol and hexane for lipid extraction; DHA, docosahexaenoic acid; EPA, eicosapentaenoic acid; GC-FID, capillary gas chromatography coupled with flameionization detection; UPLC-TQ-MS/MS, ultraperformance liquid chromatography-triple quadrupole tandem mass spectrometry; HILIC-QTrap-MS, hydrophilic interaction liquid chromatography-hybrid triple quadrupole-linear ion trap, mass spectrometry; ESI-QTrap-MS/MS, electrospray ionization-hybrid triple quadrupole-linear ion trap, tandem mass spectrometry; UPLC-QTrap-MS/MS, ultraperformance liquid chromatography-hybrid triple quadrupole-linear ion trap, tandem mass spectrometry; UPLC-Q-Exactive-Orbitrap-MS/MS, ultraperformance liquid chromatography coupled to quadrupole exactive orbitrap high resolution tandem mass spectrometry; UPLC-TripleTOF-MS/MS, ultraperformance liquid chromatography-triple time-of flight tandem mass spectrometry; MALDI-TOF MS, matrix-assisted laser desorption and ionization time-of-flight mass spectrometry; MALDI-MSI, matrix-assisted laser desorption/ionization mass spectrometric imaging; NMR, nuclear magnetic resonance spectroscopy; ANOVA, analysis of variance; PCA, principal component analysis; PLS-DA, partial least squares discriminant analysis; OPLS-DA, orthogonal partial least squares discriminant analysis; HCA, hierarchical cluster analysis; VIP, variable importance in projection; RSD, relative standard deviations; TGs, triglycerides; DGs, diglycerides; TAGs, triacylglycerols; PAs, phosphatidic acids; PCs, phosphatidylcholines; PEs, phosphatidylethanolamines; PGs, phosphatidylglycerols; PSs, phosphatidylserines; PIs, phosphatidylinositols; LPGs, lysophosphatidylglycerols; LPCs, lysophosphatidylcholines; LPSs, lysophosphatidylserines; LPEs, lysophosphatidylethanolamines; LDPGs, lyso-diphosphatidylglycerols; CLs, cardiolipins; SMs, sphingomyelines; SPHs, sphingosine bases; CERs, ceramides; FFAs, free fatty acids; MUFAs, monounsaturated fatty acids; PUFAs, polyunsaturated fatty acids; SFAs, saturated fatty acids; FAMEs, fatty acid methyl esters; KEGG, service of Kyoto Encyclopedia of Genes and Genomes; MSEA, metabolite set enrichment analysis.

(10, 13, 52, 53, 59–63), consequently determining the fat deposition, lipolysis, and lipidomics profile (9, 20). In most cases, PLs are the main substrates for lipolysis in dry-cured meat products (10). However, some protein chaperones (heat shock protein 90, Hsp90) are reported to stabilize cell membranes and preserve membrane integrity in muscle tissues, and particularly act as an inherent antioxidant by providing additional protection against ROS-induced PLs oxidation (64). For seafood, such as in fish fillets, the total lipid content generally decreases during cold storage as TGs and PLs are either hydrolyzed by lipolytic enzymes, such as lipase and PLA_2 and/or susceptible to oxidative damage from the myoglobin-mediated mechanism of action (39, 65, 66), though the activity of mitochondrial enzymes may be different during subsequent thawing. Indeed, the water-enriched external medium could induce hydrostatic pressure in cells and impair plasma membrane integrity, provoking an enrichment of intracellular enzymes in the final exudate (39). These knowledge of the adipose tissue TGs and PLs hydrolysis and oxidation during meat processing suggests a complicated overall lipid degradation mechanism and cellular protection under oxidative stress. A more comprehensive understanding based on multi-omics techniques is still required for improving both the quality and nutritional value of specific end products.

CONCLUSION

During the transition from "farm-to-fork" to the modern meat industry, the lipidomics disciplines successfully encompass a comprehensive and high-throughput understanding of meat composition, nutritional value, and safety with a combination of biochemical and mechanical mechanisms. Overall, the techniques for lipidomics have been steadily progressing, particularly regarding the omics-data-mining and multivariate statistical analyses, whereby new efforts are contributed toward new algorithms of developed prediction models for identified lipid biomarkers. Untargeted MS-/NMR-based lipidomics gives molecular insight into meat origin/adulteration and microbial safety with more tentative lipid markers being screened out on a global scale, though additional targeted analytes (e.g., the lipolysis fate of PLs resulting from foodborne microbe bred in muscle) still require further validation in their adulteration detection. In addition, the exhaustive analysis of lipids and their alterations during meat production favors the selective design of processing methods for specific muscle matrices (e.g., irradiation and PEF). Many putative lipid biomarkers following computational approaches and possible metabolism pathways enriched by bioinformatics provide valuable suggestions on food safety and health concerns regarding their potential during the treatment with preservatives, fermentation, aging, and storage. However, challenges remain due to the complexity of meat lipidome, the nature of key intermediate lipid-metabolites, and their evaluation concerning the quality and nutritional value of the final product.

AUTHOR CONTRIBUTIONS

CL and BO-K performed literature review, analyzed and interpreted the data, and drafted the manuscript. CL, BO-K, and GJ reviewed the first draft and revised the manuscript accordingly. All authors contributed to the article and approved the final submitted version.

FUNDING

This research was supported by the National Natural Science Foundation of China (No. 31871824).

REFERENCES

1. OECD/Food and Agriculture Organization of the United Nations. *"Meat", in OECD-FAO Agricultural Outlook 2021-2030*. Paris: OECD Publishing (2021). doi: 10.1787/cf68bf79-en
2. De Smet S, Vossen E. Meat: the balance between nutrition and health. A review. *Meat Sci.* (2016) 120:145–56. doi: 10.1016/j.meatsci.2016.04.008
3. Chen Y, Jia X, Sun F, Jiang S, Liu H, Liu Q, et al. Using a stable pre-emulsified canola oil system that includes porcine plasma protein hydrolysates and oxidized tannic acid to partially replace pork fat in frankfurters. *Meat Sci.* (2020) 160:107968. doi: 10.1016/j.meatsci.2019.107968
4. Han X, Ye H. Overview of lipidomic analysis of triglyceride molecular species in biological lipid extracts. *J Agric Food Chem.* (2021) 69:8895–909. doi: 10.1021/acs.jafc.0c07175
5. Jia W, Di C, Zhang R, Shi L. Application of liquid chromatography mass spectrometry-based lipidomics to dairy products research: an emerging modulator of gut microbiota and human metabolic disease risk. *Food Res Int.* (2022) 157:111206. doi: 10.1016/j.foodres.2022.111206
6. Fahy E, Cotter D, Sud M, Subramaniam S. Lipid classification, structures and tools. *Biochim Biophys Acta Mol Cell Biol Lipids.* (2011) 1811:637–47. doi: 10.1016/j.bbalip.2011.06.009
7. Liu Z, Rochfort S, Cocks B. Milk lipidomics: what we know and what we don't. *Prog Lipid Res.* (2018) 71:70–85. doi: 10.1016/j.plipres.2018.06.002
8. Chiesa LM, Di Cesare F, Mosconi G, Pavlovic R, Campaniello M, Tomaiuolo M, et al. Lipidomics profile of irradiated ground meat to support food safety. *Food Chem.* (2022) 375:131700. doi: 10.1016/j.foodchem.2021.131700
9. Wood JD, Enser M, Fisher AV, Nute GR, Sheard PR, Richardson RI, et al. Fat deposition, fatty acid composition and meat quality: a review. *Meat Sci.* (2008) 78:343–58. doi: 10.1016/j.meatsci.2007.07.019
10. Wang D, Zhang M, Bian H, Xu W, Xu X, Zhu Y, et al. Changes of phospholipase A2 and C activities during dry-cured duck processing and their relationship with intramuscular phospholipid degradation. *Food Chem.* (2014) 145:997–1001. doi: 10.1016/j.foodchem.2013.09.007
11. Chao MD, Donaldson EA, Wu W, Welter AA, O'Quinn TG, Hsu WW, et al. Characterizing membrane phospholipid hydrolysis of pork loins throughout three aging periods. *Meat Sci.* (2020) 163:108065. doi: 10.1016/j.meatsci.2020.108065
12. Merrill AH Jr, Schmelz EM, Wang E, Schroeder JJ, Dillehay DL, Riley RT. Role of dietary sphingolipids and inhibitors of sphingolipid metabolism in cancer and other diseases. *J Nutr.* (1995) 125:1677S–82S. doi: 10.1093/jn/125.suppl_6.1677S
13. Li C, He L, Jin G, Ma S, Wu W, Gai L. Effect of different irradiation dose treatment on the lipid oxidation, instrumental color and volatiles of fresh pork and their changes during storage. *Meat Sci.* (2017) 128:68–76. doi: 10.1016/j.meatsci.2017.02.009
14. Man KY, Chan CO, Tang HH, Dong NP, Capozzi F, Wong KH, et al. Mass spectrometry-based untargeted metabolomics approach for differentiation of

beef of different geographic origins. *Food Chem.* (2021) 338:127847. doi: 10.1016/j.foodchem.2020.127847
15. Wu B, Wei F, Xu S, Xie Y, Lv X, Chen H, et al. Mass spectrometry-based lipidomics as a powerful platform in foodomics research. *Trends Food Sci Technol.* (2021) 107:358–76. doi: 10.1016/j.tifs.2020.10.045
16. Wagner L, Peukert M, Kranz B, Gerhardt N, Andr S, Busch U, et al. Comparison of targeted (HPLC) and nontargeted (GC-MS and NMR) approaches for the detection of undeclared addition of protein hydrolysates in Turkey breast muscle. *Foods.* (2020) 9:1084. doi: 10.3390/foods9081084
17. Ahmmed MK, Carne A, Tian HS, Bekhit AEDA. The effect of pulsed electric fields on the extracted total lipid yield and the lipidomic profile of hoki roe. *Food Chem.* (2022) 384:132476. doi: 10.1016/j.foodchem.2022.132476
18. Artegoitia VM, Foote AP, Lewis RM, Freetly HC. Metabolomics profile and targeted lipidomics in multiple tissues associated with feed efficiency in beef steers. *ACS Omega.* (2019) 4:3973–82. doi: 10.1021/acsomega.8b02494
19. Liu H, Hui T, Zheng X, Li S, Wei X, Li P, et al. Characterization of key lipids for binding and generating aroma compounds in roasted mutton by UPLC-ESI-MS/MS and Orbitrap Exploris GC. *Food Chem.* (2022) 374:131723. doi: 10.1016/j.foodchem.2021.131723
20. Muroya S, Ueda S, Komatsu T, Miyakawa T, Ertbjerg P. MEATabolomics: muscle and meat metabolomics in domestic animals. *Metabolites.* (2020) 10:188. doi: 10.3390/metabo10050188
21. Gu X, Sun W, Yi K, Yang L, Chi F, Luo Z, et al. Comparison of muscle lipidomes between cattle-yak, yak, and cattle using UPLC–MS/MS. *J Food Compos Anal.* (2021) 103:104113. doi: 10.1016/j.jfca.2021.104113
22. Dannenberger D, Süss R, Teuber K, Fuchs B, Nuernberg K, Schiller J. The intact muscle lipid composition of bulls: an investigation by MALDI-TOF MS and 31P NMR. *Chem Phys Lipids.* (2010) 163:157–64. doi: 10.1016/j.chemphyslip.2009.10.011
23. Wang K, Xu L, Wang X, Chen A, Xu Z. Discrimination of beef from different origins based on lipidomics: a comparison study of DART-QTOF and LC-ESI-QTOF. *LWT Food Sci Technol.* (2021) 149:1–10. doi: 10.1016/j.lwt.2021.111838
24. Trivedi DK, Hollywood KA, Rattray NJW, Ward H, Trivedi DK, Greenwood J, et al. Meat, the metabolites: an integrated metabolite profiling and lipidomics approach for the detection of the adulteration of beef with pork. *Analyst.* (2016) 141:2155–64. doi: 10.1039/c6an00108d
25. Zhang Z, Liao Q, Sun Y, Pan T, Liu S, Miao W, et al. Lipidomic and transcriptomic analysis of the longissimus muscle of Luchuan and Duroc pigs. *Front Nutr.* (2021) 8:667622. doi: 10.3389/fnut.2021.667622
26. Mi S, Shang K, Li X, Zhang CH, Liu JQ, Huang DQ. Characterization and discrimination of selected China's domestic pork using an LC-MS-based lipidomics approach. *Food Control.* (2019) 100:305–14. doi: 10.1016/j.foodcont.2019.02.001
27. Cao M, Han Q, Zhang J, Zhang R, Wang J, Gu W, et al. An untargeted and pseudotargeted metabolomic combination approach to identify differential markers to distinguish live from dead pork meat by liquid chromatography–mass spectrometry. *J Chromatogr A.* (2020) 1610:460553. doi: 10.1016/j.chroma.2019.460553
28. Wang J, Xu Z, Zhang H, Wang Y, Liu X, Wang Q, et al. Meat differentiation between pasture-fed and concentrate-fed sheep/goats by liquid chromatography quadrupole time-of-flight mass spectrometry combined with metabolomic and lipidomic profiling. *Meat Sci.* (2021) 173:108374. doi: 10.1016/j.meatsci.2020.108374
29. Wang X, Jin M, Cheng X, Hu X, Zhao M, Yuan Y, et al. Hepatopancreas transcriptomic and lipidomic analyses reveal the molecular responses of mud crab (*Scylla paramamosain*) to dietary ratio of docosahexaenoic acid to eicosapentaenoic acid. *Aquaculture.* (2022) 551:737903. doi: 10.1016/j.aquaculture.2022.737903
30. Chen J, Kong Q, Sun Z, Liu J. Freshness analysis based on lipidomics for farmed Atlantic salmon (*Salmo salar* L.) stored at different times. *Food Chem.* (2022) 373:131564. doi: 10.1016/j.foodchem.2021.131564
31. Chen Y, Ning Q, Wang S, Chen Y, Mo X, Liang P, et al. Effects of cold treatments on lipidomics profiles of large yellow croaker (*Larimichthys crocea*) fillets by UPLC-Q-Exactive Orbitrap MS analysis. *J Food Compos Anal.* (2022) 109:104481. doi: 10.1016/j.jfca.2022.104481
32. Wang Y, Zhang H. Tracking phospholipid profiling of muscle from *Ctennopharyngodon idellus* during storage by shotgun lipidomics. *J Agric Food Chem.* (2011) 59:11635–42. doi: 10.1021/jf2030852
33. Hayashi E, Maeda T, Hasegawa R, Tomita T. The effect of myo-inositol deficiency on lipid metabolism in rats: III. The mechanism of an enhancement in lipolysis due to myo-inositol deficiency in rats. *Biochim Biophys Acta Lipids Lipid Metab.* (1978) 531:197–205. doi: 10.1016/0005-2760(78)90143-1
34. Li J, Tang C, Zhao Q, Yang Y, Li F, Qin Y, et al. Integrated lipidomics and targeted metabolomics analyses reveal changes in flavor precursors in psoas major muscle of castrated lambs. *Food Chem.* (2020) 333:127451. doi: 10.1016/j.foodchem.2020.127451
35. Jia W, Li R, Wu X, Liu S, Shi L. UHPLC-Q-Orbitrap HRMS-based quantitative lipidomics reveals the chemical changes of phospholipids during thermal processing methods of Tan sheep meat. *Food Chem.* (2021) 360:130153. doi: 10.1016/j.foodchem.2021.130153
36. Castrica M, Pavlovic R, Balzaretti CM, Curone G, Brecchia G, Copelotti E, et al. Effect of high-pressure processing on physico-chemical, microbiological and sensory traits in fresh fish fillets (*Salmo salar* and *Pleuronectes platessa*). *Foods.* (2021) 10:1775. doi: 10.3390/foods10081775
37. Jia W, Shi Q, Shi L. Effect of irradiation treatment on the lipid composition and nutritional quality of goat meat. *Food Chem.* (2021) 351:129295. doi: 10.1016/j.foodchem.2021.129295
38. Panseri S, Arioli F, Pavlovic R, Di Cesare F, Nobile M, Mosconi G, et al. Impact of irradiation on metabolomics profile of ground meat and its implications toward food safety. *LWT.* (2022) 161:113305. doi: 10.1016/j.lwt.2022.113305
39. Chiesa LM, Pavlovic R, Nobile M, Di Cesare F, Malandra R, Pessina D, et al. Discrimination between fresh and frozen-thawed fish involved in food safety and fraud protection. *Foods.* (2020) 9:1–15. doi: 10.3390/foods9121896
40. Tu CH, Qi XE, Shui SS, Lin HM, Benjakul S, Zhang B. Investigation of the changes in lipid profiles induced by hydroxyl radicals in whiteleg shrimp (*Litopenaeus vannamei*) muscle using LC/MS-based lipidomics analysis. *Food Chem.* (2022) 369:130925. doi: 10.1016/j.foodchem.2021.130925
41. Huang Q, Dong K, Wang Q, Huang X, Wang G, An F, et al. Changes in volatile flavor of yak meat during oxidation based on multi-omics. *Food Chem.* (2022) 371:131103. doi: 10.1016/j.foodchem.2021.131103
42. Dyer JM, Deb-Choudhury S, Cornellison CD, Krsinic G, Dobbie P, Rosenvold K, et al. Spatial and temporal mass spectrometric profiling and imaging of lipid degradation in bovine *M. longissimus* dorsi lumborum. *J Food Compos Anal.* (2014) 33:203–9. doi: 10.1016/j.jfca.2013.12.001
43. Li C, Li X, Huang Q, Zhuo Y, Xu B, Wang Z. Changes in the phospholipid molecular species in water-boiled salted duck during processing based on shotgun lipidomics. *Food Res Int.* (2020) 132:109064. doi: 10.1016/j.foodres.2020.109064
44. Li C, Li X, Huang Q, Zhou Y, Xu B, Wang Z. Influence of salt content used for dry-curing on lipidomic profiles during the processing of water-boiled salted duck. *J Agric Food Chem.* (2020) 68:4017–26. doi: 10.1021/acs.jafc.0c01513
45. Wang J, Wang H, Lu W, Zhang M, Xue J, Yu X, et al. Low-salted salmon: effects of salt reduction on physicochemical, lipidomic, and sensory characteristics. *LWT.* (2021) 152:112311. doi: 10.1016/j.lwt.2021.112311
46. Guo X, Shi D, Liu C, Huang Y, Wang Q, Wang J, et al. UPLC-MS-MS-based lipidomics for the evaluation of changes in lipids during dry-cured mutton ham processing. *Food Chem.* (2022) 377:131977. doi: 10.1016/j.foodchem.2021.131977
47. Jia W, Wu X, Zhang R, Shi L. UHPLC-Q-Orbitrap-based lipidomics reveals molecular mechanism of lipid changes during preservatives treatment of Hengshan goat meat sausages. *Food Chem.* (2022) 369:130948. doi: 10.1016/j.foodchem.2021.130948
48. Corino C, Mourot J, Magni S, Pastorelli G, Rosi F. Influence of dietary conjugated linoleic acid on growth, meat quality, lipogenesis, plasma leptin and physiological variables of lipid metabolism in rabbits. *J Anim Sci.* (2002) 80:1020–8. doi: 10.2527/2002.8041020x
49. Xu L, Zheng Y, Zhou C, Pan D, Geng F, Cao J, et al. Kinetic response of conformational variation of duck liver globular protein to ultrasonic stimulation and its impact on the binding behavior of n-alkenals. *LWT.* (2021) 150:111890. doi: 10.1016/j.lwt.2021.111890
50. Pateiro M, Domínguez R, Munekata PES, Barba FJ, Lorenzo JM. Lipids and fatty acids. In: Barba FJ, Saraiva JMA, Cravotto G, Lorenzo JM, editors. *Innovative Thermal and Non-Thermal Processing, Bioaccessibility and*

Bioavailability of Nutrients and Bioactive Compounds. Cambridge: Woodhead Publishing (2019). p. 107–37.
51. Xia Q, Zheng Y, Liu Z, Cao J, Chen X, Liu L, et al. Nonthermally driven volatilome evolution of food matrices: the case of high pressure processing. *Trends Food Sci Technol.* (2020) 106:365–81. doi: 10.1016/j.tifs.2020.10.026
52. Toldrá F. Proteolysis and lipolysis in flavour development of dry-cured meat products. *Meat Sci.* (1998) 49:S101–10. doi: 10.1016/s0309-1740(98)90041-9
53. Xiao S, Zhang W, Yang Y, Ma C, Ahn DU, Li X, et al. Changes of hormone-sensitive lipase (HSL), adipose tissue triglyceride lipase (ATGL) and free fatty acids in subcutaneous adipose tissues throughout the ripening process of dry-cured ham. *Food Chem.* (2010) 121:191–5. doi: 10.1016/j.foodchem.2009.12.029
54. Aldana J, Romero-Otero A, Cala MP. Exploring the lipidome: current lipid extraction techniques for mass spectrometry analysis. *Metabolites.* (2020) 10:231. doi: 10.3390/metabo10060231
55. Zhou J, Wang M, Saraiva JA, Martins AP, Pinto CA, Prieto MA, et al. Extraction of lipids from microalgae using classical and innovative approaches. *Food Chem.* (2022) 384:132236. doi: 10.1016/j.foodchem.2022.132236
56. Shen Q, Dai Z, Huang YW, Cheung HY. Lipidomic profiling of dried seahorses by hydrophilic interaction chromatography coupled to mass spectrometry. *Food Chem.* (2016) 205:89–96. doi: 10.1016/j.foodchem.2016.02.151
57. Jadhav HB, Annapure US, Deshmukh RR. Non-thermal technologies for food processing. *Front Nutr.* (2021) 8:657090. doi: 10.3389/fnut.2021.657090
58. Chiesa L, Panseri S, Bonacci S, Procopio A, Zecconi A, Arioli F, et al. Authentication of Italian PDO lard using NIR spectroscopy, volatile profile and fatty acid composition combined with chemometrics. *Food Chem.* (2016) 212:296–304. doi: 10.1016/j.foodchem.2016.05.180
59. Petrón MJ, Muriel E, Timón ML, Martín L, Antequera T. Fatty acids and triacylglycerols profiles from different types of Iberian dry-cured hams. *Meat Sci.* (2004) 68:71–7. doi: 10.1016/j.meatsci.2004.01.012
60. Zhou GH, Zhao GM. Biochemical changes during processing of traditional Jinhua ham. *Meat Sci.* (2007) 77:114–20. doi: 10.1016/j.meatsci.2007.03.028
61. Siciliano C, Belsito E, De Marco R, Di Gioia ML, Leggio A, Liguori A. Quantitative determination of fatty acid chain composition in pork meat products by high resolution 1H NMR spectroscopy. *Food Chem.* (2013) 136:546–54. doi: 10.1016/j.foodchem.2012.08.058
62. Ying W, Ya-Ting J, Jin-Xuan C, Yin-Ji C, Yang-Ying S, Xiao-Qun Z, et al. Study on lipolysis-oxidation and volatile flavour compounds of dry-cured goose with different curing salt content during production. *Food Chem.* (2016) 190:33–40. doi: 10.1016/j.foodchem.2015.05.048
63. Pan J, Zhao S, He L, Zhang M, Li C, Huang S, et al. Promotion effect of salt on intramuscular neutral lipid hydrolysis during dry-salting process of porcine (biceps femoris) muscles by inducing phosphorylation of ATGL, HSL and their regulatory proteins of perilipin1, ABHD5 and G0S2. *Food Chem.* (2022) 373:131597. doi: 10.1016/j.foodchem.2021.131597
64. Zhang M, Wang D, Geng Z, Li P, Sun Z, Xu W. Effect of heat shock protein 90 against ROS-induced phospholipid oxidation. *Food Chem.* (2018) 240:642–7. doi: 10.1016/j.foodchem.2017.08.005
65. Wu H, Richards MP, Undeland I. Lipid oxidation and antioxidant delivery systems in muscle food. *Compr Rev Food Sci Food Saf.* (2022) 21:1275–99. doi: 10.1111/1541-4337.12890
66. Tatiyaborworntham N, Oz F, Richards MP, Wu H. Paradoxical effects of lipolysis on the lipid oxidation inmeat and meat products. *Food Chem X.* (2022) 14:100317. doi: 10.1016/j.fochx.2022.100317

Conflict of Interest: The authors declare that the research was conducted in the absence of any commercial or financial relationships that could be construed as a potential conflict of interest.

Publisher's Note: All claims expressed in this article are solely those of the authors and do not necessarily represent those of their affiliated organizations, or those of the publisher, the editors and the reviewers. Any product that may be evaluated in this article, or claim that may be made by its manufacturer, is not guaranteed or endorsed by the publisher.

frontiers | Frontiers in Nutrition

ORIGINAL RESEARCH
published: 09 June 2022
doi: 10.3389/fnut.2022.910589

Influence of Fluid Food Viscosity on Internal Flow Characteristics of Conveying Pump

XiaoQi Jia[1], Qingyang Chu[1], ZuChao Zhu[1], Qiangmin Ding[2] and Panlong Gao[2]*

[1] *Key Laboratory of Fluid Transmission Technology of Zhejiang Province, Zhejiang Sci-Tech University, Hangzhou, China,*
[2] *Hefei General Machinery Research Institute, Hefei, China*

A fluid food conveying pump is used to convey edible or nutritional fluids and semi-fluids (containing suspended soft and hard particles and with different viscosities), such as water, glycerin, yogurt, and juice concentrate. Since different fluid food have different viscosities, the internal flow characteristics and conveying performance of food conveying pump are greatly affected by viscosity. To obtain the influence law of fluid food viscosity on the internal flow characteristics of the pump, the internal flow characteristics of food conveying pump when conveying food of 4 different viscosities (water, glycerin, 67.2 °Bx wild jujube juice, and 71.0 °Bx haw juice) were compared and observed in this study. The results showed that, with the increase in food viscosity, the overall flow loss in the pump, the entropy generation, and the proportion of total entropy generation in the pump chamber increase, but the conveying performance of the food conveying pump gets worse; however, the pressure pulsation intensity caused by static and dynamic interferences decreases with the increase in viscosity.

Keywords: external characteristic, pressure pulsation, radial force, entropy production, viscosity, conveying pump

OPEN ACCESS

Edited by:
Qiang Xia,
Ningbo University, China

Reviewed by:
Xun Sun,
Shandong University, China
Xingtao Xu,
National Institute for Materials Science, Japan

****Correspondence:***
ZuChao Zhu
zhuzuchao01@163.com

Specialty section:
This article was submitted to Food Chemistry, a section of the journal Frontiers in Nutrition

Received: *01 April 2022*
Accepted: *13 May 2022*
Published: *09 June 2022*

Citation:
Jia X, Chu Q, Zhu Z, Ding Q and Gao P (2022) Influence of Fluid Food Viscosity on Internal Flow Characteristics of Conveying Pump. Front. Nutr. 9:910589. doi: 10.3389/fnut.2022.910589

INTRODUCTION

The processing and manufacturing of food is a critical part of the food industry. Making raw materials into semi-finished and finished products requires complicated processes. A pump is an indispensable part in the manufacturing of fluid food. It pressurizes fluid food and conveys it to each production link. Since the internal flow characteristics and conveying performance of a conveying pump are greatly affected by the fluid food viscosity, in order to ensure smooth food processing, it is very important to study the influence of viscosity on the internal flow and conveying characteristics of the pump during food conveying. The main flow losses in the food conveying pump are caused by viscous dissipative vortex flow, mainly including backflow (1), jet flow-wake flow (2), secondary flow (3), and shedding vortex (4). In Li (5), the stable-state flow of fluids of different viscosities in a centrifugal pump was studied. The results showed that the decrease in turbo performance is mainly caused by the increase in wall shear stress. In Li (6), the conveying performance and internal flow losses of the pump when conveying media of different viscosities were studied. The results showed that the increase in the friction losses between the front and

rear cover plates and the outer disk of the impeller and the increase in hydraulic loss in the pump runner is caused by high viscosity. In Yuan et al. (7), the pressure pulsation of the impeller and volute in the runner under design conditions was studied. The results showed that with the increase of radius, the peak of the pressure pulsation in the impeller increases and is maximized at the outlet. However, the numerical value in the diffuser decreases gradually. In Jia et al. (8), a dynamic pressure test was conducted on the centrifugal pump at a given viscosity. The results showed that the pressure of the volute close to the tongue first increases rapidly and then slowly at a low flow rate; however, the pressure decreases sharply at a high flow rate. In Sinha et al. (9), the occurrence and development of the rotating stall of a centrifugal pump with a vane diffuser were studied by particle image velocimetry (PIV) and pressure fluctuation measurement. The results showed that, under design conditions, there is a consistently high-speed leakage flow in the clearance between the impeller and the diffuser from the outlet side to the beginning of the volute. The separation of the leakage flow from the diffuser vane causes the start of the stall. The leakage rate and the velocity distribution in the clearance depend on the direction of the impeller vane. The results (10) showed that the unsteady flow force exerted by the viscous force of the fluid on the impeller is related to the number of vanes and shows a star distribution. Zhang et al. (11) found that, under rotating stall conditions, there are multiple viscous vortex structures in the impeller of the pump. These viscous vortex structures develop with the development of the rotating impeller. Some vane channels are seriously blocked, showing strong unsteady characteristics. In terms of the study of the internal flow characteristics of the food conveying pump, in Zhang et al. (12), the distribution of the boundary vorticity flux (BVF) at the suction surface and the pressure surface of the two pumps was analyzed. The results showed that the optimization design based on BVF diagnosis helps inhibit the bad flow of the centrifugal pump and improve its hydraulic performance. The results (13) showed that the BVF-based flow field diagnosis helps effectively capture the unsteady flow in the pump and optimize the design of the pump impeller by adjusting geometric parameters and modifying the vane shape. In Gu et al. (14), the influence of the static and dynamic interferences of the main vane and splitter vane in the pump and the volute tongue on the internal flow characteristics of the pump was studied; and the energy loss and vorticity distribution in the middle section of the pump were analyzed. The results showed that, after vane cutting, the energy loss and vorticity around the tongue increase obviously; and the splitter vane produces more unsteady energy dissipation than the main vane. In Ji et al. (15), the influence of the distance between the impeller and the guide vane on the internal flow loss distribution and total power loss was studied by entropy generation based on numerical results. In Cui and Zhang (16) and Li et al. (17), entropy generation was used for the numerical analysis of the energy loss of the centrifugal pump; besides, the energy distribution of pressure pulsation and vibration at different flow rates was evaluated according to the experimental results. In Xu et al. (18), the effects of low-frequency ultrasound (US) induced conformational variation of duck liver globular proteins (DLGPs) on the binding behavior of n-alkanes were investigated. This work suggests the great potential of specific conformational variations of DLGPs induced by ultrasonic pretreatments to modulate flavor features of protein-based products. In Sun et al. (19), the present review summarizes the recent advances in the HC (hydrodynamic cavitation)-based pretreatment of LCB (lignocellulosic biomass). The principle of HC is introduced, and the enhancement mechanism of HC is analyzed. In Xuan et al. (20), various synthetic methods for preparing low-dimensional metal-organic frameworks (LD MOFs) are summarized. The synthesis principle and catalytic performance of LD MOFs were explored. For the first time, genetic algorithms (GA) and computational fluid dynamics (CFD) are combined to study and determine the optimal structure of the representative ARHCR (advanced rotational hydrodynamic cavitation reactors) cavity-generating unit (21). In conclusion, most of the previous studies focused on conventional and single fluid media. Relatively few studies compared the influence of fluid food of different viscosities on the internal flow characteristics and conveying performance of the conveying pump. Therefore, it is necessary to study the influence of fluid food of different viscosities on the internal flow characteristics and conveying performance of the conveying pump.

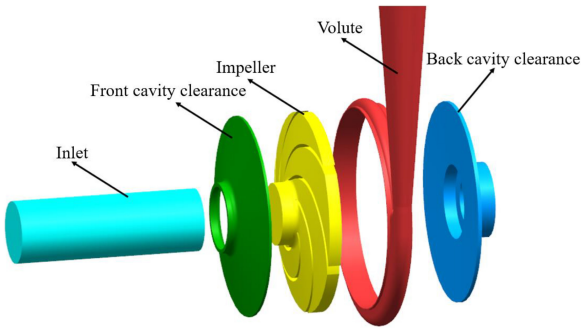

FIGURE 1 | Diagram of the computational domain of flow field.

CENTRIFUGAL PUMP MODEL

In this study, the speed of the model pump, n = 2,950 r/min; the design flow, Q_d = 11 m^3/h; and the rated lift, H_d = 38 m. The pump inlet diameter, D_s = 50 mm; the outlet diameter, D_o = 40 mm; the impeller inlet diameter, D_1 = 50 mm; the impeller outlet diameter, D_2 = 160 mm; the impeller outlet width, b_2 = 10 mm; the number of impeller blades, Z = 6; the blade inlet angle, β_1 = 23°; the blade outlet angle, β_2 = 23°; the blade thickness, δ = 2.7 mm; the volute base circle diameter, D_b = 165 mm; and the volute inlet width, b_2 = 15 mm. The model pump is shown in **Figure 1**. The main geometric parameters of the model pump are listed in **Table 1**.

In this study, the same centrifugal pump was used to convey water, glycerin, 67.2 °Bx wild jujube juice, and 71.0 °Bx haw juice of four different viscosities by numerical simulation. The density and viscosity of such food at 25°C are listed in **Table 2**.

NUMERICAL CALCULATION METHOD AND TEST APPARATUS

Numerical Calculation Method

The turbulence model in this study was SST k–ω model. When the compressibility of the fluid is not considered, this model can be expressed as follows (22, 23):

$$\frac{\partial(\rho k)}{\partial t}+\frac{\partial(\rho k u_i)}{\partial x_i}=\frac{\partial}{\partial x_j}\left[\left(\mu+\frac{\mu_t}{\sigma_k}\right)\frac{\partial k}{\partial x_j}\right]+G_k+\rho k\omega\beta^* \quad (1)$$

$$\frac{\partial(\rho\omega)}{\partial t}+\frac{\partial(\rho\omega\overline{u}_i)}{\partial x_i}=\frac{\partial}{\partial x_j}\left[\left(\mu+\frac{\mu_t}{\sigma_\omega}\right)\frac{\partial\omega}{\partial x_j}\right]+\frac{\partial_\omega}{k}G_k-\rho\omega^2\beta+2(1-F_1)\rho\frac{1}{\omega\sigma_\omega}\frac{\partial k}{\partial x_j}\frac{\partial\omega}{\partial x_j} \quad (2)$$

$$\mu_t=\frac{\rho k}{\omega} \quad (3)$$

where $\sigma_k=0.5$, $\sigma_w=0.5$, $\beta=0.075$, $\beta^*=0.09$, $\alpha=5/9$.

Boundary vorticity flow (BVF) is the core concept of boundary vorticity dynamics. It reflects the rate of boundary vorticity generation and refers to the vortex flux entering the fluid through a unit area in unit time. This concept was proposed by Lighthill in 1963 (24) and was defined as follows:

$$\sigma=\nu\frac{\partial\omega}{\partial n} \quad (4)$$

where σ is the value of BVF, ω is the vorticity, ν is the kinematic viscosity coefficient, and $\boldsymbol{n}$ is the unit vector in the normal direction outside the fluid surface.

For a general centrifugal pump, when the vane rotates uniformly, the fluid cannot be compressed, the Reynolds number is great, there is no slip on the wall, and the body force is ignored (25). BVF only has the component produced by the pressure gradient σ_p,

$$\sigma=\sigma_p=\frac{1}{\rho}n\times\nabla p \quad (5)$$

Entropy generation (EGR) is a dissipative effect of energy loss, which cannot be avoided in the process of energy conversion. According to the thermodynamic definition, the irreversible process is inevitably accompanied by entropy generation. For the interior of the centrifugal pump, when the heat transfer is not considered, the viscous force in the boundary layer near the wall will cause the mechanical energy in the fluid to be converted into internal energy, which is irreversible; the turbulent pulsation in the high Reynolds number region will cause energy loss and entropy generation. Therefore, the entropy generation theory was

TABLE 1 | Performance parameters and geometric parameters of the centrifugal pump.

Parameter/Symbol	Value	Parameter/Symbol	Value
Head/H_{des}	40 m	Rotate speed /n_{des}	2,950 rpm
Flow rate/Q_{des}	10.8 m^3/h	Specific speed /n_s	37.08
Pump outlet diameter/D_o	40 mm	Impeller inlet diameter /D_1	50 mm
Blade thickness/δ	2.7 mm	Impeller outlet diameter /D_2	160 mm
Blade inlet angle/β_1	23°	Volute inlet diameter /D_b	165 mm
Blade outlet angle /β_2	23°	Blade outlet width / b_1	10 mm
Blade number /Z	6	Volute inlet width /b_2	15 mm

TABLE 2 | Density and viscosity of four kinds of food liquid at 25°C.

Food liquid	Density/(kg/m^3)	Dynamic viscosity/(mPa·s)
Water	1000.0	0.8949
Glycerin	1261.7	56.0
Wild jujube juice	1339.6	167.0
Hawthorn juice	1350.4	260.4

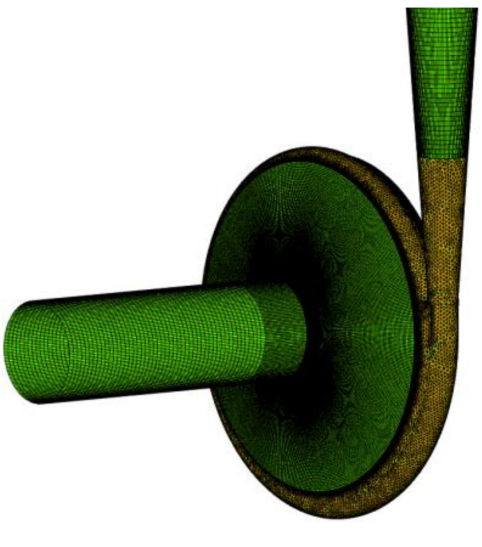

FIGURE 2 | Diagram of flow field domain.

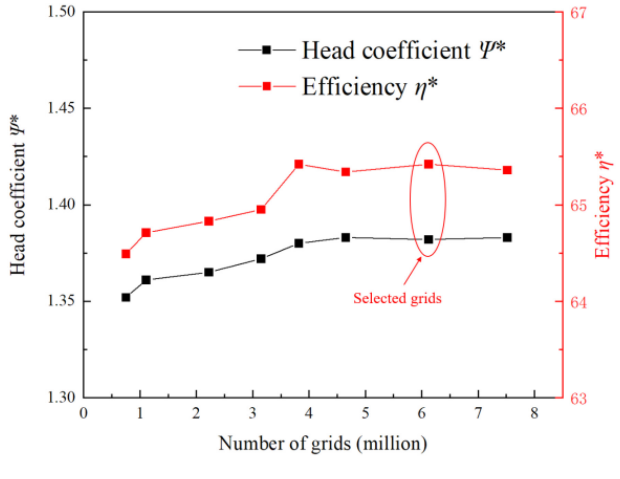

FIGURE 3 | Diagram of flow field mesh independence.

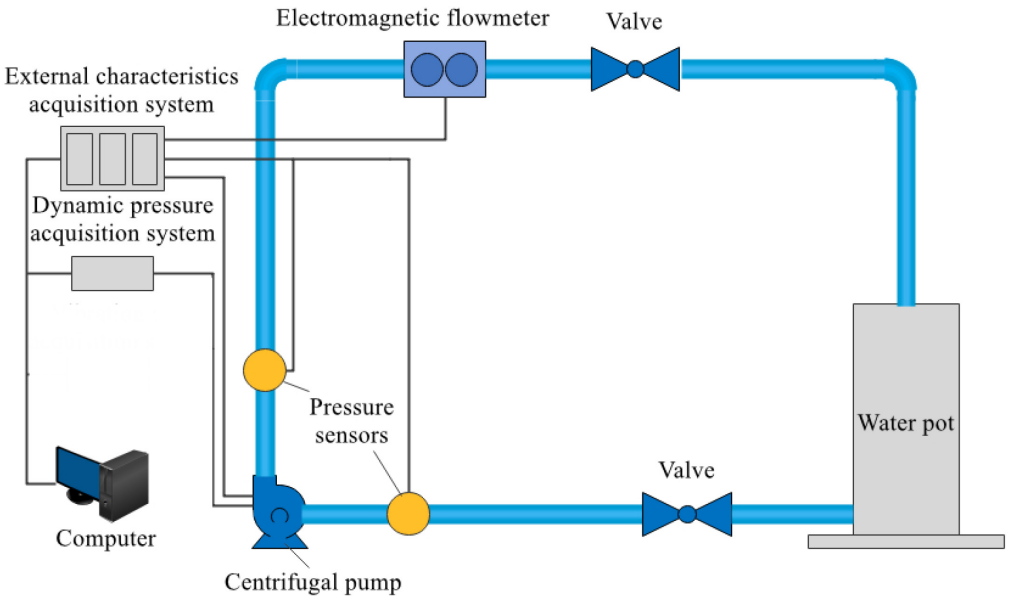

FIGURE 4 | Testing system of the centrifugal pump.

used in this study for the study and analysis of the energy loss in the centrifugal pump flow.

For turbulent flow, entropy generation is divided into two parts, namely, entropy generation caused by time-averaged movement and entropy generation caused by velocity fluctuation (23, 26).

$$\dot{S}_D''' = \dot{S}_{\overline{D}}''' + \dot{S}_{D'}''' \tag{6}$$

where $\dot{S}_{\overline{D}}'''$ is the entropy generation caused by time-averaged movement, and $\dot{S}_{D'}'''$ is the entropy generation caused by velocity fluctuation.

The entropy generation caused by time-averaged movement can be calculated using the following formula:

$$\dot{S}_{\overline{D}}''' = \frac{\mu}{T}\left\{2\left[\left(\frac{\partial \overline{u}}{\partial x}\right)^2 + \left(\frac{\partial \overline{v}}{\partial y}\right)^2 + \left(\frac{\partial \overline{w}}{\partial z}\right)^2\right] + \left[\left(\frac{\partial \overline{v}}{\partial x} + \frac{\partial \overline{u}}{\partial y}\right)^2 + \left(\frac{\partial \overline{w}}{\partial x} + \frac{\partial \overline{u}}{\partial z}\right)^2 + \left(\frac{\partial \overline{v}}{\partial z} + \frac{\partial \overline{w}}{\partial y}\right)^2\right]\right\} \tag{7}$$

The entropy generation caused by velocity fluctuation can be calculated using the following formula:

$$\dot{S}_{D'}''' = \frac{\mu}{T}\left\{2\left[\left(\frac{\partial u'}{\partial x}\right)^2 + \left(\frac{\partial v'}{\partial y}\right)^2 + \left(\frac{\partial w'}{\partial z}\right)^2\right] + \left[\left(\frac{\partial v'}{\partial x} + \frac{\partial u'}{\partial y}\right)^2 + \left(\frac{\partial w'}{\partial x} + \frac{\partial u'}{\partial z}\right)^2 + \left(\frac{\partial v'}{\partial z} + \frac{\partial w'}{\partial y}\right)^2\right]\right\} \tag{8}$$

Since the entropy generation caused by velocity fluctuation cannot be directly calculated in the numerical calculation model selected in this study, Kock (27) proposed calculating it with the following formula:

$$\dot{S}_{D'}''' = \frac{\rho\varepsilon}{T} \tag{9}$$

where ρ is the medium density, and ε is the turbulent dissipation rate.

Therefore, the total entropy generation in the flow field can be obtained by performing volume integral on it.

$$\dot{S}_{\overline{D}} = \int_V \dot{S}_{\overline{D}}''' \, dV \tag{10}$$

$$\dot{S}_{D'} = \int_V \dot{S}_{D'}''' \, dV \tag{11}$$

In this study, the whole flow field of the centrifugal pump was numerically calculated by the inlet velocity and the free outlet velocity. The walls in the impeller flow area and the wall in contact with the impeller solid area were set as rotating walls. The walls in other flow domains were set to fixed walls. All walls were set to be smooth. The coupling between speed and pressure was realized by the SIMPLEC algorithm. Second-order upwind and central difference schemes were adopted for the spatial dispersion of convective and diffusive terms, respectively. In the unsteady calculation of the whole flow field, the time step of every 1° rotation of the impeller was taken as a time step, and a rotation cycle contained 120 time steps in total. The speed of the model pump was 2,950 r/min; the time step was 1.69492×10^{-4} s; and the convergence residual accuracy of each physical quantity was set to 10^{-5}. **Figure 2** shows the diagram of the flow field domain and mesh. **Figure 3** shows the mesh independence verification diagram of the flow field domain.

According to mesh independence verification, the number of mesh cells finally selected herein for the flow field was 6.12×10^6. The head coefficient ψ^* is 1.382, and the efficiency coefficient η^* is 65.42.

Test Apparatus

The test bench for the operation stability of the centrifugal pump designed in this study is mainly composed of a characteristic data acquisition systems, a centrifugal pump, water tank, high-precision electromagnetic flowmeter, valve, inlet and outlet water pipes, and motor. **Figure 4** shows the circuit of the test system for the centrifugal pump. The test object in this study was a low-specific speed centrifugal pump at 2,950 r/min. The installation position of the GYS-I dynamic pressure sensor is shown in **Figure 5** and **Table 3**. The measurement accuracy of the GYS-I pressure sensor is 0.2, the range is −0.1∼1.0 MPa, and the response frequency is 10,000 Hz. (On the premise of ensuring that effective data can be obtained, monitoring points should be arranged in key locations with large pressure changes as far as possible to ensure accurate judgment of the performance of the food delivery pump. This explains why the pressure test points are asymmetrical on the casing).

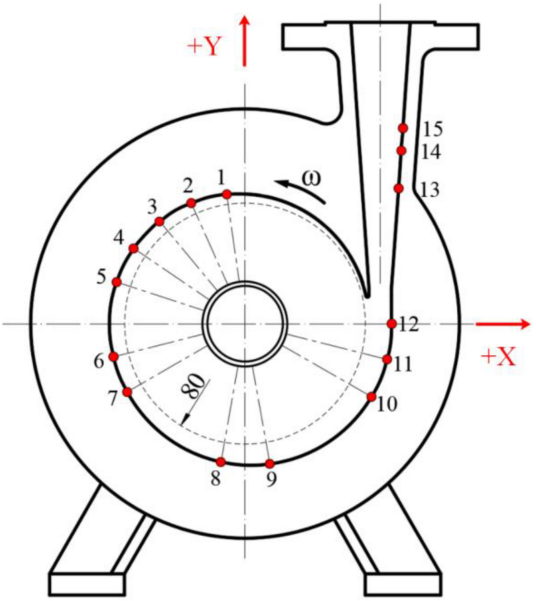

FIGURE 5 | Installation position of the pressure sensor.

TABLE 3 | Installation position of the pressure sensor.

No.	Location	No.	Location
1	θ = 8°	9	θ = 190°
2	θ = 24°	10	θ = 240°
3	θ = 40°	11	θ = 255°
4	θ = 56°	12	θ = 270°
5	θ = 72°	13	h = 90 mm
6	θ = 104°	14	h = 115 mm
7	θ = 120°	15	h = 130 mm
8	θ = 170°		

Angle θ represents the included angle between the line between the center of the measurement point and the origin and the positive direction of the Y-axis. H represents the vertical height between the centerline of the pressure measuring hole at the outlet and the X-axis of the pump.

RESULTS AND DISCUSSION

Figure 6 shows the comparison diagram for the simulated value and experimental value of the food conveying pump. The maximum error of the head and efficiency were 7.6 and 7.3%, respectively. According to **Figure 6**, the simulated value was slightly higher than the actual experimental value. The reason for this is that there may be mechanical seal leakage in practice. Such leakage will cause a decrease in the volumetric efficiency of pumps. Moreover, the wall of the flow parts is rough rather than completely smooth during machining. Besides, energy loss may be caused by the friction between flowing fluids and solid parts. Therefore, both the head and efficiency were slightly lower than the simulated value. Generally speaking, the results of the numerical simulation calculation were consistent with the experimental results, proving the accuracy of the numerical simulation calculation method adopted herein.

Figure 7 shows the external characteristic curve of the conveying pump for fluid food of four different viscosities at the flow rate of 0.2 Q_d, 0.6 Q_d, 1.0 Q_d, and 1.3Q_d. It can be seen from **Figure 7** that the head and efficiency of the pump were the highest when conveying water and the lowest when conveying haw juice. This indicates that the lower the viscosity of fluid food, the closer the conveying performance of the pump to the performance when conveying an eater; the greater the viscosity, the greater the difference. The head and efficiency of the pump gradually decreased with the increase in fluid food viscosity. Under design conditions, the head was 42.66 m, 32 m, 23.88 m, and 21.24 m, respectively, and the efficiencies were 65.42, 47.32, 37.83, and

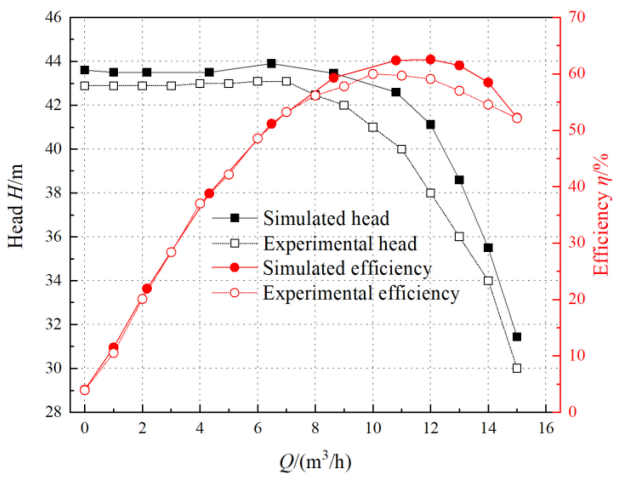

FIGURE 6 | Comparison of external characteristics between simulated and experimental values.

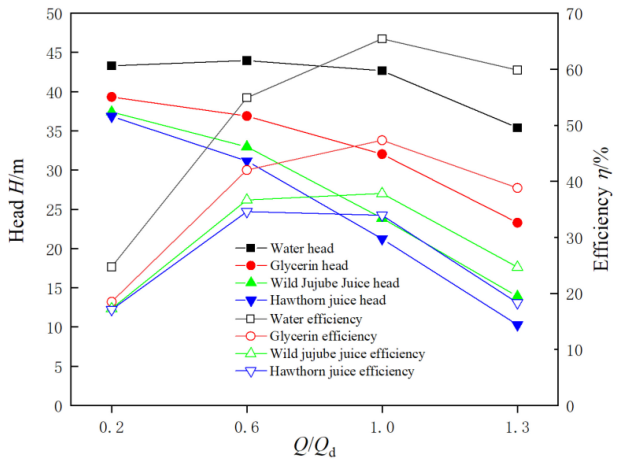

FIGURE 7 | External characteristics of the centrifugal pump with different viscosity.

34.59%, respectively. It can be seen that the higher the viscosity of the medium, the lower the head and the lower the hydraulic efficiency, which is mainly caused by the friction loss of the high viscosity fluid.

Figure 8 shows the total pressure distribution of fluid food of different viscosities on the midsection of the centrifugal pump under design conditions. According to **Figure 8**, the pressure distribution in the pump is relatively uniform when conveying water. However, the pressure distribution in the pump is not uniform when conveying glycerin, wild jujube juice, and haw juice. With the increase in viscosity, the high-pressure area near the volute outlet gradually shifted toward the side away from the tongue, resulting in an increase in the pressure gradient on that side. Flow separation occurred at the tongue after the fluid impacted the tongue. Consequently, the pressure near the wall of the volute was lower, and the area of the low-pressure area also increased gradually with the increase in viscosity. The friction resistance of the medium also increased with the increase in fluid viscosity. In addition, at the same volume flow rate, the mass flow rate increased with the increase in fluid density, and the centrifugal force generated by the mass fluid at the same speed was also great, resulting in greater pressure. The friction resistance generated by the viscosity will offset the centrifugal force generated by the fluid during the rotation of the impeller. It can be seen from the figure that, at the design flow rate, the impact of density on pressure is greater than that of viscosity on pressure. This explains why the greater the viscosity, the greater the total pressure.

Figure 9 shows the circumferential distribution of total pressure on the wall of the volute at the design flow rate when conveying four food fluids of different viscosities. As shown in the figure, the circumferential pressure on the volute wall changed irregularly with the increase in the density and viscosity of the medium. The circumferential pressure on the volute wall conveying water showed no great fluctuations. However, when conveying glycerin, wild jujube juice, and haw juice, the pressure at the same monitoring point decreased with the increase in viscosity. This is consistent with the pressure distribution on the volute wall as shown in **Figure 8**. The pressure decreased with the increase in viscosity at monitoring points at the pump outlet away from the impeller and diaphragm (monitoring

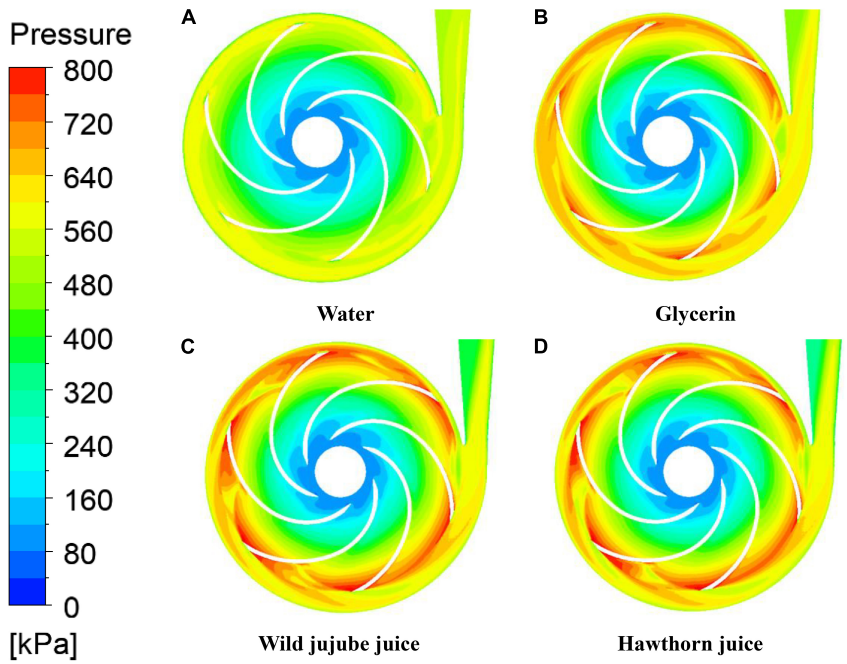

FIGURE 8 | Total pressure of the centrifugal pump with different viscosity. **(A)** Water, **(B)** Glycerin, **(C)** Wild jujube juice and **(D)** Hawthorn juice.

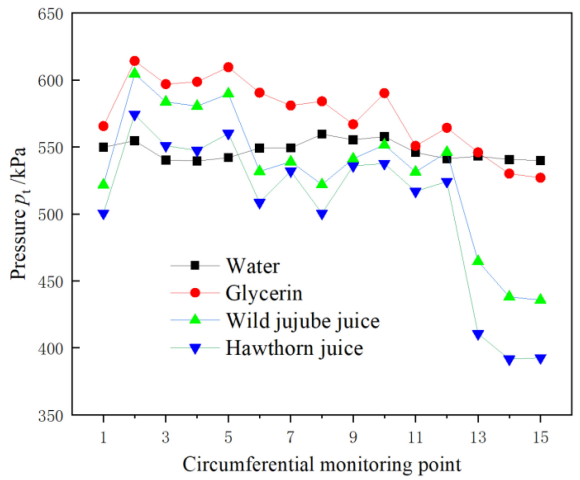

FIGURE 9 | Total pressure on volute casing of the centrifugal pump with different viscosity.

points 13–15). Nevertheless, the pressure decreased with the increase in viscosity. The higher the viscosity, the greater the decrease in pressure.

Figure 10 shows the time-domain diagram of pressure pulsation over time at five representative monitoring points on the circumferential wall of the volute. At different viscosities, the pressure pulsation at each monitoring point showed a certain periodicity, there were 6 obvious peaks and troughs, and the number was exactly the number of blades of the impeller. The difference was the difference in pressure amplitude corresponding to the peaks and troughs. This further indicates that the pressure pulsation was significantly affected by the interference of the blade tongue. Monitoring point 1 was the first monitoring point along the helix from the separator. After the impact of the fluid flow and the separator, a great flow separation occurred; and the influence of the separator on the pressure pulsation was shifted to monitoring point 1. The pulsation amplitude of glycerin at this point was the greatest, reaching about 40 kPa; at monitoring points 6 and 9, far away from the tongue, the pressure pulsation amplitude of haw juice was the greatest, and the amplitude of glycerin was the smallest; the pressure pulsation curves of the four fluids at monitoring points 12 and 15 were closer, indicating that these points were mainly affected by the dynamic and static interferences of the tongue, rather than the viscosity.

To express the pressure pulsation rules at each monitoring point more clearly, a fast Fourier transform (FFT) was performed on the pressure pulsation value at each point to analyze the

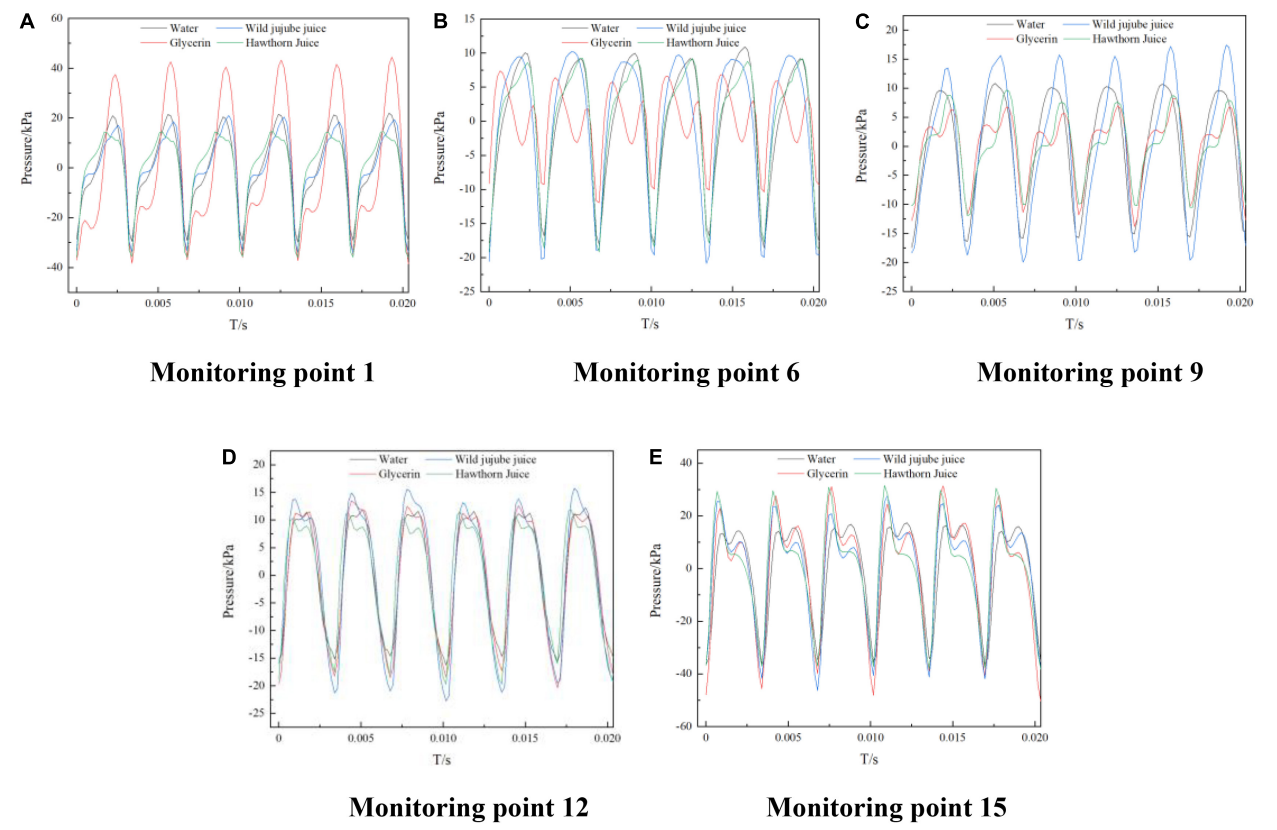

FIGURE 10 | Time-domain distribution of pressure pulsation on volute casing of the centrifugal pump with different viscosities. **(A)** Monitoring Point 1, **(B)** Monitoring Point 6, **(C)** Monitoring Point 9, **(D)** Monitoring Point 12 and **(E)** Monitoring Point 15.

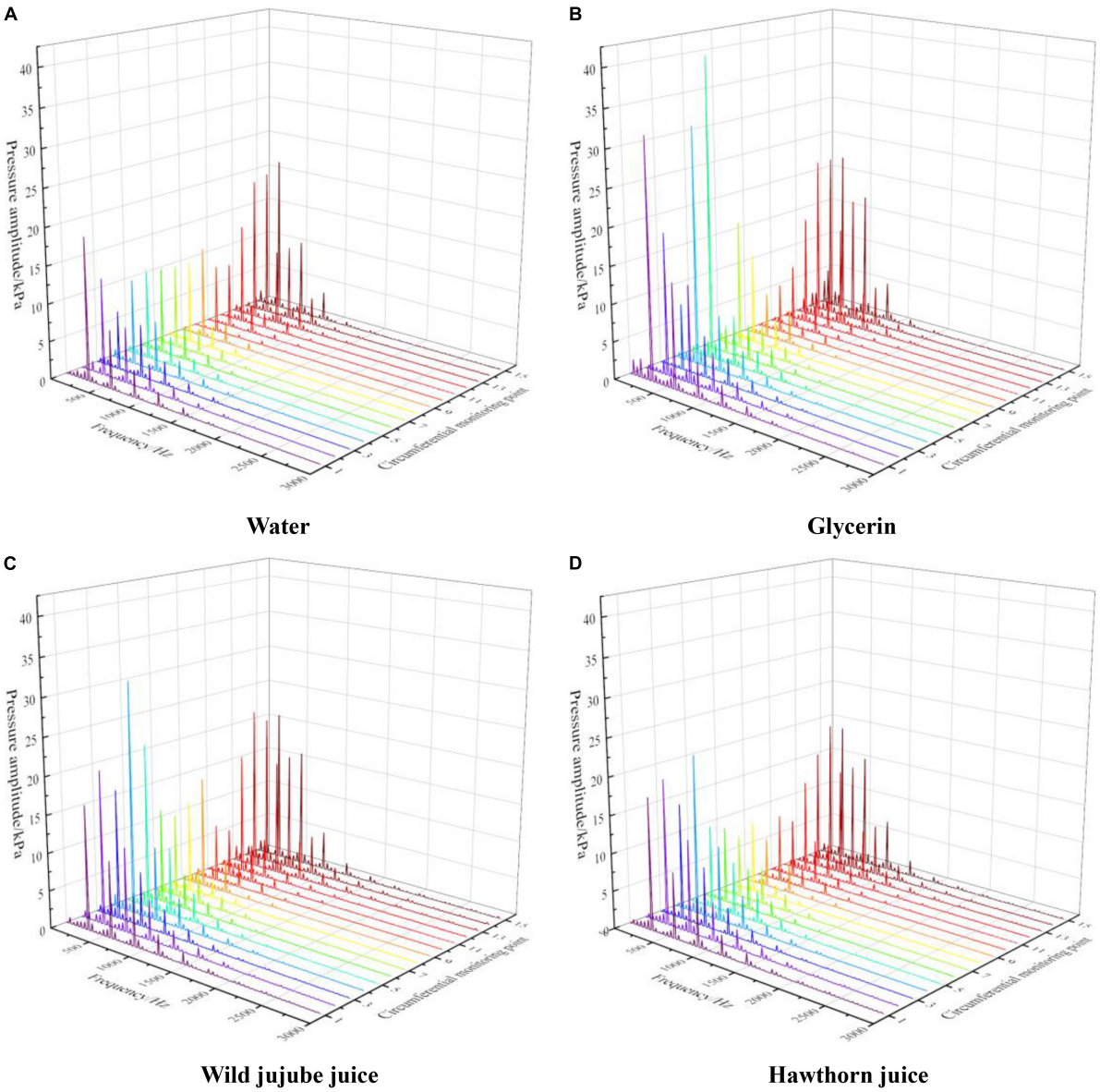

FIGURE 11 | Frequency domain distribution of pressure pulsation on volute casing of the centrifugal pump with different viscosities. **(A)** Water, **(B)** Glycerin, **(C)** Wild jujube juice and **(D)** Hawthorn juice.

frequency domain characteristics of pressure pulsation at each monitoring point in the centrifugal pump. **Figure 11** shows the frequency domain diagram for the circumferential pressure pulsation at all monitoring points on the volute wall. It can be seen that the pressure pulsation amplitude at each monitoring point appeared at the blade frequency and its frequency was doubled. The amplitude at the blade frequency of f = 295 Hz was the greatest. For the same fluid, the pressure pulsation amplitude at the blade frequency of the monitoring point near the circumferential wall of the volute was greater than that of the monitoring point far from the tongue of the volute. The pulsation amplitude at each monitoring point showed a downward trend on the whole with the increase in viscosity, which also indicates that the flow near the circumferential wall of the volute became more stable with the increase in viscosity.

In viscous fluid mechanics, a vortex is one of the main causes of the energy loss of fluid flow. Therefore, the study of the viscous flow (especially secondary flow) in the centrifugal pump cannot be separated from the movement of vortices. It is generally recognized that the peak of BVF causes the peak of downstream boundary vorticity. Therefore, the pressure surface and suction surface of blades were analyzed by BVF in this study. **Figure 12** shows the BVF distribution diagram and velocity streamline for the blade of four fluids. According to the figure, the maximum of BVF appeared near the blade inlet where the blade contacted the fluid for the first time and the flow was unstable. The peak

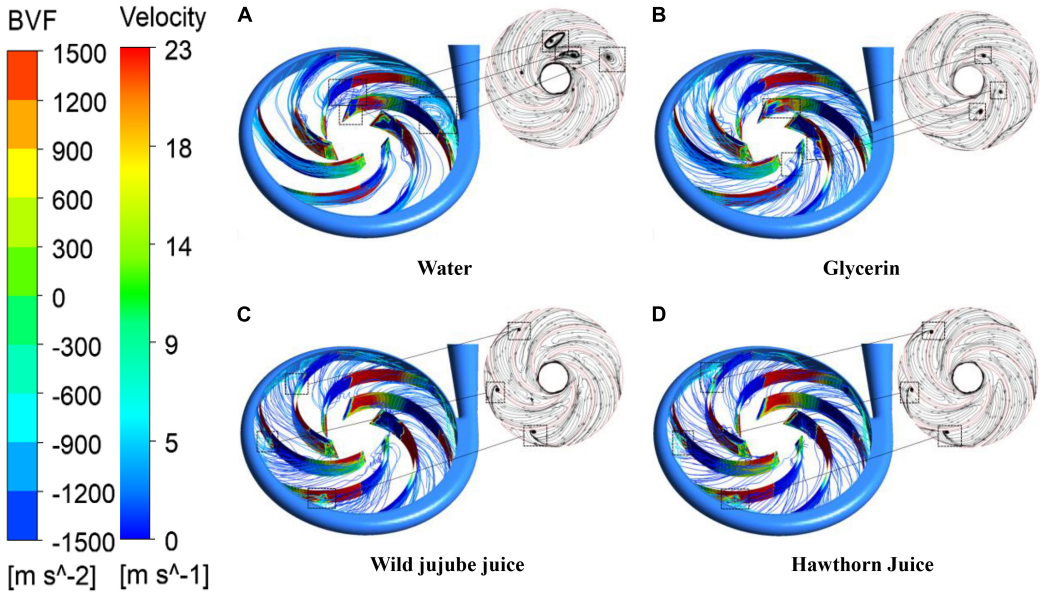

FIGURE 12 | BVF distribution on blades and streamline distribution in the impeller channel with different viscosities. **(A)** Water, **(B)** Glycerin, **(C)** Wild jujube juice and **(D)** Hawthorn juice.

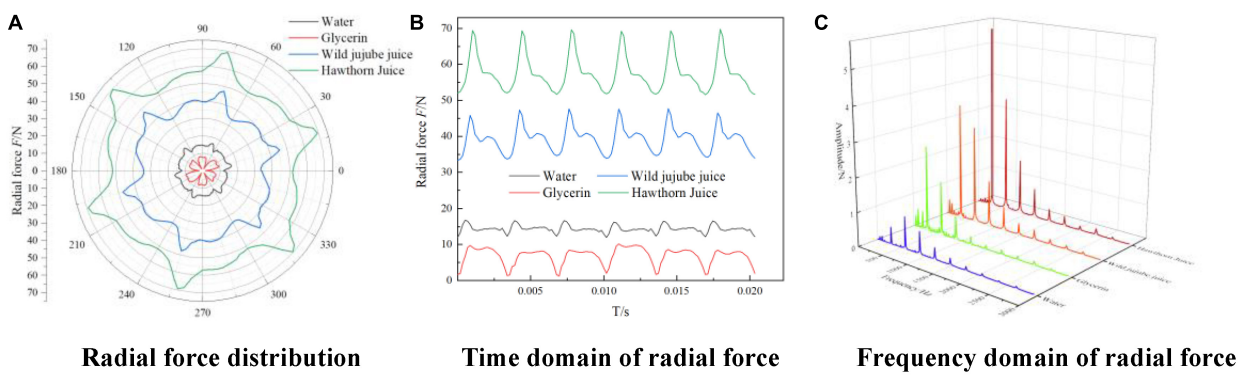

FIGURE 13 | Time-frequency domain distribution of impeller radial force with different viscosities. **(A)** Radial force distribution, **(B)** Time domain of radial force and **(C)** Frequency domain of radial force.

of BVF might be caused by the unreasonable design of the blade inlet placement angle. It can be seen from **Figure 12** that large or small vortexes appeared in the streamlines flowing through the area with alternating BVF positive and negative peaks, indicating that there was a large flow separation. The vortexes in the impeller flow domain with water flow were derived from the flow separation of the blade inlet near the suction surface and the pressure surface near the tongue. The vortices of the other three fluids were mainly generated on the suction surface of the blade, and the vortex structure was gradually transferred to the impeller outlet with the increase in viscosity.

Figure 13A shows the radial flow force vector distribution diagram received by the impeller during a rotating period at the design flow rate in the rotating coordinate system for four different types of fluid food with different viscosities. **Figure 13B** shows the time-domain diagram of the radial flow force received by the impeller for media with different viscosities at the design flow rate. It can be seen from **Figures 13A,B** that the radial force received by the impeller for four fluids showed very regular periodic fluctuation, the number of peaks and troughs was consistent with the number of the centrifugal pump blades, and the transient radial force trajectory of the centrifugal pump impeller is symmetric about the central axis as a whole.

With the increase in medium density and viscosity, the radial force of the impeller showed irregular changes; the radial force for glycerin was smaller than that for water, while the radial force for wild jujube juice and haw juice increased with the increase in medium density and viscosity. The density of wild jujube juice and haw juice was close; the radial force was mainly affected by the viscosity, which caused different inlet and outlet pressures,

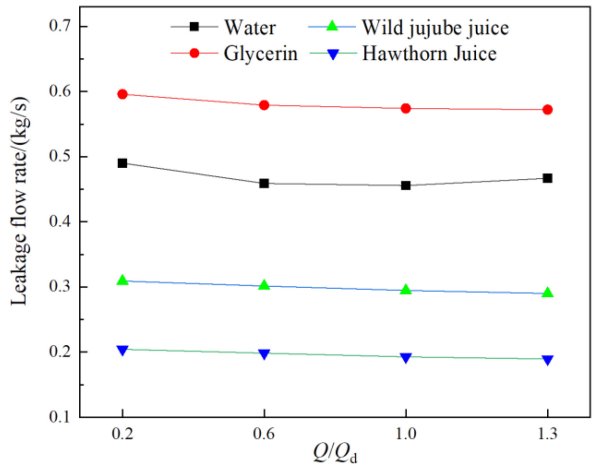

FIGURE 14 | Leakage of the front cavity of a centrifugal pump with different viscosities.

thus causing different radial forces. Since the radial force came from the reaction force of the diffuser to the impeller through fluids, according to 12,The vortex structures in the impeller passage for water were more distributed and asymmetrical under design conditions. Such asymmetric flow caused an uneven force on the runner, resulting in a great radial force. For fluids with a high viscosity, the radial force showed obvious unilateral irregular changes with the medium viscosity. For fluids with low viscosity, however, the radial force showed irregular changes with the medium viscosity.

Figure 13C shows the frequency domain diagram for the radial force on the impeller for media of different viscosities at the design flow rate. Since the speed of the conveying pump was 2,950 r/min, the theoretical shaft frequency was 2,950/60 = 49.17 Hz. Meanwhile, the pump had 6 blades. Therefore, its theoretical blade passing frequency (blade frequency) was 295 Hz. According to **Figure 13**, the main component of the frequency was blade frequency of f = 295 Hz and its frequency doubling. At blade frequency of f = 295 Hz, the amplitudes were 0.5133 N, 2.5226 N, 3.4654 N, and 5.5537 N, respectively. The amplitude at the blade frequency also increased with the increase in viscosity. It can be seen from **Figures 13A,B** that the radial force for glycerin was relatively small, but it showed great fluctuations. As a result, the amplitude at the blade frequency was greater than that for water.

Figure 14 shows the diagram of the leakage rate in the antechamber of the centrifugal pump for fluid food of different viscosities under design conditions. Generally, the leakage rate decreased gradually due to the positive proportion of the leakage rate in the clearance to the pressure difference between both ends.

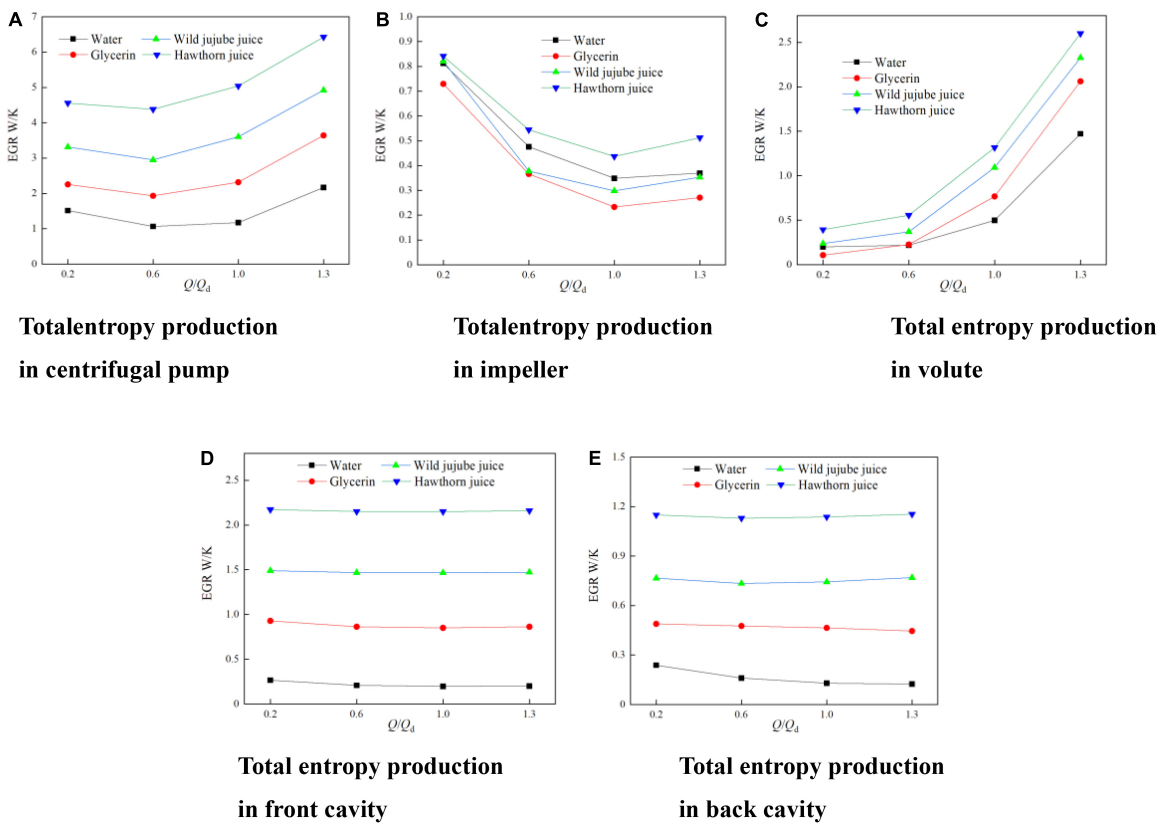

FIGURE 15 | Entropy production in each fluid domain of centrifugal pump with different viscosities. **(A)** Total entropy production in centrifugal pump, **(B)** Total entropy production in impeller, **(C)** Total entropy production in volute, **(D)** Total entropy production in front cavity and **(E)** Total entropy production in back cavity.

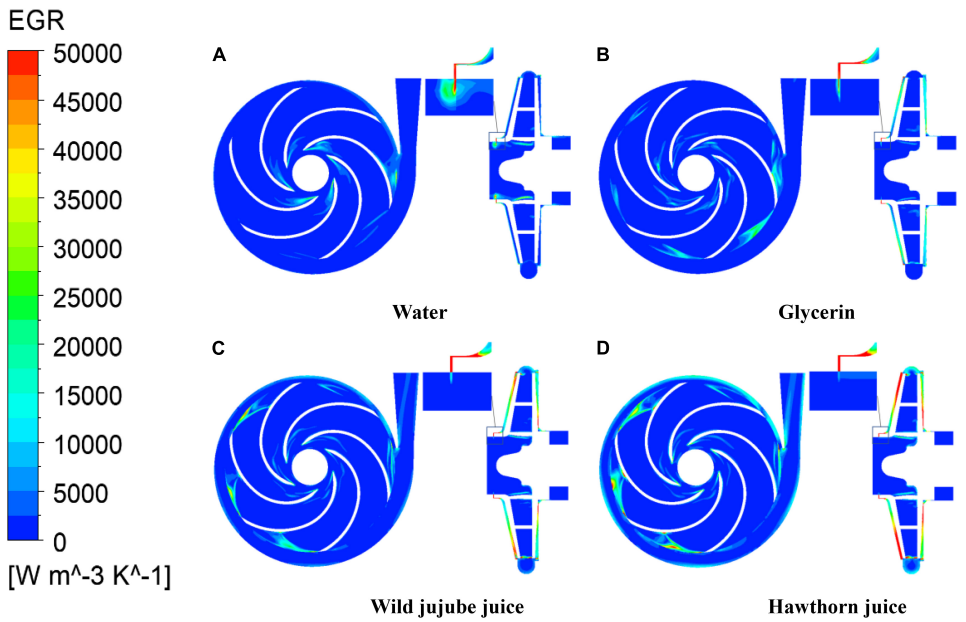

FIGURE 16 | Entropy production distribution of impeller and volute in the middle and y = 0 section. **(A)** Water, **(B)** Glycerin, **(C)** Wild jujube juice and **(D)** Hawthorn juice.

When the flow rate increased, the pressure at the impeller outlet gradually decreased, reducing the pressure difference between both ends of the ante-chamber flow domain. This resulted in a decrease in the leakage rate. Under the same conditions, the higher the viscosity, the lower the leakage rate. According to **Figure 12**, under design conditions, there were more vortex structures in the impeller passage for water, reducing the pressure difference between both ends of the ante-chamber flow domain and resulting in a lower leakage rate for water than that for glycerin. This is consistent with the law of radial force and further indicates that the leakage rate has a certain influence on the radial force. The leakage rate in the ante-wear-ring clearance for water, glycerin, wild jujube juice, and haw juice at the design flow was 0.4556 kg/s, 0.5741 kg/s, 0.2946 kg/s, and 0.1928 kg/s, respectively.

To analyze and compare the influence of fluid food of different viscosities on the flow losses in each flow domain of the conveying pump, the whole flow field in the pump was divided into four parts, namely, the impeller, the volute, ante-chamber, and rear-chamber flow domains. **Figure 15** shows the comparison diagram for the total entropy generation in each flow domain of the pump at different viscosities of fluid food. According to **Figures 15B,C**, the entropy generation in the centrifugal pump is mainly concentrated in the impeller flow domain at low flow rates, indicating that the complicated unsteady flow in the impeller is the main factor causing entropy generation; the entropy generation in each flow domain decreases with the increase of the flow rate, making the flow in each flow domain more orderly; and the total entropy generation is minimized near the design flow rate. Then, as the flow rate increases from $1.0Q_d$ to $1.3Q_d$, the entropy generation in the volute increases sharply. At this time, the flow loss is mainly concentrated in the volute. In combination with **Figure 12**, since there is a large vortex structure in the impeller passage of water and the energy loss caused by the vortex structure is much greater than the dissipation caused by viscosity. As a result, the entropy generation in the impeller flow domain of water is greater than that of glycerin and wild jujube juice. According to **Figures 15D,E**, the entropy generation in the pump chamber is less affected by flow rate and more by fluid food viscosity. With the increase in viscosity, the proportion of the total entropy generation in the pump chamber increases. The proportion of the entropy generation in the pump chamber of fluid food of four different viscosities at the design flow rate is 27.84, 56.80, 61.37, and 65.21%, respectively. This indicates that the flow loss in the pump chamber is the major source of the flow loss in the centrifugal pump conveying high viscosity fluid.

Under each condition, with the increase in fluid food viscosity, the entropy generation in each flow domain in the pump increases, and the total entropy generation increases accordingly. The total entropy generation of water, glycerin, wild jujube juice, and haw juice at the design flow rate is 1.17 W/K, 2.32 W/K, 3.60 W/K, and 5.04 W/K, respectively. Besides, it indicates that the overall flow loss in the centrifugal pump increases with the increase in fluid viscosity.

Figure 16 shows the entropy generation distribution on the midsection between the impeller and volute of the centrifugal pump and the axial y = 0 section under design conditions. On the midsection between the impeller and volute, the high entropy generation areas of water (entropy generation greater than 25,000 W/K/m^3) are mainly distributed in the impeller inlet and near the tongue; the high entropy generation areas in the impeller of glycerin are mainly distributed in the impeller passage near the vane outlet, especially near the tongue. In the impeller of

wild jujube juice, the high entropy generation areas are mainly distributed at the vane outlet of each runner; and the entropy generation begins to appear in a large area near the volute tongue. In the impeller of haw juice, the high entropy generation areas are mainly distributed at the vane outlet of each runner and the volute near the tongue; and with the increase in viscosity, the entropy generation gradually decreases along the spiral line of the volute. This indicates that the fluid impact loss at the impeller inlet and the flow loss caused by dynamic and static interferences between the impeller and volute tongue are major sources of entropy generation. On the axial $y = 0$ section, there are large high entropy generation areas near the wear-ring, the reason for which is that partial fluid at the outlet of the impeller enters the wear-ring clearance through the ante-chamber of the pump and then returns to the pump inlet area. Meanwhile, due to the narrow flow area at the wear-ring clearance, the velocity of the fluid is excited there, which forms a jet when flowing to the inlet, thus aggravating the flow loss. With the increase in viscosity, the flow loss at the wear-ring clearance decreases, while the entropy generation decreases accordingly.

CONCLUSION

In this study, the lift, efficiency, and the internal unsteady flow characteristics for four kinds of fluid food of different viscosities (i.e., water, glycerin, 67.2 °Bx wild jujube juice, and 71.0 °Bx haw juice) were investigated. The main conclusions are as follows:

(1) With the increase in viscosity, the flow loss in the conveying pump increases; and the conveying performance for fluid food gets worse. Under design conditions, the head is 42.66 m, 32 m, 23.88 m, and 21.24 m, respectively, and the efficiencies are 65.42, 47.32, 37.83, and 34.59%, respectively. At the design flow rate, the total pressure increases with the increase in viscosity due to the greater influence of density on pressure than that of viscosity.

(2) The circumferential pressure on the volute wall shows irregular changes with the increase in medium density and viscosity. When conveying water, the pressure on the circumferential wall of the volute of the pump shows no great fluctuations. However, with the increase in fluid food viscosity, the pressure in the pump gradually decreases; however, the pressure drop increases.

(3) For fluids with high viscosity, the radial force shows obvious unilateral irregular changes with the medium viscosity. For fluids with low viscosity, however, the radial force shows irregular changes with the medium viscosity. The amplitude of the radial force at the blade frequency also increases with the increase in viscosity. At the blade frequency of $f = 295$ Hz, the amplitudes are 0.5133 N, 2.5226 N, 3.4654 N, and 5.5537 N, respectively.

(4) With the increase in viscosity, the flow loss at the wear-ring clearance decreases, while the entropy generation decreases accordingly. The flow loss in the pump chamber is the major source of the flow loss in the centrifugal pump conveying high viscosity fluid. The proportion of the total entropy production value of the pump cavity increases, and the proportion of the entropy production of the pump cavity under the design flow rate is 27.84%, 56.80%, 61.37%, and 65.21%, respectively.

Overall, the study on food viscosity can provide a useful reference for the efficient and stable operation of food conveying pump.

DATA AVAILABILITY STATEMENT

The original contributions presented in this study are included in the article/supplementary material, further inquiries can be directed to the corresponding author/s.

AUTHOR CONTRIBUTIONS

XJ: methodology, writing – review, and editing. QC: formal analysis, data curation, visualization, and writing – original draft. ZZ: conceptualization. QD: supervision. PG: project administration. All authors contributed to the article and approved the submitted version.

FUNDING

This study was supported by the National Natural Science Foundation of China (Grant Nos. 51906221 and 51876110) and the Key Research and Development Program of Zhejiang Province (Grant No. 2022C01148).

REFERENCES

1. Yamamoto K, Tsujimoto Y. Backflow vortex cavitation and its effects on cavitation instabilities. *Int J Fluid Mach Syst.* (2009) 2:40–54. doi: 10.5293/IJFMS.2009.2.1.040
2. Furukawa A, Takahara H, Nakagawa T. Pressure fluctuation in a vaned diffuser downstream from a centrifugal pump impeller. *Int J Rotat Mach.* (2003) 9:285–92. doi: 10.1155/S1023621X03000265
3. Westra RW, Broersma L, Andel KV, Kruyt NP. PIV measurements and CFD computations of secondary flow in a centrifugal pump impeller. *J Fluids Eng.* (2010) 132:153. doi: 10.1115/1.4001803
4. Cui B, Zhang Y, Huang Y. Analysis of the pressure pulsation and vibration in a low-specific-speed centrifugal pump. *J Fluids Eng.* (2021) 143:021201. doi: 10.1115/1.4048691
5. Li WG. Effects of viscosity on turbine mode performance and flow of a low specific speed centrifugal pump. *Appl Math Model.* (2016) 40:904–26. doi: 10.1016/j.apm.2015.06.015
6. Li WG. Effects of viscosity of fluids on centrifugal pump performance and flow pattern in the impeller. *Int J Heat Fluid Flow.* (2000) 21:207–12. doi: 10.1016/S0142-727X(99)00078-8
7. Yuan S, Yongyan NI, Pan Z, Yuan J. Unsteady turbulent simulation and pressure fluctuation analysis for centrifugal pumps. *Chin J Mech Eng.* (2009) 22:64–9. doi: 10.3901/CJME.2009.01.064
8. Jia XQ, Cui BL, Zhu ZC, Zhang YL. Experimental investigation of pressure fluctuations on inner wall of a centrifugal pump. *Int J Turbo Jet Engines.* (2017) 36. doi: 10.1515/tjj-2016-0078
9. Sinha M, Pinarbasi A, Katz J. The flow structure during onset and developed states of rotating stall within a vaned diffuser of a centrifugal pump. *ASME J Fluids Eng.* (2001) 123:490–9. doi: 10.1115/1.1374213

10. Si Q, Yuan J, Yuan S, Wang W, Zhu L, Bois G. Numerical investigation of pressure fluctuation in centrifugal pump volute based on sas model and experimental validation. *Adv Mech Eng.* (2015). 6:972081. doi: 10.1155/2014/972081
11. Zhang N, Yang M, Gao B, Li Z, Ni D. Unsteady pressure pulsation and rotating stall characteristics in a centrifugal pump with slope volute. *Adv Mech Eng.* (2014) 2014:710791. doi: 10.1155/2014/710791
12. Zhang Y, Long C, Xin Z, Jiang C, Min S. Hydraulic design and bvf diagnosis of high efficiency centrifugal pump. *J Drain Irrig Mach Eng.* (2013) 15:032024. doi: 10.1088/1755-1315/15/3/032024
13. Zhang Y. Design optimization of the impeller for a high specific-speed pump based on BVF diagnosis. *J Eng Thermophys.* (2010) 31:765–8.
14. Gu Y, Yuan S, Pei J, Zhang J, Zhang F, Huang X. Effects of the impeller–volute tongue interaction on the internal flow in a low-specific-speed centrifugal pump with splitter blades. *Proc Instit Mech Eng Part A J Power Energy.* (2017). 232:170–80. doi: 10.1177/0957650917718117
15. Ji P, Fan M, Li Y, Yuan S, Jia C. Effects of distance between impeller and guide vane on losses in a low head pump by entropy production analysis. *Adv Mech Eng.* (2016) 8:1687814016679568. doi: 10.1177/1687814016679568
16. Cui B, Zhang C. Investigation on energy loss in centrifugal pump based on entropy generation and high-order spectrum analysis. *J Fluids Eng.* (2020) 142:091205. doi: 10.1115/1.4047231
17. Li J, Meng D, Qiao X. Numerical investigation of flow field and energy loss in a centrifugal pump as turbine. *Shock Vibr.* (2020). 2020:1–12. doi: 10.1155/2020/8884385
18. Xu L, Zheng Y, Zhou C, Pan D, Geng F, Cao J, et al. Kinetic response of conformational variation of duck liver globular protein to ultrasonic stimulation and its impact on the binding behavior of n-alkenals. *LWT.* (2021) 150:111890. doi: 10.1016/j.lwt.2021.111890
19. Sun X, Liu S, Zhang X, Tao Y, Boczkaj G, Yong JY, et al. Recent advances in hydrodynamic cavitation-based pretreatments of lignocellulosic biomass for valorization. *Bioresour Technol.* (2022) 345:126251. doi: 10.1016/j.biortech.2021.126251
20. Xuan X, Wang M, Zhang M, Kaneti YV, Xu X, Sun X, et al. Nanoarchitectonics of low-dimensional metal-organic frameworks toward photo/electrochemical CO2 reduction reactions. *J CO2 Util.* (2022) 57:101883. doi: 10.1016/j.jcou.2022.101883
21. Sun X, Yang Z, Wei X, Tao Y, Boczkaj G, Yong YJ, et al. Multi-objective optimization of the cavitation generation unit structure of an advanced rotational hydrodynamic cavitation reactor. *Ultrason Sonochem.* (2021) 80:105771. doi: 10.1016/j.ultsonch.2021.105771
22. Versteeg HK, Malalasekera W. *An introduction to Computational Fluid Dynamics*. London: Longman Group Ltd (1995).
23. Menter FR. Influence of freestream values on k-ω turbulence model predictions. *AIAA J.* (1992) 30:1651–9. doi: 10.2514/3.11115
24. Lighthill MJ. Attachment and separation in three dimensional flow. *Laminar Bound Layers.* (1963).
25. Wu JZ, Wu JM. Interactions between a solid surface and a viscous compressible flow field. *J Fluid Mech.* (1993) 254:183–211. doi: 10.1017/S0022112093002083
26. Si Q, Yuan S, Yuan J, Liang Y. Investigation on flow-induced noise due to backflow in low specific speed centrifugal pumps. *Adv Mech Eng.* (2015) 5:631–5. doi: 10.1155/2013/109048
27. Kock F, Herwig H. Local entropy production in turbulent shear flows: a high-Reynolds number model with wall functions. *Int J Heat Mass Trans.* (2004) 47:2205–15. doi: 10.1016/j.ijheatmasstransfer.2003.11.025

Conflict of Interest: The authors declare that the research was conducted in the absence of any commercial or financial relationships that could be construed as a potential conflict of interest.

Publisher's Note: All claims expressed in this article are solely those of the authors and do not necessarily represent those of their affiliated organizations, or those of the publisher, the editors and the reviewers. Any product that may be evaluated in this article, or claim that may be made by its manufacturer, is not guaranteed or endorsed by the publisher.

frontiers | Frontiers in Nutrition

ORIGINAL RESEARCH
published: 06 July 2022
doi: 10.3389/fnut.2022.880370

Effects of Ozone Water Combined With Ultra-High Pressure on Quality and Microorganism of Catfish Fillets (*Lctalurus punctatus*) During Refrigeration

Yuzhao Ling[1,2†], Mingzhu Zhou[1,3†], Yu Qiao[1], Guangquan Xiong[1]*, Lingyun Wei[2], Lan Wang[1], Wenjin Wu[1], Liu Shi[1], Anzi Ding[1] and Xin Li[1]*

[1] Key Laboratory of Cold Chain Logistics Technology for Agro-Product, Ministry of Agriculture and Rural Affairs, Institute of Agro-Products Processing and Nuclear Agricultural Technology, Hubei Academy of Agricultural Sciences, Wuhan, China, [2] School of Environmental Ecology and Biological Engineering, Wuhan Institute of Technology, Wuhan, China, [3] School of Bioengineering and Food, Hubei University of Technology, Wuhan, China

OPEN ACCESS

Edited by:
Qiang Xia,
Ningbo University, China

Reviewed by:
Wenshui Xia,
Jiangnan University, China
Tao Yin,
Huazhong Agricultural University, China

***Correspondence:**
Yu Qiao
qiaoyu412@sina.com
Guangquan Xiong
xiongguangquan@163.com

[†] These authors have contributed equally to this work and share first authorship

Specialty section:
This article was submitted to Food Chemistry, a section of the journal Frontiers in Nutrition

Received: 21 February 2022
Accepted: 11 April 2022
Published: 06 July 2022

Citation:
Ling Y, Zhou M, Qiao Y, Xiong G, Wei L, Wang L, Wu W, Shi L, Ding A and Li X (2022) Effects of Ozone Water Combined With Ultra-High Pressure on Quality and Microorganism of Catfish Fillets (Lctalurus punctatus) During Refrigeration. Front. Nutr. 9:880370. doi: 10.3389/fnut.2022.880370

This study described the quality and microbial influence on ozone water (OW) and ultra-high pressure (UHP) processing alone or in combination with refrigerated catfish fillets. The analysis parameters included total volatile base nitrogen (TVBN), thiobarbituric acid reactive substances (TBARs), chromaticity, microbial enumeration, 16S rRNA gene sequencing, electronic nose (E-nose), and sensory score. The study found that compared with the control (CK), ozone water combined with ultra-high pressure (OCU) delayed the accumulation of TVBN and TBARs. The results of sensory evaluation illustrated that OCU obtained a satisfactory overall sensory acceptability. The counting results suggested that compared to CK, OCU significantly ($p < 0.05$) delayed the stack of TVC, *Enterobacteriaceae*, *Pseudomonas*, lactic acid bacteria (LAB), and hydrogen sulfide-producing bacteria (HSPB) during the storage of catfish fillets. The sequencing results reflected that the dominant were *Proteobacteria*, *Firmicutes*, *Bacteroidetes*, and *Actinobacteria* at the phylum level, and the dominant were *Acinetobacter*, *Pseudomonas*, *Lelliottia*, *Serratia*, *Shewanella*, *Yersinia*, and *Aeromonas* at the genus level. The dominant was *Acinetobacter* in initial storage, while *Pseudomonas* and *Shewanella* were in anaphase storage. Based on the TVC and TVBN, the shelf life of catfish fillets was extended by at least 3 days compared to the control. In short, the combination of ozone water and ultra-high-pressure processing is a favorable strategy to control microbial quality and delay lipid oxidation during catfish storage.

Keywords: ultra-high pressure, ozone water, catfish fillets, lipid oxidation, microbial enumeration, 16S rRNA gene sequencing

Abbreviations: OW, ozone water; UHP, ultra-high pressure; OCU, ozone water combined with ultra-high pressure; TVBN, total volatile basic nitrogen; TBARs, thiobarbituric acid reactive substances; MDA, malondialdehyde; ΔE, chromatic aberration; TVC, total viable count; LAB, lactic acid bacteria; HSPB, hydrogen sulfide-producing bacteria; OTU, operational taxon units; PCoA, principal co-ordinates analysis; E-nose, electronic nose; PCA, principal components analysis.

INTRODUCTION

Channel catfish (*Lctalurus punctatus*) is the main cultured fish in the United States (1), while there are limited types of processed catfish products in China, mainly frozen fish fillets (2). The endogenous enzymatic reactions, oxidation, and microbial activities that occur after fish die could reduce sensory acceptance and nutritional value (3). Therefore, it is necessary to take timely preservation measures for catfish to maintain their economic value. Biological preservatives are natural and harmless, while their high acquisition cost and difficulty in adapting to industrialization are still critical reasons for not being commercialized (4). Certain chemical preservatives, for example, nitrite, are powerful in the preservation of meat products, but their potential carcinogenic ability keeps most consumers away (5). Based on the above, food processors are looking for harmless and efficient alternatives to extend the shelf life of catfish. Considering fresh aquatic products, non-pasteurization is the first choice. Common physical food processing technologies include electromagnetic field, cold plasma, irradiation, high pressure, high hydrostatic pressure, ozone, ultrasonic, microwave, ultraviolet, pulsed light, pulsed electric field, and shockwaves (6, 7).

Ozone is a powerful bactericide, which can quickly kill all kinds of pathogens, including protozoa, bacteria, and viruses due to its strong oxidizing property (8, 9). In the food industry, ozone water has been widely used in the disinfection of aquatic products. Pastoriza et al. (10) reported that the replacement treatment of ozone water resulted in a reduction in the total viable count (TVC) and hydrogen sulfide-producing bacteria (HSPB) compared to seawater cleaning and ice making. However, ozone water alone is not enough to effectively inhibit certain spoilage bacteria for example *Pseudomonas*. Tachikawa et al. (11) found that *Pseudomonas fluorescens* and *Pseudomonas aeruginosa* in biofilms were more resistant to ozone damage than suspension cells. Therefore, hurdle technology is used as a strategy to enhance the bactericidal effectiveness. Ultra-high pressure processing (UHP), also known as ultra-high hydrostatic pressure processing, is considered to be an emerging and promising physical alternative to heat sterilization (12). UHP (usually 100–800 MPa) has been proven to inactivate a variety of microbes and endogenous enzymes while retaining the sensory properties and nutritional value of food (6, 13–15). Specifically, UHP can cause membrane damage and increase the permeability of the cell membrane, which is the main reason for the destruction of microbes. In addition, the destruction of organelles and genetic material may also be critical reasons (16). In the food industry, UHP has been widely used as a pasteurization step after food packaging (17). Ye et al. (18) reported the effect of high-pressure treatment (300 MPa/20 min) on crab meat during storage at 4°C, and the results showed that the TVC (5.71 $\log_{10}$ CFU/g) on the 8th day was still lower than the limit value (6 $\log_{10}$ CFU/g) recommended by the International Committee of Microbiological Specializations on Food (ICMSF). But expensive equipment, localized packaging options, limited inactivation of spores, cooked appearance, and lipid oxidation are major restrictions to the widespread application of ultra-high pressure (13, 16).

Microbial activity and lipid oxidation are the main factors that limit the shelf life of fish (4). Two emerging technologies, ozone water and ultra-high pressure are considered harmless, effective, and economical methods, and are widely used in food technology. Ozone water or ultra-high pressure alone used to effectively control food spoilage has been widely reported. However, there are rare reports to probe the effects of ozone water combined with ultra-high pressure on refrigerated catfish for all we know. In this study, we checked the changes in the quality of refrigerated catfish fillets treated by single or combined ultra-high pressure through physicochemical parameters [total volatile base nitrogen (TVBN), thiobarbituric acid reactive substances (TBARs), chromaticity, and electronic nose], microbial analysis (microbial plate count and next-generation sequencing), and sensory evaluation.

MATERIALS AND METHODS

Fillet Samples Preparation

The live catfish (mean weight and body length were about 2.0 ± 0.5 kg and 50 ± 5.0 cm, respectively) purchased from a local Wushang supermarket (Hongshan District, Wuhan, China), were transported to the laboratory in 1 h. Cleaned catfish were slaughtered, and then the back muscles were cut into small blocks (mean weight of about 50 g). All untreated fish fillets were divided into four groups as follows: ultrapure water immersion for 10 min set as the control (lot CK), 13.28 mg/L ozone water immersion for 10 min (lot OW), 200 MPa high-pressure treatment for 10 min (lot UHP), and first 13.28 mg/L ozone water immersion for 10 min followed by 200 MPa high-pressure treatment for 10 min (lot OCU). In detail, a gas–liquid mixer (HPSJ-25, Wuhan, China) combined with an ozone generator (GCQJ-1-3, Wuhan, China) was used to produce ozone water, and the flow rate was adjusted to change the concentration of ozone water. The soaked fish fillets were packed in cooking bags, and then the cooking bags were placed in a vacuum sealer (DZD-400/S, Tengtong Co. Ltd., Nantong, China). In addition, the packaged fillets from UHP and OCU were sent to an ultra-high pressure processing machine (HPPL2-600MPa/2L, Huataisenmiao Inc., Tianjin, China). All packaged fillets were stored at 4°C, and the physicochemical, microbiological, and sensory parameters of the catfish fillets were evaluated on the 0th, 3rd, 6th, 9th, and 12th days, respectively (unless otherwise specified).

Measurement of Total Volatile Base Nitrogen

Accurately 10.0 g minced catfish meats and 90.0 ml of 7.5% (*w/v*) trichloroacetic acid solution were homogenized at 5,000 rpm for 1 min, and then the mixture was filtered with a GE Whatman medium-speed qualitative filter paper after centrifuging at 5,000 rpm for 10 min at 4°C. The semi-micro-quantitative nitrogen method was used to determine TVBN in catfish fillets according to the fore method (19) with a slight modification. Concretely, 5 ml of obtained filtrate and 5 ml of 1% (*w/v*)

magnesium oxide were boiled in a reaction chamber for 6 min, and the receiving parts were 10 ml of 2% (*w/v*) boric acid absorption solution and a few drops of indicator (methyl red and bromocresol green at a ratio of 1:5). After the reaction, 0.01 mol/L hydrochloric acid standard solution was used to turn the indicator blue–violet. TVBN of the reactant was converted by the volume of hydrochloric acid standard solution, and its value was expressed as mg N per 100 g of catfish fillets. Each catfish fillet was measured in triplicate.

Measurement of Thiobarbituric Acid Reactive Substances

Accurately 5 g of minced catfish muscles were homogenized with 45 ml of 20% (*w/v*) trichloroacetic acid solution. After standing for 30 min, the mixture was centrifuged at 5,000 rpm for 10 min at 4°C. The centrifugal liquid obtained was collected after passing through a GE Whatman medium-speed qualitative filter paper. About 5 ml of supernatant and 5 ml of 0.02 mol/L thiobarbituric acid (TBA) were seethed for 30 min. The reacting substance was measured at 532 nm using a UV-vis spectrophotometer (UV-3802, Unico Instrument Co. Ltd., China) after cooling in an ice bath. 1,1,3,3-Tetraethoxypropane was used in the preparation of the standard curve, and then TBARs was expressed as mg malondialdehyde (MDA) per kilogram of catfish fillets. Each catfish fillet was measured in triplicate.

Examination of Chromaticity

The L* (representing brightness value), a* (representing red or green value), and b* (representing yellow or blue value) of catfish fillets with a thickness of 40 mm were measured by a portable colorimeter (CR-400, Konica Minolta Inc., Japan), and the colorimeter was corrected by a white standard board (L* = 85.6, a* = 0.3162, b* = 0.3238) before testing. The chromaticity of three catfish fillets was measured in triplicate, and random testing parts of each catfish fillet were selected. The whiteness and chromatic aberration (ΔE) were expressed with the following equation (20, 21):

$$\text{Whiteness} = 100-\sqrt{(100-\text{L})^2+\text{a}^2+\text{b}^2}$$

$$\Delta\text{E} = \sqrt{(\Delta\text{L})^2+(\Delta\text{a})^2+(\Delta\text{b})^2}$$

Where ΔL*, Δa*, and Δb* represent the aberration in the L*, a*, and b* values of different processing and raw catfish fillets.

Microbiological Evaluation

Microbial Enumeration

Precisely 10.0 g of chopped catfish muscles was thoroughly mixed with 90 ml of sterile 0.85% (*w/v*) saline and sterile grass beads to obtain a sample suspension. Then, 1 ml of the suspension was taken at an appropriate dilution to a petri dish containing approximately 20 ml of agar medium, while gently rotating the petri dish to fully mix the bacterial solution and the culture medium. After the agar medium had solidified, the plates were placed upside down into an artificial constant temperature incubator (HPX-9082 MBE, Boxun Inc., China). These procedures were completed in the ultra-clean workbench (HFsafe-1200LC, Lishen Inc., China). The strategy of microbial selective counting was customized based on the previous studies (22, 23): (a) the total viable count (TVC) was cultivated on Plate Count Agar (Hopebio, China) at 30°C for 3 days, (b) *Enterobacteriaceae* were incubated on Violet Red Bile Glucose Agar (Hopebio, China) at 30°C for 2 days, (c) *Pseudomonas* were cultivated on Cetrimide Fucidin Cephaloridine Agar (Hopebio, China) added with selective supplements at 30°C for 3 days, (d) lactic acid bacteria (LAB) were incubated on De Man Rogosa Sharpe Agar (Hopebio, China) at 30°C for 3 days, and (e) hydrogen sulfide-producing bacteria (HSPB) were incubated on Triple Sugar Iron Agar (Hopebio, China) at 30°C for 3 days (the production of black colonies). Two fish fillets from each treatment were respectively used for microbial enumeration. The counting results from the plates with 30–300 colonies were converted to the colony-forming units (CFU) and expressed in the form of $\log_{10}$ CFU/g.

Microbial Diversity

The 0th and 6th days of CK were used for sequencing analysis given the previously obtained results of the TVC threshold. Similarly, OW and UHP: the 0th and 9th days; OCU: the 0th and 12th days. The cotton swabs contaminated with the contents were stored at −80°C and then sent to Meiji Biomedical Technology Co. Ltd. (Shanghai, China) for microbial sequencing. The QIAamp® DNA Tool Mini Kit was used to extract bacterial DNA from swabs, and 2.0% agarose gel electrophoresis was used to determine the DNA quality. Universal primer 1 (338-F) and primer 2 (806-R) were used to amplify the V3-V4 region of the 16S rRNA gene according to Zhang et al. (24) with appropriate modification. The PCR mix included TE buffer, 10 ng of DNA template, 4 μl of 5 × FastPfu buffer, 0.4 μl of FastPfu DNA polymerase, 0.8 μl of primer 1, 0.8 μl of primer 2, and 2 μl of dNTP (2.5 mM). The PCR amplification procedures are listed as follows: 94°C for 2 min, and followed by 30 cycles: degeneration at 94°C for 1 min, renaturation at 55°C for 40 s, elongation at 72°C for 40 s, and finally, extension at 72°C for 10 min. The amplification process was completed in the ABI GeneAmp® 9700 PCR sprint. The concentration of amplified DNA was identified by 2.0% agarose gel electrophoresis, and the TruSeq® Nano DNA LT Sample Prep Kit (Illumina Inc., San Diego, CA, United States) was used to purify the amplified DNA, and then the sequencing library was established.

The Illumina HiSeq platform (Beijing Novogene Bioinformation Science and Technology Co. Ltd., China) was used to sequence the amplified DNA. The Flash (v1.2.11) software was used to splice, denoise, merge, and non-chimeric the sequences to obtain high-quality sequences. The Uparse (v7.0.1090) software clustered high-quality sequences into the same operational taxon units (OTU) with a similarity of 97%. OTU could be converted into a genus or a phylum. To obtain the species classification information corresponding to each OTU, the silva132/16S_bacteria database was used for taxonomic comparison of species classification, and Ribosomal Database Project (RDP) classifier (v2.11). The confidence percentage of species classification was set as 70%. This procedure was

carried out on the free online platform from Shanghai Majorbio Bio-pharm Technology Co. Ltd. Plotting was based on data with software R (v3.3.1), including Principal Co-ordinates Analysis (PCoA), Barplot, and Heat-map to visualize bacteria community.

Electronic Nose Analysis

The electronic nose (E-Nose) (PEN3, AIRSENSE Co. Ltd., Germany) was used to analyze the odor difference of the crayfish samples. About 2.0 g of shredded catfish muscles and 4 ml of saturated saline were placed in a 20.0 ml headspace and sealed with an E-Z Crimper (Huifen Co. Ltd., China). The headspace bottle was placed in a 45°C water bath to equilibrate for 2 min and then analyzed in the E-nose system. The test parameters were as follows: flush time and measurement time were set as 100 and 120 s, respectively, and chamber flow was set as 600 ml/min. The E-nose system consists of 10 metal oxide sensors, which are sensitive to different volatile components. The response values of the sensor from 115 to 119 s were used to visualize the odor difference between the samples, and this procedure was completed in the software WinMuster built into the E-nose system. The samples from day 0 and day 12 were used for the E-nose test, and each sample was tested in triplicate.

Sensory Evaluation

Sensory evaluation was evaluated through four indexes: smell, color, muscle tissue, and elasticity, and slightly modified by Li et al. (25). Each indicator included four summary descriptive words based on sensory. The descriptors respectively represented four excellent quality levels (representing 8–9 score), good (representing 6–7 score), average (representing 4–5 score), and poor (representing 2–3 score). Five experienced food professionals (three males and two females) aged 22–26 in the laboratory scored the descriptors, and the results were averaged.

Statistical Analysis

Excel 2010 (Microsoft Corporation, United States) was used to calculate data, and Origin 9.4 (Origin Lab Corporation, Northampton, MA, United States) was used to form the chart. SPSS 18.0 for Windows (SPSS Inc., Chicago, IL, United States) was used for multiple comparisons (one-way analysis of variance with the Duncan method) between data, and a confidence interval of 95% ($p < 0.05$) was set as the significance level. The results were expressed as means ± standard deviation (SD).

RESULTS AND DISCUSSION

Total Volatile Base Nitrogen

As shown in **Figure 1**, the TVC of the different treatments gradually increased with the prolonged storage. The TVBN value of all treatments was less than 12 mg/100 g on day 0. After that, the TVBN of CK increased rapidly and exceeded the freshwater fish threshold (20 mg/100 g) defined by the Chinese National Food Safety Standard (GB 2733–2015) on the 9th day. The combined treatment did not reach this spoilage point until the 12th day, which prolonged the shelf life by at least 3 days compared with the control. In brief, the TVBN of OCU was

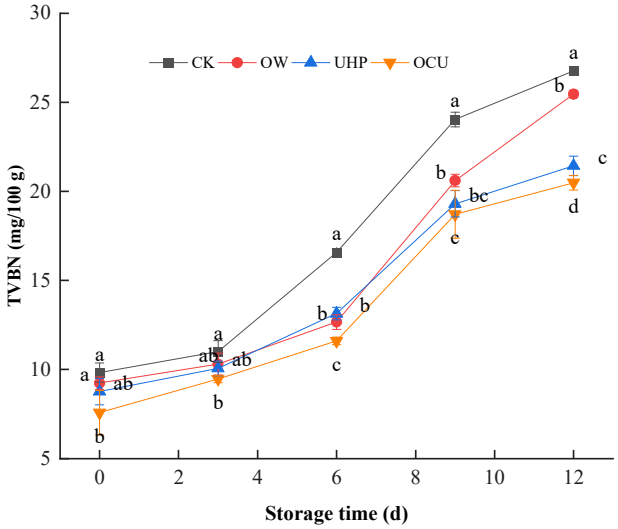

FIGURE 1 | Changes in total volatile basic nitrogen (TVBN) of refrigerated catfish fillets. Error bars were derived from the standard deviation of means. Significant differences ($p < 0.05$) were expressed as alphabets (a, b, c, and d) in different treatments at the same storage time, respectively. CK, the control; OW, ozone water; UHP, ultra-high pressure; OCU, ozone water combined with ultra-high pressure.

significantly ($p < 0.05$) lower than that of CK during the entire storage, which suggested that ozone water combined with ultra-high pressure could effectively reduce the accumulation of TVBN produced by spoilage bacteria and endogenous protein enzymes. Similarly, studies reported that TVBN of red mullet and coho salmon was reduced to varying degrees at different pressure levels compared to unpressured treatments (26, 27). On the other hand, we observed that the TVBN of UHP was lower than OW in general, and this phenomenon was more pronounced in anaphase storage (9–12 days).

Thiobarbituric Acid Reactive Substances

The TBARs monitoring of various secondary oxidation products is a valuable parameter to characterize lipid oxidative rancidity. As shown in **Figure 2**, with the storage prolongation, the TBARs of CK, OW, UHP, and OCU increased gradually. Previous studies have found that ozone water or ultra-high pressure processing could lead to increased TBARs (28–32). The TBARs of the three processing methods were lower than that of the control in early storage. The TBARs of OCU were significantly ($p < 0.05$) lower than that of CK during the entire storage, which suggested that ozone water combined with ultra-high pressure could effectively restrain rancidity. Pressurization could prevent the development of lipid oxidation by inhibiting the activity of endogenous enzymes (lipoxygenase, peroxidase, etc.) (15). Torres et al. (33) found that high-pressure treatment partially inhibited the development of lipid oxidation in Atlantic horse mackerel during frozen storage. The TBARs of OCU that we observed may be due to the better enzymatic inactivation effect of the combined treatment than either UHP or OW alone. The milder pressurization level used in this study (pressure is

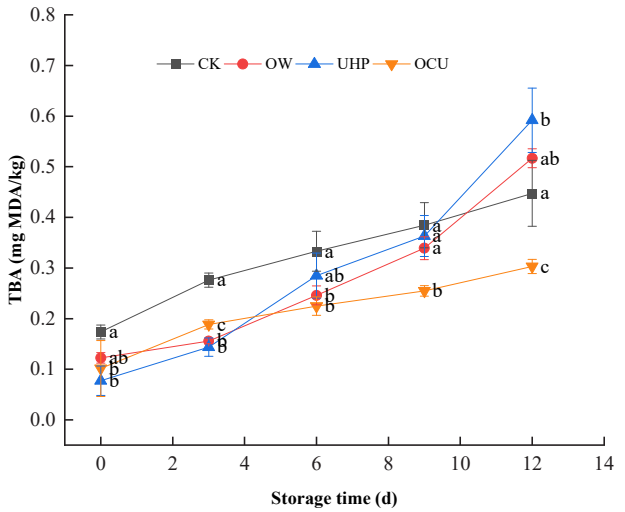

FIGURE 2 | Changes in thiobarbituric acid reactive substances (TBARs) in refrigerated catfish fillets. Error bars were derived from the standard deviation of means. Significant differences ($p < 0.05$) were expressed as alphabets (a, b, c, and d) in different treatments at the same storage time, respectively. CK, the control; OW, ozone water; UHP, ultra-high pressure; OCU, ozone water combined with ultra-high pressure.

200 MPa, and the holding time is only 10 min) may also be a reason for not complying with the UHP effect on lipid oxidation. The explanation of these phenomena was also classified as the differences in the composition and content of lipids in the species (34), the position of muscle containing heme proteins, and the pressurized level (such as pressure and duration) (31, 35).

Chromaticity

The whiteness (**Figure 3A**) of OW was significantly ($p < 0.05$) lower than that of CK until the storage destination. In general, individual ozonation results in increased whiteness (36, 37). Ozone water causes the color difference of species. de Mendonça Silva et al. (32) found that ozone water processing did not affect the color of Nile tilapia fillets. These discrepancies may be due to factors such as the biological conditions of the species, storage conditions, and the treated load they receive. In addition, the whiteness of OCU was lower than that of CK until the 6th day. In detail, the whiteness of CK decreased from 61.48 on day 0 to 55.48 on day 6, while the whiteness of OCU increased from 52.38 on day 0 to 54.65 on day 6, indicating that OCU reduced the bleaching of the fillets compared to CK until storage middle. Subsequently, storage was prolonged, contrary to the serial decline of CK, the whiteness of UHP and OCU continued to rise. The results we observed reflected that catfish fillets treated with ultra-high pressure developed a cooked color, which may be attributed to the degeneration of the myofibrils and sarcoplasmic proteins that lead to changes in the surface of the meat (28). Similarly, studies have reported that high pressure processing contributed to the cooked appearance of meat (38, 39). Globin denaturation, oxidation of myoglobin, the disintegration of myofibrillar protein, lack of active pigments, and protein

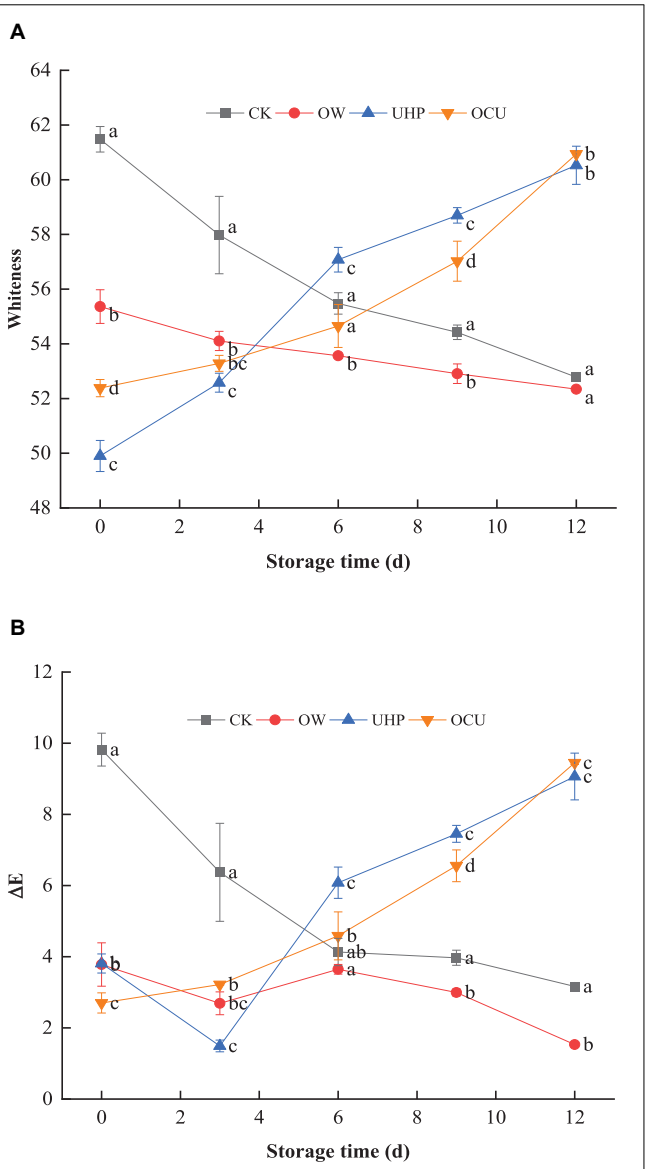

FIGURE 3 | Panels **(A,B)** were respectively whiteness and chromatic aberration of refrigerated catfish fillets. Error bars were derived from the standard deviation of means. Significant differences ($p < 0.05$) were expressed as alphabets (a, b, c, and d) in different treatments at the same storage time, respectively. CK, the control; OW, ozone water; UHP, ultra-high pressure; OCU, ozone water combined with ultra-high pressure.

coagulation were also considered to be contributing factors to the whitish color (30, 40–43). And pressurization intensity could also affect color differences. Ragazzo-Sanchez et al. (44) reported that 600 MPa pressure treatment for 180 s did not affect the color of the shrimp paste samples. The converted ΔE (**Figure 3B**) and whiteness displayed the same trend. The L*, a*, and b* of raw catfish fillets were 51.74, 2.35, and 0.98, respectively (data not shown). Moreover, OCU contributed to the minimum of ΔE on day 0 ($p < 0.05$), and its increase was proportional to the prolonged storage. See the **Supplementary Material** for the actual photos of refrigerated catfish fillets.

Microbial Count

As shown in **Figure 4A**, the TVC of different processing was positively correlated with prolonged storage. Specifically, TVC of OW, UHP, and OCU was 4.28, 4.88, and 4.06 $\log_{10}$ CFU/g at day 0, respectively, which were all lower than 5.35 $\log_{10}$ CFU/g of CK. The initial bacterial count of CK was relatively high and exceeded the threshold (6 $\log_{10}$ CFU/g) stipulated in Al–Dagal et al. (45) on the 6th day. The OCU did not reach this spoilage point until the 9th day, which prolonged the shelf life by at least 3 days compared with the control. The microbial activity was also evaluated by chemical parameters, for example, TVBN (27). Dramatically, the TVC results we observed were consistent with the formerly described TVBN. The latest evidence confirmed that there was a significant correlation between alkaline volatile nitrogen and microbial proliferation (46). In brief, TVC of OCU was significantly ($p < 0.05$) lower than that of CK during the entire storage, which suggested that ozone water combined with ultra-high pressure could effectively reduce the accumulation of bacteria and fungi. On the other hand, we observed that the microbial loading of UHP was lower than OW in general, and this phenomenon was more significant ($p < 0.05$) in 6 –12 days. Zhao et al. (47) found that *Toona sinensis* treated with UHP reduced more TVC compared with ozonation. The lower initial microbial load of OW may be attributed to the sublethal damage to the cells. After the harsh stress is eliminated, cell metabolism can be partially or completely repaired (44, 48). The explanation of OCU may be attributed to ultra-high pressure further ruptured the cells damaged by oxidation, resulting in irreversible degeneration. Then, we emphasized the potential of ozone water combined with ultra-high pressure to control the microbial quality of catfish fillets.

Enterobacteriaceae (**Figure 4B**), *Pseudomonas* (**Figure 4C**), LAB (**Figure 4D**), and HSPB (**Figure 4E**) gradually increased during storage. Both *Enterobacteriaceae* and *Pseudomonas* from combined treatment were significantly ($p < 0.05$) less than from the control during storage. In summary, the combined processing postponed the accumulation of the main genera of *Proteobacteria* in the entire storage. Spoilage microorganisms such as *Pseudomonas* and *Shewanella* could metabolize free amino acids in the muscles to produce volatile nitrogen compounds (49), resulting in unacceptable sensory quality. The counting results showed that *Pseudomonas* has the potential to survive in ozone water based on a large increase of OW in mid-to-late storage. And preceding reports also stated that *Pseudomonas* has the advantage of tolerating a fairly high dose of ozone water (50). The results we found suggested that UHP could effectively rupture the cell membrane of *Pseudomonas*. Similarly, ultra-high pressure reduced the initial load of *Pseudomonas* (27). Moreover, Rivas-Canedo et al. (51) reported that the presence of some gram-negative bacteria such as *Pseudomonas* and *Aeromonas* was directly related to accelerated lipid oxidation. Our reduced *Pseudomonas* may also contribute to the reduced TBARs as described earlier. The oxygen-free environment caused by vacuum is conducive to facultative anaerobes propagation, which also explained that certain LAB can become dominant

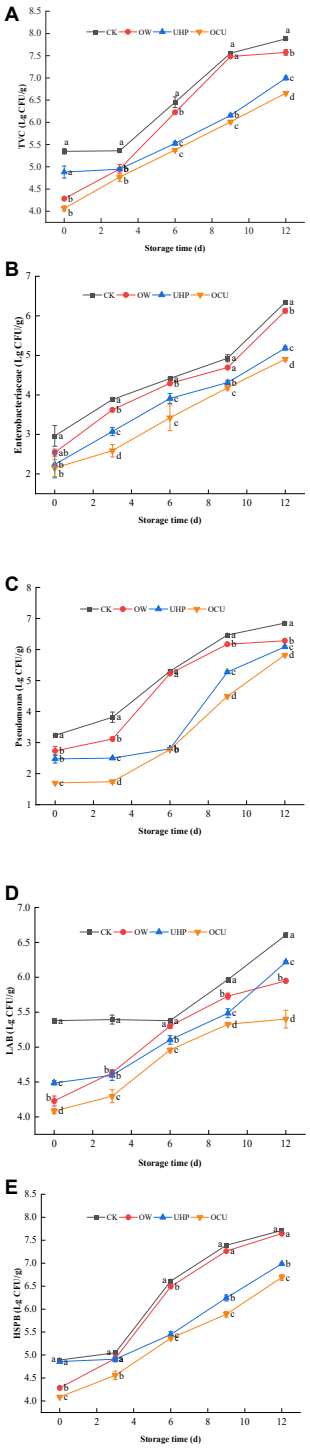

FIGURE 4 | Microbial count of refrigerated catfish fillets, including **(A)** total viable count (TVC), **(B)** *Enterobacteriaceae*, **(C)** *Pseudomonas*, **(D)** lactic acid bacteria (LAB), and **(E)** hydrogen sulfide-producing bacteria (HSPB). Error bars were derived from the standard deviation of means. Significant differences ($p < 0.05$) were expressed as alphabets (a, b, c, and d) in different treatments at the same storage time, respectively. CK, the control; OW, ozone water; UHP, ultra-high pressure; OCU, ozone water combined with ultra-high pressure.

bacteria in later storage (52). In short, the LAB of ultra-high-pressure treatments was significantly ($p < 0.05$) reduced compared with the control. The study reported that the same pressure (200 MPa) treatment can effectively reduce the LAB of salmon fillets during refrigeration, no matter at the beginning or end of storage (53). Compared to the control, the LAB of beef and chicken breast pressure-treated at 400 MPa/10 min decreased significantly (51). H_2S is described as a strong characteristic spoilage odor of "spoiled eggs." In general, the trend of HSPB was not much different from that of TVC. Ozone water lethality to HSPB during entire storage was mild on the whole except for the significant ($p < 0.05$) decline on day 6. The low initial bacterial load of OW was explained as ozone water processing may cause sublethal bacterial damage, and this damage gradually recovers as prolonged storage. Compared with OW, OCU significantly ($p < 0.05$) reduced the load of HSPB during storage, which also indicated that the inactivation efficacy of the combined treatment mainly came from ultra-high pressure. A previous study found that *Shewanella* (a representative genus producing hydrogen sulfide) achieved varying degrees of reduction through ultra-high pressure levels (27). In brief, the combination of ozone water and ultra-high-pressure processing has achieved a significant bacterial inactivation amount.

Microbial Diversity

Most OTU belonged to four bacteria phyla (**Figure 5A**), namely *Proteobacteria*, *Firmicutes*, *Bacteroidetes*, and *Actinobacteria*. Based on the results on day 0, the relative abundance of the most abundant phylum *Proteobacteria* from UHP and OCU decreased compared to CK, but excluding OW. In detail, the relative abundance of CK, OW, UHP, and OCU was 60.03, 68.82, 19.85, and 22.16%, respectively. The results emphasized that ultra-high pressure has better bacteria reduction ability than ozone water, which complied with our previous results of TVBN and TVC. Generally, compared with gram-negative bacteria, gram-positive bacteria survived more due to their thicker cell walls with 40 layers of peptidoglycan and their ability to resist ultra-high pressure (44).

A total of twenty-five of relative abundance value >1% (at least 1 sample) was identified at the genus level (**Figure 5B**). OTU of most genera increased with prolonged storage. On day 0, the combined processing significantly reduced the relative abundance of *Acinetobacter* and *Pseudomonas* belonging to the phylum *Proteobacteria*, while the ozone water processing alone stimulated the vitality of genera. Concretely, *Acinetobacter* and *Pseudomonas* were reduced by 33.73 and 4.26%, respectively. In this work, *Acinetobacter* showed high relative abundance in initial storage, while *Pseudomonas* became the most dominant bacteria in anaphase storage, which may be attributed to competition between species. A previous study reported that *Acinetobacter*, which dominated fresh fish, was replaced by *Pseudomonas* or *Aeromonas* under different treatments (54). In addition, the abundances of *Lelliottia*, *Serratia*, *Shewanella*, and *Yersinia* belonging to the phylum *Proteobacteria* were less than 1% (all samples) after combined processing (OCU). *Serratia* belonging to *Enterobacteriaceae* was widely considered to be typical conditional rot-causing bacteria (55, 56). Belletti

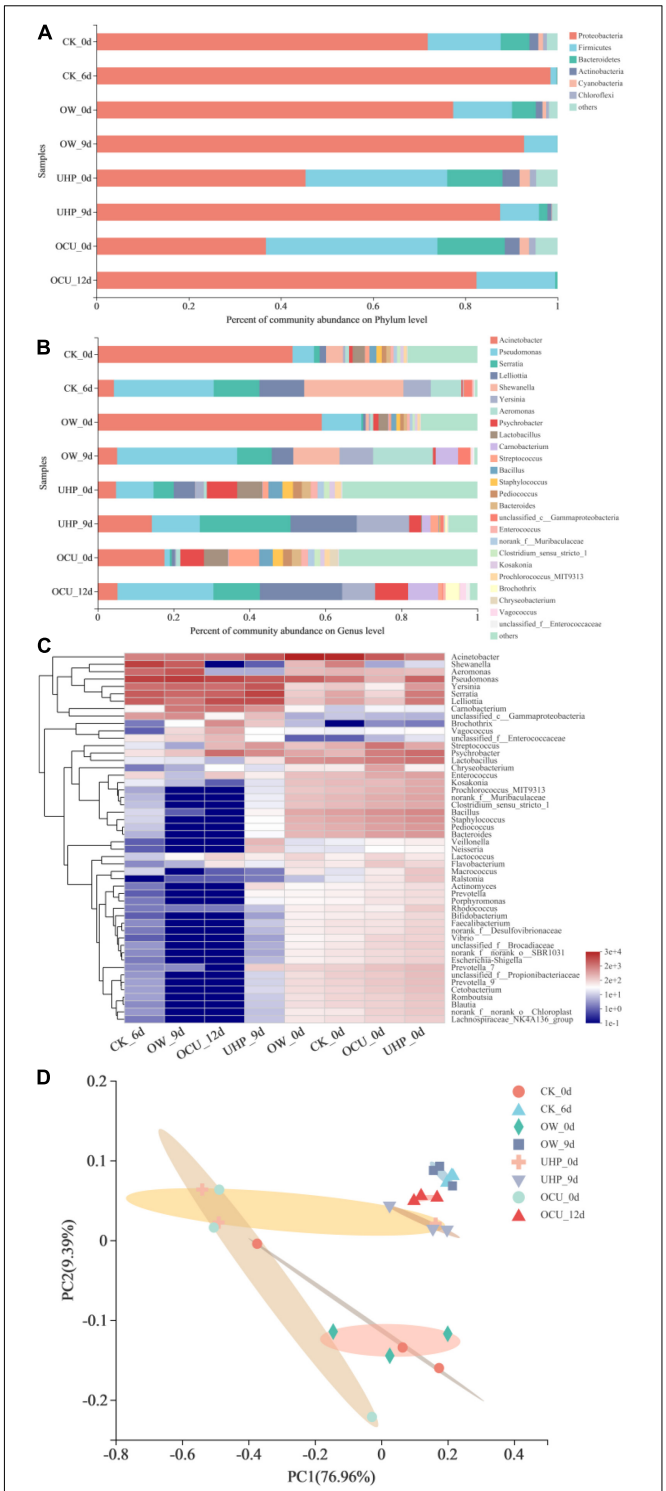

FIGURE 5 | The relative abundance of bacterial community phylum **(A)** and genus **(B)** level in refrigerated catfish fillets. Among panel **(B)**, genera with a relative abundance of less than 1% (all samples) were classified as "other"; panel **(C)** was bacterial community analysis at the genus level, presented in the form of a Heat-map (readers can choose the online version of this article to refer to the colors in the Heat-map); panel **(D)** was principal co-ordinates analysis (PCoA) at the species level. CK, the control; OW, ozone water; UHP, ultra-high pressure; OCU, ozone water combined with ultra-high pressure.

et al. (57) expressed the fact that *Serratia* was affected by high pressure. In short, the results at the genus level corresponded to those at the phylum level as well as the *Enterobacteriaceae* count. At the same time, these phenomena indicated that ozone water combined with ultra-high pressure effectively deactivated *Enterobacteriaceae* of the *Proteobacteria*. *Shewanella* belonging to *Proteobacteria* was recognized as the main contributor to hydrogen sulfide during the storage of aquatic products (58). As for *Shewanella*, its relative abundance was reduced in the ultra-high-pressure treatments (UHP and OCU) compared to the control during storage, and the effective reduction of *Shewanella* in ultra-high pressure followed the previous HSPB count result. On the other hand, certain gram-positive bacteria such as *Lactobacillus*, *Bacillus*, *Staphylococcus*, *Pediococcus*, and *Enterococcus* were insensitive to ultra-high-pressure processing given increased relative abundance in initial storage. Due to the presence of thick film or endospores, the gram-positive bacteria can effectively withstand ultra-high pressure (48). The study reported that the gram-negative bacteria group and coliforms decreased more than TVC and LAB under the same pressure level treatment (51).

The top fifty microbial genera in total abundance emerged in the Heat-map (**Figure 5C**). The colors of most genera that characterize relative abundance had obvious differences between the early and late storages, which indicated that the dominant microbiota had changed. The Principal Co-ordinates Analysis (PCoA) plot showing species clustering is exhibited in **Figure 5D**. The PCoA visualized the differences in microbial species between different processing methods. The first principal component (PC1) and the second principal component (PC2) were 44.33 and 20.08%, respectively. In initial storage, OTU were clustered into two areas, one formed between UHP and OCU, and the other between CK and OW. The species composition similarity between UHP and OCU was attributed to the inactivated effects of ultra-high pressure on microbial communities. In addition, OW was closest to CK due to the limitation of the bactericidal effect of ozone water. Consistent with the previous microbial enumeration results, the inactivation of ultra-high pressure was more recognized than that of ozone water.

Electronic Nose

Electronic nose technology was considered a simple and fast parameter for characterizing complex odors in food samples (59). **Figure 6** is principal components analysis (PCA), showing the odor clustering of refrigerated catfish fillets from different processing. The sample variance of PC1 and PC2 was 96.63 and 2.33%, respectively, which almost characterized the volatile odor components of all catfish fillets. An overlap area was created between CK, OW, UHP, and OCU due to fresh samples, which suggested that the contribution of the samples with several processing methods to the collection of volatile odors was almost equal in the initial storage. The obvious odor difference between the samples was reflected in the anaphase storage. The interlaced area of CK and OW may be attributed to the weaker bactericidal effect of ozone water. There was a great overlap area between UHP and OCU, indicating that the odor properties of the two were approximately equal. Generally, volatile odors are mainly derived from metabolites produced by protein degradation and

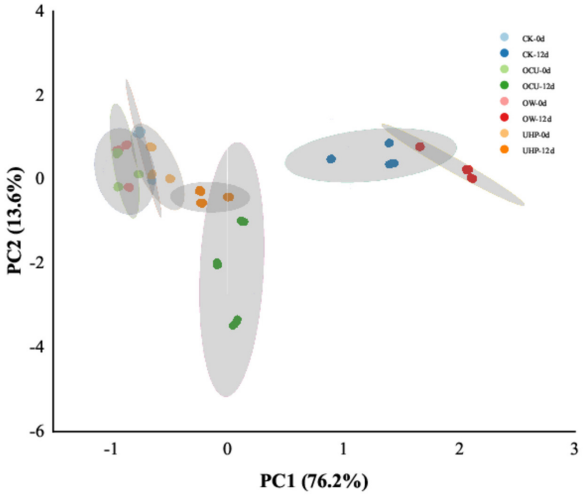

FIGURE 6 | Principal components analysis (PCA) of electronic nose (E-nose) odor clustering in refrigerated catfish fillets. CK, the control; OW, ozone water; UHP, ultra-high pressure; OCU, ozone water combined with ultra-high pressure.

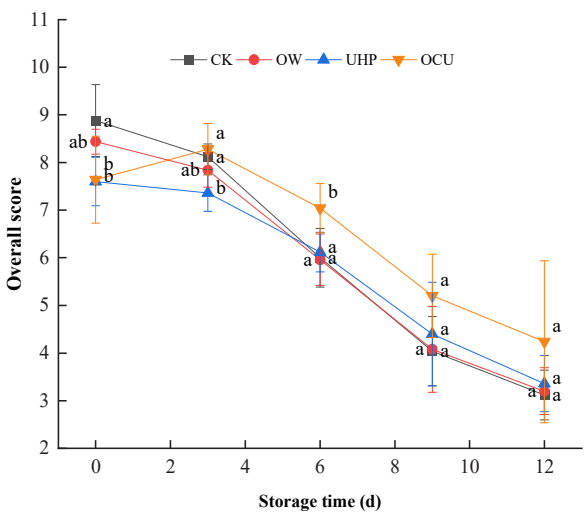

FIGURE 7 | Overall sensory score of refrigerated catfish fillets. CK, the control; OW, ozone water; UHP, ultra-high pressure; OCU, ozone water combined with ultra-high pressure. Significant differences ($p < 0.05$) were expressed as lowercase alphabets in different treatments at the same storage time, respectively. CK, the control; OW, ozone water; UHP, ultra-high pressure; OCU, ozone water combined with ultra-high pressure.

fat oxidation during storage as well as microbial catabolites (18). The odor distance of the ultra-high-pressure processing (UHP and OCU) on day 12 was closer to that of the fresh samples, probably because UHP inhibited the growth of putrefying bacteria and reduced the generation of some spoilage odors, which still requires further study to confirm.

Sensory Score

Figure 7 shows the overall sensory acceptability of the samples during storage. The sensory scores of all samples decreased with prolonged storage. The scores of UHP and OCU on day

0 were 7.60 and 7.64, respectively, which attribute to cooked color caused by ultra-high-pressure treatment. From the 3rd day, OCU consistently maintained the highest overall acceptability compared with other samples. A score of 5 could be considered a threshold for not being accepted by consumers (60). CK (4.04 score), OW (4.08 score), and UHP (4.40 score) all reached levels of sensory rejection on day 9, while OCU (4.24) reached this threshold on day 12. Sensory rejection is related to microbial consumption of meat nutrients (61). The reason for the high sensory score of OCU in our results can be considered to be the synergistic inactivation effect of ozone water combined with ultra-high pressure. These sensory scores followed the changes in E-nose, indicating that the combined treatment effectively improved the sensory quality of refrigerated catfish fillets.

CONCLUSION

This study suggested that ozone water combined with ultra-high pressure effectively decreased TVBN value and microbial load in catfish fillets during refrigeration. All analytical results suggested that the combined treatment inhibited catfish fillet spoilage, especially showing a significant reduction of *Enterobacteriaceae*, *Pseudomonas*, LAB, and HSPB. On the other hand, 16S rRNA gene sequencing analysis showed that the dominant bacteria in fresh catfish fillets were *Acinetobacter*, while the dominant bacteria in spoiled catfish fillets were mainly *Pseudomonas* and *Shewanella*. Further work needs to be performed to better understand the potential synergistic active mechanisms of ozone water and ultra-high pressure on spoilage bacteria, and to apply this method to extend the shelf life of catfish fillets during refrigeration.

DATA AVAILABILITY STATEMENT

The data presented in this study are deposited in the National Center for Biotechnology Information (NCBI) repository, accession number PRJNA837024.

AUTHOR CONTRIBUTIONS

YL: experiments, statistical analysis of data, visualization, and manuscript writing and revision. MZ: experiments and manuscript revision. YQ: experimental design and conceptualization. GX: project proposal and research methodology. LWe: supervision. LWa, WW, LS, AD, and XL: review and editing. All authors contributed to the article and approved the submitted version.

FUNDING

This work was funded by the China Agriculture Research System (CARS-46) and the Major Project of Scientific and Technological R&D of Hubei Agricultural Scientific and Technological Innovation Center (2020-620-000-002-03).

SUPPLEMENTARY MATERIAL

The Supplementary Material for this article can be found online at: https://www.frontiersin.org/articles/10.3389/fnut.2022.880370/full#supplementary-material

REFERENCES

1. Liu Z, Liu S, Yao J, Bao L, Zhang J, Li Y, et al. The channel catfish genome sequence provides insights into the evolution of scale formation in teleosts. *Nat Commun.* (2016) 7:11757. doi: 10.1038/ncomms11757
2. Zhong L, Song C, Chen X, Deng W, Xiao Y, Wang M, et al. Channel catfish in china: historical aspects, current status, and problems. *Aquaculture.* (2016) 465:367–73. doi: 10.1016/j.aquaculture.2016.09.032
3. Karoui R, Hassoun A. Efficiency of rosemary and basil essential oils on the shelf-life extension of Atlantic mackerel (*Scomber scombrus*) fillets stored at 2°C. *J AOAC Int.* (2019) 100:335–44. doi: 10.5740/jaoacint.16-0410
4. Hussain MA, Sumon TA, Mazumder SK, Ali MM, Jang WJ, Abualreesh MH, et al. Essential oils and chitosan as alternatives to chemical preservatives for fish and fisheries products: a review. *Food Control.* (2021) 129:108244. doi: 10.1016/j.foodcont.2021.108244
5. Anand S, Sati N. Artificial preservatives and their harmful effects: looking toward nature for safer alternatives. *Int J Pharm Sci Res.* (2013) 4:2496. doi: 10.13040/ijpsr.0975-8232.4(7).2496-01
6. Deng LZ, Mujumdar AS, Pan Z, Vidyarthi SK, Xu J, Zielinska M, et al. Emerging chemical and physical disinfection technologies of fruits and vegetables: a comprehensive review. *Crit Rev Food Sci Nutr.* (2020) 60:2481–508. doi: 10.1080/10408398.2019.1649633
7. Shi H, Shahidi F, Wang J, Huang Y, Zou Y, Xu W, et al. Techniques for postmortem tenderisation in meat processing: effectiveness, application and possible mechanisms. *Food Prod Process Nutr.* (2021) 3:21. doi: 10.1186/s43014-021-00062-0
8. Rodrigues AAZ, Queiroz M, Neves AA, Oliveira AF, Prates LHF, Freitas JF, et al. Use of ozone and detergent for removal of pesticides and improving storage quality of tomato. *Food Res Int.* (2019) 125:108626. doi: 10.1016/j.foodres.2019.108626
9. da Silva S, Luvielmo M, Geyer M, Pra I. Potencialidades do uso do ozônio no processamento de alimentos potential use of ozone in the food processing. *Semina Ciências Agrárias.* (2011) 32:659–82. doi: 10.5433/1679-0359.2011v32n2p659
10. Pastoriza L, Bernárdez M, Sampedro G, Cabo ML, Herrera JJR. Use of sterile and ozonized water as a strategy to stabilize the quality of stored refrigerated fresh fish. *Food Control.* (2008) 19:772–80. doi: 10.1016/j.foodcont.2007.08.003
11. Tachikawa M, Yamanaka K, Nakamuro K. Studies on the disinfection and removal of biofilms by ozone water using an artificial microbial biofilm system. *Ozone Sci Eng.* (2009) 31:3–9. doi: 10.1080/01919510802586566
12. Abera G, Yildiz F. Review on high-pressure processing of foods. *Cogent Food Agric.* (2019) 5:1568725. doi: 10.1080/23311932.2019.1568725
13. Truong BQ, Buckow R, Stathopoulos CE, Nguyen MH. Advances in High-pressure processing of fish muscles. *Food Eng Rev.* (2014) 7:109–29. doi: 10.1007/s12393-014-9084-9
14. Aubourg SP. Impact of high-pressure processing on chemical constituents and nutritional properties in aquatic foods: a review. *Int J Food Sci Technol.* (2018) 53:873–91. doi: 10.1111/ijfs.13693
15. Vázquez M, Fidalgo LG, Saraiva JA, Aubourg SP. Preservative effect of a previous high-pressure treatment on the chemical changes related to quality loss in frozen hake (*Merluccius merluccius*). *Food Bioprocess Technol.* (2017) 11:293–304. doi: 10.1007/s11947-017-2010-4

16. Zhao YM, de Alba M, Sun DW, Tiwari B. Principles and recent applications of novel non-thermal processing technologies for the fish industry-a review. *Crit Rev Food Sci Nutr.* (2019) 59:728–42. doi: 10.1080/10408398.2018.1495613
17. Sevenich R, Mathys A. Continuous versus discontinuous ultra-high-pressure systems for food sterilization with focus on ultra-high-pressure homogenization and high-pressure thermal sterilization: a review. *Compr Rev Food Sci Food Saf.* (2018) 17:646–62. doi: 10.1111/1541-4337.12348
18. Ye T, Chen X, Chen Z, Yao H, Wang Y, Lin L, et al. Quality and microbial community of high pressure shucked crab (*Eriocheir sinensis*) meat stored at 4°C. *J Food Process Preserv.* (2021) 45:e15330. doi: 10.1111/jfpp.15330
19. Yu D, Zhao W, Yang F, Jiang Q, Xu Y, Xia WA. Strategy of ultrasound-assisted processing to improve the performance of bio-based coating preservation for refrigerated carp fillets (*Ctenopharyngodon idellus*). *Food Chem.* (2021) 345:128862. doi: 10.1016/j.foodchem.2020.128862
20. Cao Y, Li B, Fan X, Wang J, Zhu Z, Huang J, et al. Synergistic recovery and enhancement of gelling properties of oxidatively damaged myofibrillar protein by L-lysine and transglutaminase. *Food Chem.* (2021) 358:129860. doi: 10.1016/j.foodchem.2021.129860
21. Wang Y-Y, Yan J-K, Ding Y, Rashid MT, Ma H. Effect of sweep frequency ultrasound and fixed frequency ultrasound thawing on gelling properties of myofibrillar protein from quick-frozen small yellow croaker and its possible mechanisms. *Lwt.* (2021) 150:111922. doi: 10.1016/j.lwt.2021.111922
22. Carrion-Granda X, Fernandez-Pan I, Jaime I, Rovira J, Mate JI. improvement of the microbiological quality of ready-to-eat peeled shrimps (*Penaeus vannamei*) by the use of chitosan coatings. *Int J Food Microbiol.* (2016) 232:144–9. doi: 10.1016/j.ijfoodmicro.2016.05.029
23. Li B, Wang X, Gao X, Ma X, Zhang L, Mei J, et al. Shelf-life extension of large yellow croaker (*Larimichthys crocea*) using active coatings containing lemon verbena (*Lippa citriodora* Kunth.) essential oil. *Front Nutr.* (2021) 8:678643. doi: 10.3389/fnut.2021.678643
24. Zhang J, Li Y, Yang X, Liu X, Hong H, Luo Y. Effects of oregano essential oil and nisin on the shelf life of modified atmosphere packed grass carp (*Ctenopharyngodon idellus*). *Lwt.* (2021) 147:111609. doi: 10.1016/j.lwt.2021.111609
25. Li P, Peng Y, Mei J, Xie J. Effects of microencapsulated eugenol emulsions on microbiological, chemical and organoleptic qualities of farmed Japanese sea bass (*Lateolabrax japonicus*) during cold storage. *Lwt.* (2020) 118:108831. doi: 10.1016/j.lwt.2019.108831
26. Erkan N, Üretener G, Alpas H. Effect of high pressure (Hp) on the quality and shelf life of red mullet (*Mullus surmelutus*). *Innovative Food Sci Emerg Technol.* (2010) 11:259–64. doi: 10.1016/j.ifset.2010.01.001
27. Aubourg SP, Tabilo-Munizaga G, Reyes JE, Rodríguez A, Pérez-Won M. Effect of high-pressure treatment on microbial activity and lipid oxidation in chilled coho salmon. *Eur J Lipid Sci Technol.* (2010) 112:362–72. doi: 10.1002/ejlt.200900173
28. Chevalier D, Le Bail A, Ghoul M. Effects of high pressure treatment (100–200 Mpa) at low temperature on turbot (*Scophthalmus maximus*) muscle. *Food Res Int.* (2001) 34:425–9. doi: 10.1016/s0963-9969(00)00187-3
29. Yagiz Y, Kristinsson HG, Balaban MO, Marshall MR. Effect of high pressure treatment on the quality of rainbow trout (*Oncorhynchus mykiss*) and Mahi Mahi (*Coryphaena hippurus*). *J Food Sci.* (2007) 72:C509–15. doi: 10.1111/j.1750-3841.2007.00560.x
30. Han G, Chen Q, Xia X, Liu Q, Kong B, Wang H. High hydrostatic pressure combined with moisture regulators improves the tenderness and quality of beef jerky. *Meat Sci.* (2021) 181:108617. doi: 10.1016/j.meatsci.2021.108617
31. Ramirez-Suarez JC, Morrissey MT. Effect of high pressure processing (Hpp) on shelf life of albacore tuna (*Thunnus alalunga*) minced muscle. *Innov Food Sci Emerg Technol.* (2006) 7:19–27. doi: 10.1016/j.ifset.2005.08.004
32. de Mendonça Silva AM, Gonçalves AA. Effect of aqueous ozone on microbial and physicochemical quality of Nile tilapia processing. *J Food Process Preserv.* (2017) 41:e13298. doi: 10.1111/jfpp.13298
33. Torres JA, Vázquez M, Saraiva JA, Gallardo JM, Aubourg SP. Lipid damage inhibition by previous high pressure processing in white muscle of frozen horse mackerel. *Eur J Lipid Sci Technol.* (2013) 115:1454–61. doi: 10.1002/ejlt.201300027
34. Montiel R, De Alba M, Bravo D, Gaya P, Medina M. Effect of high pressure treatments on smoked cod quality during refrigerated storage. *Food Control.* (2012) 23:429–36. doi: 10.1016/j.foodcont.2011.08.011
35. Campus M. High pressure processing of meat, meat products and seafood. *Food Eng Rev.* (2010) 2:256–73. doi: 10.1007/s12393-010-9028-y
36. Aday MS, Caner C. Individual and combined effects of ultrasound, ozone and chlorine dioxide on strawberry storage life. *LWT Food Sci Technol.* (2014) 57:344–51. doi: 10.1016/j.lwt.2014.01.006
37. Glowacz M, Rees D. Exposure to ozone reduces postharvest quality loss in red and green chilli peppers. *Food Chem.* (2016) 210:305–10. doi: 10.1016/j.foodchem.2016.04.119
38. Chéret R, Chapleau N, Delbarre-Ladrat C, Verrez-Bagnis V, Lamballerie MD. Effects of high pressure on texture and microstructure of sea bass (*Dicentrarchus labrax* L.) fillets. *J Food Sci.* (2005) 70:e477–83. doi: 10.1111/j.1365-2621.2005.tb11518.x
39. Techarang J, Apichartsrangkoon A. Physical, chemical and rheological parameters of pressurized Swai-fish (*Pangasius hypophthalmus*) emulsion incorporating fermented soybeans. *Food Bioprod Process.* (2015) 94:649–56. doi: 10.1016/j.fbp.2014.09.002
40. Ma Y, Yuan Y, Bi X, Zhang L, Xing Y, Che Z. Tenderization of yak meat by the combination of papain and high-pressure processing treatments. *Food Bioprocess Technol.* (2019) 12:681–93. doi: 10.1007/s11947-019-2245-3
41. Liu C, Gu Z, Lin X, Wang Y, Wang A, Sun Y, et al. Effects of high hydrostatic pressure (Hhp) and storage temperature on bacterial counts, color change, fatty acids and non-volatile taste active compounds of oysters (*Crassostrea ariakensis*). *Food Chem.* (2021) 372:131247. doi: 10.1016/j.foodchem.2021.131247
42. Lowder AC, Mireles Dewitt CA. Impact of high pressure processing on the functional aspects of beef muscle injected with salt and/or sodium phosphates. *J Food Process Preserv.* (2014) 38:1840–8. doi: 10.1111/jfpp.12155
43. Canto ACVCS, Lima BRCC, Cruz AG, Lázaro CA, Freitas DGC, Faria JAF, et al. Effect of high hydrostatic pressure on the color and texture parameters of refrigerated caiman (*Caiman crocodilus* Yacare) tail meat. *Meat Sci.* (2012) 91:255–60. doi: 10.1016/j.meatsci.2012.01.023
44. Ragazzo-Sanchez JA, Gutierrez-Sanchez Q, Ramirez-de-Leon JA, Ortiz-Basurto RI, Calderon-Santoyo M. Application of high hydrostatic pressure on pacific white shrimp (*Litopenaeus vannamei*) pate: microbiological, physicochemical and consumer acceptance. *Food Sci Technol Int.* (2018) 24:713–23. doi: 10.1177/1082013218792955
45. Al-Dagal MM, Bazaraa WA. Extension of shelf life of whole and peeled shrimp with organic acid salts and bifidobacteria. *J Food Protect.* (1999) 62:51–6. doi: 10.4315/0362-028X-62.1.51
46. Yu D, Wu L, Regenstein JM, Jiang Q, Yang F, Xu Y, et al. Recent advances in quality retention of non-frozen fish and fishery products: a review. *Crit Rev Food Sci Nutr.* (2020) 60:1747–59. doi: 10.1080/10408398.2019.1596067
47. Zhao f, Sun x-j, Yu P-F, Chen W, Liu C-J. Effects of different cold sterilization technology on quality change in toona sinensis during storage. *Food Res Dev.* (2018) 39:188–92. doi: 10.3969/j.issn.1005-6521.2018.04.035
48. Zhang Z-H, Wang L-H, Zeng X-A, Han Z, Brennan CS. Non-thermal technologies and its current and future application in the food industry: a review. *Int J Food Sci Technol.* (2019) 54:1–13. doi: 10.1111/ijfs.13903
49. Parlapani FF, Michailidou S, Anagnostopoulos DA, Koromilas S, Kios K, Pasentsis K, et al. Bacterial communities and potential spoilage markers of whole blue crab (*Callinectes sapidus*) stored under commercial simulated conditions. *Food Microbiology.* (2019) 82:325–33. doi: 10.1016/j.fm.2019.03.011
50. Fournaud J, Lauret R. Influence of ozone on the surface microbial flora of frozen beef and during thawing. *Industr Aliment Agric.* (1972) 89:585–9.
51. Rivas-Canedo A, Fernandez-Garcia E, Nunez M. Volatile compounds in fresh meats subjected to high pressure processing: effect of the packaging material. *Meat Sci.* (2009) 81:321–8. doi: 10.1016/j.meatsci.2008.08.008
52. Zhang J, Li Y, Liu X, Lei Y, Regenstein JM, Luo Y. Characterization of the microbial composition and quality of lightly salted grass carp (*Ctenopharyngodon idellus*) fillets with vacuum or modified atmosphere packaging. *Int J Food Microbiol.* (2019) 293:87–93. doi: 10.1016/j.ijfoodmicro.2018.12.022
53. Park DH, Jung JG, Jung BR, Kim G, Lee H, Kim HA, et al. Changes in salmon (*Oncorhynchus keta*) flesh quality following ultra-high pressure treatment and 30 D of chilled storage. *J Food Sci.* (2015) 80:M142–6. doi: 10.1111/1750-3841.12714
54. Liu X, Zhang Y, Li D, Luo Y. Characterization of the microbiota in lightly salted bighead carp (*Aristichthys nobilis*) fillets stored at 4

degrees C. *Food Microbiol.* (2017) 62:106–11. doi: 10.1016/j.fm.2016.10.007
55. Lavizzari T, Breccia M, Bover-Cid S, Vidal-Carou MC, Veciana-Nogues MT. Histamine, cadaverine, and putrescine produced *in vitro* by *Enterobacteriaceae* and pseudomonadaceae isolated from spinach. *J Food Prot.* (2010) 73:385–9. doi: 10.4315/0362-028x-73.2.385
56. Marino M, Maifreni M, Moret S, Rondinini G. The capacity of *Enterobacteriaceae* species to produce biogenic amines in cheese. *Lett Appl Microbiol.* (2000) 31:169–73. doi: 10.1046/j.1365-2672.2000.00783.x
57. Belletti N, Garriga M, Aymerich T, Bover-Cid S. Inactivation of *Serratia* liquefaciens on dry-cured ham by high pressure processing. *Food Microbiol.* (2013) 35:34–7. doi: 10.1016/j.fm.2013.03.001
58. Yang SP, Xie J, Qian YF. Determination of spoilage microbiota of pacific white shrimp during ambient and cold storage using next-generation sequencing and culture-dependent method. *J Food Sci.* (2017) 82:1178–83. doi: 10.1111/1750-3841.13705
59. Zhao D, Hu J, Chen W. Analysis of the relationship between microorganisms and flavour development in dry-cured grass carp by high-throughput sequencing, volatile flavour analysis and metabolomics. *Food Chem.* (2022) 368:130889. doi: 10.1016/j.foodchem.2021.130889
60. Li Y, Yang Z, Li J. Shelf-life extension of pacific white shrimp using algae extracts during refrigerated storage. *J Sci Food Agric.* (2017) 97:291–8. doi: 10.1002/jsfa.7730
61. Casaburi A, Nasi A, Ferrocino I, Di Monaco R, Mauriello G, Villani F, et al. Spoilage-related activity of carnobacterium maltaromaticum strains in air-stored and vacuum-packed meat. *Appl Environ Microbiol.* (2011) 77:7382–93. doi: 10.1128/AEM.05304-11

Conflict of Interest: The authors declare that the research was conducted in the absence of any commercial or financial relationships that could be construed as a potential conflict of interest.

Publisher's Note: All claims expressed in this article are solely those of the authors and do not necessarily represent those of their affiliated organizations, or those of the publisher, the editors and the reviewers. Any product that may be evaluated in this article, or claim that may be made by its manufacturer, is not guaranteed or endorsed by the publisher.

frontiers | Frontiers in Nutrition

TYPE Mini Review
PUBLISHED 03 August 2022
DOI 10.3389/fnut.2022.960712

OPEN ACCESS

EDITED BY
Qiang Xia,
Ningbo University, China

REVIEWED BY
Wei Zou,
Sichuan University of Science and Engineering, China

*CORRESPONDENCE
Jian Zhou
zhoujian@swust.edu.cn
Guiqiang He
guiqianghe@swust.edu.cn

SPECIALTY SECTION
This article was submitted to Food Chemistry, a section of the journal Frontiers in Nutrition

RECEIVED 03 June 2022
ACCEPTED 11 July 2022
PUBLISHED 03 August 2022

CITATION
Gao L, Zhou J and He G (2022) Effect of microbial interaction on flavor quality in Chinese baijiu fermentation. *Front. Nutr.* 9:960712. doi: 10.3389/fnut.2022.960712

Effect of microbial interaction on flavor quality in Chinese baijiu fermentation

Lei Gao[1], Jian Zhou[1,2]* and Guiqiang He[1,2]*

[1]School of Life Science and Engineering, Southwest University of Science and Technology, Mianyang, China, [2]Engineering Research Center of Biomass Materials, Ministry of Education, Southwest University of Science and Technology, Mianyang, China

Chinese baijiu brewing is an open, complex, and synergetic functional microbiota fermentation process. Microbial interaction is pivotal for the regulation of microbial structure and function in the brewing microecosystem, consequently affecting the flavor and quality of baijiu. This article mainly summarizes the effect of microbial interactions among functional microbiota on the growth performance, flavor formation, and safe quality of baijiu fermentation process. In addition, the review specifically emphasizes on the microbial interactions for the regulation of "Ethyl Caproate-Increasing and Ethyl Lactate-Decreasing" in Chinese strong-flavor baijiu. Furthermore, the construction of synthetic microbiota by metabolic characteristics of the functional microbes and their interactions for regulating and controlling flavor quality of Chinese baijiu is also reviewed and prospected.

KEYWORDS

Chinese baijiu, flavor quality, microbial interaction, synergistic fermentation, synthetic microbiota

Introduction

Chinese baijiu, one of the well-known traditional fermented foods, possesses strong ethnic characteristics in Chinese culture and industrial advantages in the national economy. For example, owing to its unique flavor and aroma, the output and revenue of Chinese baijiu achieved 7.1 billion liters and 583.6 billion RMB in 2020, respectively, reaching a total profit of 131.2 billion RMB. The distinctive flavor and taste of Chinese baijiu is attributed to the composition and proportion of multifarious flavor compounds. Typically, four organic acids (acetic acid, lactic acid, butanoic acid, and hexanoic acid) and their corresponding ethyl esters, especially, caproic acid and ethyl caproate, have been confirmed to be dominant compounds and important contributors to the characteristic flavor of strong-flavor baijiu (1, 2). In fact, 12 flavor types of Chinese baijiu contain more than 1,870 flavor compounds, namely, acids, alcohols, esters, ketones, aldehydes, aromatics, nitrogenous compounds, terpenes, and sulfur compounds (3). In addition, the potential functional component in Chinese baijiu was also uncovered

in recent years. For instance, a tetrapeptide (Ala-Lys-Arg-Ala) had been successfully identified in sesame-flavor baijiu and exhibited preventive effects against 2,2-Azobis (2-methyl-propanimidamidine) dihydrochloride-induced oxidative stress in HepG2 cells (4).

The formation of these flavor and functional compounds is extremely complicated and can be fluctuated mainly by dynamic succession of functional microbiota during the fermentation process. These functional microbes are supposed responsible for the production of flavor compounds by their extensive interactions. For example, the flavor compounds, namely, fatty acids, esters, terpenes, and aromatic compounds produced by *Saccharomyces cerevisiae* were correlated with the mixing ratio of *Bacillus licheniformis* in Chinese maotai−flavor baijiu fermentation (5). Moreover, the microbial interaction is a crucial factor for maintaining the co-occurring in microbiota structure, which will influence the microbial metabolism and flavor formation during the wine fermentation (6). Therefore, revealing the mechanism of the microbial interactions on flavor metabolism is important for regulation of Chinese baijiu fermentation. Based on this, some related studies have already been focused on the microbial interactions and how to achieve the targeted regulation by these interactions in baijiu fermentation (7, 8).

In this review, recent researches relating to the effect of microbial interactions on growth metabolism, flavor formation, and safe quality in Chinese baijiu fermentation (**Figure 1A**), especially for regulation of "Ethyl Caproate-Increasing and Ethyl Lactate-Decreasing" in strong-flavor baijiu (**Figure 1B**) are summarized and discussed. Furthermore, the construction of synthetic microbiota by considering the metabolic features of functional microbes and their interactions (**Figure 1C**), is also described and prospected in the regulation of flavor quality for Chinese baijiu fermentation.

Interactions among functional microbes

Chinese baijiu is produced by the traditional spontaneous solid-state fermentation process containing various functional microbes and their complex interactions (9). In general, microbial interactions are mainly classified through ecological typing into competition, mutualism (cooperation), commensalism, amensalism, or parasitism, and these interactions can be regulated by modifying the metabolic pathway, intercellular communication, and spatial structures, thereby accomplishing the specific functions (10). In fact, there are mainly synergistic (cooperation) and antagonistic (competition) effects involved in the microbial interactions in the baijiu brewing microecosystem. Here, we describe the effect of interactions among functional microbes on the growth performance, flavor formation, and safety characteristic (**Figure 1A**) in the baijiu fermentation process.

Effect of microbial interactions on growth performance

In fact, microbial interactions are usually deemed as cooperative networks with functional microbiota working together toward an ultimate goal during the baijiu-brewing process. This implicates that the cooperation and interaction can influence growth performance and even metabolic activity of the microbial consortia. For example, the biomass of *S. cerevisiae* increased when it was co-cultured with *Aspergillus oryzae* at the ratios of 1:0.1, 1:0.5, and 1:1, and this was attributed to providing more glucose for *S. cerevisiae* growth by inducing enzyme system of starch hydrolyzation in *A. oryzae* (11). This means that the metabolites produced by microbe have synergistic or antagonistic effect on other microbes, also known as metabolite regulation mechanism of the microbial interactions. But, on the contrary, the antagonistic interaction between both species was also uncovered. The growth and biomass of *S. cerevisiae* and *A. oryzae* were inhibited in the mixed culture system, but the protein synthesis for the cell wall of *S. cerevisiae* was significantly promoted (12). In addition, the occurrence and effectiveness of synergistic interactions within functional microbiota are affected easily and restricted by the environmental factors in the natural succession process (13). For instance, the growth of *Zygosaccharomyces bailii* was normal at 30°C, but was inhibited at 37°C in the co-culture system with *B. licheniformis* for Chinese maotai-flavor baijiu fermentation (14). This is mainly related to the stress mechanism of fermentation environment, that is, the growth and survival of brewing microbiota are declined under multiple environmental stresses, namely, alcoholic, acidic, thermal, and oxidative during baijiu production.

Most notably, the antagonistic effect between non-*Saccharomyces* yeasts and *S. cerevisiae* is essential for Chinese baijiu brewing. Many researches have demonstrated that *S. cerevisiae* could inhibit the growth of non-*Saccharomyces* such as *Z. bailii* (15), *Wickerhamomyces anomalus* (16), and *Issatchenkia orientalis* (17) when they were co-cultured. These interactions might be resulted from the non-specific competition for nutrients among yeasts (18) and the inhibition of metabolites (such as ethanol) produced by *S. cerevisiae* (19). So, microbial interactions inevitably influence the growth performance of brewing microbiome during the baijiu fermentation process, consequently altering the metabolic activity and even the flavor formation of the final products.

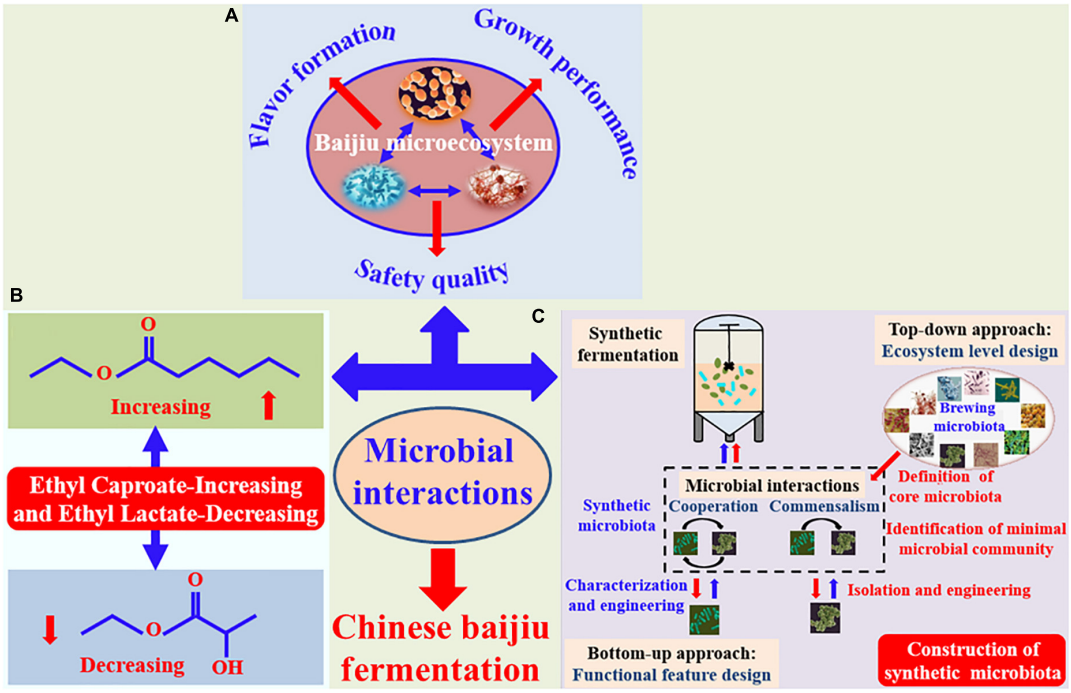

FIGURE 1
Effect of microbial interactions on regulation of growth and flavor metabolism **(A)** and "Ethyl Caproate-Increasing and Ethyl Lactate-Decreasing" **(B)**, as well as construction of synthetic microbiota ("top-down" approach was red arrows, and "bottom-up" approach was blue arrows) **(C)** in Chinese baijiu fermentation process.

Effect of microbial interactions on flavor formation

There are multifarious strategies for improving the flavor quality of traditional fermented foods (20, 21), and the core point of strategy is regulation of the microbial community and their interactions in the fermentation process. For example, the contents of caproic acid and ethyl caproate were improved in strong-flavor baijiu microecosystem by increasing the abundances of caproic acid bacteria and methanogens and also the hydrogen transfer interaction among them with fortified Daqu fermentation (22). Interestingly, although the growth performances of functional strains are repressed, their activities of flavor metabolism are not weakened in the co-culture fermentation system. For instance, when *Z. bailii* and *B. licheniformis* were coexisted, the growth of *B. licheniformis* was significantly inhibited, but the genes, namely, *GAPDH*, *PGM1*, *ENO1*, *PDC1*, *COX1*, and *MEP2* involved in glycolysis, Ehrlich, and oxidative phosphorylation pathways in *Z. bailii* were upregulated, thereby producing more alcohols, acids, esters, and aldehydes in co-culture (15). Actually, the inhibition of growth but promotion of flavor metabolism activity in the co-culture system with non-*Saccharomyces* yeasts and *S. cerevisiae* is ubiquitous in the baijiu fermentation process (15–17). For instance, compared with the single culture of *W. anomalus*, higher yield of ethyl acetate was observed when *S. cerevisiae* and *W. anomalus* were co-cultured (16). This result indicated that the higher content of ethyl acetate could be attributed to synergy between non-*Saccharomyces* yeast and *S. cerevisiae* in co-culture (23). *S. cerevisiae* could produce acetic acid and ethanol, which were critical for *W. anomalus* in generating ethyl acetate in co-culture synergistic fermentation.

Besides aforementioned, some microbes have really poor ability to produce flavor compounds in the fermentation process, but they can coordinate the metabolic activity with those flavor producers. For example, *Bacillus amyloliquefaciens* and *Pichia membranaefaciens* were not effective flavor producers, but they could improve the flavor compounds with *S. cerevisiae*, *I. orientalis*, and *B. licheniformis* co-cultured in the sesame-flavor baijiu fermentation (17). In examples like this, the synergetic interactions between yeasts and lactic acid bacteria are the most widespread in the fermented alcoholic beverages (24). For instance, the content of ethyl lactate was significantly increased when co-cultured with *P. membranifaciens* and *Lactobacillus acetotolerans* in the strong-flavor baijiu fermentation compared with the mono-culture of *P. membranifaciens* (25). In addition, He et al. (26) reported that improvement of esters production and fruity flavor of strong-flavor baijiu was observed when fermented with the fortified Daqu in the brewing process, in which the

synergistic interaction between *Lactobacillus* and *Candida* was considered to be an important driving factor. Another example of synergistic effect on higher production of 3-(methylthio)-1-propanol and dimethyl disulfide was also obtained by co-culturing *S. cerevisiae* with *Lactobacillus buchneri* in baijiu fermentation (27). This synergy mechanism between *S. cerevisiae* and *L. buchneri* was revealed by transcriptome analysis. *S. cerevisiae* upregulated expression of genes for generation of 3-(methylthio)-1-propanol and dimethyl disulfide in the presence of *L. buchneri*, which can regenerate the precursors methionine and S-adenosylmethionine by methyl recycle (27). On the contrary, yeast and lactic acid bacteria could provide nutrients to each other, and promote the growth metabolism of them (28).

Effect of microbial interactions on safe quality

Although the traditional baijiu brewing has been produced for thousands of years, traditional hand-making in an open and complex brewing environment without strict control leads to low production, inconsistent quality, and even security risk (29). Based on the security of baijiu, current researches mainly pay attentions to the regulation and reduction of ethyl carbamate (EC), a class 2A carcinogen (30). For example, there are reports already that the concentrations of EC and its precursor cyanide effectively decreased in raw baijiu by pot still second distillation process (31, 32). Unfortunately, the flavor and quality of baijiu would be affected in part by altering the production process to eliminate the EC content. So, some researchers have focused on the microbial intervention methods for removing the EC, especially for microbial interactions (33, 34). For instance, low amounts of urea (the precursor of EC) was produced by *Lactobacillus* species with non-conventional yeasts, namely, *Pichia*, *Schizosaccharomyces*, and *Zygosaccharomyces* species co-fermentation in Chinese maotai-flavor baijiu (35). Moreover, Fang et al. (36) reported that EC generation by *S. cerevisiae* was significantly inhibited in the co-culture with *Lactobacillus brevis* and provided valuable insights into the molecular mechanism of EC formation by transcriptomic analysis.

Besides EC, some odor compounds were also detected in the baijiu fermentation process, thereby affecting the flavor and safety quality. For example, the compound *p*-cresol is the major off-odor and toxic component of strong-flavor baijiu (37). Another research indicated that *Clostridium* was the primary microbial source for *p*-cresol production and the formation of *p*-cresol could be inhibited by increasing the proportions of *Lactobacillus* (38). In particular, the concentration of *p*-cresol in sesame-flavored baijiu is decreased by hydrogen bond interactions with the non-volatile tetrapeptide Ala-Lys-Arg-Ala (39). Taken together, these studies inspire that intensification of interspecies interactions between *Clostridium* with relevant *Lactobacillus* or Ala-Lys-Arg-Ala-producing strains is a possible strategy for eliminating the *p*-cresol in baijiu fermentation.

Regulation of "Ethyl Caproate-Increasing and Ethyl Lactate-Decreasing" by microbial interactions

At present, one of the tricky problems for many Chinese strong-flavor baijiu production enterprises is how to decrease lactic acid and increase caproic acid accumulation during the fermentation process (40). This technical challenge inevitably results in weakness of the body aroma by ethyl caproate, thinness of flavor and texture, and shortness of aftertaste, which consequently destroys the typical style of strong-flavor baijiu. To address this problem, many researches have been devoted to regulate and control the process parameters during the fermentation, such as scientific construction of fermentation cellar, optimization of pit mud, improvement the quality of fermentation starter, and regulation of the conditions for pit entry (41). However, these works focused mainly on uncovering the correlations between the lactic acid and caproic acid contents with the technical parameters in the baijiu fermentation process. The vital information related to the alteration of functional microbiota caused by these process parameters for regulation of "Ethyl Caproate-Increasing and Ethyl Lactate-Decreasing" is still fragmented.

According to this, some researchers have paid attentions on microbial interactions for regulation of "Ethyl Caproate-Increasing and Ethyl Lactate-Decreasing" (**Figure 1B**) in these years. For instance, the co-culture fermentation broth with *Clostridium kluyveri* and *Methanogen* was subjected to strong-flavor baijiu pit-entry fermentation, the concentration of caproic acid and ethyl caproate in the raw baijiu, respectively, increased by 114.7 and 142.8%, while that of ethyl lactate decreased by 64.1% (42). Interestingly, recent study indicated the relative abundance of caproic acid bacteria significantly increased after 15-day fed-batch fermentation with lactate as carbon sources, which meaned that the brewing microbiota exhibited a regular and directional evolutionary pattern for effectively achieving "Ethyl Caproate-Increasing and Ethyl Lactate-Decreasing" (43). However, in general, it is difficult to control the natural evolution of microbiota and easily fluctuated by environmental factors and process parameters.

Thus, it is of urgent need to develop feasible strategy for directionally regulating fermentation and accelerate the enrichment of functional microbiota. Most notably, an effective regulation approach is the interspecies hydrogen transfer interactions between the hexanoic acid producers and methanogenic archaea (44). The synergistic interaction between caproic acid bacteria and methanogens

is extensively existed in baijiu-brewing microecosystem, which is conducive to maintain the stability of the microbial succession and also produce more caproic acid and ethyl caproate (42, 45, 46). In addition, considering the negative correlations between *Lactobacillus* and *Bacillus* reported by many researches, He et al. (22) performed a novel strategy for regulating strong-flavor baijiu fermentation by directional bioturbation with fortified Daqu (inoculation of *Bacillus subtilis* and *Bacillus velezensis*). The results demonstrated that the bioturbation by fortified Daqu was feasible for "Ethyl Caproate-Increasing and Ethyl Lactate-Decreasing" by interspecies interactions of functional microbiota, namely, *Bacillus*, *Lactobacillus*, *Caproiciproducens*, *Clostridium*, *Candida*, *Aspergillus*, *Methanobacterium*, and *Methanosarcina*.

Construction of synthetic microbiota by the microbial interactions

Synthetic microbiota, constructed artificially by co-culturing of multiple species with well-defined genetic background and specific functions, is provided with low complexity, high controllability, and stability (47, 48). In recent years, some researchers have focused on how to transform to the synthetic fermentation from spontaneous fermentation for regulation of microbial metabolism and production of high-quality foods. For example, *Acetobacter pasteurianus*, *Lactobacillus brevis*, and *Lactobacillus fermentum* were co-cultured and constructed an acetoin-producing synthetic community, when it was applied in the traditional vinegar fermentation, the content of acetoin in vinegar increased significantly (49). In addition, it was reported that a tractable microbiota system was constructed by 24 widely distributed and culturable genera and conducted to the cheese rind fermentation (50). These studies provide references for synthetic microbiota in the different fermented foods. It means that the manipulation and repeatability of microbial succession and dynamic can be obtained *in vitro*. This also affords an opportunity to construct a synthetic microbiota system for food fermentation with prospective flavor and quality.

However, Chinese baijiu brewing is an open, complex, and synergetic of the functional microbiota fermentation process. It seems arduous to construct the synthetic microbiota for regulation and control of the flavor compounds formation in such a microecosystem. Fortunately, the methods of synthetic biology and microbiome make it possible by identification and isolation of the core microbiota with the development of modern biotechnology (51). For the construction of synthetic microbiota, revealing the phylogeny, metabolic functions, especially interspecies interaction of the selected strains are of paramount importance (52). Synthetic microbiota is generally constructed according to the top–down or bottom–up approach (**Figure 1C**), and the microbial interactions play an important role in the construction process by both the approaches (53).

For example, although the growth performances of *S. cerevisiae*, *P. membranaefaciens*, *I. orientalis*, *B. licheniformis*, and *B. amyloliquefaciens* were inhibited by each other, the co-culture of these five species could coordinate the metabolic activities by their interactions and produce the largest amount of flavor compounds in the Chinese sesame-flavor baijiu (17). For another example, the microbial interaction was analyzed by co-occurring network and the synthetic microbiota composed by *L. acetotolerans*, *Pichia kudriavzevii*, *Geotrichum candidum*, *Candida vini*, and *S. cerevisiae* was constructed, 77.27% of the flavor compounds produced by the synthetic microbiota exhibited a similar dynamic profile with that *in situ* system, and the flavor profile presented a similar composition (54). In recent, the core microbiota, namely, *Lactobacillus*, *Thermoactinomyces*, *Aquabacterium*, *Aspergillus*, and *Kazachstania* was identified in the fermented grains of Chinese strong-flavor baijiu by finding ubiquitous, dominant, flavor associated, and co-occurring microbiota together (55). And, the results lay the foundation of construction the synthetic microbiota for regulating the baijiu fermentation process and achieving the homogenization of product quality. Therefore, once we can understand the interaction mechanism of functional microbiota for constructing the synthetic microbiota, we will be able to regulate and control the fermentation process for production of high-quality baijiu.

Conclusion

Chinese baijiu is produced by the spontaneous solid-state fermentation process involved in the multifarious microbes and their extensive and complex interactions. These interactions are propitious to flavor and safety improvement, such as "Ethyl Caproate-Increasing and Ethyl Lactate-Decreasing," and to stability enhancement of baijiu-brewing microecosystem. Moreover, revealing the mechanism of microbial interactions is beneficial for rational construction of synthetic microbiota, and achieving the directional regulation for flavor quality in Chinese baijiu fermentation process.

Author contributions

LG performed the literature search and wrote the manuscript. JZ performed the literature search and contributed to the manuscript revision. GH contributed to the literature summary, manuscript revision, and overall support of this

work. All authors contributed to the article and approved the submitted version.

Funding

This work was funded by the Sichuan Province Key Research and Development Project (2021YFS0340), Doctoral Scientific Fund Project of Southwest University of Science and Technology (20zx7130), and Open Fund of Key Laboratory in Luzhou (NJ202201).

Acknowledgments

We would like to thank Southwest University of Science and Technology for supporting this work.

Conflict of interest

The authors declare that the research was conducted in the absence of any commercial or financial relationships that could be construed as a potential conflict of interest.

Publisher's note

References

1. Fan W, Qian M. Characterization of aroma compounds of Chinese "Wuliangye" and "jiannanchun" liquors by aroma extract dilution analysis. *J Agric Food Chem.* (2006) 54:2695–704. doi: 10.1021/jf052635t

2. Fan W, Qian M. Identification of aroma compounds in Chinese "Yanghe Daqu" liquor by normal phase chromatography fractionation followed by gas chromatography/olfactometry. *Flavour Frag J.* (2010) 21:333–42. doi: 10.1002/ffj.1621

3. Liu H, Sun B. Effect of fermentation processing on the flavor of baijiu. *J Agric Food Chem.* (2018) 66:5425–32. doi: 10.1021/acs.jafc.8b00692

4. Wu J, Huo J, Huang M, Zhao M, Luo X, Sun B. Structural characterization of a tetrapeptide from sesame flavor-type baijiu and its preventive effects against AAPH-induced oxidative stress in HepG2 cells. *J Agric Food Chem.* (2017) 65:10495–504. doi: 10.1021/acs.jafc.7b04815

5. Meng X, Wu Q, Wang L, Wang D, Chen L, Xu Y. Improving flavor metabolism of *Saccharomyces cerevisiae* by mixed culture with *Bacillus licheniformis* for Chinese maotai-flavor liquor making. *J Ind Microbiol Biot.* (2015) 42:1601–8. doi: 10.1007/s10295-015-1647-0

6. Ciani M, Comitini F. Yeast interactions in multi-starter wine fermentation. *Curr Opin Food Sci.* (2015) 1:1–6. doi: 10.1016/j.cofs.2014.07.001

7. Wang B, Wu Q, Xu Y, Sun B. Synergistic effect of multi-saccharifying enzymes on alcoholic fermentation for Chinese baijiu production. *Appl Environ Microb.* (2020) 86:e00013–20. doi: 10.1128/AEM.00013-20

8. Wang B, Wu Q, Xu Y, Sun B. Multiple sugars promote microbial interactions in Chinese baijiu fermentation. *LWT Food Sci Technol.* (2021) 138:110631. doi: 10.1016/j.lwt.2020.110631

9. Zou W, Zhao C, Luo H. Diversity and function of microbial community in Chinese strong-flavor baijiu ecosystem: a review. *Front Microbiol.* (2018) 9:671. doi: 10.3389/fmicb.2018.00671

10. Song H, Ding M, Jia X, Ma Q, Yuan Y. Synthetic microbial consortia: from systematic analysis to construction and applications. *Chem Soc Rev.* (2014) 43:6954–81. doi: 10.1039/c4cs00114a

11. Wu Q, Chen B, Xu Y. Regulating yeast flavor metabolism by controlling saccharification reaction rate in simultaneous saccharification and fermentation of Chinese maotai-flavor liquor. *Int J Food Microbiol.* (2015) 200C:39–46. doi: 10.1016/j.ijfoodmicro.2015.01.012

12. Ge X, Qian H, Zhang W. Influence of mixed culture system on the growth performance of *Aspergillus oryzae* and *Saccharomyces cerevisiae*. *Afr J Biotechnol.* (2013) 12:3272–7. doi: 10.5897/AJB09.025

13. Nuno MO, Rene N, Kevin R. Evolutionary limits to cooperation in microbial communities. *Proc Natl Acad Sci USA.* (2014) 111:17941–6. doi: 10.1073/pnas.1412673111

14. Zhuang X, Wu Q, Xu Y. Physiological characteristics of *Zygosaccharomyces bailii* and its interaction with *Bacillus licheniformis* in Chinese maotai-flavor liquor making. *Microbiol China.* (2017) 44:251–62. doi: 10.13344/j.microbiol.china.160174

15. Xu Y, Wu Q, Xu Y. Effects of main functional strains on *Zygosaccharomyces bailii* in Chinese maotai-flavor liquor fermentation. *Microbiol China.* (2018) 45:42–53. doi: 10.13344/j.microbiol.china.170190

16. Zha M, Sun B, Wu Y, Yin S, Wang C. Improving flavor metabolism of *Saccharomyces cerevisiae* by mixed culture with *Wickerhamomyces anomalus* for Chinese baijiu making. *J Biosci Bioeng.* (2018) 126:189–95. doi: 10.1016/j.jbiosc.2018.02.010

17. Wu Q, Ling J, Xu Y. Starter culture selection for making Chinese sesame-flavored liquor based on microbial metabolic activity in mixed-culture fermentation. *Appl Environ Microb.* (2014) 80:4450–9. doi: 10.1128/AEM.00905-14

18. Tang J, Wang H, Xu Y. Effect of mixed culture of *Saccharomyces cerevisiae* and *Pichia anomala* on fermentation efficiency and flavor compounds in Chinese liquor. *Microbiol China.* (2012) 39:921–30.

19. Wu Q, Kong Y, Xu Y. Flavor profile of Chinese liquor is altered by interactions of intrinsic and extrinsic microbes. *Appl Environ Microb.* (2016) 82:422–30. doi: 10.1128/AEM.02518-15

20. Xu L, Zheng Y, Zhou C, Pan D, Geng F, Cao J, et al. Kinetic response of conformational variation of duck liver globular protein to ultrasonic stimulation and its impact on the binding behavior of n-alkenals. *LWT Food Sci Technol.* (2021) 150:111890. doi: 10.1016/j.lwt.2021.111890

21. Lin X, Tang Y, Hu Y, Lu Y, Sun Q, Lv Y, et al. Sodium reduction in traditional fermented foods: challenges, strategies, and perspectives. *J Agric Food Chem.* (2021) 69:8065–80. doi: 10.1021/acs.jafc.1c01687

22. He G, Huang J, Wu C, Jin Y, Zhou R. Bioturbation effect of fortified Daqu on microbial community and flavor metabolite in Chinese strong-flavor liquor brewing microecosystem. *Food Res Int.* (2019) 129:108851. doi: 10.1016/j.foodres.2019.108851

23. Sadoudi M, Tourdot R, Rousseaux S, Steyer D, Gallardo J, Ballester J, et al. Yeast-yeast interactions revealed by aromatic profile analysis of sauvignon Blanc wine fermented by single or co-culture of non-saccharomyces and *Saccharomyces yeasts*. *Food Microbiol.* (2012) 32:243–53. doi: 10.1016/j.fm.2012.06.006

24. Gammacurta M, Marchand S, Moine V, Revel G. Influence of different yeast/lactic acid bacteria combinations on the aromatic profile of red bordeaux wine. *J Sci Food Agr.* (2017) 97:4046–57. doi: 10.1002/jsfa.8272

25. Luo Q, Zheng J, Zhao D, Qiao Z, An M, Zhang X, et al. Interaction between dominant lactic acid bacteria and yeasts strains in strong aroma baijiu. *China J Appl Environ Biol.* (2019) 25:1192–9. doi: 10.19675/j.cnki.1006-687x.2018.12031

26. He G, Huang J, Zhou R, Wu C, Jin Y. Effect of fortified Daqu on the microbial community and flavor in Chinese strong-flavor liquor brewing process. *Front Microbiol.* (2019) 10:56. doi: 10.3389/fmicb.2019.00056

27. Liu J, Wu Q, Wang P, Lin J, Huang L, Xu Y. Synergistic effect in core microbiota associated with sulfur metabolism in spontaneous Chinese liquor fermentation. *Appl Environ Microb.* (2017) 83:e01475–17. doi: 10.1128/stocktickerAEM.01475-17

28. Mendes F, Sieuwerts S, de Hulster E, Almering MJ, Luttik MA, Pronk JT, et al. Transcriptome-based characterization of interactions between *Saccharomyces cerevisiae* and *Lactobacillus delbrueckii* subsp. bulgaricus in lactose-grown chemostat cocultures. *Appl Environ Microb.* (2013) 79:5949–61. doi: 10.1128/AEM.01115-13

29. Jin G, Zhu Y, Xu Y. Mystery behind Chinese liquor fermentation. *Trends Food Sci Tech.* (2017) 63:18–28. doi: 10.1016/j.tifs.2017.02.016

30. Wang C, Wang M, Zhang M. Ethyl carbamate in Chinese liquor (baijiu): presence, analysis, formation, and control. *Appl Microbiol Biot.* (2021) 105:4383–95. doi: 10.1007/s00253-021-11348-1

31. Wu C, Fan W, Xu Y. Influence of different types of double distillation on removal efficiency of ethyl carbamate in Chinese strong aroma type liquor. *Food Ferment Ind.* (2015) 41:1–7. doi: 10.13995/j.cnki.11-1802/ts.201506001

32. Wang J, Fan W, Xu Y, Yang J, Xie G, Sun L, et al. Influence of pilot scale pot still second distillation on ethyl carbamate and cyanide in baijiu and the quality of raw liquor. *Food Ferment Ind.* (2022) 48:53–7. doi: 10.13995/j.cnki.11-1802/ts.030800

33. Cui K, Wu Q, Xu Y. Biodegradation of ethyl carbamate and urea with *Lysinibacillus sphaericus* MT33 in Chinese liquor fermentation. *J Agric Food Chem.* (2018) 66:1583–90. doi: 10.1021/acs.jafc.7b05190

34. Wei T, Jiao Z, Hu J, Lou H, Chen Q. Chinese yellow rice wine processing with reduced ethyl carbamate formation by deleting transcriptional regulator Dal80p in *Saccharomyces cerevisiae*. *Molecules.* (2020) 25:3580. doi: 10.3390/molecules25163580

35. Du H, Song Z, Xu Y. Ethyl carbamate formation regulated by lactic acid bacteria and nonconventional yeasts in solid-state fermentation of Chinese moutai-flavor liquor. *J Agric Food Chem.* (2017) 66:387–92. doi: 10.1021/acs.jafc.7b05034

36. Fang L, Zhou W, Chen Q. Ethyl carbamate regulation and genomic expression of *Saccharomyces cerevisiae* during mixed-culture yellow rice wine fermentation with *Lactobacillus* sp. *Food Chem.* (2019) 292:90–7. doi: 10.1016/j.foodchem.2019.04.014

37. Dong W, Guo R, Liu M, Shen C, Sun X, Zhao M, et al. Characterization of key odorants causing the roasted and mud-like aromas in strong-aroma types of base baijiu. *Food Res Int.* (2019) 125:108546. doi: 10.1016/j.foodres.2019.108546

38. Du H, Liu B, Wang X, Xu Y. Exploring the microbial origins of p-cresol and its co-occurrence pattern in the Chinese liquor-making process. *Int J Food Microbiol.* (2017) 260:27–35. doi: 10.1016/j.ijfoodmicro.2017.08.016

39. Huang M, Huo J, Wu J, Zhao M, Zheng F, Sun J, et al. Interactions between p-cresol and Ala-Lys-Arg-Ala (AKRA) from sesame-flavor-type baijiu. *Langmuir.* (2018) 34:12549–59. doi: 10.1021/acs.langmuir.8b02662

40. Tao Y, Hu X, Zhu X, Jin H, Xu Z, Tang Q, et al. Production of butyrate from lactate by a newly isolated *Clostridium* sp. BPY5. *Appl Biochem Biotech.* (2016) 179:361–74. doi: 10.1007/s12010-016-1999-6

41. He P, Hu X, Zheng Y, Shen X, Li S, Li X, et al. Research and application progress of "Ethyl Caproate-increasing and Ethyl Lactate-decreasing" in brewing of Chinese luzhou-flavor liquor. *J Light Ind.* (2018) 33:1–12. doi: 10.3969/j.issn.2096-1553.2018.04.001

42. Yan S, Dong D. Improvement of caproic acid production in a *Clostridium kluyveri* H068 and Methanogen 166 co-culture fermentation system. *AMB Expr.* (2018) 8:175. doi: 10.1186/s13568-018-0705-1

43. Chai L, Qian W, Zhong X, Zhang X, Lu Z, Zhang S, et al. Mining the factors driving the evolution of the pit mud microbiome under the impact of long-term production of strong-flavor baijiu. *Appl Environ Microb.* (2021) 87:e0088521. doi: 10.1128/AEM.00885-21

44. Thauer R, Kaster A, Seedorf H, Buckel W, Hedderich R. Methanogenic archaea: ecologically relevant differences in energy conservation. *Nat Rev Microbiol.* (2008) 6:579–91. doi: 10.1038/nrmicro1931

45. Hu X, Du H, Ren C, Xu Y. Illuminating anaerobic microbial community and cooccurrence patterns across a quality gradient in Chinese liquor fermentation pit muds. *Appl Environ Microb.* (2016) 82:2506–15. doi: 10.1128/AEM.03409-15

46. Tao Y, Wang X, Li X, Wei N, Jin H, Xu Z, et al. The functional potential and active populations of the pit mud microbiome for the production of Chinese strong-flavour liquor. *Microb Biotechnol.* (2017) 10:1603–15. doi: 10.1111/1751-7915.12729

47. Roy K, Marzorati M, Abbeele P, Wiele T, Boon N. Synthetic microbial ecosystems: an exciting tool to understand and apply microbial communities. *Environ Microbiol.* (2014) 16:1472–81. doi: 10.1111/1462-2920.12343

48. Shong J, Diaz M, Collins C. Towards synthetic microbial consortia for bioprocessing. *Curr Opin Biotech.* (2012) 23:798–802. doi: 10.1016/j.copbio.2012.02.001

49. Lu Z, Liu N, Wang L, Wu L, Gong J, Yu Y, et al. Elucidating and regulating the acetoin production role of microbial functional groups in multispecies acetic acid fermentation. *Appl Environ Microb.* (2016) 82:5860–8. doi: 10.1128/AEM.01331-16

50. Wolfe B, Button J, Santarelli M, Dutton R. Cheese rind communities provide tractable systems for in situ and in vitro studies of microbial diversity. *Cell.* (2014) 158:422–33. doi: 10.1016/j.cell.2014.05.041

51. Wu Q, Zhu Y, Fang C, Wijffels R, Xu Y. Can we control microbiota in spontaneous food fermentation? – Chinese liquor as a case example. *Trends Food Sci Tech.* (2021) 110:321–31. doi: 10.1016/j.tifs.2021.02.011

52. Vorholt J, Vogel C, Carlstrm C, Müller D. Establishincg ausality: opportunities of synthetic communities for plant microbiome research. *Cell Host Microbe.* (2017) 22:142–55. doi: 10.1016/j.chom.2017.07.004

53. Lawson C, Harcombe W, Hatzenpichler R, Lindemann S, Mcmahon K. Common principles and best practices for engineering microbiomes. *Nat Rev Microbiol.* (2019) 17:725–41. doi: 10.1038/s41579-019-0255-9

54. Wang S, Wu Q, Nie Y, Wu J, Xu Y. Construction of synthetic microbiota for reproducible flavor metabolism in Chinese light aroma type liquor produced by solid-state fermentation. *Appl Environ Microb.* (2019) 85:e03090–18. doi: 10.1101/510610

55. Jiao W, Xie F, Gao L, Du L, Wei Y, Zhou J, et al. Identification of core microbiota in the fermented grains of a Chinese strong-flavor liquor from Sichuan. *LWT Food Sci Technol.* (2022) 158:113140. doi: 10.1016/j.lwt.2022.113140

Advantages of publishing in Frontiers

OPEN ACCESS
Articles are free to read for greatest visibility and readership

FAST PUBLICATION
Around 90 days from submission to decision

HIGH QUALITY PEER-REVIEW
Rigorous, collaborative, and constructive peer-review

TRANSPARENT PEER-REVIEW
Editors and reviewers acknowledged by name on published articles

Frontiers
Avenue du Tribunal-Fédéral 34
1005 Lausanne | Switzerland

Visit us: www.frontiersin.org
Contact us: frontiersin.org/about/contact

REPRODUCIBILITY OF RESEARCH
Support open data and methods to enhance research reproducibility

DIGITAL PUBLISHING
Articles designed for optimal readership across devices

FOLLOW US
@frontiersin

IMPACT METRICS
Advanced article metrics track visibility across digital media

EXTENSIVE PROMOTION
Marketing and promotion of impactful research

LOOP RESEARCH NETWORK
Our network increases your article's readership